

2013

## Development of a framework for scaling surfactant enhanced CO<sub>2</sub> flooding from laboratory scale to field implementation

Gbolahan I. Afonja

*Louisiana State University and Agricultural and Mechanical College*

Follow this and additional works at: [https://digitalcommons.lsu.edu/gradschool\\_dissertations](https://digitalcommons.lsu.edu/gradschool_dissertations)



Part of the [Petroleum Engineering Commons](#)

---

### Recommended Citation

Afonja, Gbolahan I., "Development of a framework for scaling surfactant enhanced CO<sub>2</sub> flooding from laboratory scale to field implementation" (2013). *LSU Doctoral Dissertations*. 527.

[https://digitalcommons.lsu.edu/gradschool\\_dissertations/527](https://digitalcommons.lsu.edu/gradschool_dissertations/527)

This Dissertation is brought to you for free and open access by the Graduate School at LSU Digital Commons. It has been accepted for inclusion in LSU Doctoral Dissertations by an authorized graduate school editor of LSU Digital Commons. For more information, please contact [gradetd@lsu.edu](mailto:gradetd@lsu.edu).

DEVELOPMENT OF A FRAMEWORK FOR SCALING SURFACTANT ENHANCED CO<sub>2</sub>  
FLOODING FROM LABORATORY SCALE TO FIELD IMPLEMENTATION

A Dissertation

Submitted to the Graduate Faculty of the  
Louisiana State University and  
Agricultural and Mechanical College  
in partial fulfillment of the  
requirements for the degree of  
Doctor of Philosophy

in

The Craft & Hawkins Department of Petroleum Engineering

by

Gbolahan I. Afonja

B.S., Morgan State University, 2004

M.S., West Virginia University, 2006

August 2013

# Acknowledgments

All through the time I have spent here, I have received guidance, support and encouragement from a number of individuals. Many thanks to my research adviser, Dr. Richard Hughes. His assistance, support and mentoring approach helped move this project from an idea to a complete work. I would like to thank my dissertation committee members, Dr. Mileva Radonjic, Dr. Dandina Rao, and Dr. Christopher White, who offered guidance and support. It is a pleasure also to thank Dr. Gerald Knapp, the Dean's Representative, for his time and help.

I would like to acknowledge the financial, academic and technical support of the Craft and Hawkins Department of Petroleum Engineering, Louisiana State University. In particular, I would like to thank Janet Dugas, Andi Donmeyer, Darryl Bourgoyne and Fenelon Nunez for their invaluable help during the course of my studies. I would also like to thank Telisha Snell, my program officer at the Graduate School, for her numerous advices on navigating through University policies. In addition, support for this work was provided in part by the U.S. Department of Energy under award number DE-FC-26-04NT15536.

My appreciation also goes out to my colleagues (past and present) for their moral support and in some cases, help in the lab or analysis of my results: Didem Senocak, Venu Nagineni, Shrinidhi Shetty, Danelle Bagoo, Ruiz Paidin, Paulina Mwangi, Chukwudozie Chukwudi, Lu Jin, Abiola Olabode, William Armah, Arome Oyibo, Hakeem Adedehinbo, Bamidele Adediji, Jean-Michel Ngaleu and Law Dickerson.

And, finally, thanks to my wonderful parents, Mr. and Mrs. Afonja, and numerous other family members and friends such as Kunle Afonja, Tosin Folorunso, Mopelola Afonja, Tunde Afonja, Sanya Soyannwo, Ossie Okeke, Debo and Tope Fadesere, Eloho Okeze, Wale and Shakirat Olanrewaju, Judith Udeke, and Lanre Alli. This wonderful group of people endured this long process with me, and did not hesitate to offer assistance and encouragement.

# Table of Contents

<b>Acknowledgments</b>	<b>ii</b>
<b>List of Tables</b>	<b>v</b>
<b>List of Figures</b>	<b>vii</b>
<b>Abstract</b>	<b>ix</b>
<b>Chapter 1: Introduction</b>	<b>1</b>
1.1 Sweep Efficiency Improvement Techniques	1
1.1.1 Water-Alternating-Gas	2
1.1.2 Polymers	2
1.1.3 Surfactants	4
1.2 Impact of Reservoir Heterogeneity	5
1.3 Description of Surfactants	6
1.4 Modeling Surfactant in Porous Media	6
1.5 Dimensionless Scaling Groups	8
1.6 Motivation and Purpose	10
1.7 Strategy	11
<b>Chapter 2: Mathematical Model and Scaling Groups</b>	<b>12</b>
2.1 General Assumptions and Simplifications	12
2.2 Derivation of Dimensionless Groups	13
2.2.1 Governing Equations	13
2.3 Definition of Dimensionless Groups	15
2.3.1 Peclet Number	15
2.3.2 Effective Aspect Ratio	17
2.3.3 Mobility Ratio	18
2.3.4 Capillary Number	18
2.3.5 Gravity Number	19
<b>Chapter 3: Laboratory Experiments</b>	<b>20</b>
3.1 Equipment Setup	20
3.1.1 Injection and Fluid Delivery Unit	20
3.1.2 The Core Unit	22
3.1.3 The Production Unit	22
3.1.4 The Data Acquisition Unit	22
3.2 Experimental Fluids	23
3.2.1 Oil	23
3.2.2 Brine	23
3.2.3 Cleaning Fluids	23
3.2.4 Carbon Dioxide	24
3.2.5 Surfactant Solution	24
3.3 Experimental Procedure	24
3.3.1 Core Cleaning Procedure	24
3.3.2 Pore Volume and Porosity Determination	25
3.3.3 Brine Absolute Permeability Determination	26
3.3.4 Brine- and Surfactant-CO <sub>2</sub> Co-Injection in Oil-free Core	26

3.3.5	Oil Flood	27
3.3.6	Waterflood	27
3.3.7	Co-Injection of Surfactant Solution and CO <sub>2</sub>	28
3.4	Experimental Results	28
3.4.1	Determination of Mobility Reduction Factor (MRF)	29
3.4.2	Oil Recovery Experiments	33
3.5	Summary	36
3.5.1	Field Implementation	36
<b>Chapter 4:</b>	<b>Reservoir Simulation</b>	<b>39</b>
4.1	Foam Model	39
4.2	Foam Generation and Sustenance Modeling	40
4.3	Simulation of Laboratory Floods	41
4.4	Simulation of Synthetic Reservoirs	46
4.4.1	Reduction of fluid velocity for use in Larger Models	46
4.4.2	Scaling Reaction Frequency Factor for use in Larger Models	46
4.5	Simulation Results	47
4.5.1	Coreflooding	47
4.5.2	Synthetic Reservoirs	59
4.6	Conclusions	64
<b>Chapter 5:</b>	<b>Design of Experiments</b>	<b>72</b>
5.1	Overview of Design of Experiments Methods	72
5.1.1	Classical Design of Experiments	73
5.1.2	Modern Design of Experiments	73
5.2	Methodology	73
5.2.1	Permeability Distribution	75
5.2.2	Application of Regression Analysis	76
5.3	Results	77
5.3.1	Validation of the Regression Model	79
5.3.2	Summary	86
<b>Chapter 6:</b>	<b>Conclusions and Recommendations</b>	<b>87</b>
6.1	Conclusions	87
6.2	Recommendations	89
<b>References</b>		<b>92</b>
<b>Appendix A:</b>	<b>Dimensionless Groups</b>	<b>100</b>
<b>Appendix B:</b>	<b>Auxiliary Laboratory Experiments</b>	<b>117</b>
<b>Appendix C:</b>	<b>Inputs and Outputs for Design of Experiments</b>	<b>123</b>
<b>Appendix D:</b>	<b>Code for Hammersley Sequence Sampling</b>	<b>144</b>
<b>Appendix E:</b>	<b>Nomenclature</b>	<b>146</b>
<b>Vita</b>		<b>151</b>

# List of Tables

2.1	Surfactant component-phase chart . . . . .	12
2.2	Dimensionless Groups from Inspectional Analysis . . . . .	14
3.1	Summary of results from MRF experiments . . . . .	31
3.2	Summary of results from auxiliary experiments . . . . .	33
4.1	Minimum and maximum values for the $D_{Lo1}$ and $D_{To1}$ for $CO_2$ in the oleic phase	46
4.2	Dimensional parameters for core experiments and synthetic reservoirs . . . . .	48
4.3	Values of $FM$ parameters used to match laboratory results . . . . .	50
4.4	Values of wetting and non-wetting interpolation parameters . . . . .	50
4.5	Values of stoichiometric parameters used to match laboratory results . . . . .	55
4.6	Comparison of Reaction Frequency Factors, $r_{rate}$ . . . . .	55
4.7	Dimensionless numbers for core and synthetic models for 0.1% wt . . . . .	56
4.8	Dimensionless numbers for core and synthetic models for 0.5% wt . . . . .	59
4.9	Layer thickness and permeability distribution for sample reservoirs . . . . .	60
5.1	Minimum and maximum values for 9 dimensionless numbers . . . . .	75
5.2	Descriptive statistics of input and output variables used in Experimental Design	78
5.3	Coefficients for oil $RF$ and $\Delta p$ obtained from linear regression . . . . .	79
5.4	Coefficients for oil $RF$ and $\Delta p$ obtained from quadratic regression . . . . .	80
5.5	R Squared values for linear and quadratic regression models . . . . .	80
5.6	Minimum and maximum values for regression model validation . . . . .	83
5.7	R Squared values for linear and quadratic regression models . . . . .	83
A.1	Initial Dimensionless Groups from Inspectional Analysis . . . . .	109
B.1	Summary of results from auxilliary experiments . . . . .	117
B.2	Properties of fluids . . . . .	117
B.3	Fluid volumes used to calculate core pore volume and porosity . . . . .	118
B.4	Flow rates and corresponding average $\Delta p$ used to determine $k_{abs}$ . . . . .	118
B.5	Fluid volumes used to calculate $S_{wirr}$ and $S_{oi}$ from oil injection . . . . .	118

B.6	Fluid volumes used to calculate $S_{wi}$ and $S_{or}$ from waterflood . . . . .	119
B.7	Fluid saturations after surfactant and CO <sub>2</sub> coinjection . . . . .	119
C.1	Design space for raw sampling points for dimensionless groups (128 runs) . .	123
C.2	Design space for actual sampling points for dimensionless groups (128 runs)	126
C.3	Part 1: Dimensional properties calculated from dimensionless numbers . . .	128
C.4	Part 2: Dimensional properties calculated from dimensionless numbers . . .	130
C.5	Part 3: Dimensional properties calculated from dimensionless numbers . . .	132
C.6	Part 4: Dimensional properties calculated from dimensionless numbers . . .	135
C.7	Measured and linear- and quadratic-regression predicted values of $RF$ and $\Delta p$	137
C.8	Design space for sampling points for dimensionless groups (32 prediction runs)	139
C.9	Part 1: Dimensional properties for cases to be predicted . . . . .	140
C.10	Part 2: Dimensional properties for cases to be predicted . . . . .	141
C.11	Part 3: Dimensional properties for cases to be predicted . . . . .	141
C.12	Part 4: Dimensional properties for cases to be predicted . . . . .	142
C.13	Measured and regression results of predicted values of $RF$ and $\Delta p$ (32 cases)	143

# List of Figures

3.1	Schematic of coreflood experimental setup . . . . .	21
3.2	Comparison of $\Delta p$ . . . . .	30
3.3	Comparison of foam mobility . . . . .	30
3.4	Comparison of produced fluid (brine or surfactant solution) $RF$ . . . . .	32
3.5	Comparison of $CO_2$ $RF$ . . . . .	32
3.6	$\Delta p$ for 0.1 % wt and 0.5 % wt surfactant concentrations . . . . .	35
3.7	Foam mobility for 0.1 % wt and 0.5 % wt surfactant concentrations . . . . .	35
3.8	Oil $RF$ for 0.1 % wt and 0.5 % wt surfactant concentrations . . . . .	37
3.9	$CO_2$ $RF$ for 0.1 % wt and 0.5 % wt surfactant concentrations . . . . .	37
3.10	Surfactant solution $RF$ for 0.1 % wt and 0.5 % wt surfactant concentrations . .	38
4.1	Set of relative permeability curves for 0.1% wt surfactant concentration . . . .	44
4.2	Set of relative permeability curves for 0.5% wt surfactant concentration . . . .	45
4.3	Simulation and experimental results for oil $RF$ . . . . .	51
4.4	Simulation and experimental results for $CO_2$ PV recovered . . . . .	52
4.5	Simulation and experimental results for brine/surfactant PV recovered . . . .	53
4.6	Simulation and experimental results for $\Delta p$ . . . . .	54
4.7	Property distribution in the core for 0.1% wt surfactant concentration . . . . .	57
4.8	Property distribution in the core for 0.5% wt surfactant concentration . . . . .	58
4.9	Oil $RF$ and $\Delta p$ for 0.1% wt surfactant concentration . . . . .	62
4.10	Oil $RF$ and $\Delta p$ for 0.5% wt surfactant concentration . . . . .	63
4.11	Property distribution for synthetic model R1 for 0.1% wt surfactant concentration	65
4.12	Property distribution for synthetic model R2 for 0.1% wt surfactant concentration	66
4.13	Property distribution for synthetic model R3 for 0.1% wt surfactant concentration	67
4.14	Property distribution for synthetic model R1 for 0.5% wt surfactant concentration	68
4.15	Property distribution for synthetic model R2 for 0.5% wt surfactant concentration	69
4.16	Property distribution for synthetic model R3 for 0.5% wt surfactant concentration	70



5.1	Scatter plot for measured and predicted $RF$ and $\Delta p$ for linear models . . . . .	81
5.2	Scatter plot for measured and predicted $RF$ and $\Delta p$ for quadratic models . . .	82
5.3	Scatter plot for measured and predicted $RF$ and $\Delta p$ for sample linear models .	84
5.4	Scatter plot for measured and predicted $RF$ and $\Delta p$ for sample quadratic models	85
B.1	Cumulative oil and water produced for oil flood (pre 0.1% wt) . . . . .	120
B.2	Cumulative oil and water produced for oil flood (pre 0.5% wt) . . . . .	121
B.3	Plot of raw data of $\Delta p$ . . . . .	122
B.4	Plot of raw data of foam mobility . . . . .	122

# Abstract

The efficiency of the use of CO<sub>2</sub> as a displacement fluid in oil recovery is hampered by the existence of an unfavorable mobility ratio that is caused by the large difference in viscosity between the injected fluid (CO<sub>2</sub>) and the reservoir fluids. This viscosity contrast results in early CO<sub>2</sub> breakthrough, viscous fingering, gas channeling, and consequently, the inability of CO<sub>2</sub> to effectively contact much of the reservoir and the oil it contains.

Improvement of sweep efficiency and mobility control in CO<sub>2</sub> injection require solutions to these problems. The use of surfactants and other chemical means for mobility control has been studied extensively and offer promising results, as they provide ways of increasing the viscosity of CO<sub>2</sub> and/or block high permeability zones.

One common problem that researchers encounter occurs when moving from core-scale experiments to field-scale implementation. Results obtained from laboratory experiments serve as inputs to reservoir simulators for modeling field-scale processes and estimating surfactant requirements. Generally, core-scale permeability is assumed to be homogeneous. While this assumption simplifies laboratory experiments and provides information of some flow properties, it does not present in-depth knowledge on the true heterogeneity of a reservoir system as a whole, and how the varying permeability affects recovery. Core-scale results also typically imply that chemical requirements for field-scale implementation are uneconomic. It is thereby crucial to develop a method to characterize scaling of results from the core-scale to the field-scale, especially as it pertains to the amount of chemical to use in this recovery method. This will provide an insight into the dynamics of water, oil, surfactant and CO<sub>2</sub> flow within a stratified system using results obtained from laboratory experiments.

This study focused on the development, evaluation and validation of scaling (dimensionless) groups for surfactant transport in porous media that affect sweep efficiency. The groups were obtained through dimensional and inspectional analysis and verified through practical laboratory coreflood experiments and numerical simulation. Design of experiments was used to generate an appropriate sample space for the dimensionless groups from which a model

that is capable of predicting oil recovery and pressure difference is developed. The scaling groups derived correspond to existing scaling methods for homogeneous systems. Therefore, Dykstra-Parson's coefficient,  $V_{DP}$ , was introduced so as to incorporate heterogeneity for the evaluation of surfactant requirements.

Borchardt et al. (1985), Yin et al. (2009), Bian et al. (2012) and Emadi et al. (2012) have conducted experimental studies to understand the mechanism of foam generation and propagation from CO<sub>2</sub> and surfactant solution in the presence of oil. The findings reported by these researchers were based solely on laboratory investigations as they did not utilize numerical simulation to further understand the behavior of their respective systems. One researcher, Ren (2012b), used history-matching to relate surfactant transport properties measured during core experiments to a simulator-derived Mobility Reduction Factor, *MRF*. While very good matches were obtained, Ren (2012b) reported that each of the fitted parameters that led to a good fit of pressure and saturation data may not represent actual foam physics. For the first time, a comprehensive study that interfaced laboratory experiments and numerical simulation, while maintaining realistic interactions between phases, was conducted.

This research work led to the development of a process that can be used to design a CO<sub>2</sub>-surfactant oil recovery project. This process is very flexible, and can be applied to a wide range of reservoir types as long as there is physical commonality between the laboratory and field models. The process allows for the assessment of ranges of parameters such as surfactant concentration and Dykstra-Parsons coefficients so as to aid in the selection of the optimum and economic surfactant concentration and to account for uncertainties due to heterogeneity.

# 1 Introduction

The goal of this chapter is to, first, identify the need for an improved methodology for an efficient, yet economic CO<sub>2</sub> injection operation, and second, to propose a combination of techniques to achieve this goal. This will be carried out by presenting a developmental framework that integrates the examination of previous and current research to identify well-established procedures, their advantages and limitations, which will assist in illustrating the benefits of the proposed technique that this study addresses. Furthermore, the examination of the experimental, analytical and numerical tools that will be utilized in this work will provide insight to better understand the fundamental ideas on which this research is based and also emphasize areas where improvements are required.

This chapter discusses the merits of various sweep efficiency and mobility control schemes, and through this, builds a case for CO<sub>2</sub>-foam. Discussion on the role of reservoir heterogeneity as it affects scaling from laboratory to field realization and the effect of foam is presented. The nature of foam and various methods of modeling its propagation through porous media are also examined. The theoretical foundations of the application of dimensional analysis and experimental design to oil recovery, and in particular to this study, are discussed.

## 1.1 Sweep Efficiency Improvement Techniques

The utilization of CO<sub>2</sub> as an oil recovery fluid began when Whorton et al. (1952) obtained the first patent for the injection of a gas containing CO<sub>2</sub> into an oil reservoir with the goal of increasing the recovered volume when compared to previously used methods. Since then, CO<sub>2</sub> injection has been widely used, especially in the United States (Lake and Walsh, 2008) and much research work has been carried out to understand and improve the process. The continuous injection of CO<sub>2</sub> into a reservoir is often successful at recovering oil initially, but declines dramatically as the sweep efficiency of CO<sub>2</sub> as a displacing fluid can be poor due to its unfavorable mobility ratio. Therefore, large volumes of CO<sub>2</sub> are required to sweep significant portions of the reservoir. Various techniques have been introduced to ameliorate the problem

of unfavorable sweep efficiency. These techniques include: water-alternating-gas (WAG) and chemical injection, such as surfactants and polymers.

#### **1.1.1 Water-Alternating-Gas**

In 1976, Amoco Production Company began a pilot WAG process at the previously water-flooded Slaughter Estate Unit (Rowe et al., 1981). The researchers reported excellent tertiary recovery, a reduction in CO<sub>2</sub> injectivity, and an improved areal sweep. One of the problems encountered by Rowe et al. was the rather lengthy time it took to produce tertiary oil, which they attributed to the high volume of water injected, mechanical problems, and limits on rates imposed on some of the injectors. Their evaluation suggested that alternate injection of water and CO<sub>2</sub> led to significant increases in water saturation, trapping of oil by water which prevented CO<sub>2</sub> from contacting part of the oil, and ultimately delayed oil production. Jackson et al. (1985), Huang and Holm (1988), and Nezhad et al. (2006) conducted laboratory experiments to determine the effect of WAG on wettability and they discovered that it was not an advantageous procedure in sandstones that are predominantly water-wet.

#### **1.1.2 Polymers**

In a polymer-supported waterflood, polymer is added to water to reduce its mobility by increasing its viscosity. This viscosity increase, along with a decrease in aqueous phase permeability leads to a more favorable mobility ratio, and consequently results in a larger volumetric sweep efficiency. This same principle can be applicable to CO<sub>2</sub>-polymer floods. Most of the polymer flow and displacement models available in literature focus on polymer-augmented waterfloods, with little information available for polymer-based CO<sub>2</sub> floods. Available literature examines the use of polymers for increasing the viscosity of CO<sub>2</sub>.

Initial work to study the use of thickeners for CO<sub>2</sub> was done by Heller et al. (1985). Their paper explains efforts in an experimental search for polymers that are efficiently able to dissolve in dense CO<sub>2</sub>, and hence serve as mobility control agents. They designed an apparatus to measure the solubility and viscosity of the resulting mixture, as there were no commercially available viscometers able to measure the resulting viscosity. The carbon dioxide solubility

experiments were carried out at 77°F, with density of CO<sub>2</sub> maintained between 0.82 - 0.92 g/cc. The researchers discovered that there are no water-soluble polymers that can dissolve in CO<sub>2</sub> and generally, CO<sub>2</sub>-insoluble polymers have higher molecular weights and solubility parameters than CO<sub>2</sub>-soluble polymers. Terry et al. (1987) introduced a way to increase the viscosity of CO<sub>2</sub> by insitu polymerization of monomers that are miscible with CO<sub>2</sub>. Terry and coworkers constructed an apparatus that allowed insitu generation of polymers in supercritical CO<sub>2</sub>, and allowed the measurement of the resultant viscosity for CO<sub>2</sub> and polymer mixtures. The laboratory experiment was carried out at 160°F and 1800 psi. Their methodology was based on identifying a monomer that can be polymerized, and the resulting polymer tested for solubility in CO<sub>2</sub>. If solubility was achieved, the viscosity of the CO<sub>2</sub>/polymer mixture was compared to that of pure CO<sub>2</sub>. Their goal was to increase viscosity by a factor of 20-30 so as to improve sweep efficiency. The researchers were able to develop soluble polymers, but did not observe any increase in viscosity for CO<sub>2</sub>.

Xu (2003) carried out research to design and evaluate direct CO<sub>2</sub> thickeners which will dissolve CO<sub>2</sub> without incorporating a cosolvent. None of the polymers fully met design considerations. One type of polymer, the poly vinyl acetate or PVAc, offered the most promising results. Unfortunately, PVAc required pressures higher than the CO<sub>2</sub>-oil minimum miscibility pressure in order to dissolve in CO<sub>2</sub>. Therefore, PVAc was considered not CO<sub>2</sub>-philic enough. Other types of polymers considered, such as carbonyl-rich polymers, were found to be less soluble or incompletely soluble in CO<sub>2</sub> due to their crystallinity.

Enick et al. (2001) identified four types of polymers that yielded significant increase in CO<sub>2</sub> viscosity. These polymers are fluoroacrylate-styrene copolymers (polyFAST), fluorinated telechelic ionomers, semi-fluorinated trialkyltin fluorides and small fluorinated hydrogen-bonding compounds. PolyFAST provided the best results. PolyFast increased the viscosity of CO<sub>2</sub> by a factor of 8 and 19 at concentrations of 1% wt and 1.5% wt. The major setbacks in utilizing these polymers in field cases include the high cost of production, environmental impact, and unavailability of large amounts of chemicals to manufacture the polymers. Enick

(2009) confirmed the issues associated with utilizing CO<sub>2</sub> thickeners, and further stated that new research will be directed towards developing surfactant-based solutions to CO<sub>2</sub> sweep issues.

### **1.1.3 Surfactants**

The inadequacies associated with the water-alternating-gas and polymer-CO<sub>2</sub> injection processes for improving sweep efficiency can be addressed by the application of a procedure that enables CO<sub>2</sub> to contact a significant portion of the reservoir, and can be modeled based on either a viscosity increase, a decrease in relative permeability of the displacing fluid, or a combination of these two techniques. The use of surfactant solution and CO<sub>2</sub> to generate foams provide very promising results that lead to increased oil recovery over WAG and pure CO<sub>2</sub> injection (Bernard et al., 1980; Casteel and Djabbarah, 1988; Claridge et al., 1988).

To obtain a stable foam for effective CO<sub>2</sub> mobility control, the right conditions have to be imposed on the system. Liu et al. (2005) investigated the effect of surfactant concentration, temperature and pressure on CO<sub>2</sub>-foam stability. They discovered that foam stability occurred at all tested temperatures (25°C to 75°C) at surfactant concentrations above 0.1 wt% and at all tested pressures (800 psi to 2000 psi) at concentrations above 0.025 wt%. The surfactant concentration ranged from 0.0005 wt% to 1 wt%. The impact of pressure on CO<sub>2</sub>-foam experiments at pressures below and above the minimum miscibility pressure (MMP) using visualization models was examined by Chang et al. (1994). In this study, CO<sub>2</sub> and surfactant were simultaneously injected in a glass micromodel, and foam was generated in situ. For reference and comparison to CO<sub>2</sub>-foam displacement, simultaneous injection of CO<sub>2</sub> and brine (WAG), and continuous CO<sub>2</sub> injection were carried out. The authors observed generally poor sweep efficiencies at pressures lower than the MMP for all injection schemes. In comparing the effect of pressure for the injecting schemes, Chang et al. (1994) report that pressure effects on sweep efficiency were less for the CO<sub>2</sub>-foam scheme when evaluated against WAG, and were much lower when compared to pure CO<sub>2</sub> injection. The experiments in the study by Chang et al. (1994) were conducted in the absence of oil. Yaghoobi (1994) conducted

laboratory experiments, with no oil present, to study the effect of foam mobility on flow rate, flow quality, surfactant type, surfactant concentration and rock permeability. They utilized four commercially available surfactants at 500 ppm and 2500 ppm concentrations in 2% wt brine. Some of the experimental conditions included: pressure (2100 psig), temperature (101°F), range of flow rates (0.5 cc/hr to 109.75 cc/hr), CO<sub>2</sub>/brine or surfactant solution volumetric flow ratio (4:1, with 80% CO<sub>2</sub>), core type (consolidated Berea sandstone), porosity (21%), and core permeability (140, 490 and 985 md). The researchers reported that foam mobility increased with injection flow rate for all surfactants used; foams were generated at all flow rates; surfactant concentration significantly affected foam flow performance; some of the surfactants used performed better than others; pressure drop increased while corresponding mobility curves decreased, with increasing liquid viscosity at a fixed gas rate; and foam mobility increased with increasing foam quality.

## **1.2 Impact of Reservoir Heterogeneity**

While most previous studies on foam transport focused on homogeneous systems, some researchers have investigated foam flow through heterogenous porous media with the aim of better understanding field situations. Bertin et al. (1998) conducted research to examine the formation and propagation of nitrogen-based foam in an annularly heterogenous porous media. Experiments were designed with and without crossflow between layers and the ratio of the high to low permeability values was 67 to 1. Despite this high ratio, foamed gas was diverted to the low permeability layer.

A flow model experiment scaled to North Sea conditions to study the recovery process for stratified heterogeneous reservoirs using CO<sub>2</sub>-foam was conducted by Hanssen et al. (1994). The authors compared conventional WAG to SAG (alternate injection of surfactant solution and gas). Poor performance was observed for the WAG case as mainly the high permeability layer was swept. The SAG scheme was more successful as the researchers observed diversion of gas into the low permeability layer that led to a more comprehensive reservoir sweep.



Therefore, foam, apart from being an effective gas mobility reducing material, has been known to exhibit a feature whereby the mobility reduction of CO<sub>2</sub> is more in a high permeability system than in lower permeability rocks. This characteristic is known as Selective Mobility Reduction (SMR).

Tsau and Heller (1996) present results to show the relationship between the mobility of CO<sub>2</sub>-foams and permeability. They also introduce a modeling strategy to evaluate the advantages of SMR to oil recovery. The authors report that the success of oil recovery is dependent on the extent of SMR and difference in permeability between layers.

### **1.3 Description of Surfactants**

Various studies have been carried out to better understand the generation, stability, transport, and destruction of foam generated by surfactants in porous media. Kovscek and Radke (1994) describe foam as a gas phase dispersed within a liquid phase. Surfactant absorbed at the gas/liquid interface stabilizes the gas phase. The authors identified three pore-level foam generation mechanisms: snap-off, lamella division, and leave-behind. Snap-off occurs when capillary action causes the wetting fluid to accumulate in a pore-throat that was initially occupied by a non-wetting phase (Rossen, 2000). The wetting phase fingers and stretches across the pore-throat, obstructing flow. Kovscek and Radke (1994) assert that snap-off is the dominant foam generation mechanism. Lamella division is described as the breaking or separation of foam bubbles. It can occur when a flowing bubble reaches a branched flow path, and divides into separate bubbles to flow through the divided paths. Leave-behind is considered to generate coarse and ineffective foam, and is applied only to drainage processes (Kam and Rossen, 2003).

### **1.4 Modeling Surfactant in Porous Media**

Various methods have been introduced to model foam flow and displacement in porous media. These techniques include population balance models, percolation models, modifications of gas-phase mobilities, local equilibrium models, and fractional flow theories. The population balance model provides a description of the evolution of foam texture and its resulting reduc-

tions in gas mobility during foam displacement. The model is described as mechanistic, as it explains pore-level events. In this model, a separate conservation equation is introduced to account for evolution of bubble size. The transient population balance equation on the mean bubble size provided by Kovscek et al. (1995); Kovscek and Radke (1994); Patzek (1998) is as follows:

$$\phi \frac{\partial}{\partial t} (S_g x_f n_f + \phi S_g (1 - x_f) n_t) + \nabla(u_g n_f) = \phi S_g (G_f - C_f) \quad (1.1)$$

where the subscripts  $f$  and  $t$  are flowing and trapped foam respectively,  $\phi$  is porosity,  $S_g$  is gas saturation,  $x_f$  is flowing gas fraction,  $n$  is the bubble concentration (bubbles per unit volume of gas),  $u_g$  is gas velocity,  $G_f$  is bubble generation rate, and  $C_f$  is bubble coalescence rate. The bubble generation and coalescence rates are expressed on a per volume of gas basis, and they are important terms as they control bubble texture. Generally, the population balance model assumes that there are two phases present in the medium. These are the aqueous phase (made up of water and surfactant) and the gas phase (or foam phase).

Description of the generation and displacement of foam in porous media by percolation and network models have been utilized by Chou (1990) and Rossen and Gauglitz (1990). The theory assumes that lamellae are generated by the snap-off mechanism, and also accommodates constrained pore throat and body size distribution functions that describe the complex and interconnected nature of pore geometry (Chou, 1990). The description provided by Chou (1990) is based on a statistical network model that calculates the probability of snap-off and percolating conductivity of the pore network. Rossen and Gauglitz (1990) point out that foam mobilization initializes at a minimum pressure gradient or a corresponding minimum gas velocity. In their study, percolation theory is used to estimate the pressure gradient at which lamellae are displaced from pore throats.

Application of fractional flow theory to model foam displacement was developed by Fisher et al. (1990) and developed further by Rossen and Zhou (1995). It provides a basis for describing foam flow in porous media in terms of spreading or shock waves at a fixed phase

saturation. The central idea is that if capillary pressure is below a limiting value, foam in the matrix is stabilized. Rossen and Zhou made various assumptions, and among them are:

1. One-dimensional flow with no phase change
2. Incompressible fluids and matrix
3. Dispersion and viscous fingering are ignored
4. No more than two phases are present:
  - A gas phase that contains only gas
  - An aqueous phase that contains water, or water and surfactant
5. No more than 3 components present - water, gas and surfactant
6. Foam generated only causes a reduction in the gas phase permeability and has no effect on other phase permeability

An empirical method was developed by the Computer Modelling Group for use in their commercial simulator, STARS. The method utilizes a reduction factor to adjust gas relative permeability in the presence of foam (CMG, 2009). This reduction parameter is dependent on dimensionless values obtained from fluid concentrations and saturations, capillary number, and a mobility reduction factor. This model has been successfully applied to steam floods and nitrogen injection by Coombe et al. (1997), Wassmuth et al. (2000), Vikingstad (2006) and Khan et al. (2006).

### **1.5 Dimensionless Scaling Groups**

Dimensionless scaling groups provide a method of studying similar processes on different scales. The goal is to simulate such processes in models (corefloods) that will enable proper understanding or prediction of larger scale operations (field). In moving from one scale to another, it is imperative to establish a set of relationships, known as scaling laws, which connect both systems. These scaling laws are typically represented as dimensionless numbers.

Two methods employed in obtaining dimensionless numbers are dimensional analysis (DA) (Buckingham, 1914; Bridgman, 1922; Langhaar, 1951; Focken, 1953) and inspectional analysis (IA) (Ruark, 1935; Birkhoff, 1950; Shook et al., 1992). Dimensional analysis is centered on the knowledge that equations originating from physical systems are dimensionally homogeneous (Hrenya, 2007), and does not require equations that explain the process being studied. Inspectional analysis is utilized when one has mathematical equations for the governing equations and initial and boundary conditions. In this case, dimensionless groups are obtained by normalizing all the related equations and conditions. As IA makes use of a complete set of mathematical equations, it is considered more robust than DA, as it may lead to a more advanced level of similarity (Sonin, 2001).

From the perspective of fluid flow in porous media, various researchers have applied scaling in their studies. One of the pioneer applications of developing dimensionless numbers for oil-field behavior was carried out by Leverett et al. (1942). The authors design two models to simulate an oil well and the sand in its immediate environment for a distance of 16 ft and to simulate linear flow through linear sands with the aim of studying the feasibility of various well completion techniques and factors affecting oil recovery from linear sands. Pozzi and Blackwell (1963) classify scaling criteria into 5 groups that include:

1. Geometry description
2. Relating viscous and gravitational forces (Gravity Number)
3. Boundary and initial conditions
4. Fluid properties
5. Effects of mixing or microscopic distribution.

Other groups include those that relate gravity forces to capillary forces (Bond Number), and viscous forces to capillary forces (Capillary Number).

Gharbi et al. (1998) investigated scaling miscible displacements in porous media using inspectional analysis. The groups obtained control the process of miscible displacement in a 2-dimensional, homogeneous, anisotropic vertical cross section. Nine dimensionless groups were obtained, of which one was found not to have any effect on miscible displacement performance. Islam and Farouq-Ali (1989) developed new scaling groups that deal with the flow of polymers, emulsions and foams. They emphasized the importance of mass transfer between phases, interfacial tension, fractional flow, dispersion, adsorption, entrapment and slug size. New sets of scaling criteria that provide a thorough mathematical description for cosurfactant-enhanced alkaline/polymer floods with the inclusion of interfacial tension and relative permeability models were developed by Islam and Farouq-Ali (1990). Bai et al. (2008) derived a set of scaling criteria using inspectional analysis. Their method involves gravity and capillary force, oil, water and rock compressibilities, non-Newtonian properties of polymer solution, adsorption, and dispersion. They further proposed a technique to numerically compute the dominance of the scaling groups obtained.

## **1.6 Motivation and Purpose**

Extensive work has been carried out in the areas of sweep efficiency and mobility control improvement for carbon dioxide floods. Some researchers have focused on single chemical EOR methods, while others have carried out comparative studies on different techniques. Developmental and evaluative work for dimensionless groups has also been performed for various types of chemical recovery processes. Unfortunately, there has been little or no studies carried out that fundamentally unifies the development of scaling groups for chemical EOR with a critical investigation of a realistic scale-based comparison of the quantity of injected chemicals in a core-scale laboratory experiment with the amount needed for a field-scale process. Verification of the process-driven dimensionless numbers through corefloods and numerical simulation, the application of experimental design, and how they can be used to increase sweep efficiency and improve mobility control is also lacking.

As the scale of measurement increases from lab to reservoir, surfactant volume requirements increase, perhaps astronomically, and the effects of reservoir heterogeneity is emphasized. Addressing this issue, is the main objective of this research work.

### **1.7 Strategy**

Dimensional and inspectional analysis, laboratory corefloods, design of experiments, and numerical simulation are the major tools that will be employed in this work. This study aims to investigate ways to combat the problems associated with the injection of CO<sub>2</sub> into oil reservoirs by:

- developing new and improving existing dimensionless groups for surfactant based EOR methods
- utilizing experimental design in reducing the number of scaling groups to be studied, and experiments to be performed
- performing extensive testing and validation of obtained dimensionless groups through laboratory corefloods and numerical simulation
- determine the groups that have the most significant effects (positive and negative) on pressure drop and recovery, and how they in-turn impact sweep enhancement, mobility control, and surfactant requirements.
- scaling up from lab to field scale and simulating displacement of oil by CO<sub>2</sub> with foam to identify mobility control methods and optimized surfactant volume to enhance sweep efficiency and conformance control
- predicting possible outcomes and developing an optimal operating strategy

## 2 Mathematical Model and Scaling Groups

The mathematical model used to derive the scaling groups that describe the use of surfactant as a CO<sub>2</sub> mobility reduction agent in a miscible flood in the presence of oil and water is based on partial differential equations, supporting equations, and boundary and initial conditions. This model is made up of a multicomponent multiphase displacement process that includes the oleic, aqueous, and gaseous phases. The components include CO<sub>2</sub>, oil, brine, and surfactant. The oleic phase contains oil and CO<sub>2</sub> components, the aqueous phase contains brine and surfactant components, and the gaseous phase contains only CO<sub>2</sub>. This is based on the assumption that some of the components might be unreactive in the phases in which they are found (Panday and Corapcioglu, 1989).

The interaction between phases and components for surfactant/CO<sub>2</sub> enhanced oil recovery is shown in Table 2.1.

Table 2.1: Surfactant component-phase chart

		Components			
		Water	Oil	Surfactant	CO <sub>2</sub>
Phases	Aqueous	X		X	
	Oleic		X		X
	Gaseous				X

### 2.1 General Assumptions and Simplifications

In order to reduce the complexity associated with modeling the interactions between CO<sub>2</sub>, decane, brine, surfactant, and reservoir rocks, the following assumptions are made:

1. Darcy's law is valid
2. Fickian dispersion occurs
3. Isothermal flow
4. Immobile solid phase
5. Ideal mixing

6. Porosity does not change with pressure and is constant with time
7. There is no intrinsic permeability reduction due to the generation of foam
8. Flow is two-dimensional in the x- and z-direction
9. Mass transfer between brine and oil, and surfactant and oil are negligible

## **2.2 Derivation of Dimensionless Groups**

Inspectional Analysis (IA) was carried out on the mass balance transport equations for gas, oil and water phases, along with the constitutive equations, initial and boundary conditions, and constraints.

Every variable utilized to model the system being studied is translated into a multiplicative factor that consists of two terms. The first term describes the dimensionless quantity and can be identified with the subscript 'D', and the second term represents a scaling or reference factor which can be assumed to be an arbitrary quantity with a subscript 'R'. The variables in the governing equations were expanded by substituting them with their corresponding scaling factors. The extensive derivation of the scaling groups is shown in Appendix A.

### **2.2.1 Governing Equations**

From the process of Inspectional Analysis, 45 groups were obtained. Since it was assumed that the reference variables are arbitrary, these groups can be set to 0, 1, or equal to another group. This leads to a further reduction in the number of groups. The resulting 19 dimensionless groups that remain following this process are shown in Table 2.2.

Further reduction of the number of groups can be obtained by assuming a particular component has no hydrodynamic dispersion effect within the phase in which it is found. For example, in considering the dispersion coefficients of the brine component within the aqueous phase,  $K_{Lw3}$  and  $K_{Tw3}$ , an assumption can be made that since brine is the major component in the aqueous phase, its velocity is the same as the mass weighted velocity of the aqueous phase (Panday and Corapcioglu, 1989). The same concept can be applied to the dispersion coefficients of the decane component in the oleic phase,  $K_{Lo2}$  and  $K_{To2}$ . The dispersion coefficients



Table 2.2: Dimensionless Groups from Inspectional Analysis (See Appendix A for variable definitions)

$G_1 = \frac{\phi K_{Lo1}}{Lu_T}$	$G_7 = \frac{\phi K_{Lw1}}{Lu_T}$	$G_{13} = \frac{k_z L^2}{k_x H^2}$	$G_{19} = \Delta \rho_{wo} g H \frac{k_x k_{rw}}{Lu_T \mu_w}$
$G_2 = \frac{\phi K_{To1} L}{H^2 u_T}$	$G_8 = \frac{\phi K_{Tw1} L}{H^2 u_T}$	$G_{14} = \frac{\mu_o k_{rw}}{\mu_w k_{ro}}$	
$G_3 = \frac{\phi K_{Lo2}}{Lu_T}$	$G_9 = \frac{\phi K_{Lw3}}{Lu_T}$	$G_{15} = \frac{\mu_o k_{rg}}{\mu_g k_{ro}}$	
$G_4 = \frac{\phi K_{To2} L}{H^2 u_T}$	$G_{10} = \frac{\phi K_{Tw3} L}{H^2 u_T}$	$G_{16} = \frac{\sigma_{ow} k_{rw}}{Lu_T \mu_w} \sqrt{\phi k_x}$	
$G_5 = \frac{\phi K_{Lo4}}{Lu_T}$	$G_{11} = \frac{\phi K_{Lw4}}{Lu_T}$	$G_{17} = \frac{\sigma_{go} k_{rg}}{Lu_T \mu_g} \sqrt{\phi k_x}$	
$G_6 = \frac{\phi K_{To4} L}{H^2 u_T}$	$G_{12} = \frac{\phi K_{Tw4} L}{H^2 u_T}$	$G_{18} = \Delta \rho_{og} g H \frac{k_x k_{ro}}{Lu_T \mu_o}$	

of the surfactant component in the oleic phase,  $K_{Lo4}$  and  $K_{To4}$ , can also be eliminated because surfactant is unreactive in oil. As shown in Table 2.1,  $CO_2$  is present in only the oleic and gaseous phases, therefore, it was assumed that there is no mixing of  $CO_2$  into the aqueous phase, and  $K_{Lw1}$  and  $K_{Tw1}$  were eliminated. Surfactant was pre-mixed with brine before injecting it simultaneously with  $CO_2$  into the core. Since the selected surfactant, CD-1045, is aqueous phase soluble and completely dissolves in brine and just as in the case of the brine component in the aqueous phase, the velocity of the surfactant component is the same as the mass weighted velocity of the aqueous phase. This led to the elimination of  $K_{Lw4}$  and  $K_{Tw4}$ .

The gas-oil capillary number can also be eliminated because in a miscible  $CO_2$ -decane system, the associated interfacial tension,  $\sigma_{go} = 0$  (Kulkarni, 2005). The remaining 8 groups are shown below in the traditional terminology used to describe them.

- Longitudinal Peclet Number:  $1/G_1 = N_{pe(Lo1)} = \frac{Lu_T}{\phi K_{Lo1}}$
- Transverse Peclet Number:  $1/G_2 = N_{pe(To1)} = \frac{H^2 u_T}{\phi K_{To1} L}$
- Effective Aspect Ratio:  $\sqrt{G_{13}} = R_L = \frac{L}{H} \sqrt{\frac{k_z}{k_x}}$
- Water-Oil Mobility Ratio:  $G_{14} = M_{ow} = \frac{\mu_o k_{rw}}{\mu_w k_{ro}}$
- Gas-Oil Mobility Ratio:  $G_{15} = M_{go} = \frac{\mu_o k_{rg}}{\mu_g k_{ro}}$
- Oil-Water Capillary Number:  $1/G_{16} = N_{cap(ow)} = \frac{Lu_T \mu_w}{\sigma_{ow} k_{rw}} \frac{1}{\sqrt{\phi k_x}}$

- Gas-Oil Gravity Number:  $G_{18} = N_{G(og)} = \Delta\rho_{og}gH\frac{k_xk_{ro}}{Lu_T\mu_o}$
- Water-Oil Gravity Number:  $G_{19} = N_{G(wo)} = \Delta\rho_{wo}gH\frac{k_xk_{rw}}{Lu_T\mu_w}$

### 2.3 Definition of Dimensionless Groups

The dimensionless groups that were used in this study are presented in the following sections.

#### 2.3.1 Peclet Number

The Peclet number represents the ratio of convective and diffusive transport (Bruining et al., 2012) and is used to compare mixing mechanisms at the core and field scales. The mixing of miscible fluids in a porous medium occurs through diffusion and dispersion. The random movement of molecules from a phase that contains a solvent of high concentration into a solute that contains a lower concentration of the same solvent results in diffusion. For example, pure CO<sub>2</sub> that is injected into a reservoir that originally contains an aqueous and oleic phase penetrates into the oil by molecular diffusion. Generally, diffusion coefficients depend on the composition of the mixture (Sahimi et al., 2006).

The term dispersion refers to the mixing of two fluids in a porous medium where flow velocity has a significant effect. Mixing that occurs in the direction of flow is called longitudinal dispersion,  $D_L$ , while that which occurs perpendicular to the direction of flow is known as transverse dispersion,  $D_T$ .

The terms  $K_L$  and  $K_T$  represent the longitudinal and transverse diffusion-dispersion factors respectively and are the sum of the molecular diffusion coefficient,  $D_{mol}$ , and the dispersion coefficients,  $D_L$  or  $D_T$ , corresponding to the direction of mixing.

Perkins and Johnston (1963), Grogan and Pinczewski (1987), Grogan et al. (1988) and Renner (1963) have developed models, based on laboratory experiments, that can be used to estimate diffusion and dispersion coefficients. In this work, the Perkins and Johnston (1963) method will be combined with the Renner (1963) method. Renner's correlating parameters varied over the following ranges: 0.2 to 134 cp (liquid hydrocarbon viscosity), 0.0088 to 0.019

cp (gas viscosity), 14.7 to 2560 psia (system pressure), and 32 to 140°F (temperature). These parameters fall within the range used in this work.

The Perkins and Johnston (1963) correlations can be used to determine longitudinal and transverse dispersion coefficients if the molecular diffusion is known. The correlations are:

$$\frac{K_L}{D_{mol}} = \frac{1}{F\phi} + 0.5 \frac{u\sigma d_p}{D_{mol}}, \quad \frac{u\sigma d_p}{D_{mol}} < 50 \quad (2.1)$$

$$\frac{K_T}{D_{mol}} = \frac{1}{F\phi} + 0.0157 \frac{u\sigma d_p}{D_{mol}}, \quad \frac{u\sigma d_p}{D_{mol}} < 10^{-4} \quad (2.2)$$

where,

$K_L$  : overall longitudinal dispersion coefficient

$K_T$  : overall transverse dispersion coefficient

$D_{mol}$  : Molecular diffusion coefficient

$F$  : Formation electrical resistivity factor

$d_p$  : mean particle diameter in porous media

$\sigma$  : inhomogeneity of the medium

Renner (1963) developed empirical correlations for diffusion coefficients for CO<sub>2</sub> and rich-gas solvents. The values for diffusion coefficients obtained here will be used in the Johnston and Perkins correlation. Renner's correlations are:

- diffusion of CO<sub>2</sub>, CH<sub>4</sub>, C<sub>2</sub>H<sub>6</sub> and C<sub>3</sub>H<sub>8</sub> into liquid hydrocarbon

$$D_{ij} = 10^{-9} \mu_j^{-0.4562} M_i^{-0.6898} V_i^{-1.706} p^{-1.831} T^{4.524} \quad (2.3)$$

- diffusion of CO<sub>2</sub> into water/brine

$$D_{oj} = 6.391 \times 10^3 \mu_j^{-0.1584} \mu_i^{6.911} \quad (2.4)$$

where,

$D_{ij}$  : diffusion coefficient of gas  $i$  into liquid  $j$ ,  $ft^2/sec$

$\mu_j$  : viscosity of liquid,  $cp$

$\mu_i$  : viscosity of gas,  $cp$

$T$  : temperature,  $^{\circ}K$

$p$  : pressure,  $psi$

$M_i$  : molecular weight of diffusing gas  $i$ ,  $g/g.mol$

$V_i$  : molar volume of diffusing gas  $i$ ,  $cm^3/g.mol$

In their work, Hackert et al. (1996) found that at low Peclet number,  $N_{pe} < 1$ ,  $D_L$  and  $D_T$  are approximately equal and less than the molecular diffusion coefficient,  $D_{mol}$ . For values of  $N_{pe}$  between 1 and 1000,  $D_L$  and  $D_T$  start to increase with  $D_L$  increasing at a faster rate than  $D_T$ . A linear increase in both  $D_L$  and  $D_T$  is observed when  $N_{pe} > 1000$ . In utilizing the Peclet number for scale comparisons, it must be noted that dispersion is scale-dependent. Values of dispersion measured in corefloods are less than those observed in field-scale operations (John et al. (2008), Chen (1991), and Blackwell (1959)).

### 2.3.2 Effective Aspect Ratio

The effective aspect ratio,  $R_L$ , is described as the degree of crossflow of reservoir fluids in the longitudinal direction in comparison to the transverse direction. Therefore, when  $R_L = 0$ , there is no communication between fluids in the horizontal or vertical directions. Garmeh and Johns (2010) report that a large aspect ratio leads to a faster reduction of fluid fluctuations in the vertical direction relative to the horizontal direction. A smaller aspect ratio is indicative of increased fluid communication in the horizontal direction in comparison to the vertical direction (Rai, 2008). Aspect ratio affects the dispersion, hence the Peclet Number, because the level of crossflow is a critical factor that affects the mixing of fluids in a porous medium. When  $k_x = k_z$ , then  $R_L$  reduces to the ratio of the system length ( $L$ ) to the thickness ( $H$ ).

### 2.3.3 Mobility Ratio

Mobility Ratio describes the ability of fluids to move relative to one another and is defined as the ratio of a displacing fluid's mobility to that of a displaced fluid. The mobility of a fluid is expressed as:

$$\lambda_m = \frac{k_{rm}}{\mu_m} \quad (2.5)$$

In this work, water-oil and gas-oil mobility ratios are considered. For gas-oil miscible displacements, the mobility ratio is not constant due to the change in effective viscosities of the displacing CO<sub>2</sub> and displaced oil. This change in effective viscosities arise from the process of mixing (Sahimi et al., 2006). The current viscosity of a mixture of solute and solvent can be obtained from an equation introduced by Koval (1963) which is modified for the purposes of this study as:

$$\frac{1}{\mu_{mix}^{1/4}} = \left( \frac{c_{o1}}{\mu_g^{1/4}} + \frac{1 - c_{o1}}{\mu_o^{1/4}} \right) \quad (2.6)$$

Also,  $M_{go}$  is influenced by foam behavior due to the change in the apparent viscosity of CO<sub>2</sub> in the presence of foam.

### 2.3.4 Capillary Number

Capillary number is the ratio of viscous to capillary forces. Various forms of the capillary number have been used in existing literature (Cense and Berg, 2009). The most common definition depends on the Darcy velocity of the displacing fluid,  $u$ , the viscosity,  $\mu$ , porosity,  $\phi$ , and the interfacial tension  $\sigma$ , used by Foster (1973), Salager (1977), Green and Willhite (1998), and Tiab and Donaldson (2011). This definition is:

$$N_{cap} = \frac{u\mu}{\phi\sigma} \quad (2.7)$$

Using the interstitial velocity as suggested by Sheng (2011) omits  $\phi$  and reduces the equation to:

$$N_{cap} = \frac{v\mu}{\sigma} \quad (2.8)$$

Lake (1989) includes the contact angle term,  $\theta$ , to account for contact angle. The porous medium used in this study was water-wet and the cosine term can be neglected (Shetty, 2011). The form suggested by Lake (1989) is:

$$N_{cap} = \frac{v\mu}{\sigma \cos \theta} \quad (2.9)$$

The velocity term can be expanded using Darcy's law to obtain:

$$N_{cap} = \frac{kk_r \Delta p / L}{\sigma} \quad (2.10)$$

The definition of capillary number used in this study has previously been utilized by Shook et al. (1992), Algharaib et al. (2006), Wood et al. (2008), Ghomian (2008), and Jonoud and Jackson (2008). That capillary number is:

$$N_{cap(ow)} = \frac{Lu_T \mu_w}{\sigma_{ow} k_{rw}} \frac{1}{\sqrt{\phi k_x}} \quad (2.11)$$

### 2.3.5 Gravity Number

Gravity number,  $N_G$ , is the ratio of gravity forces to viscous forces. The two forms of gravity number used in this study are the gas-oil and oil-water gravity numbers, and they respectively take the form:

$$N_{G(og)} = \Delta \rho_{og} g H \frac{k_x k_{ro}}{Lu_T \mu_o} \quad (2.12)$$

$$N_{G(wo)} = \Delta \rho_{wo} g H \frac{k_x k_{rw}}{Lu_T \mu_w} \quad (2.13)$$

A large difference in density between fluids indicate larger values of  $N_G$ . In this case, a higher degree of fluid segregation occurs in the reservoir. When using a fluid such as  $\text{CO}_2$  to displace oil, gravity segregation is more pronounced as the heavier oil moves downward in the reservoir and  $\text{CO}_2$  flows above it. and leads to smaller sweep efficiencies. Therefore, an increase in  $N_G$  results in a decrease in oil recovery. Based on the experimental conditions utilized in this study (pressure of 2400psi and temperature of approximately 70°F), the difference in the densities of  $\text{CO}_2$  and decane is not very large. Therefore, it is expected that gravity segregation will not have a profound impact on the system.

### 3 Laboratory Experiments

The goal of the laboratory experiments is to evaluate the scaling criteria obtained and identify key process variables that will ultimately assist in the derivation of a functional framework for transitioning from lab to field-scale. This is also the first stage in the field application of many EOR processes and understanding how to utilize this data is also a goal of this project.

#### 3.1 Equipment Setup

The experimental apparatus is made up of four units: the injection and fluid delivery unit, the core unit, the production unit, and the data acquisition unit. Figure 3.1 shows a schematic of the equipment setup.

##### 3.1.1 Injection and Fluid Delivery Unit

The injection unit is designed to deliver the various fluids used in the experiments into the core system. It consists of two Teledyne-ISCO syringe pumps, transfer vessels, flow tubes, valves, and joints.

The Teledyne-ISCO 260D syringe pump setup is made up of two pumps, A and B, that are connected by a continuous flow valve that meters flow of one fluid and alternate or co-injection of two different fluids. The maximum pressure rating is 7500 psi. The volume capacity of one pump is  $266\text{ cm}^3$  and the flow rate range is  $0.001 - 107\text{ cm}^3/\text{min}$ . Pump A was used for  $\text{CO}_2$  injection and pump B was used for water and surfactant solution.

Four transfer vessels that hold decane and core cleaning chemicals (methylene chloride, toluene, and methanol) are connected to pump B and their internal piston is driven with water. The working pressure and temperature rating for all accumulators are 5000 psi and 350 °F.

The flow tubes, valves, and joints are made of aluminum and can withstand pressures of up to 5000 psi. They are also resistant to the corrosive effects of  $\text{CO}_2$ .

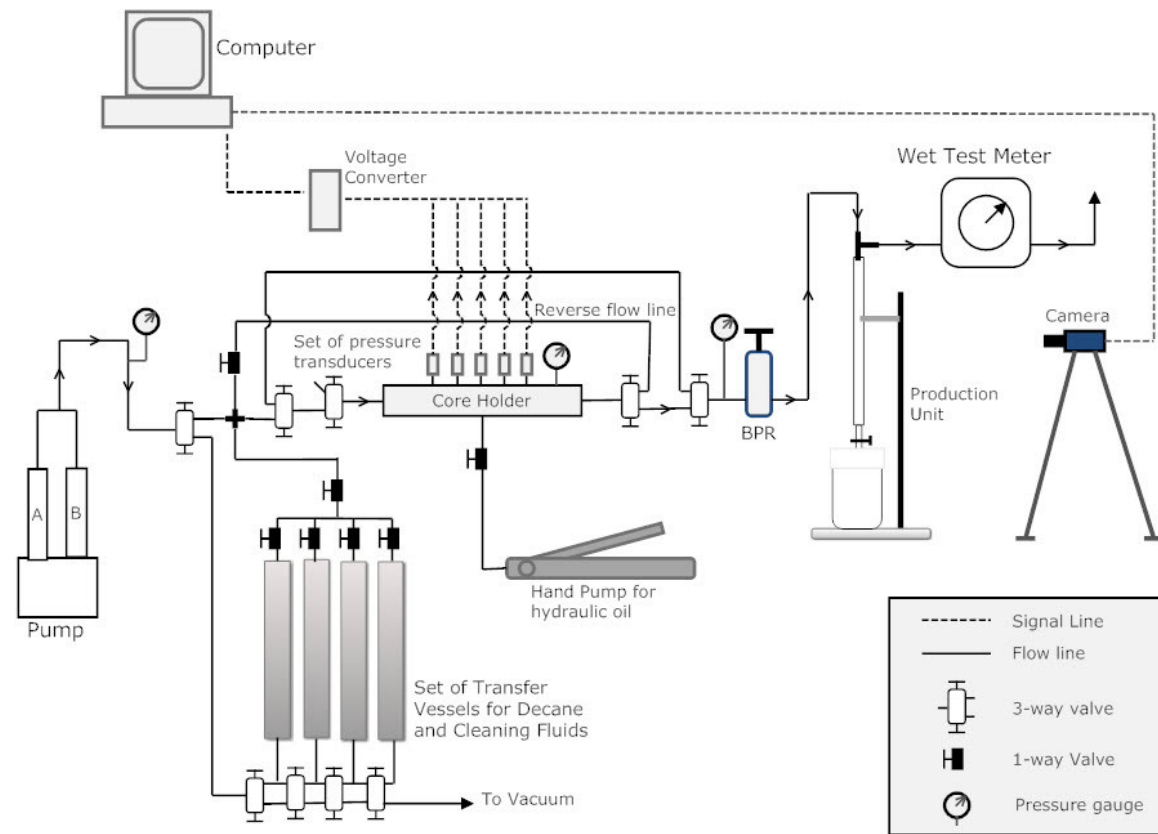


Figure 3.1: Schematic of coreflood experimental setup



### **3.1.2 The Core Unit**

The core unit is composed of a core and a core holder and arranged such that the core is contained within the core holder. Berea sandstone core is used in this study. The cores are cylindrical and measure one inch in diameter and 3 inches in length.

The core holder used in all experiments is a Hassler-type with a pressure rating of 5000 psi. The core is placed within a 1/4-inch thick Viton<sup>®</sup> sleeve, which is in turn housed within the core holder. The Viton<sup>®</sup> sleeve is compressed against the core to prevent radial flow of injected fluid around the core by pumping hydraulic fluid in the annulus between the core holder and the sleeve. Five pressure taps are placed along the top of the coreholder to measure pressure within the core and they are spaced 2-inches apart at 2-, 4-, 6-, 8- and 10-inch positions. The 3 inch core was positioned between the 5.5- and 8.5-inch points within the core holder. Hence the pressure taps at the 6- and 8-inch positions were used to monitor pressure. A sixth pressure tap is used to monitor the annulus pressure. Metal spacers fill the regions from the inlet to the core and from the core to the outlet.

### **3.1.3 The Production Unit**

A backpressure regulator (BPR) that is set to maintain an approximately constant system pressure of 2500 psi is connected to the outlet of the core holder. The BPR used in this study is manufactured by TESCO, with the ability to impose a maximum pressure of 5000 psi. It was observed that the backpressure regulator fluctuated within a span of  $\pm 9\%$ .

The outlet of the BPR is connected to a graduated burette to collect produced liquid. Produced gas flows along with the produced liquid from the BPR to the graduated burette. It then exits in the top of the burette and out to the atmosphere after flowing through a wet-test meter.

### **3.1.4 The Data Acquisition Unit**

The data acquisition unit includes a personal computer (PC), pressure transducers, signal converters, signal transmitters, various software packages, and a camera.

The pressure transducers are connected to converter modules that convert analog input signals to digital data which is then transmitted to the PC. A camera is used to monitor the volume of liquids produced by distinguishing and measuring the rise of the interface separating the fluids. The visual interpretation by the camera is transmitted to the PC and transformed into digital values by LabView<sup>®</sup> version 8.0 software.

### **3.2 Experimental Fluids**

The various fluids that were utilized in conducting the experiments for this study are outlined in the following sections.

#### **3.2.1 Oil**

Wettability effects would be studied in a typical field application and impacts the ability of the surfactant to generate foam. Because there are few studies utilizing CO<sub>2</sub>-foam with oil present, it was decided to use fluids that are neutrally wetting and effect little or no changes to the wettability state of the core. N-decane was used as the oleic phase because it does not change the wettability of the core (Kulkarni, 2003). SUDAN-4 dye was used to color the decane to distinguish the aqueous from the oleic phase.

#### **3.2.2 Brine**

The brine used was a 2 wt% calcium chloride solution that was prepared by mixing de-ionized water and CaCl<sub>2</sub> salt. It is used for saturating the core, waterflooding, and as a component in the surfactant solution. Brine was used, rather than fresh water, because it suppresses swelling of any clays present in the sandstone cores, and thus prevents drastic reductions in permeability values. It also mimics the expected field conditions.

#### **3.2.3 Cleaning Fluids**

Chemicals such as methylene chloride, methanol, and toluene were used as core cleaning fluids. Methylene Chloride acts as a buffer between the various cleaning fluids to prevent direct contact between them (Shetty, 2011) and helps to dissolve some of the oil present (Mwangi, 2010). Methanol is a dehydrating agent that helps to remove brine from the core. Shetty (2011) and Mwangi (2010) recommend the use of Methanol over other stronger

dehydrating agents like Acetone due to its incompatibility with the Viton<sup>®</sup> sleeve. Toluene is an oil solvent that is effective in removing oil (Mwangi, 2010).

#### **3.2.4 Carbon Dioxide**

CO<sub>2</sub> was used as the tertiary recovery fluid. It was contained within a cylinder and drawn from the bottom of the cylinder into pump A for injection into the system. CO<sub>2</sub>, as used in this study, exists in a dense state because pressure values are all above 1000 psi and room temperature at 24°C is less than the critical temperature of 31°C.

#### **3.2.5 Surfactant Solution**

Chevron's CD-1045 surfactant was selected for use in this study because it has been identified as one of the most effective foaming agents, based on studies carried out by Yaghoobi (1994), Heller (1994) and Moradi-Araghi et al. (1997). The surfactant was mixed with brine to formulate the surfactant solution.

### **3.3 Experimental Procedure**

The experiments were conducted under similar conditions to evaluate and compare the performance of each. As the tertiary recovery fluid was CO<sub>2</sub> and the oleic phase to be recovered was decane, the minimum miscibility pressure for the fluid combination was estimated to be 1880 psi at 160°F and about 1000 psi at 82°F (Kulkarni, 2003).

#### **3.3.1 Core Cleaning Procedure**

It is essential to thoroughly clean the core after it has been exposed to decane, brine, CO<sub>2</sub>, and surfactant. This allows the core to be returned, as close as possible, to its state prior to the introduction of fluids and thus ensure repeatability of subsequent experiments. The core was cleaned after every experiment, and the cleaning fluids were injected in the forward and backward directions. The cleaning procedure followed is a modified version of that used by Shetty (2011) and Mwangi (2010) and is listed below:

1. Back pressure was set at 2350 psi and all fluids were injected at  $3.00 \text{ cm}^3/\text{min}$

2. 6 pore volumes of brine was injected into the core to mobilize and displace CO<sub>2</sub> and surfactant
3. 3 pore volumes of Methylene Chloride was injected to act as buffer between brine and the subsequently injected Toluene
4. Toluene was injected at 3 pore volumes to dissolve decane left in the core
5. Methylene Chloride was injected at 3 pore volumes as a buffer for Toluene and Methanol
6. To remove brine, 3 pore volumes of Methanol was injected
7. 3 pore volumes of Methylene Chloride was injected
8. 6 pore volumes of brine was injected to displace any Methylene Chloride left in the core
9. Vacuum was applied to the system overnight to remove any residual air or fluids left in the core.

The sequence outlined above was repeated in the backward directed, that is, injecting through the production end and producing via the injector.

### 3.3.2 Pore Volume and Porosity Determination

The bulk volume of the core was determined by multiplying its length by the area. The core was placed in a glass chamber and air was evacuated from the system by a vacuum pump. The vacuum was applied for 6 - 8 hours to ensure a thorough extraction of air. Brine was allowed to flow into the chamber until the core was completely submerged and allowed to sit for 25 - 30 minutes. The volume of brine that was absorbed by the core, is the pore volume. The pore volume (13.07cm<sup>3</sup>) and the porosity (33.2%) were calculated respectively using:

$$\text{Pore Volume} = \frac{\text{Weight of dry core} - \text{Weight of wet core}}{\text{Density of brine}} \quad (3.1)$$

$$\phi = \frac{\text{Pore Volume}}{\text{Bulk Volume}} \quad (3.2)$$

The density of brine used to calculate the pore volume of the core was obtained from measurements carried out by Shetty (2011). Details of the pore volume and porosity calculations are presented in Appendix B.

### 3.3.3 Brine Absolute Permeability Determination

The core was placed in the core holder and brine was injected at a flow rate of  $3 \text{ cm}^3/\text{min}$  until it was completely saturated. More brine was then injected at rates of  $1.0 \text{ cm}^3/\text{min}$ ,  $1.5 \text{ cm}^3/\text{min}$ ,  $2.0 \text{ cm}^3/\text{min}$ ,  $2.5 \text{ cm}^3/\text{min}$  and  $3.0 \text{ cm}^3/\text{min}$ , for 1 pore volume each. The backpressure regulator was set at 2500 psi. Stabilized pressure drop across the core for each flow rate was averaged and used to calculate the absolute permeability using Darcy's Law (Equation 3.3). The permeability of the core was 19.96mD. Details of results obtained are shown in Appendix B.

$$k_{abs} = \frac{Q\mu L}{A\Delta P} \quad (3.3)$$

where,

$Q$  : flow rate,  $\text{cm}^3/\text{s}$

$k_{abs}$  : permeability, *Darcy*

$A$  : cross section area of core,  $\text{cm}^2$

$L$  : length of core,  $\text{cm}$

$\Delta P$  : pressure drop across core, *atm*

$\mu$  : viscosity, *cp*

### 3.3.4 Brine- and Surfactant-CO<sub>2</sub> Co-Injection in Oil-free Core

CO<sub>2</sub> and brine were simultaneously injected into the core. The core was cleaned and then foam was generated by co-injecting CO<sub>2</sub> with surfactant solution at maximum concentration (1 wt %). CO<sub>2</sub> and brine or surfactant solution were injected at rates of  $0.04 \text{ cm}^3/\text{min}$  for 2.0 PV and  $0.12 \text{ cm}^3/\text{min}$  for 6.0 PV respectively. These flowrates give a volumetric flow ratio of

1:3 and foam quality of 75 %. Backpressure was set at 2350 psi. The pressure drops obtained in both experiments were used to determine a Mobility Reduction factor (MRF) which will be defined further in this work. Results from these experiments provided the opportunity to observe the effect of foam formation on pressure difference across the core and as input in the reservoir simulator to determine gas relative permeability by history matching. The core was cleaned and vacuum was applied overnight to remove any residual fluids.

### 3.3.5 Oil Flood

Brine was injected into the core to 100% saturation. Following this, 3 pore volumes of oil were then injected at  $3 \text{ cm}^3/\text{min}$ . At this point, the water saturation in the core was reduced to connate saturation. System pressure was set at 2350 psi via the backpressure regulator. Oil was injected at different flow rates of  $2.5 \text{ cm}^3/\text{min}$ ,  $2.0 \text{ cm}^3/\text{min}$ ,  $1.5 \text{ cm}^3/\text{min}$  and  $1.0 \text{ cm}^3/\text{min}$ , for 1 pore volume each to obtain a stabilized pressure drop for each rate. Oil and brine recovery were also monitored. The effective permeability ( $k_{eff}$ ) was determined from Darcy's equation. The endpoint relative permeability to oil was calculated from:

$$k_{ro}^* = \frac{k_{eff}}{k_{abs}} \quad (3.4)$$

where,

$k_{ro}^*$  : endpoint relative permeability to oil

$k_{eff}$  : effective permeability

The results are presented in Appendix B.

### 3.3.6 Waterflood

Brine was injected at  $3.0 \text{ cm}^3/\text{min}$  for 2 pore volumes, with the backpressure set at 2350 psi. After waterflooding, material balance was used to determine the residual oil saturation. Flow rate was changed to  $2.5 \text{ cm}^3/\text{min}$ ,  $2.0 \text{ cm}^3/\text{min}$ ,  $1.5 \text{ cm}^3/\text{min}$  and  $1.0 \text{ cm}^3/\text{min}$ , and the corresponding stabilized pressure drop was obtained and averaged for each rate and used

with Darcy's equation calculate effective permeability of water in the presence of residual oil. The endpoint relative permeability to water was also calculated. Oil and brine recovery were also monitored and recorded.

### **3.3.7 Co-Injection of Surfactant Solution and CO<sub>2</sub>**

Surfactant solution at 0.1 % wt concentration and CO<sub>2</sub> were simultaneously injected into the core which was fully saturated with brine and oil. The core was thoroughly cleaned and vacuumed overnight to remove any traces of CO<sub>2</sub>, decane, brine, surfactant, or cleaning fluids. After cleaning, the core was filled with brine, and another sequence of oilflood and waterflood was carried out. A 0.5 % wt surfactant concentration was injected along with CO<sub>2</sub>. Surfactant solution at both concentrations were injected at 0.04 cm<sup>3</sup>/min for 2 pore volumes and 6.0 PV of CO<sub>2</sub> at 0.12 cm<sup>3</sup>/min.

In order to carry out optimal analysis of results obtained from this work, the use of stable foam was required. In their work, Liu et al. (2005) reported that at all tested temperatures, foam began to be stable at surfactant concentrations of 0.1% wt and above. Hence concentrations of 0.1% wt and 0.5% wt were selected to correspond to concentrations at or above the minimum value for the generation of stable foam to occur.

## **3.4 Experimental Results**

The various experiments carried out in this study can be grouped under two categories, auxiliary and primary experiments. The auxiliary experiments include porosity and permeability measurements and determination of connate water and residual oil saturation from oilflood and waterflood procedures respectively. Detailed results obtained are shown in Appendix B.

The primary experiments, which include the co-injection of brine or surfactant solution with CO<sub>2</sub> in the presence or absence of oil, provide information on about the parameters that impact the implementation of a laboratory to field scale-up procedure. From these experiments, the following can be determined:

- an appropriate value for the Mobility Reduction Factor, *MRF*

- the effect of surfactant concentration on pressure drop,  $\Delta p$ ; capillary number; residual oil saturation; and CO<sub>2</sub> trapping
- the impact of core length on scale dependent dispersion
- the parameters that will be used as inputs in a reservoir simulator and in an Experimental Design (ED) process.

#### 3.4.1 Determination of Mobility Reduction Factor (MRF)

MRF is defined as the ratio of the pressure difference across the core during the simultaneous injection of CO<sub>2</sub> and surfactant solution at the maximum concentration utilized (1.0% wt in this case) to the pressure difference obtained during the co-injection of CO<sub>2</sub> and brine, with no oil present in both cases. Both injection schemes were carried out at the same flow rates. The pressure drops used in the calculation of MRF are average values of all measured pressure points obtained during the flow process. MRF is defined as:

$$MRF = \frac{\Delta p_{foam}}{\Delta p_{brine}} \quad (3.5)$$

where,

$\Delta p_{foam}$  : Average pressure difference during CO<sub>2</sub> and surfactant solution co-injection

$\Delta p_{brine}$  : Average pressure difference during CO<sub>2</sub> and brine co-injection

Table 3.1 is a summary of results obtained from experiments conducted to measure MRF. The Mobility Reduction Factor was 45.37 for the 1% wt surfactant solution.

Figures 3.2 and 3.3 show the graphs comparing the pressure difference and foam mobility respectively measured during the coinjection sequence in the absence of oil.

In both graphs, a moving average over 3 periods was applied to the raw data for pressure difference and foam mobility to reduce the noise that was caused by backpressure fluctuations.



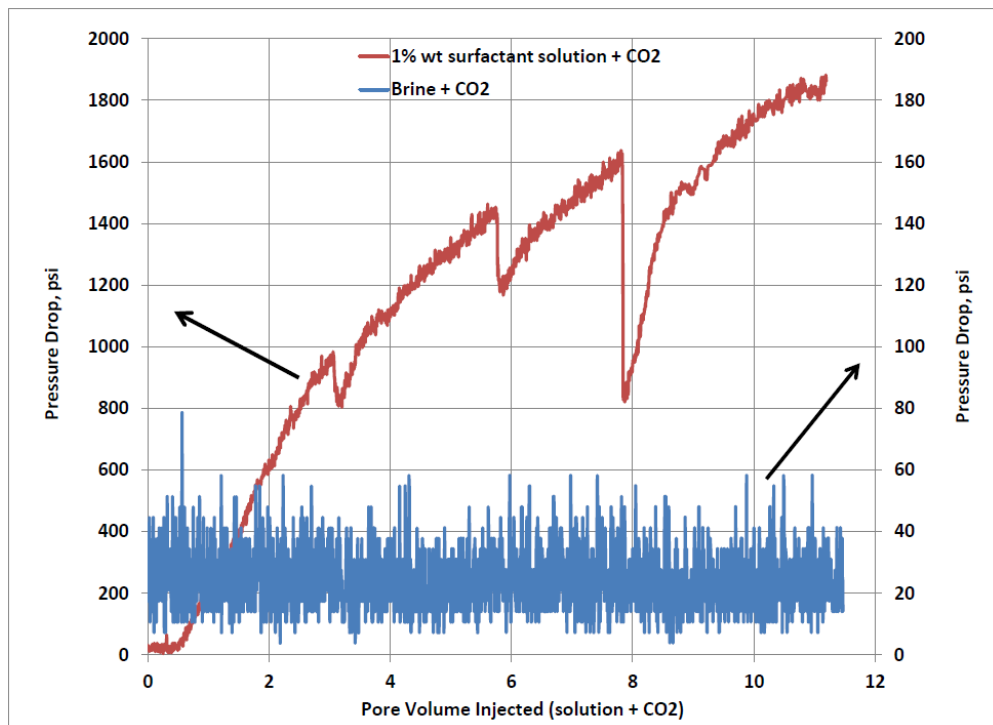


Figure 3.2: Comparison of pressure difference between coinjection of CO<sub>2</sub> with brine (no surfactant) and coinjection of CO<sub>2</sub> with a solution of brine and 1.0% wt surfactant in a 1" (dia.) × 3" (long) Berea core

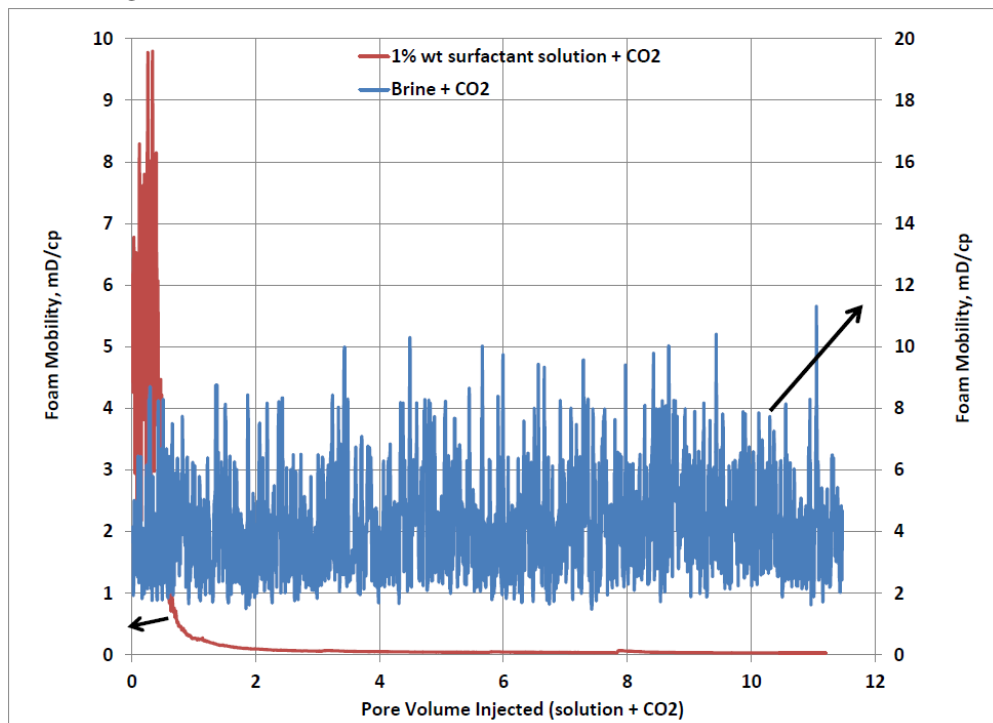


Figure 3.3: Comparison of foam mobility between coinjection of CO<sub>2</sub> with brine (no surfactant) and maximum surfactant concentration (1.0% wt) in a 1" (dia.) × 3" (long) Berea core

Table 3.1: Summary of results from MRF experiments

	Brine	1.0% wt surfactant
PVI (CO <sub>2</sub> + Solution)	11.47	11.20
Maximum $\Delta P$ , psi	136.40	1923.26
Average $\Delta P$ , psi	24.31	1103.01
CO <sub>2</sub> breakthrough PVI	0.37	1.35

Plots of the raw data are shown in Appendix B. During the co-injection of CO<sub>2</sub> and 1.0% wt surfactant solution, pressure at the inlet of the core rose steadily through the course of the experiment. The increase in injection pressure and the escape of some amount of CO<sub>2</sub> into the annulus exerted pressure on the overburden. At approximately 3.0, 5.8, and 7.9 pore volumes of injected CO<sub>2</sub> and solution, pressure was released from the annulus because the overburden pressure was approaching the maximum working value for the apparatus. The increase in annulus pressure led to a corresponding increase in pressure difference across the core.

At a higher surfactant concentration, a continuously increasing pressure drop along the core was observed when compared to the case with no surfactant present, which appeared to be relatively flat. The increase in pressure observed during the injection of CO<sub>2</sub> and 1.0 wt % surfactant solution leads to a corresponding increase in foam apparent viscosity. This effect of pressure increase was also observed by Li et al. (2010). Reduction in foam mobility with an increase in the surfactant concentration is evidence of the increase in foam apparent viscosity. As noted above, the annular pressure (and hence inlet pressure) needed to be reduced during certain stages of the experiment. Thus the apparent viscosity shown is actually smaller than what would have been measured had the apparatus had a higher working pressure. The reduction of the annular pressure also led to the measurement of a lower *MRF* value than would have been obtained.

The graphs in Figures 3.4 and 3.5 show the effect of surfactant concentration on brine or surfactant solution and CO<sub>2</sub> production respectively. A lower recovery factor for brine was measured for the coinjection of CO<sub>2</sub> and brine when compared to that obtained for CO<sub>2</sub>

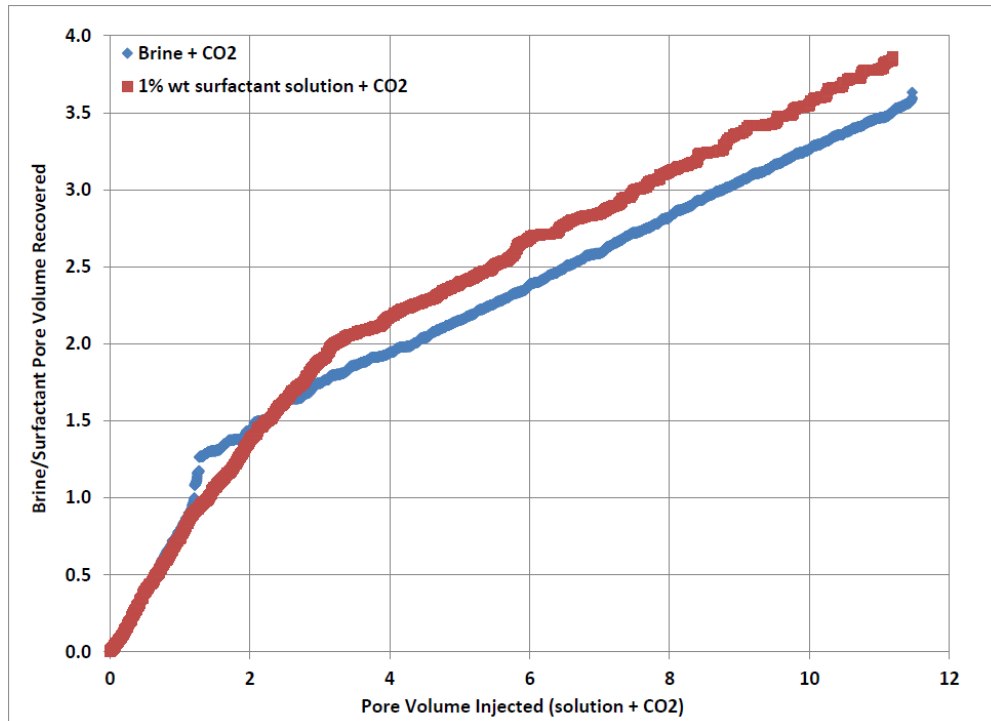


Figure 3.4: Comparison of volume of produced fluid (brine or surfactant solution) between coinjection of CO<sub>2</sub> with brine (no surfactant) and maximum surfactant concentration (1.0% wt) in a 1" (dia.) × 3" (long) Berea core

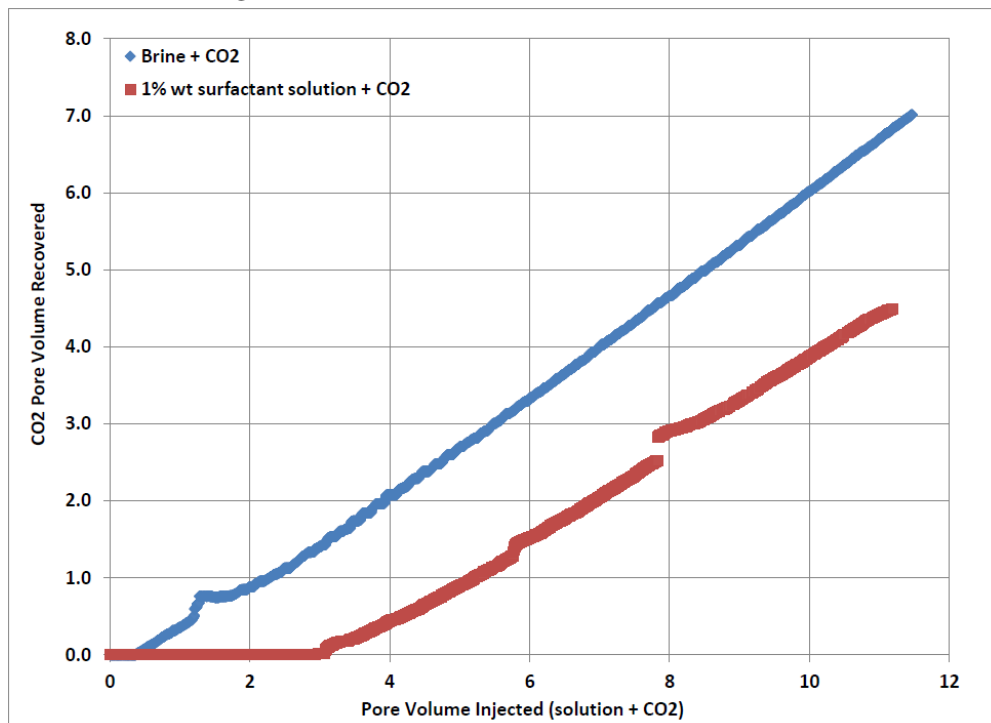


Figure 3.5: Comparison of CO<sub>2</sub> produced between coinjection of CO<sub>2</sub> with brine (no surfactant) and maximum surfactant concentration (1.0% wt) in a 1" (dia.) × 3" (long) Berea core

and 1.0 wt % surfactant solution. This is because  $\text{CO}_2$  mobility is higher when it displaces and flows along a less viscous fluid such as brine, as opposed to a more viscous fluid like surfactant solution. When  $\text{CO}_2$  was injected with surfactant solution to generate foam, the more viscous surfactant solution aided in displacing more of the resident brine contained in the core, thus allowing more  $\text{CO}_2$  into the core. During the experiment, there was an increase in pressure at the inlet while the outlet pressure remained relatively stable. The observed increase in pressure difference indicated that foam might have been generated close to the inlet and retarded the flow of  $\text{CO}_2$  through the core. Hence, less  $\text{CO}_2$  was produced during the simultaneous injection of  $\text{CO}_2$  and 1.0 wt % surfactant solution. The degree of  $\text{CO}_2$  blockage during brine and  $\text{CO}_2$  coinjection was much less because there was no observed formation of foam to significantly hinder its flow and cause a steady increase to the inlet pressure.

### 3.4.2 Oil Recovery Experiments

$\text{CO}_2$  and surfactant solution were simultaneously injected into a core that contained brine and decane at residual oil saturation. Two surfactant concentrations, 0.1 % wt and 0.5 % wt, were utilized so as to observe the effect of surfactant concentration on oil recovery and pressure difference. Prior to coinjecting  $\text{CO}_2$  and surfactant solution, the core was subjected to initial water injection, oil injection (3 PV) to connate water saturation,  $S_{wc}$ , and water injection (2 PV) to residual oil saturation,  $S_{or}$ . Table 3.2 shows results obtained from these experiments. The low values of  $S_{wc}$  in both cases indicate an oil-wet behavior for the core used in this work.

Table 3.2: Summary of results from auxiliary experiments preceding the coinjection of  $\text{CO}_2$  and surfactant solution in the presence of oil

	0.1 % wt	0.5 % wt
$k$ , mD	19.96	19.88
$S_{wc}$ , fraction	0.12	0.10
$S_{or}$ , fraction	0.48	0.49

Figures 3.6 and Figures 3.7 respectively illustrate the effect of surfactant concentration on pressure drop and foam mobility. A moving average over 3 periods was also applied to the raw data for pressure difference and foam mobility. The same trend observed during the

*MRF* determination experiments whereby an increase in surfactant concentration led to a corresponding increase in pressure difference and a decrease in foam mobility also occurred in the oil recovery experiments. For the 0.5% wt surfactant solution, steady state conditions were not reached even after the injection of over 10 pore volumes of CO<sub>2</sub> and surfactant solution. Note that the  $\Delta p$  values for both experiments were well below those obtained in the *MRF* test (100psi and 50psi at 2 PV vs. 600psi and 60psi for the *MRF* test).

The recovery factors for oil, CO<sub>2</sub>, and brine or surfactant are shown in Figures 3.8, 3.9, and 3.10. More oil is recovered during the injection of CO<sub>2</sub> and 0.5% wt surfactant solution. Also, oil recovery started faster in comparison to that observed during the injection of CO<sub>2</sub> and 0.1% wt surfactant solution. The larger oil recovery factor obtained in the case of the 0.5 % wt surfactant solution in comparison to the 0.1% wt solution can be attributed to an increased capillary number. This increase in capillary number can be attributed to the following:

- the higher viscosity of the 0.5% wt surfactant solution which resulted in a higher apparent viscosity for CO<sub>2</sub> when compared to that obtained for the 0.1% wt surfactant solution
- surfactants are known to help in reducing interfacial tension between the oleic and aqueous phases (Behzadi and Towler, 2009), hence it is expected that a solution that contains a higher surfactant concentration will lead to a larger decrease in IFT
- Tsau and Heller (1992), Liu et al. (2005) and Grigg et al. (2007) estimated the Critical Micelle Concentration, *CMC*, of the surfactant used as 0.06% wt. The 0.1% wt concentration is only slightly above the *CMC*, while the 0.5% wt concentration is significantly above the *CMC*.

As in the case of the *MRF* determination experiments, the generation of a more dense foam at the outlet of the core during the coinjection of CO<sub>2</sub> and a higher surfactant concentration led to CO<sub>2</sub> trapping within the core. On inspection of Figure 3.10, it can be seen that more brine and surfactant solution was recovered during the simultaneous injection of CO<sub>2</sub> and 0.1 % wt surfactant solution than was produced in the case of the injection of the 0.5 %

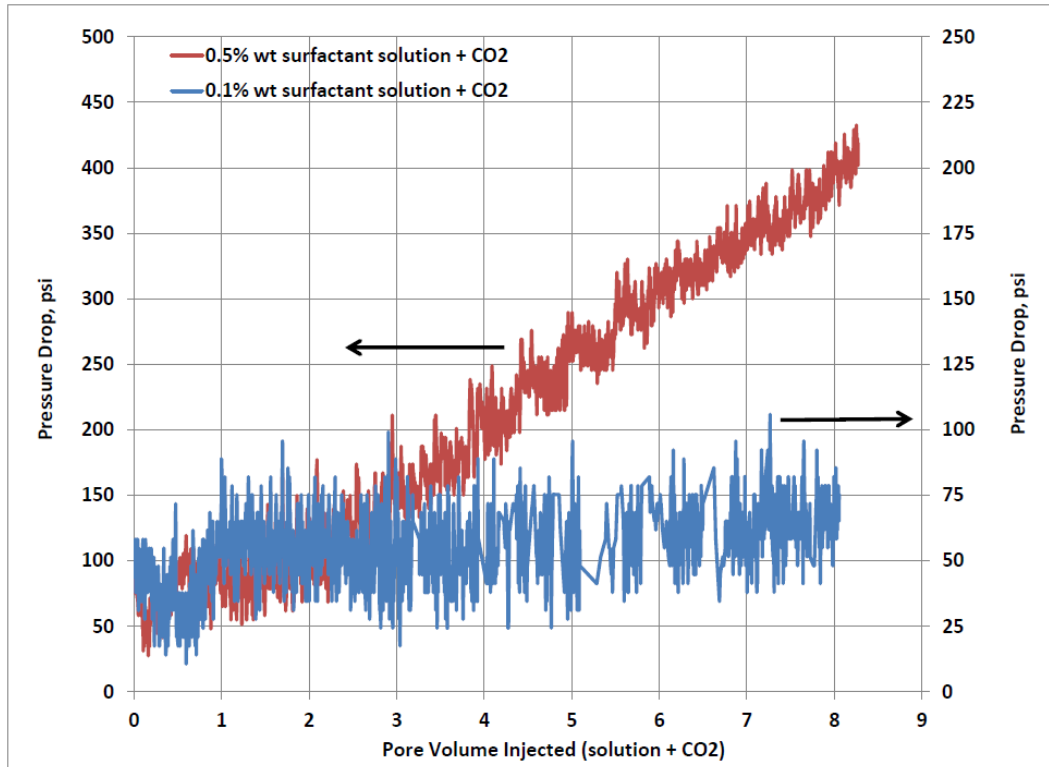


Figure 3.6: Comparison of pressure difference between coinjection of CO<sub>2</sub> with 0.1 % wt and 0.5 % wt surfactant concentration during oil recovery experiments

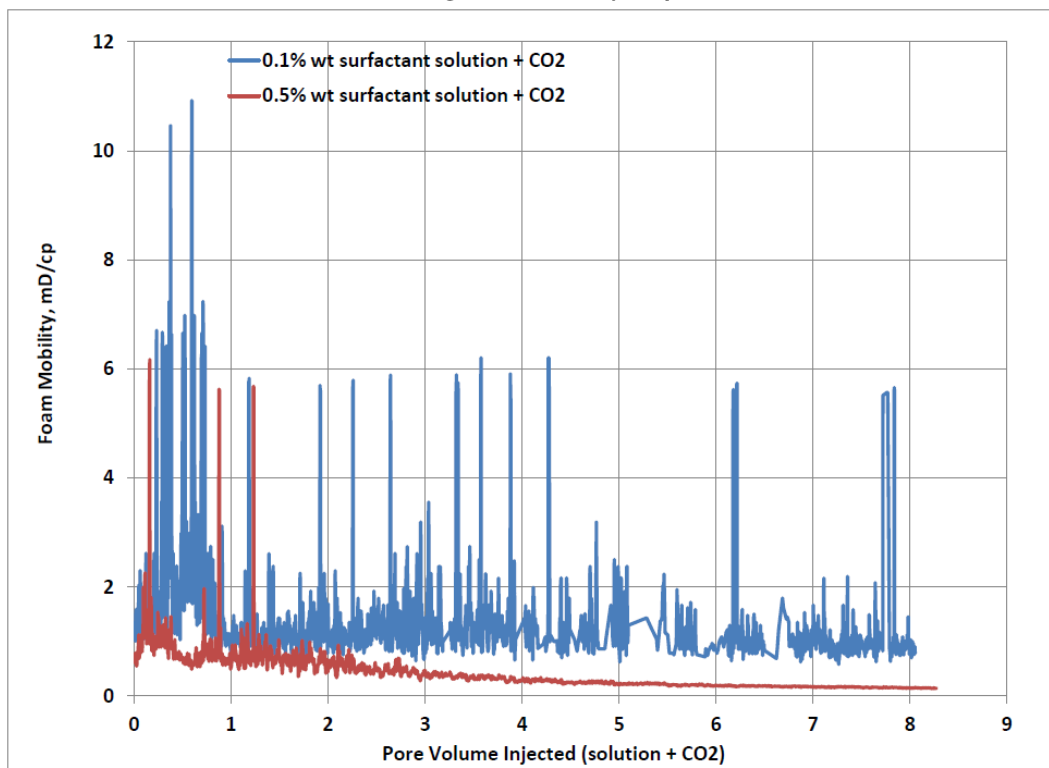


Figure 3.7: Comparison of foam mobility between coinjection of CO<sub>2</sub> with 0.1 % wt and 0.5 % wt surfactant concentration during oil recovery experiments

wt solution. This observation appears to contradict the effect of surfactant concentration on  $RF$  for brine and surfactant measured during the  $MRF$  experiments. In that case, the  $RF$  for brine and surfactant was higher during the coinjection of  $CO_2$  and the higher concentration surfactant solution. It should be recalled that the core was initially saturated with 100% brine during the  $MRF$  experiments, and initially saturated with brine and oil during the oil recovery experiments. Therefore, the more viscous surfactant solution displaced the less viscous oil and brine in the core.

There is a slight rise in oil recovery after 3.5 PVI for the 0.1% wt case and after 6.0 PVI for the 0.5% wt case. This can be attributed to the mobilization and eventual formation of an oil bank by the remaining oil in the core due to the propagation of a very stable foam. At this point, oil saturation is greatly reduced and the environment is conducive for the generation of a more stable foam as seen from the increasing  $\Delta p$  behavior especially as seen in Figure 3.6.

### **3.5 Summary**

Coreflood experiments were successfully carried out and the results obtained served as a baseline through which further analysis using numerical simulation and design of experiments were carried out. Utilizing a higher surfactant concentration led to more reduction in the residual saturation of oil after waterflood. This can be ascribed to the observed increase in pressure difference between the injector and producer in comparison to that seen in the lower surfactant concentration case. Surfactants help to reduce the interfacial tension between the oleic and aqueous phases, and the combined effect of increasing the pressure difference and reducing interfacial tension led to an increase in capillary number.

#### **3.5.1 Field Implementation**

When conducting a study to implement surfactant- $CO_2$  injection in an actual reservoir, it is advisable to execute the laboratory experiments under similar conditions that exist in the field. Factors that should be considered to ensure environment-based similarity between the core and field include oil type, surfactant type, rock type, rock wettability, reservoir pressure, oil saturation and distribution, and temperature.

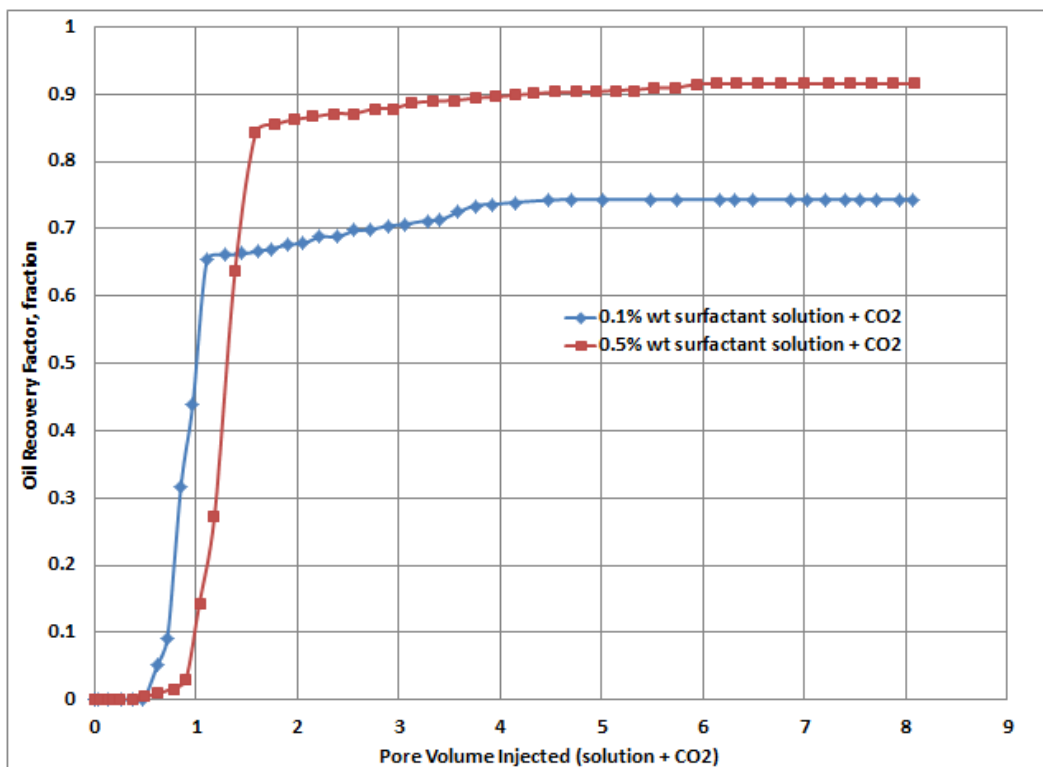


Figure 3.8: Comparison of oil recovery factor during the coinjection of CO<sub>2</sub> with 0.1 % wt and 0.5 % wt surfactant concentration during oil recovery experiments.

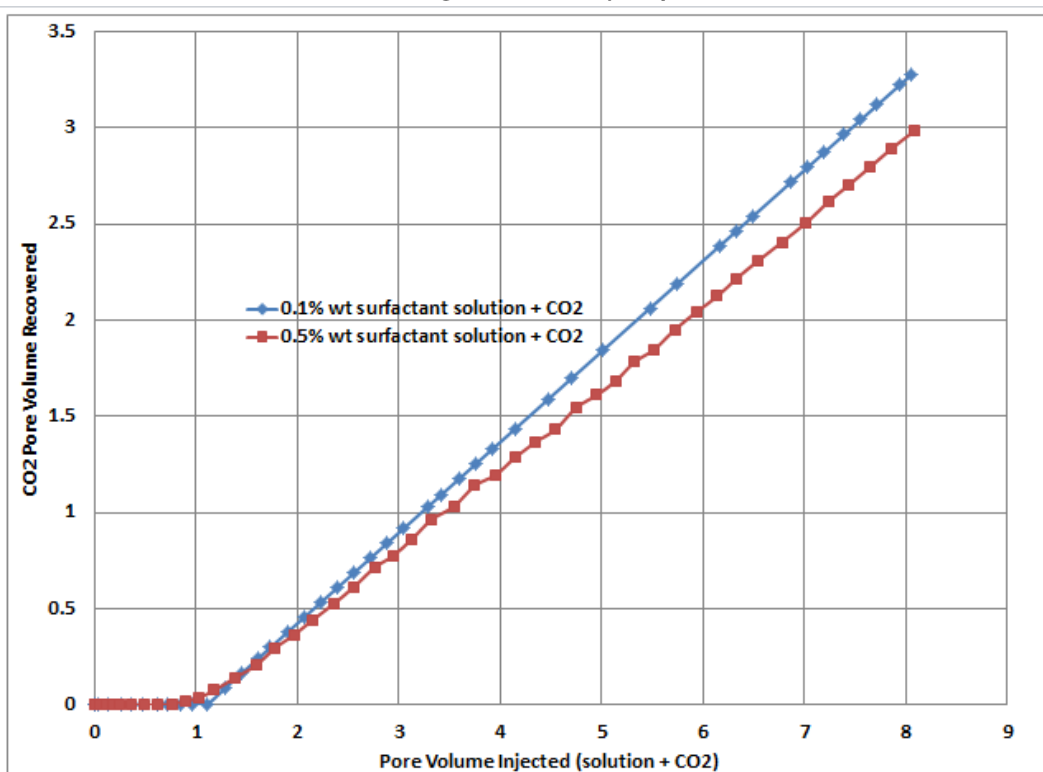


Figure 3.9: Comparison of CO<sub>2</sub> recovery factor during the coinjection of CO<sub>2</sub> with 0.1 % wt and 0.5 % wt surfactant concentration during oil recovery experiments



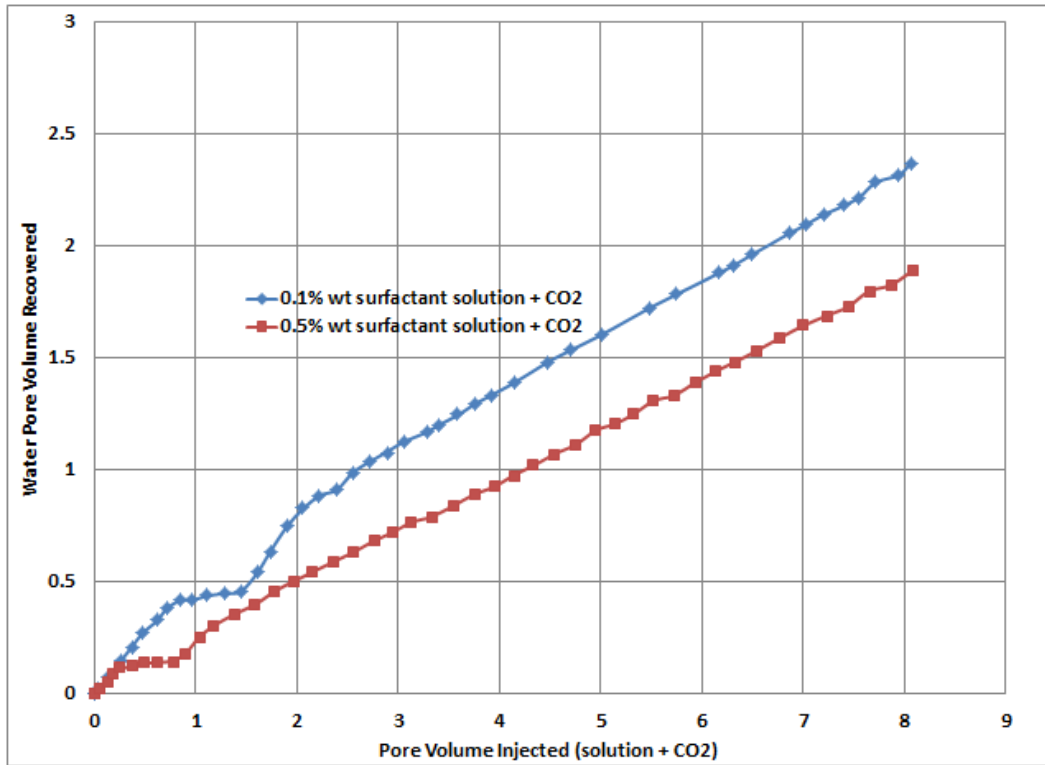


Figure 3.10: Comparison of brine and surfactant solution recovery factor during the coinjection of CO<sub>2</sub> with 0.1 % wt and 0.5 % wt surfactant concentration during oil recovery experiments

Crude oil is known to have an adverse effect on foam. In their work, Novosad et al. (1989) found that the sensitivity of foam to oil is strongly dependent on surfactant type, and even more sensitive to the type of oil. Jensen and Friedmann (1987) specified two types of foams; "oil-sensitive foams" and "oil-insensitive foams". The researchers concluded that oil-insensitive foams propagated faster than oil-sensitive foams in the presence of oil, and that oil saturation must be lowered to 0.15 for foam generation to begin when injecting an oil-sensitive foam. The physical state of CO<sub>2</sub> is dependent on the temperature and pressure of its environment. These important factors determine the degree of miscibility between CO<sub>2</sub> and oil, and the type of foam that it generated when surfactant is introduced.

## 4 Reservoir Simulation

CMG's commercial simulator, STARS, was used to model the displacement of oil using, first, water and secondly, foam generated by the simultaneous injection of supercritical CO<sub>2</sub> and surfactant solution for laboratory experiments and field scenarios. Numerical simulation helped to analyze and establish important parameters that are critical to developing a method to predict field scale performance of a CO<sub>2</sub>-foam implementation from laboratory experiments. The results obtained from laboratory experiments were history-matched with the simulator. Also, procedures that prove challenging to execute in the laboratory were modeled with STARS. One such challenge arises from the difference in time and length scales between laboratory experiments and field processes. This difference sometimes leads to a situation whereby some phenomena might be significant in the laboratory and insignificant in the field, or vice-versa (Hirasaki, 1980). When an appropriate lab model was attained with the simulator, it was scaled up to reservoir dimensions while keeping the dimensionless groups constant, and where necessary, modifications were applied to assist in appropriately translating laboratory observations to field descriptions.

### 4.1 Foam Model

The STARS foam model utilizes a modification to gas relative permeability to model the effect of foam on gas mobility (Shen, 2006). The model uses a gas relative permeability modification parameter,  $FM$ , that is dependent on the Mobility Reduction Factor,  $MRF$ , and dimensionless factors that describe the impact of surfactant concentration, oil saturation, and capillary number on recovery parameters (Afonja et al., 2012). The relationship between gas relative permeability in the absence of foam,  $k_{rg}$ , the modified gas relative permeability with foam present,  $k_{rg}^f$ ,  $MRF$ , and  $FM$  are as follows:

$$k_{rg}^f = k_{rg} FM \quad (4.1)$$

$$FM = \frac{1}{1 + MRF \left( \frac{w_s}{w_s^{max}} \right)^{es} \left( \frac{S_o^{max} - S_o}{S_o^{max}} \right)^{eo} \left( \frac{N_c^{ref}}{N_c} \right)^{ev}} \quad (4.2)$$

where,

$w_s$  : local surfactant concentration calculated by the simulator

$w_s^{max}$  : maximum surfactant concentration used in *MRF* determination experiments

$S_o$  : local oil saturation calculated by the simulator

$S_o^{max}$  : maximum oil saturation at which foam will be destroyed

$N_c$  : local capillary number calculated by the simulator

$N_c^{ref}$  : reference capillary number obtained at  $w_s^{max}$  and determined via history-match

$es, eo$  and  $ev$  : modifiable exponents used to interpolate between  $FM = 0$  and  $FM = 1$   
and determined via history-match

The maximum oil saturation at which foam will be destroyed,  $S_o^{max}$ , was determined in the laboratory by mixing surfactant solution and oil at different saturation combinations. The mixture was shaken, and visually inspected to determine the presence or absence of foam, and material balance was used to measure an approximate oil saturation value. This value was 0.8 for the 0.1% wt surfactant solution and 0.88 for the 0.5% wt solution.

#### **4.2 Foam Generation and Sustenance Modeling**

CMG's STARS simulator provides the option of incorporating a new component (foam) that is generated by the combination of existing components (brine, surfactant, and  $CO_2$ ). This feature helps to describe the formation, maintenance, and breakdown of foam in the reservoir. In this study, it is assumed that foam is formed immediately when surfactant solution contacts  $CO_2$  with the appropriate stoichiometry. CMG (2009) describes the generation and sustenance of foam as a "chemical reaction" that uses stoichiometric coefficients of "reacting" components to yield produced components. While foam generation is not a chemical process, this modeling tool does describe the physical process of foam generation and sustenance. Two stoichiometric models were utilized in modeling foam behavior. The first model describes the formation of foam such that appropriate stoichiometric coefficients of water, surfactant, and  $CO_2$  lead to

foam generation. The second model defines both the steady-state maintenance of foam as more surfactant solution and CO<sub>2</sub> are injected and the separation of components that may occur near the producer. The Reaction Frequency Factor,  $r_{rate}$ , is an important variable that is used in the foam generation and sustenance modeling to indicate reaction kinetics (rate). The unit of  $r_{rate}$  is (moles of surfactant)<sup>-1</sup>(time)<sup>-1</sup>. A history-match process is required to obtain appropriate values for  $r_{rate}$  and the stoichiometric coefficients of brine, CO<sub>2</sub>, and decane. The stoichiometric coefficients for surfactant was based on its critical micelle concentration, CMC (0.06% wt or  $3.61 \times 10^{-5}$  in mole fraction).

The stoichiometric coefficients of the components are a mass-conserving set (CMG, 2009) and must satisfy the following equation:

$$\sum M_{wi} \times \Gamma_{ri} = \sum M_{wi} \times \Gamma_{pi} \quad (4.3)$$

with  $i = 1$  to number of components

where,

$M_{wi}$  : component molecular weight

$\Gamma_{ri}$  : reacting component stoichiometric coefficient

$\Gamma_{pi}$  : produced component stoichiometric coefficient

The generation and sustenance of foam in the simulator is very sensitive to these stoichiometric coefficients. The STARS<sup>®</sup> manual states that determining these coefficients is a "non-trivial" task. The work done on this task for this dissertation was extensive and to label this as simply "non-trivial" would be a tremendous understatement.

### 4.3 Simulation of Laboratory Floods

The laboratory experiments modeled using CMG STARS include: the injection of brine into a core that was filled with oil at initial oil saturation,  $S_{oi}$ , and brine at connate water saturation,  $S_{wc}$ ; coinjection of CO<sub>2</sub> and surfactant solution at 0.1 % wt surfactant concentration; and, coinjection of CO<sub>2</sub> and 0.5 % wt surfactant concentration.

A one-dimensional model of the core with 50 gridblocks was used. The reservoir and fluid properties used to model fluid displacement in the core are presented in Table 4.2. As outlined by Afonja et al. (2012), the simulator assisted in the estimation of:

- relative permeabilities for gas, water, and oil, and the accompanying fluid saturations that are associated with the different displacement processes
- values for  $es$ ,  $eo$ , and  $ev$ , which are the respective exponents for the surfactant, oil saturation, and capillary number terms in the gas phase relative permeability modification parameter
- an appropriate history match through which values for the variables in the foam model and foam generation and sustenance modeling were obtained.

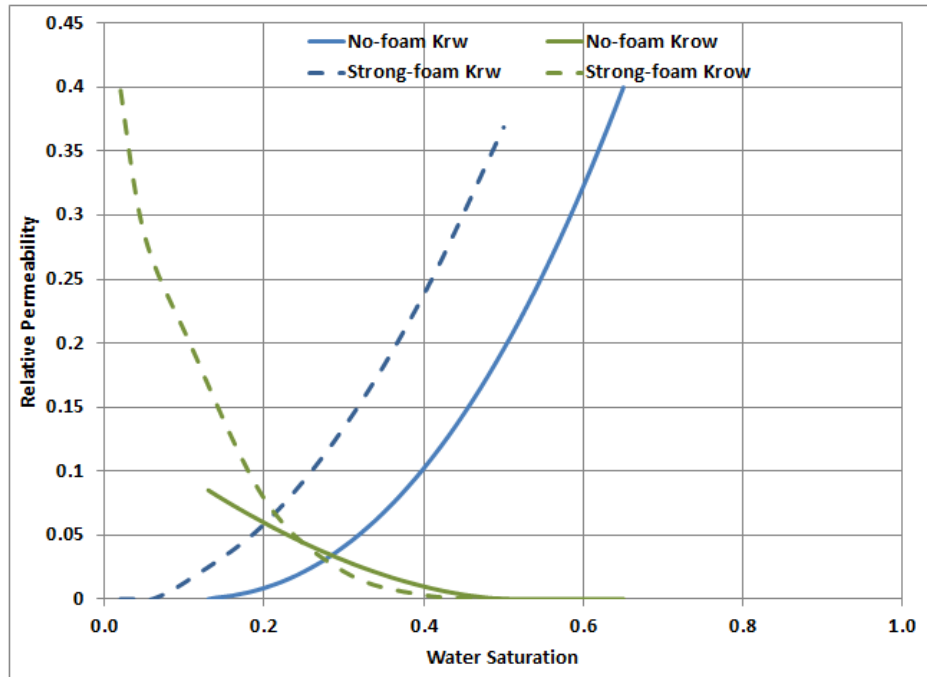
A series of gas relative permeability curves are required in order to employ CMG's empirical foam option. The first relative permeability table is for a case whereby foam is absent. Subsequent gas relative permeability curves denote the presence of foam, graded from the weakest to the strongest foam. In this study, two gas relative permeability sets are used. Figures 4.1 and 4.2 show the relative permeability curves for the no-foam case (solid lines) and strongest-foam case (dashed lines) for the 0.1% wt and 0.5% wt surfactant concentrations. The most dependable gas relative permeability curve that provided good results for a particular surfactant concentration was derived from interpolating between the sets of curves. The second set of gas relative permeability for the 0.5% wt surfactant concentration had a very low endpoint value (0.0025) denoting an almost complete blockage of the flow path due to the presence of foam. Using the measured gas relative permeability data as a baseline, history-matching was carried out to determine the parameters in Equations 4.1 and 4.2. Consistent with the results of the auxiliary experiments, the relative permeability results from the history-match would indicate oil-wet behavior. While the study of wettability effects was not a direct priority of this work, the fact that the experiments were run in what appears to be an oil-wet system is a

benefit in that oil-wet systems, especially for carbonates is suggested to be the most common wettability state in natural systems (Cosentino, 2001).

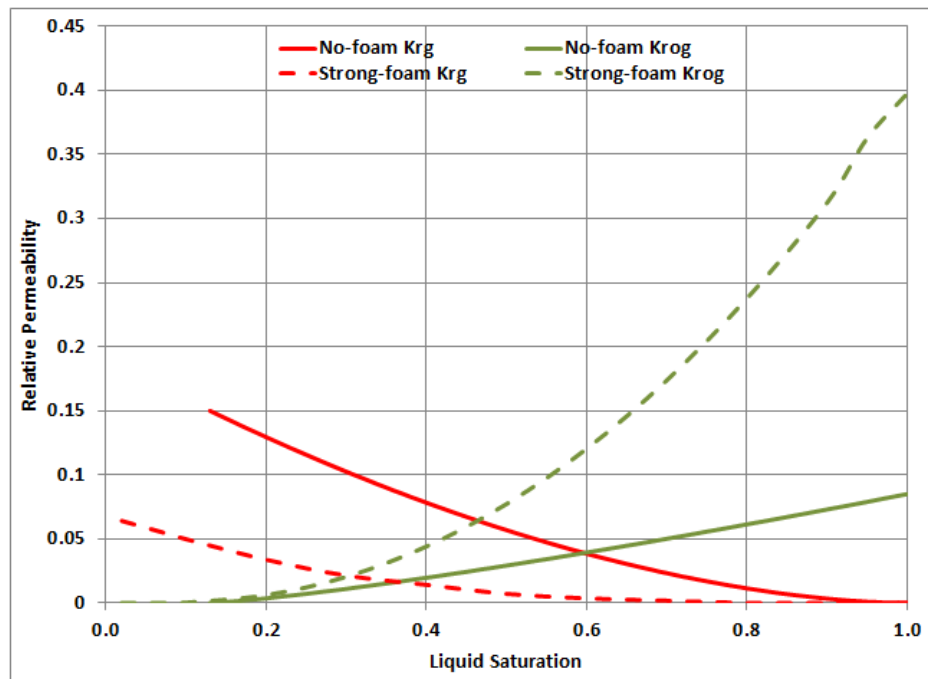
CMG STARS utilizes two additional parameters, DTRAPW and DTRAPN, to interpolate between relative permeability curves. DTRAPW and DTRAPN respectively represent the values of wetting and non-wetting phase interpolation parameter for the current relative permeability data (CMG, 2009). CMG stipulates that at least one of DTRAPW and DTRAPN must be present to enable relative permeability interpolation. Values for DTRAPW and DTRAPN are obtained via history-matching.

When carrying out a history match procedure, solutions are non-unique and it is quite possible to obtain an appropriate match with erroneous values for the matching parameters. For this study, parameters such as fluid saturations, endpoint relative permeabilities, and injection and production well pressures were constrained in order to ensure that the final match obtained was as close as possible to the results obtained experimentally.

The significance of dispersion on recovery was studied by incorporating a range of dispersion coefficients into the simulation runs for the history match process. The equations presented in Chapter 2 (Equations 2.1 to 2.4) were used to calculate dispersion coefficients. First, the method recommended by Renner (1963) was used to obtain the diffusion coefficients, which were then incorporated into the correlation used to determine dispersion coefficients that were proposed by Perkins and Johnston (1963). The use of a range of dispersion coefficients arose due to the absence of values for the average particle diameter,  $d_p$ , and a formation electrical resistivity factor,  $F$ , for Berea sandstone. Lewis (2008) suggested a range of  $0.0053\text{cm} - 0.0149\text{cm}$  for particle diameter, and  $0.3 - 0.7$  for  $F\phi$ . Bai et al. (2008) recommended using a value of 3.5 for the inhomogeneity of the medium,  $\sigma$ , for Berea sandstones. Applying the recommended ranges and values provided minimum and maximum values for the longitudinal and transverse dispersion coefficients of  $\text{CO}_2$  in the oleic phase. The calculated values are shown in Table 4.1.

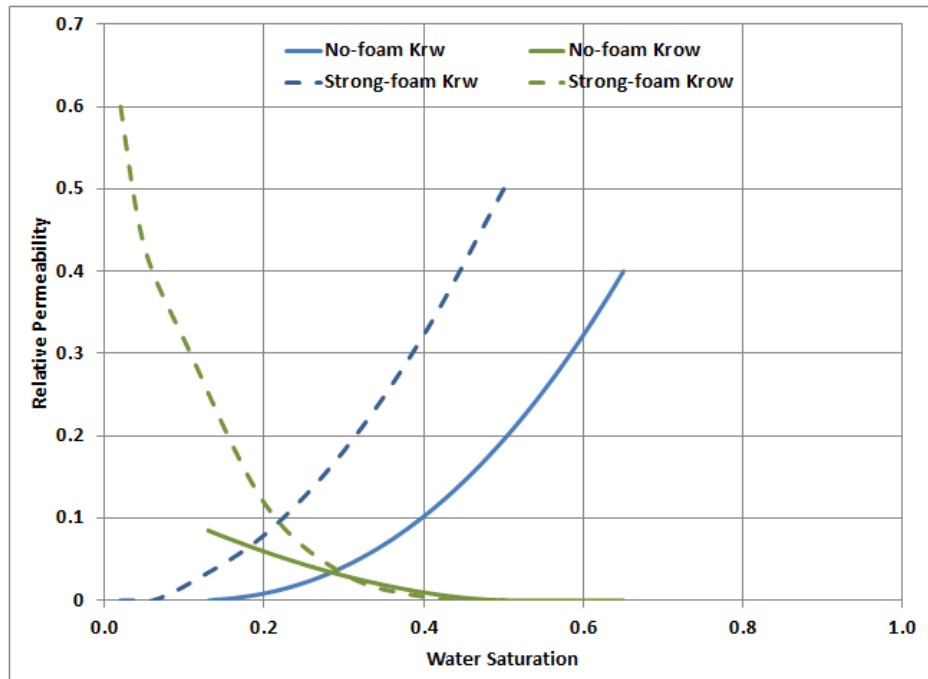


(a) Oil-water

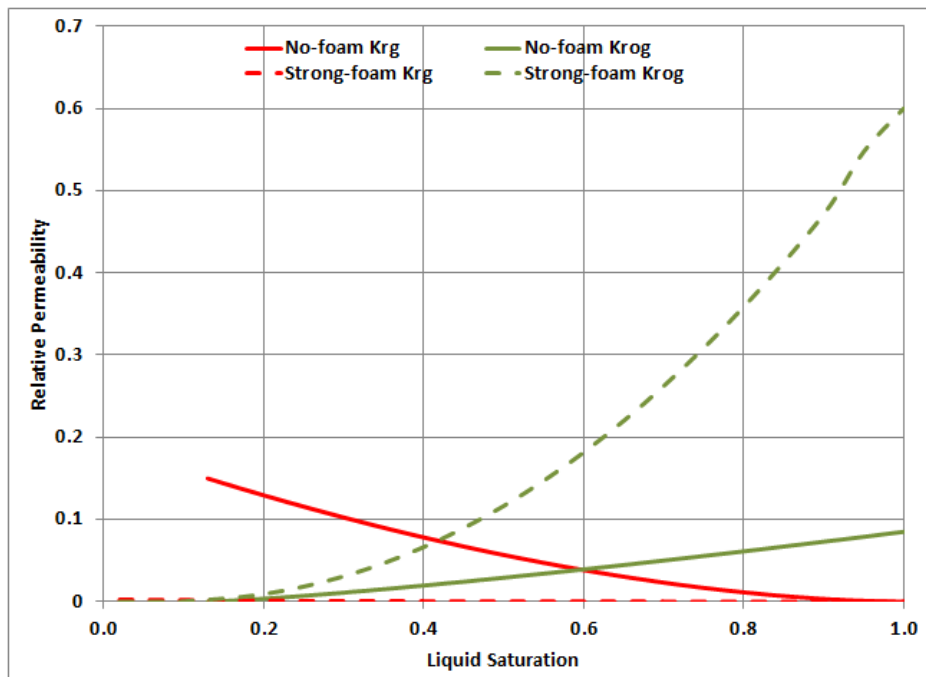


(b) Gas-oil

Figure 4.1: Set of relative permeability curves for 0.1% wt surfactant concentration for (a) Oil-water and, (b) gas-oil for no-foam and strong-foam interpolation sets



(a) Oil-water



(b) Gas-oil

Figure 4.2: Set of relative permeability curves for 0.5% wt surfactant concentration for (a) Oil-water and, (b) gas-oil for no-foam and strong-foam interpolation sets



Table 4.1: Minimum and maximum values for the longitudinal and transverse dispersion coefficients for CO<sub>2</sub> in the oleic phase

	Min	Max
$D_{Lo1}, cm^2/min$	0.0080	0.02
$D_{To1}, cm^2/min$	0.0075	0.0175

#### 4.4 Simulation of Synthetic Reservoirs

Based on the results obtained from coreflood experiments and history matching, the 8 dimensionless numbers previously derived were used to scale from laboratory to field. Ideally, different reservoirs with the same dimensionless numbers should have the same dimensionless responses. Three 2-D reservoirs (x- and z-directions) with the same dimensionless groups but different dimensional parameters were created to test the validity of the dimensionless numbers. Table 4.2 shows the dimensional parameters for the three synthetic reservoirs.

##### 4.4.1 Reduction of fluid velocity for use in Larger Models

The values of velocity used to model the synthetic reservoirs are very small. Utilizing larger values that were approximately equal to 1.0 *ft/day* caused the reservoirs to rapidly reach the set pressure limits. This made it difficult to observe the distribution of pressure along the reservoirs with time. Pujol and Boberg (1972) studied ways of accurately scaling laboratory steam flood models to field scale. Their results indicated that flowing fluids at a very low velocity brought field scale results closer to laboratory models. The longitudinal and transverse coefficients of dispersion were also reduced in order to obtain equal dimensionless numbers as the laboratory case.

##### 4.4.2 Scaling Reaction Frequency Factor for use in Larger Models

The first attempt at simulating the synthetic models using the same Reaction Frequency Factors,  $r_{rate}$ , as those used in the laboratory model resulted in a dramatic increase in pressure values. This increase was similar to those observed when the velocity used in the laboratory were directly applied during the modeling of the synthetic models. Pressures were over

6000 $psi$  for 0.1% wt and over 9000 $psi$  for 0.5% wt surfactant concentration. These high pressure values led to simulator failure as the defined limits on the simulator were exceeded.

In order to attain reasonable pressure values,  $r_{rate}$  had to be scaled using a time scale factor,  $\tau$ . This led to a reduction in the values of  $r_{rate}$  used to model the synthetic cases. This is an indication that foam generation and sustenance occurs at a faster rate in shorter systems and slower in larger systems. Reaction Frequency Factor was scaled as follows:

$$\tau = \frac{\text{Pore volume for large model}}{\text{Pore volume for laboratory model}} \quad (4.4)$$

$$\text{Large model } r_{rate} = \frac{\text{Laboratory model } r_{rate}}{\tau} \quad (4.5)$$

where,

$\tau$  : time scale factor

## 4.5 Simulation Results

The following sections show the results obtained from history matching the coreflood experiments, the application of these results to model three synthetic reservoirs so as to analyze the validity of the dimensionless numbers, and to identify and apply any possible modifications to correct inconsistencies.

### 4.5.1 Coreflooding

In the laboratory, brine was injected into a core that contained oil at initial saturation,  $S_{oi}$ , and brine at connate water saturation,  $S_{wc}$ . After waterflood was done,  $CO_2$  and surfactant solution at 0.1% wt were co-injected into a core that was saturated with brine and oil at residual oil saturation,  $S_{or}$ . The core was cleaned (following the sequence listed in Section 3.3.1) and another sequence of oil flooding and waterflooding were carried out before the simultaneous injection of  $CO_2$  and surfactant solution at 0.5% wt. Results for the waterflood are presented in Appendix B (Figures B.1 and B.2).

Table 4.2: Dimensional parameters for core experiments and synthetic reservoirs

(a) Dimensional parameters for properties with equal values used in core experiments and synthetic reservoirs

Parameters	Values
$k_z, mD$	19.96
$k_x, mD$	19.96
$k_{rg}$	0.150
$k_{ro}$	0.085
$k_{rw}$	0.400
$g, cm/s^2$	980.7
$\sigma_{ow}, dyn/cm$	49.0

(b) Dimensional parameters for 0.1 % wt surfactant concentration core experiments and synthetic reservoirs

Parameters	Core	R1	R2	R3
$L, cm [ft]$	7.65	1500 [49.2]	1800 [59.0]	3735 [122.5]
$H, cm [ft]$	2.56	502 [16.5]	602.4 [19.8]	1250 [41.0]
$u_T, cm/s$	$3.36 \times 10^{-4}$	$1.71 \times 10^{-5}$	$1.43 \times 10^{-5}$	$2.50 \times 10^{-6}$
$D_{Lo1}, cm^2/s$	$1.12 \times 10^{-4}$	$1.12 \times 10^{-3}$	$9.67 \times 10^{-4}$	$9.31 \times 10^{-4}$
$D_{To1}, cm^2/s$	$3.53 \times 10^{-6}$	$3.53 \times 10^{-5}$	$3.05 \times 10^{-5}$	$2.93 \times 10^{-5}$
$\phi$	0.332	0.332	0.385	0.400
$\mu_g @ 2500 \text{ psi}, cp$	0.125	0.125	0.125	0.125
$\mu_o @ 2500 \text{ psi}, cp$	1.03	1.03	1.03	1.03
$\mu_w @ 2500 \text{ psi}, cp$	0.99	0.99	0.99	0.99
$\rho_g @ 2500 \text{ psi}, g/cm^3$	0.942	1.001	1.002	1.003
$\rho_o @ 2500 \text{ psi}, g/cm^3$	0.683	0.988	0.991	0.998
$\rho_w @ 2500 \text{ psi}, g/cm^3$	1.020	1.005	1.005	1.005

(c) Dimensional parameters for 0.5 % wt surfactant concentration core experiments and synthetic reservoirs

Parameters	Core	R1	R2	R3
$L, cm [ft]$	7.65	1500 [49.2]	1800 [59.0]	3735 [122.5]
$H, cm [ft]$	2.56	502 [16.5]	602.4 [19.8]	1250 [41.0]
$u_T, cm/s$	$2.85 \times 10^{-4}$	$1.45 \times 10^{-5}$	$1.21 \times 10^{-5}$	$5.84 \times 10^{-6}$
$D_{Lo1}, cm^2/s$	$1.12 \times 10^{-5}$	$1.12 \times 10^{-4}$	$9.67 \times 10^{-5}$	$9.31 \times 10^{-5}$
$D_{To1}, cm^2/s$	$3.53 \times 10^{-7}$	$3.53 \times 10^{-6}$	$3.05 \times 10^{-6}$	$2.93 \times 10^{-5}$
$\phi$	0.332	0.332	0.385	0.400
$\mu_g @ 2500 \text{ psi}, cp$	0.210	0.210	0.210	0.210
$\mu_o @ 2500 \text{ psi}, cp$	1.03	1.03	1.03	1.03
$\mu_w @ 2500 \text{ psi}, cp$	0.99	0.99	0.99	0.99
$\rho_g @ 2500 \text{ psi}, g/cm^3$	0.942	1.001	1.002	1.003
$\rho_o @ 2500 \text{ psi}, g/cm^3$	0.683	0.988	0.991	0.998
$\rho_w @ 2500 \text{ psi}, g/cm^3$	1.020	1.005	1.005	1.005

Figures 4.3a and 4.3b compare recovery factors obtained from laboratory experiments and the simulator for 0.1% wt and 0.5% wt respectively. In both cases,  $RF$  calculated from simulation matched well with experimental data.

For  $CO_2$  pore volumes recovered, good matches were observed when laboratory data was analyzed against simulator results. Figures 4.4a and 4.4b show the comparison of recovered  $CO_2$  pore volumes obtained from laboratory experiments with that predicted by the simulator for 0.1% wt and 0.5% wt surfactant concentration respectively.

The simulation and experimental results for total brine and surfactant pore volumes recovered for the two cases of  $CO_2$  and surfactant solution injection are presented in Figures 4.5a and 4.5b. A reasonable match between experimental data and calculated results was obtained for both injection scenarios.

Pressure difference across the core was calculated from laboratory data and simulation results and are depicted in Figures 4.6a and 4.6b. In order to obtain reasonable matches for injector pressure, producer pressure, and the resulting pressure difference, Ren (2012a) recommended using a larger Mobility Reduction Factor ( $MRF$ ) in the simulator than the value measured in the laboratory (in some cases, as much as 3 orders of magnitude larger). In their work, Coombe et al. (1997) reported laboratory measured values in the range of 8 to 40, but required a range of 800 to 1000 to match the pressure drop observed during their laboratory experiments. Ma et al. (2012) studied the parameters used to describe foam and analyzed experimental results obtained from foam injection in a commercially available reservoir simulator. To obtain reasonable pressure matches, they utilized very high  $MRF$  values that ranged from 33,614 to 215,595. These researchers did not utilize stoichiometric relationships to model foam behavior and had to over-compensate with  $MRF$  to obtain the steady rise in pressure observed at the producer.

Tables 4.3 and 4.4 respectively show the values of  $FM$  parameters and DTRAPW and DTRAPN that were used to match laboratory results with the simulator. While the laboratory-derived  $MRF$  value of 45.37 resulted in an acceptable match, increasing  $MRF$  to 60 led to a

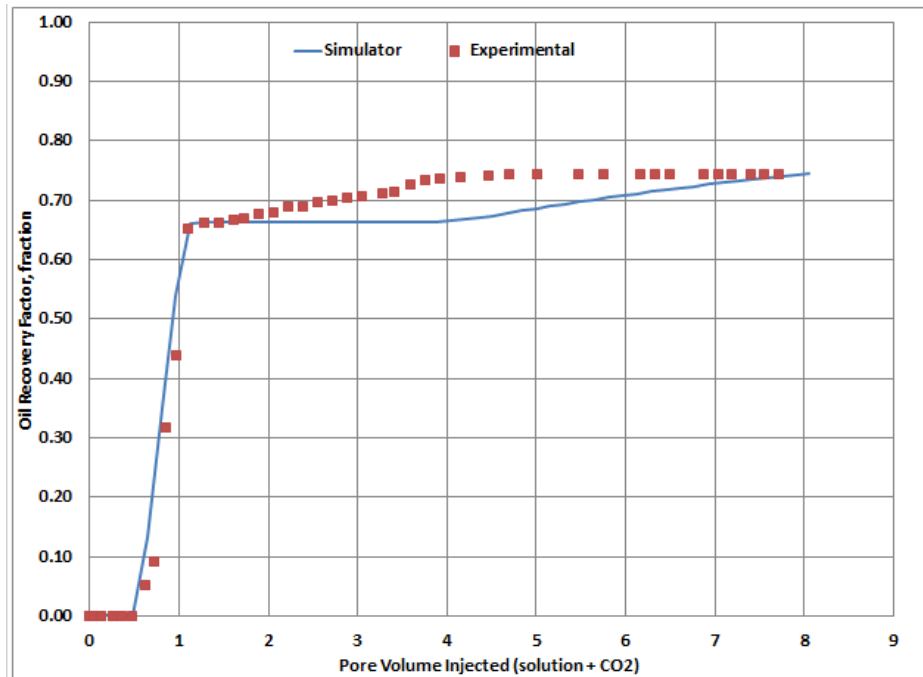
more improved match. The use of a higher  $MRF$  value is justified based on the effect on  $\Delta p$  when the annular pressure and hence the inlet pressure was reduced during the co-injection of  $\text{CO}_2$  and 1.0% wt surfactant solution (Chapter 3, Section 3.4). The values used in the stoichiometric modeling for the core model are shown in Table 4.5. For the foam formation stage, during the generation of foam, the stoichiometric coefficient of the surfactant component was  $3.61 \times 10^{-5}$ . This value is equal to the  $CMC$ , in units of mole fraction, of the surfactant utilized in this study. The value of the  $CMC$  for Chevron's CD-1045 surfactant was obtained from Tsau and Heller (1992), Liu et al. (2005) and Grigg et al. (2007). It was assumed that only half of the available surfactant is used to create foam. Hence the stoichiometric coefficient of produced surfactant was  $1.81 \times 10^{-5}$ . In the simulator, the stoichiometric coefficients are very sensitive as a change in the value of the 4th decimal number can cause a significant increase or decrease in  $RF$  and  $\Delta p$ . Table 4.6 presents the scaled values of  $r_{rate}$ , as explained in Section 4.4.2, that were used to describe the synthetic models.

Table 4.3: Values of  $FM$  parameters used to match laboratory results

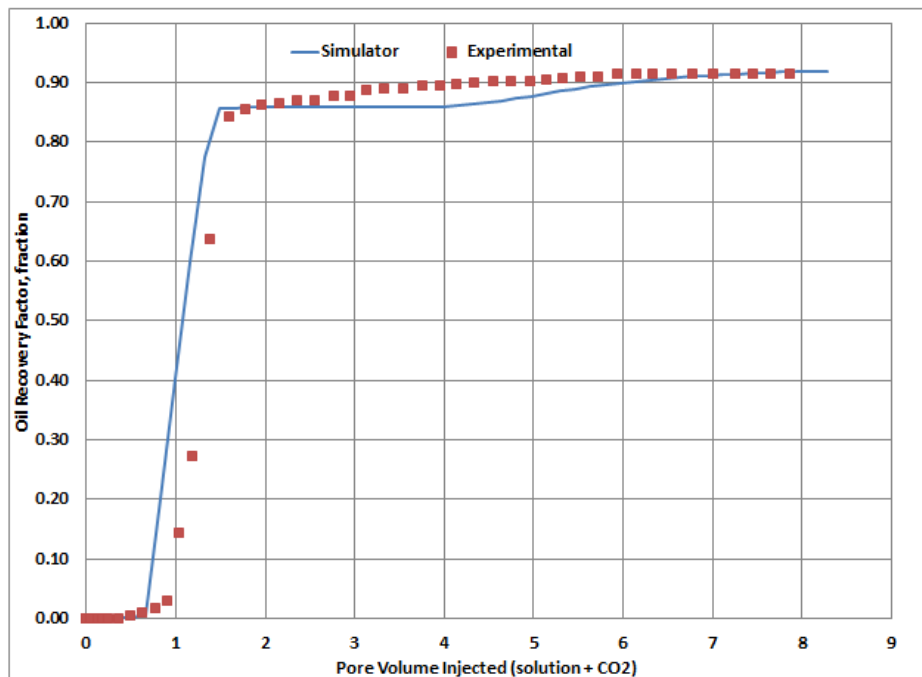
	0.1% wt	0.5% wt
Surfactant term exponent, $es$	0.12	0.36
Oil term exponent, $eo$	1.08	0.72
Capillary number term exponent, $ev$	0.48	0.36
Mobility Reduction Factor	60	60
Maximum oil saturation to foam, $S_o^{max}$	0.80	0.88
Reference capillary number, $N_c^{ref}$	$4.5 \times 10^{-6}$	$8.4 \times 10^{-6}$
Maximum surfactant concentration, $w_s^{max}$	$3.01 \times 10^{-4}$	

Table 4.4: Values of wetting and non-wetting interpolation parameters used to match laboratory results

	0.1% wt	0.5% wt
DTRAPW in first relperm set, $DTRAPW_1$	3.00	4.00
DTRAPW in second relperm set, $DTRAPW_2$	0.0167	3.00
DTRAPN in first relperm set, $DTRAPN_1$	5.00	3.50
DTRAPN in second relperm set, $DTRAPN_2$	-0.0175	3.00

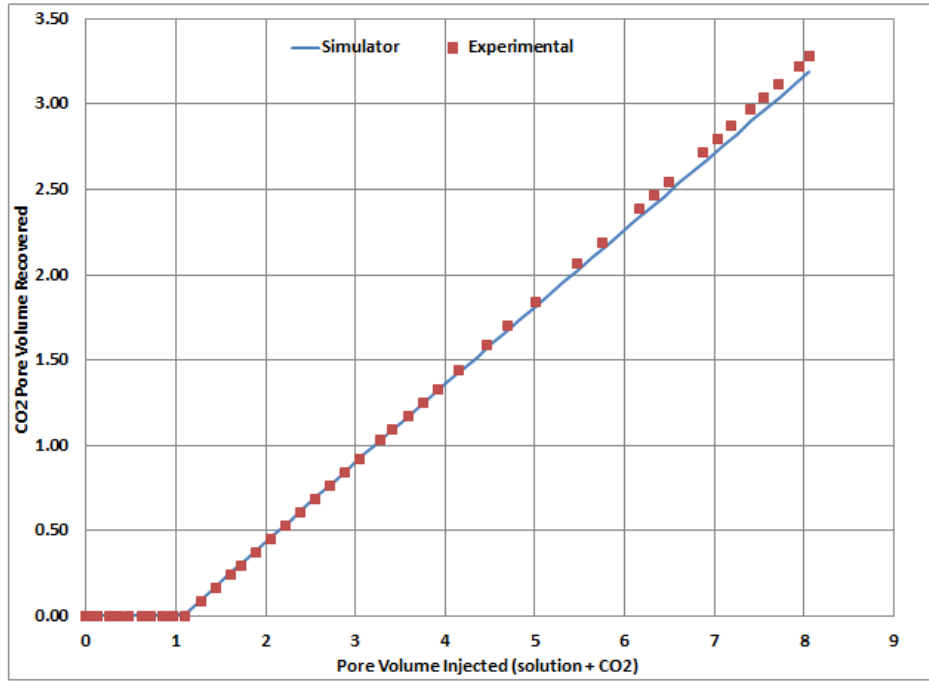


(a) 0.1% wt surfactant

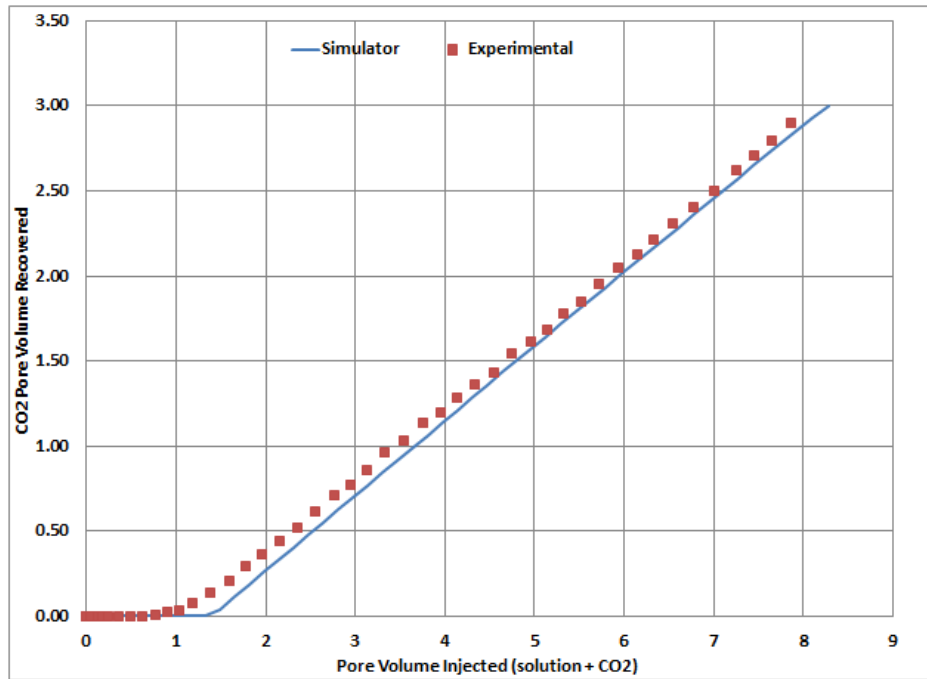


(b) 0.5% wt surfactant

Figure 4.3: Simulation and experimental results for oil recovery factor in 1" (dia.)  $\times$  3" (long) Berea core

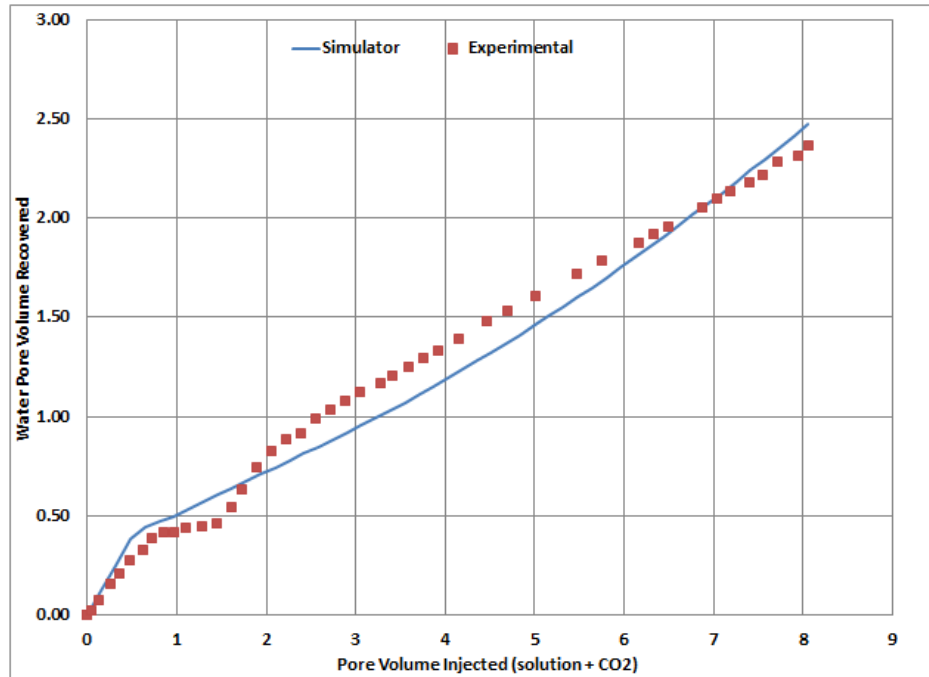


(a) 0.1% wt surfactant

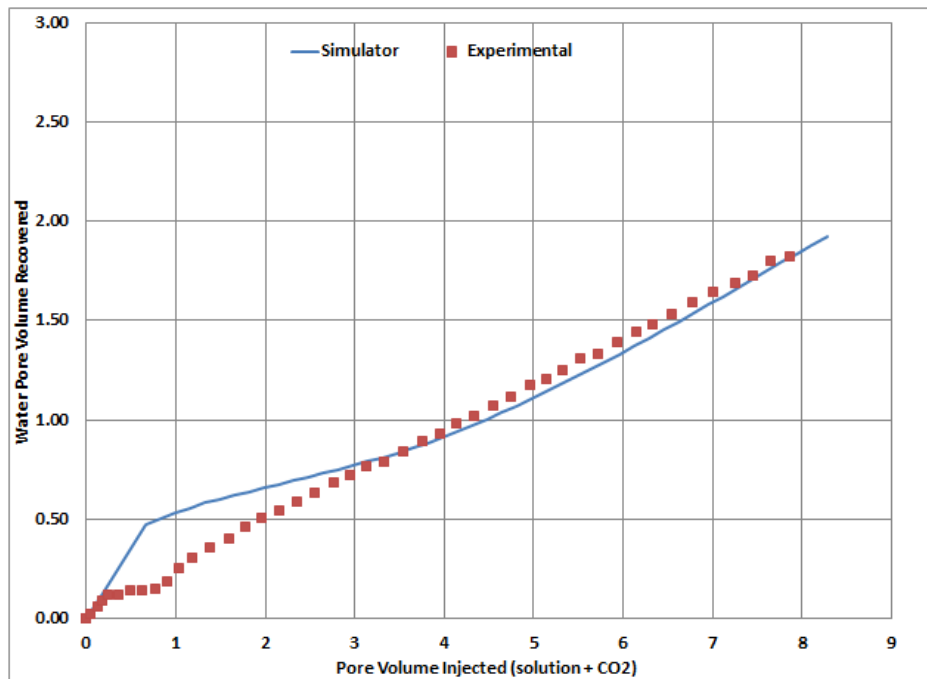


(b) 0.5% wt surfactant

Figure 4.4: Simulation and experimental results for CO<sub>2</sub> pore volume recovered in 1" (dia.) × 3" (long) Berea core



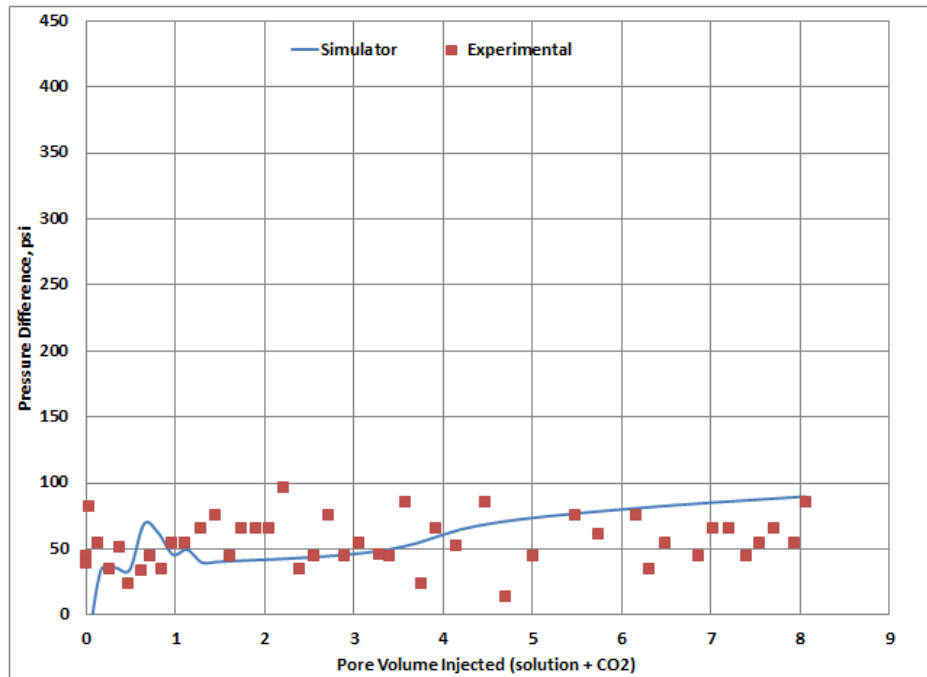
(a) 0.1% wt surfactant



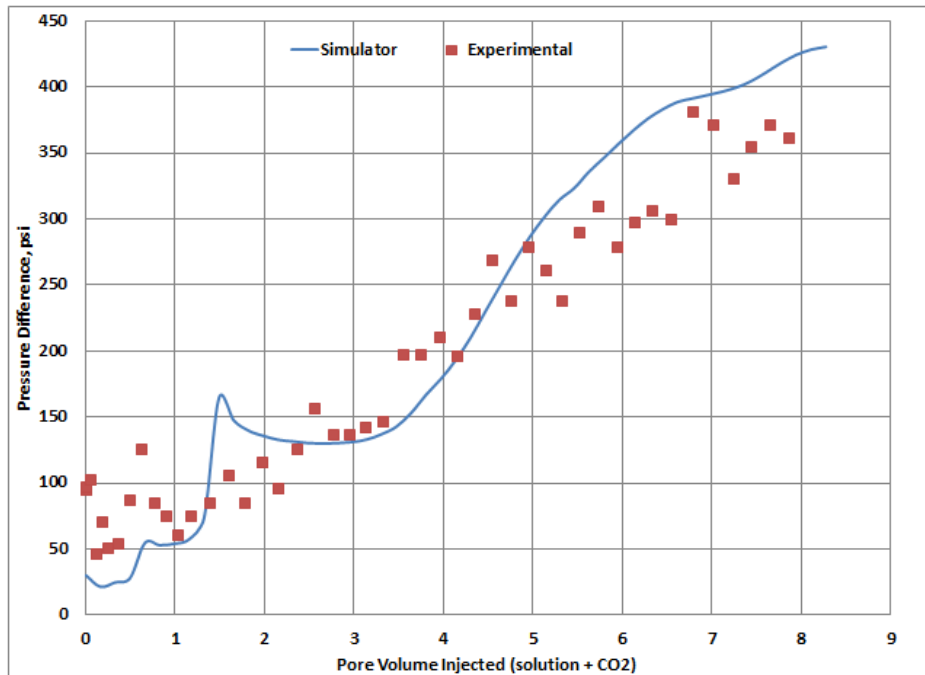
(b) 0.5% wt surfactant

Figure 4.5: Simulation and experimental results for brine and surfactant pore volume recovered in 1" (dia.)  $\times$  3" (long) Berea core





(a) 0.1% wt surfactant



(b) 0.5% wt surfactant

Figure 4.6: Simulation and experimental results for pressure difference across the 1" (dia.) × 3" (long) Berea core

Table 4.5: Values of stoichiometric modeling parameters used to match laboratory results

Surf. Concentration		Water	Surfactant	Foam	Decane	CO <sub>2</sub>
0.1% wt	Reaction coefficient	1	$3.61 \times 10^{-5}$	0	0	1
	Production coefficient	0	$1.81 \times 10^{-5}$	2	0	1
	$r_{rate}$ for formation	$2.08 \times 10^5$				
	$r_{rate}$ for sustenance	$1.92 \times 10^6$				
0.5% wt	Reaction coefficient	0	$1.81 \times 10^{-5}$	2	0	0
	Production coefficient	1	$3.61 \times 10^{-5}$	2.00325	0	0
	$r_{rate}$ for formation	$4.75 \times 10^5$				
	$r_{rate}$ for sustenance	$1.26 \times 10^6$				

Table 4.6: Comparison of Reaction Frequency Factors,  $r_{rate}$ , used for modeling coreflood and synthetic models

Surfactant Concentration	Foam Stage	Lab	R1	R2	R3
0.1% wt	Formation	$2.08 \times 10^5$	35.11	21.02	4.70
	Sustenance	$1.92 \times 10^6$	324.06	194.06	43.38
0.5% wt	Formation	$4.75 \times 10^5$	69.83	41.82	9.35
	Sustenance	$1.26 \times 10^6$	184.50	110.49	24.67

Gas relative permeability,  $k_{rg}$ , in the presence of foam, and in a particular gridblock, depends on the local surfactant concentration, the local oil saturation, and the local capillary number. Values for these parameters are calculated by the history matching optimization software, CMOST (CMG, 2009).

The distribution of gas relative permeability, global oil mole fraction, global CO<sub>2</sub> mole fraction, and global foam mole fraction are shown in Figure 4.7 for the 0.1% wt case and Figure 4.8 for the 0.5% wt case. At the start of the injection of CO<sub>2</sub> and surfactant solution, foam was generated and some CO<sub>2</sub> not utilized in foam generation moved ahead of the newly formed foam. Therefore a higher CO<sub>2</sub> and lower foam mole fraction was observed away from the injector towards the producer. As co-injection progressed, CO<sub>2</sub> and oil concentration along the core reduced and foam mole fraction increased. As CO<sub>2</sub>, stabilized by foam, propagated along the core, oil was displaced. Tortopidis and Shallcross (1994) carried out laboratory experiments to study the efficiency of CO<sub>2</sub>-foam by analyzing various types of surfactants. They observed the formation of strong foam in the upstream section of their reservoir that

slowly propagated along the length of the system. This observation led them to conclude that the first section of the core acted as an in-situ foam generator. This same concept can be applied to the results obtained in this study. In Figures 4.7c and 4.8c, it can be observed that a steady  $\text{CO}_2$  mole fraction extends along the core as injected pore volumes increased. Global foam mole fraction also approached a constant value that gradually moved along the core. The steady values for  $\text{CO}_2$  and surfactant mole fractions represent the concentrations at which maximum foam strength was generated. As the foam front moved along the core, oil and brine were displaced, and the relative permeability of gas reduced between the injector and producer. It is expected that the same behavior will be observed in field cases.

Coreflood experiments can be used to analyze a field case whereby one layer of the reservoir is being screened for  $\text{CO}_2$ -surfactant potential. Also, basic data that can be utilized for more advanced analysis can be extracted from laboratory experiments. In this study, results measured during laboratory experiments and those obtained from a history-match process were used to design and analyze synthetic reservoir models.

Table 4.7: Dimensionless numbers for core experiments and synthetic models for 0.1% wt surfactant concentration

Groups	Core	R1	R2	R3
$R_L$	3	3	3	3
$M_{ow}$	4.9	4.9	4.9	4.9
$M_{go}$	14.5	14.5	14.5	14.5
$N_{cap(ow)}$	$2.90 \times 10^{-6}$	$2.90 \times 10^{-6}$	$2.90 \times 10^{-6}$	$2.90 \times 10^{-6}$
$N_{G(og)}$	$4.19 \times 10^7$	$4.19 \times 10^7$	$4.19 \times 10^7$	$4.19 \times 10^7$
$N_{G(wo)}$	$2.66 \times 10^8$	$2.66 \times 10^8$	$2.66 \times 10^8$	$2.66 \times 10^8$
$N_{pe(Lo1)}$	69	69	69	69
$N_{pe(To1)}$	245	245	245	245

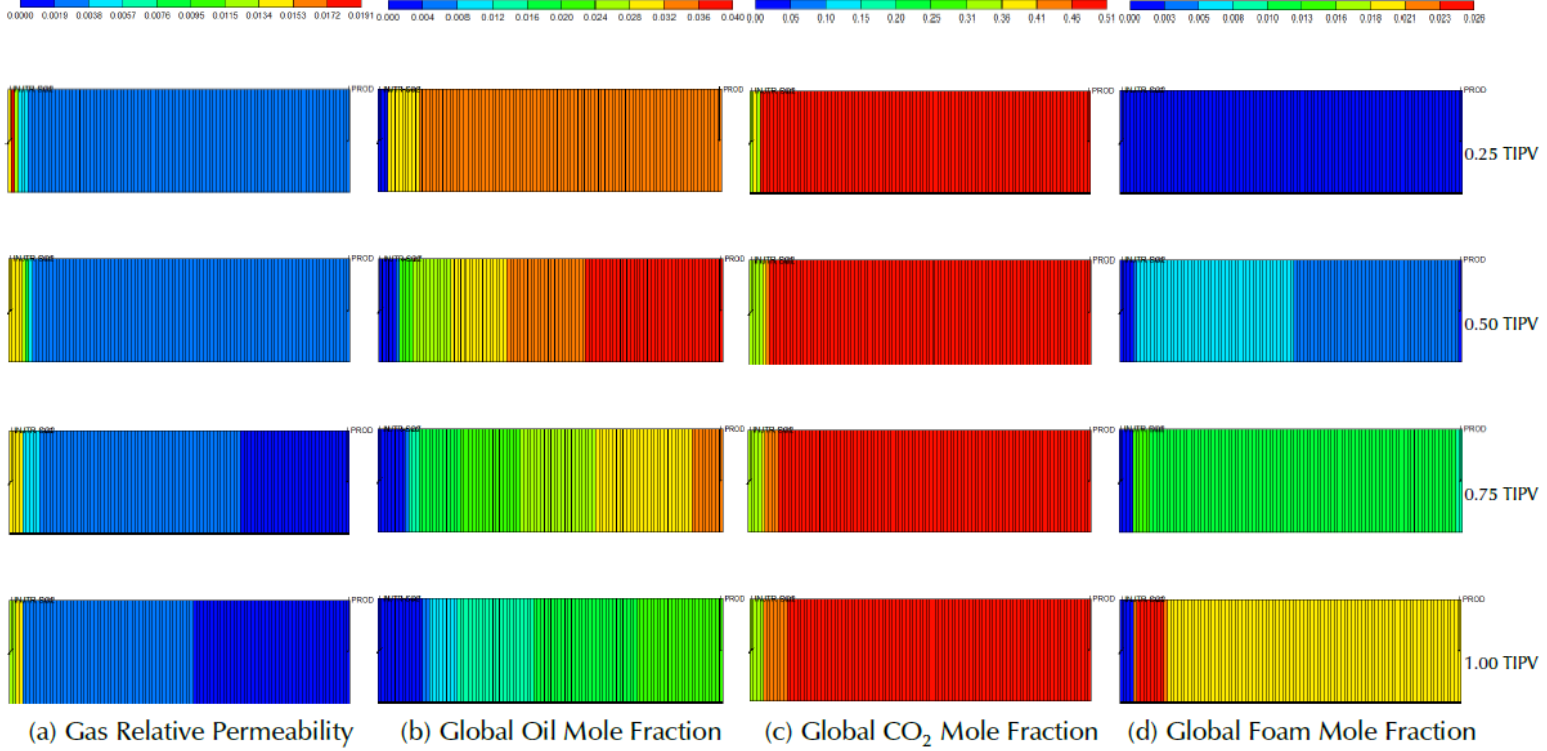


Figure 4.7: Property distribution in the core during the co-injection of 0.1% wt surfactant solution and CO<sub>2</sub> at 0.25, 0.50, 0.75 and 1.00 of total PVI

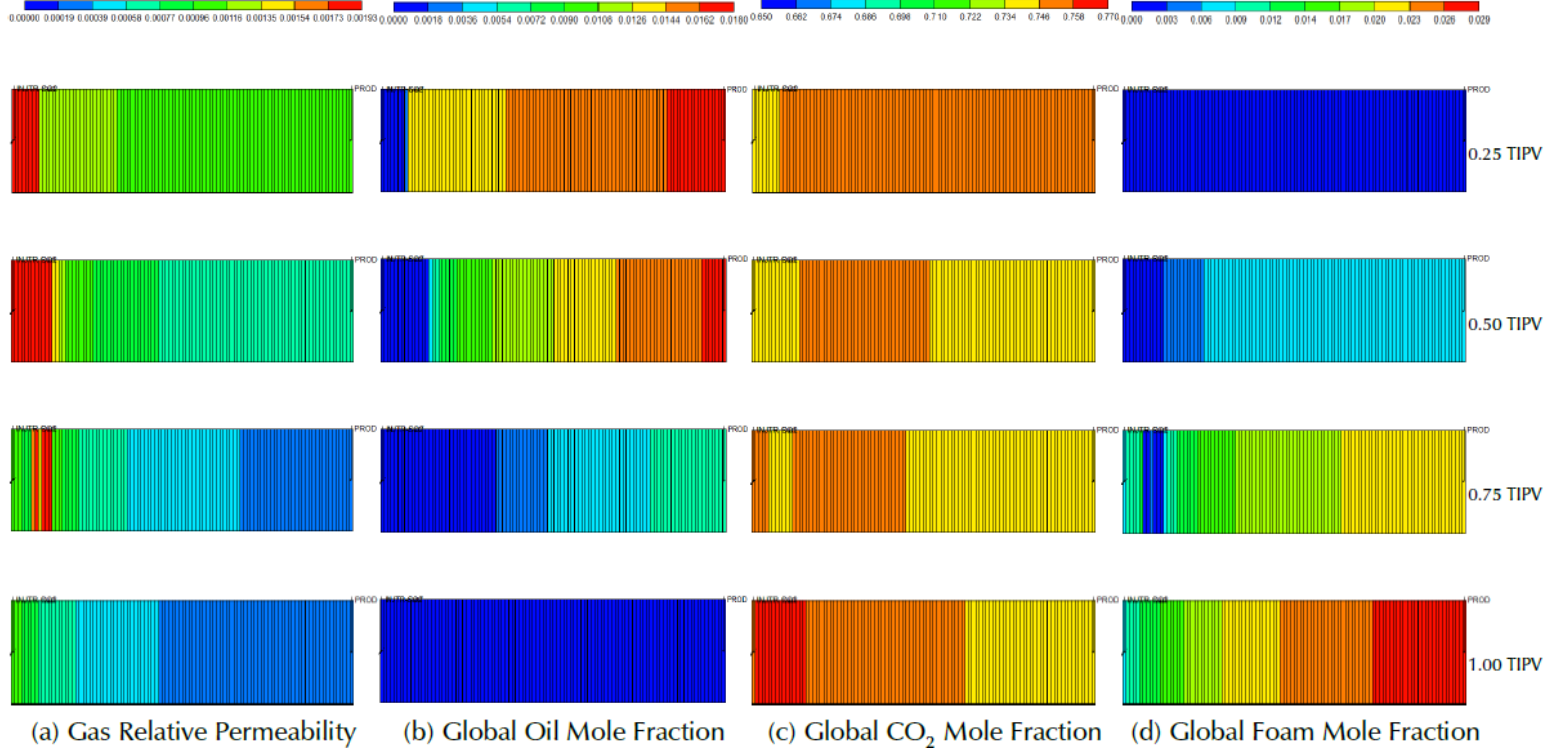


Figure 4.8: Property distribution in the core during the co-injection of 0.5% wt surfactant solution and CO<sub>2</sub> at 0.25, 0.50, 0.75 and 1.00 of total PVI

Table 4.8: Dimensionless numbers for core experiments and synthetic models for 0.5% surfactant concentration

Groups	Core	R1	R2	R3
$R_L$	3	3	3	3
$M_{ow}$	4.9	4.9	4.9	4.9
$M_{go}$	8.6	8.6	8.6	8.6
$N_{cap(ow)}$	$2.46 \times 10^{-6}$	$2.46 \times 10^{-6}$	$2.46 \times 10^{-6}$	$2.46 \times 10^{-6}$
$N_{G(og)}$	$4.93 \times 10^7$	$4.93 \times 10^7$	$4.93 \times 10^7$	$4.93 \times 10^7$
$N_{G(wo)}$	$3.13 \times 10^8$	$3.13 \times 10^8$	$3.13 \times 10^8$	$3.13 \times 10^8$
$N_{pe(Lo1)}$	585	585	585	585
$N_{pe(To1)}$	2081	2081	2081	2081

#### 4.5.2 Synthetic Reservoirs

The dimensionless numbers obtained from laboratory experiments and extended to the sample models are presented in Tables 4.7 and 4.8. The thickness and permeability distribution of the layers for the synthetic models were arbitrarily chosen. Geometric averaging was applied to the layer permeabilities in the  $x$ -direction to obtain the single values for each model that was used to calculate the dimensionless numbers. Vertical permeability,  $k_z$ , was assumed to be equal in every layer for each model. The remaining parameters were specified to maintain the laboratory dimensionless number values. Injection was along the entire set of grid cells on the inlet side of the models and production was along the entire set of grids cells on the outlet side of the model.

The first model,  $R1$ , represents a homogeneous system, divided into 6 equal layers, each with the same permeability and thickness. Case  $R2$  had 3 different permeability and thickness values that were distributed through 6 layers, with every 2 layers having the same permeability and thickness. The last model,  $R3$ , consisted of 6 layers with 5 different values of permeability and thickness. Table 4.9 shows the layer thickness and permeability distribution for the synthetic reservoir models. All models have a geometric average permeability equal to the core permeability of 20mD.

For interpolation of relative permeability curves, the same first set of data were used to model  $R1$ ,  $R2$ , and  $R3$ . The end point relative permeability values of oil, water, and gas for

the second set of curves were rescaled to characterize fluid trapping by gas trapping in the presence of foam.

Table 4.9: Layer thickness and permeability distribution for sample reservoirs

Reservoir	$L, \text{ cm [ft]}$	Layer $H, \text{ cm [ft]}$	Layer $k, \text{ mD}$
R1	1500 [49.2]	83.67 [2.8]	20
		83.67 [2.8]	20
		83.67 [2.8]	20
		83.67 [2.8]	20
		83.67 [2.8]	20
		83.67 [2.8]	20
R2	1800 [59.0]	100.2 [3.3]	37
		100.2 [3.3]	37
		66 [2.2]	10
		66 [2.2]	10
		135 [4.4]	18
		135 [4.4]	18
R3	3735 [122.5]	250 [8.2]	40
		100 [3.3]	15
		375 [12.3]	22
		175 [5.7]	30
		175 [5.7]	10
		175 [5.7]	10

Figures 4.9a and 4.10a compares oil recovery factor for laboratory core experiments and the synthetic models with equal dimensionless numbers for each respective injected surfactant concentration (0.1% and 0.5%). For the 0.1% wt case, a higher oil recovery factor was obtained from laboratory experiments when compared to those obtained for the synthetic models. It was also observed that both the rate of recovery and  $RF$  reduced with reservoir heterogeneity, primarily due to the larger size of the upper zones, and being swept by  $\text{CO}_2$ . Pressure difference for the core (Figure 4.9b) matched reasonably with the results obtained for  $R1$ ,  $R2$ , and  $R3$ . The opposite behavior was seen in the 0.5% wt injection. The synthetic models achieved almost equal  $RF$  values at very similar rates that were slightly higher than the values measured for the core. Pressure difference decreased with increased reservoir complexity (Figure 4.10b) but were still somewhat similar to those observed in the experiments. The higher pressure difference caused by the more stable foam appears to allow the displacement proceed in a

similar manner to the core experiments, whereas, the weaker foam (lower  $\Delta p$ ) causes more bypassing.

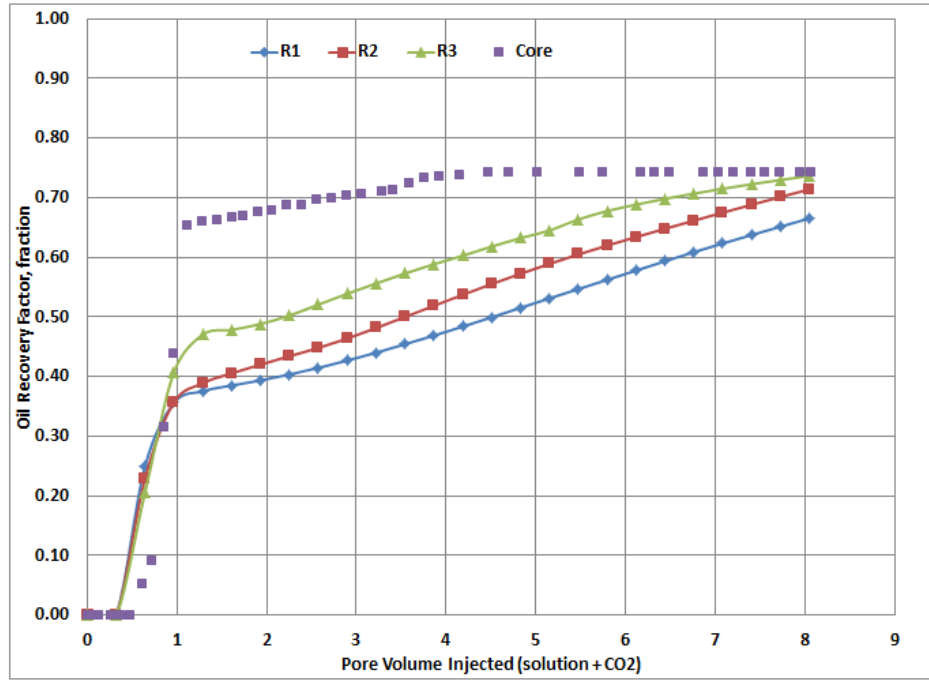
Distribution of global mole fraction of foam, CO<sub>2</sub>, and oil for the synthetic reservoirs are presented in Figure 4.11 through 4.16 at 25%, 50%, 75%, and 100% of total injected pore volumes. Similar fluid distribution patterns were observed for both cases of surfactant and CO<sub>2</sub> co-injection between the respective synthetic reservoirs. In general, the degree of heterogeneity, crossflow between layers, and the difference in density between associated fluids have a major effect on fluid distribution in the reservoir.

For the homogeneous reservoir, *R1*, the heavier foam component flowed to the bottom layers of the reservoir (Figures 4.11b and 4.14b) while the CO<sub>2</sub> flowed predominantly through the top layers (Figures 4.11c and 4.14c). In this case, the effect of gravity segregation is very pronounced. As surfactant solution and CO<sub>2</sub> are injected, oil is displaced from the top layers to the bottom layers. Here, the CO<sub>2</sub> acts as the main displacing fluid. Figures 4.11d and 4.14d show how CO<sub>2</sub>, which flows mostly at the top of the reservoir, displaces the oil initially present in these layers in addition to the displaced oil from the lower layers.

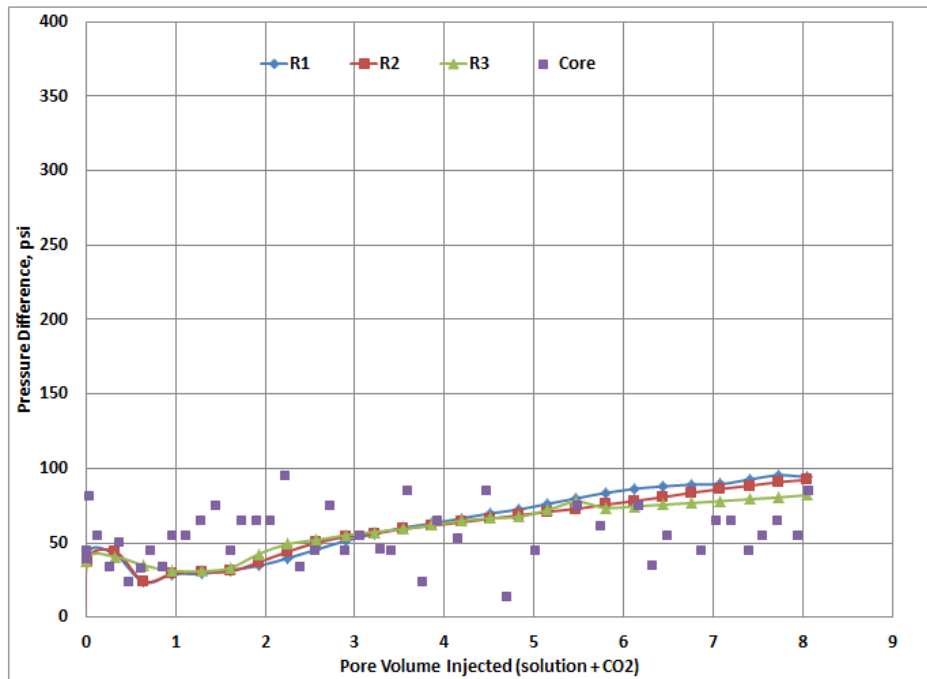
The fluid distribution patterns obtained for the second synthetic reservoir, *R2*, are very similar to those seen in reservoir *R1*. Though *R2* is a heterogeneous system, the contrast between the high and low permeability values for the layers is not very large. Foam that segregated to the last 2 layers with a permeability value of 37mD was able to divert some CO<sub>2</sub> into the lowest permeability layers. Figures 4.12b and 4.15b show the foam mole fraction map while Figures 4.12c and 4.15c show the distribution of CO<sub>2</sub> mole fraction.

A higher degree of heterogeneity is found in *R3*. The foam distribution maps in Figures 4.13b and 4.16b indicate that gravity segregation made surfactant flow to the lowest layers. Since layer 1 has a relatively low permeability value of 10mD, flow is restricted and most of the foam component is diverted into layers with higher permeability values. Figures 4.13c and 4.16c show that with most of the foam flowing into layers 5 and 6, CO<sub>2</sub> is able to flow predominantly through the top and middle layers, regardless of permeability values. Figures



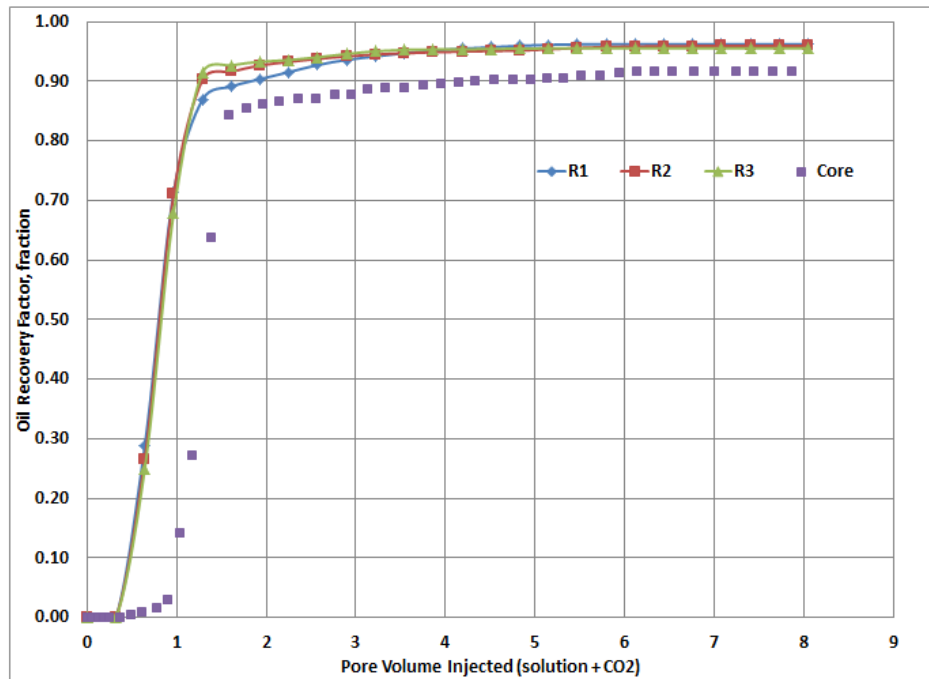


(a) Oil recovery factor

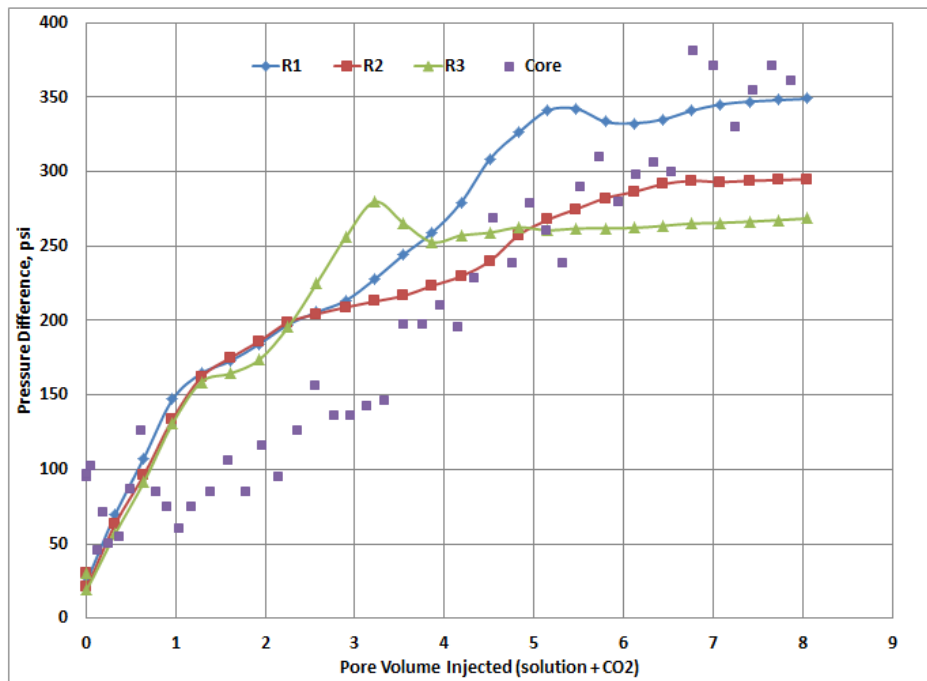


(b) Pressure difference

Figure 4.9: Comparison of oil recovery factor and pressure difference for core experiments and synthetic reservoirs with equal dimensionless numbers for 0.1% wt surfactant concentration



(a) Oil recovery factor



(b) Pressure difference

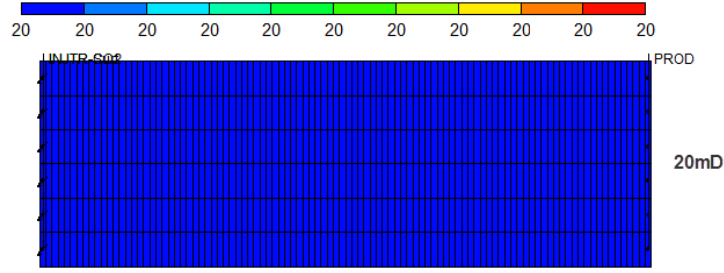
Figure 4.10: Comparison of oil recovery factor and pressure difference for core experiments and synthetic reservoirs with equal dimensionless numbers for 0.5% wt surfactant concentration

4.13d and 4.16d indicate that oil recovery occurred in a top-to-bottom pattern, that is, starting from the top layers through the bottom layers.

#### **4.6 Conclusions**

Extending the values of laboratory derived dimensionless groups to field scale implementation led to similar values of dimensionless oil recovery. There was a reasonable match between results measured for the core experiments and those obtained from numerical simulation of the synthetic cases. This is an indication that traditional dimensionless groups can predict field behavior from laboratory scale data when coupled with the gas relative permeability reduction model and foam reaction modeling that adequately describe the stoichiometry between surfactant and  $\text{CO}_2$ . History-matching was carried out to obtain similar trends with core results for pressure drop for the synthetic reservoirs. The history-matching process focused on adjusting *FM* parameters, so as to alter gas relative permeability. Obtaining an appropriate trend for pressure difference between core-scale modeling and the synthetic reservoirs was essential for meeting the condition that states that pressure should be preserved when scaling-up to field implementation (CMG (2012), Pujol and Boberg (1972), and Kimber and Farouq-Ali (1991)). This pressure difference was not obtained by scaling parameters suggested by previous authors. It was obtained with detailed history matching of the *MRF* and the parameters associated with modeling the generation and sustenance of foam.

The results obtained indicate that the degree of permeability contrast between layers has an important effect on injected fluid distribution. In reservoir *R3*, the higher permeability contrast between the layers resulted in the flow of foam through the high permeability layers, especially those found in the lower parts of the system, and  $\text{CO}_2$  was able to flow through the lower permeability zones. Coombe et al. (1997) report that in a steam-foam flood, the permeability contrast between top layers and other layers is an important factor that leads to additional oil recovery. They discovered that favorable conditions to generate and sustain foam were found in models with high permeability in the upper parts of the reservoir, and that models with normal permeability distribution are more affected by gravity segregation.



(a) Permeability distribution for R1

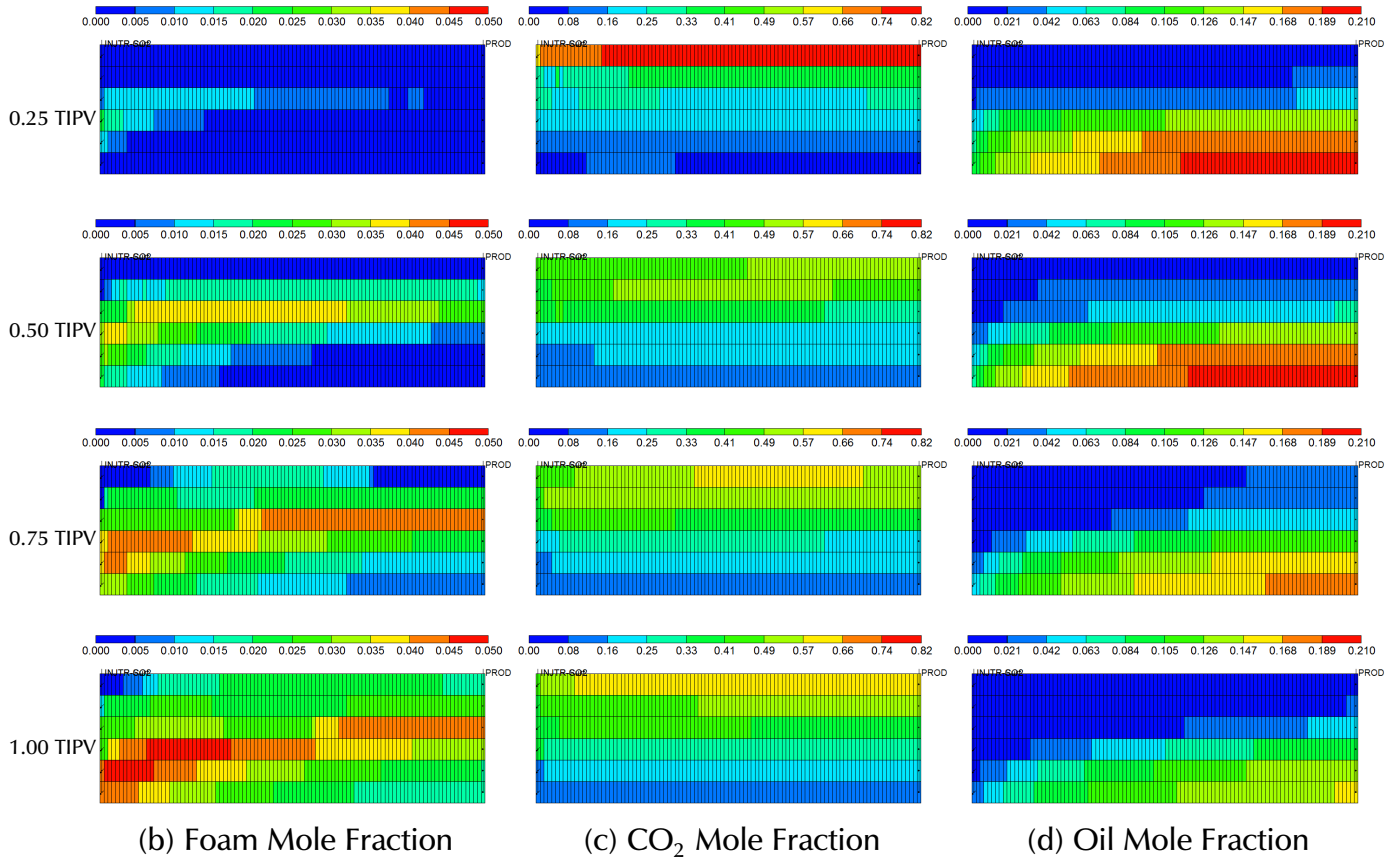
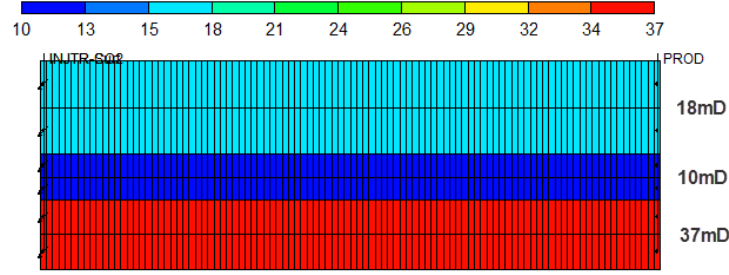


Figure 4.11: Property distribution for synthetic reservoir R1 during the co-injection of 0.1% wt surfactant solution and CO<sub>2</sub> showing (a) permeability distribution, and the global mole fraction of (b) foam, (c) CO<sub>2</sub>, and (d) oil, at 0.25, 0.50, 0.75 and 1.00 of total injected pore volume



(a) Permeability distribution for R2

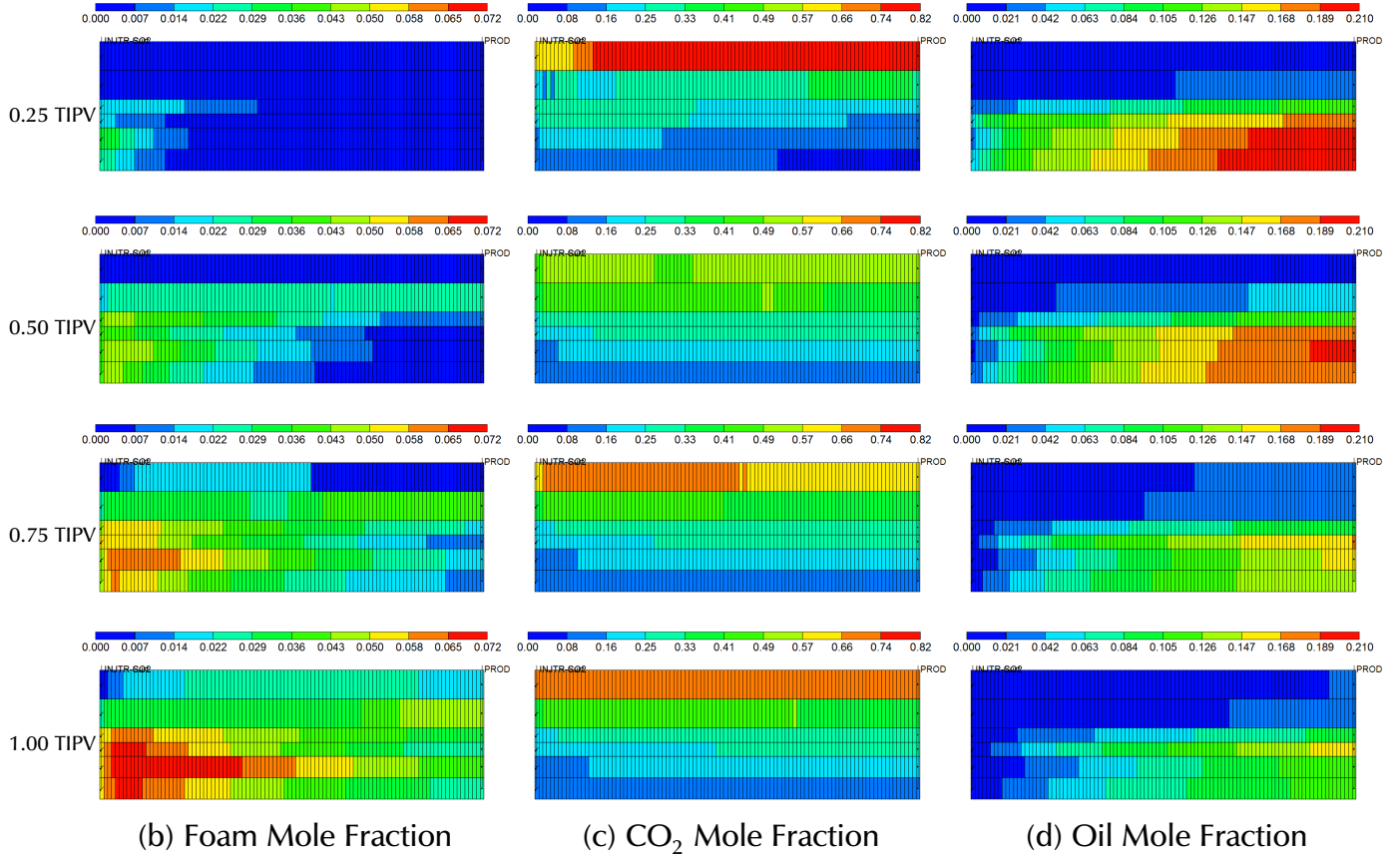
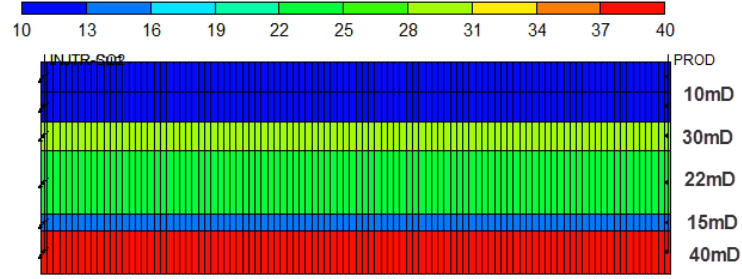


Figure 4.12: Property distribution for synthetic reservoir R2 during the co-injection of 0.1% wt surfactant solution and CO<sub>2</sub> showing (a) permeability distribution, and the global mole fraction of (b) foam, (c) CO<sub>2</sub>, and (d) oil, at 0.25, 0.50, 0.75 and 1.00 of total injected pore volume



(a) Permeability distribution for R3

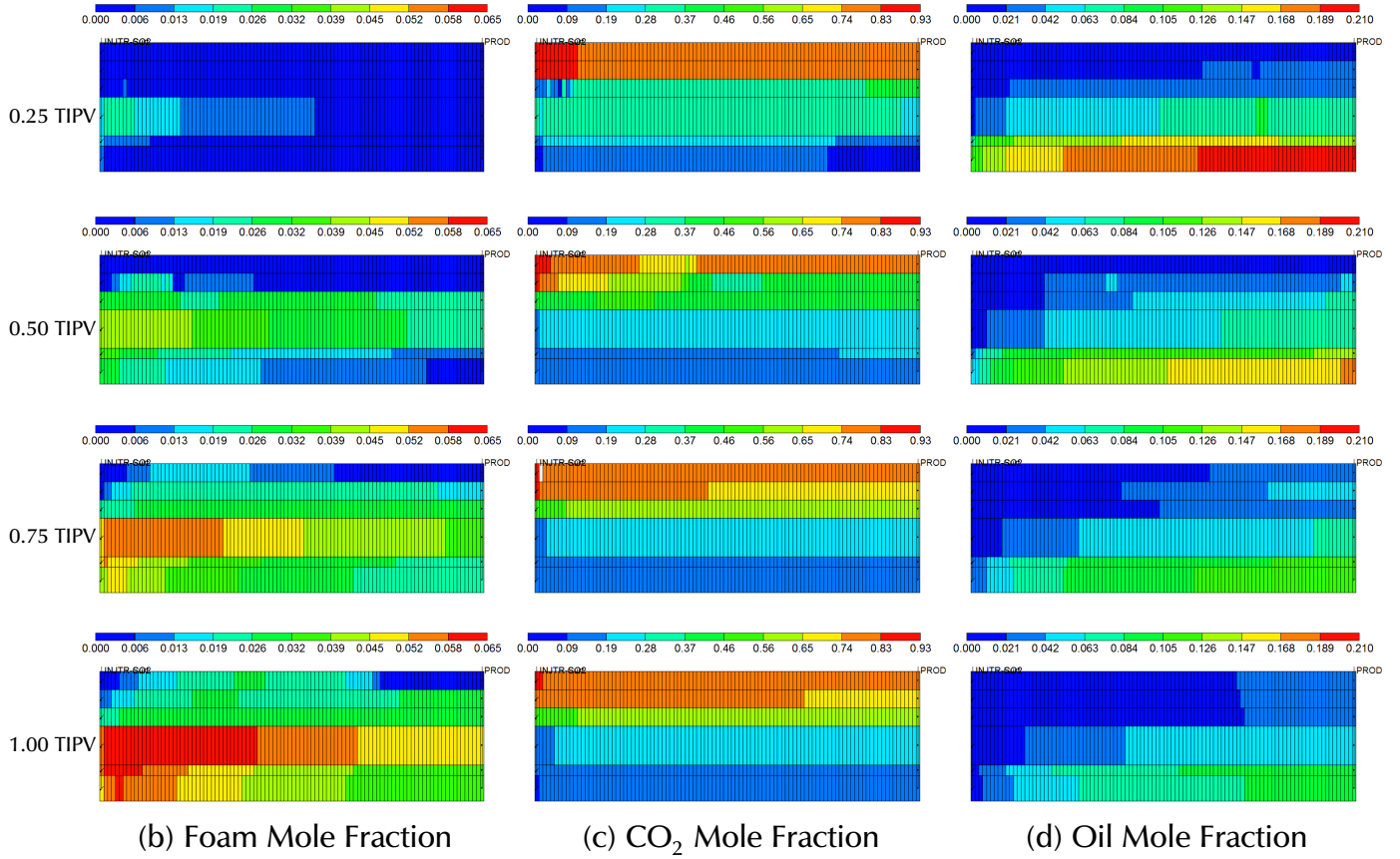
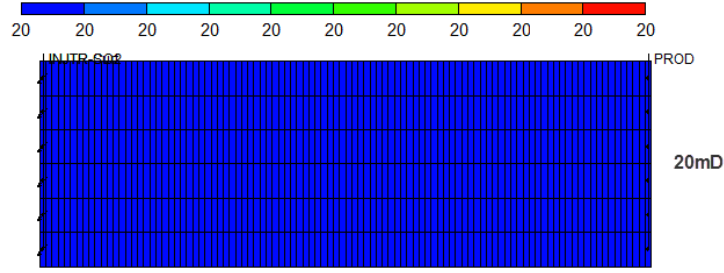


Figure 4.13: Property distribution for synthetic reservoir R3 during the co-injection of 0.1% wt surfactant solution and CO<sub>2</sub> showing (a) permeability distribution, and the global mole fraction of (b) foam, (c) CO<sub>2</sub>, and (d) oil, at 0.25, 0.50, 0.75 and 1.00 of total injected pore volume



(a) Permeability distribution for R1

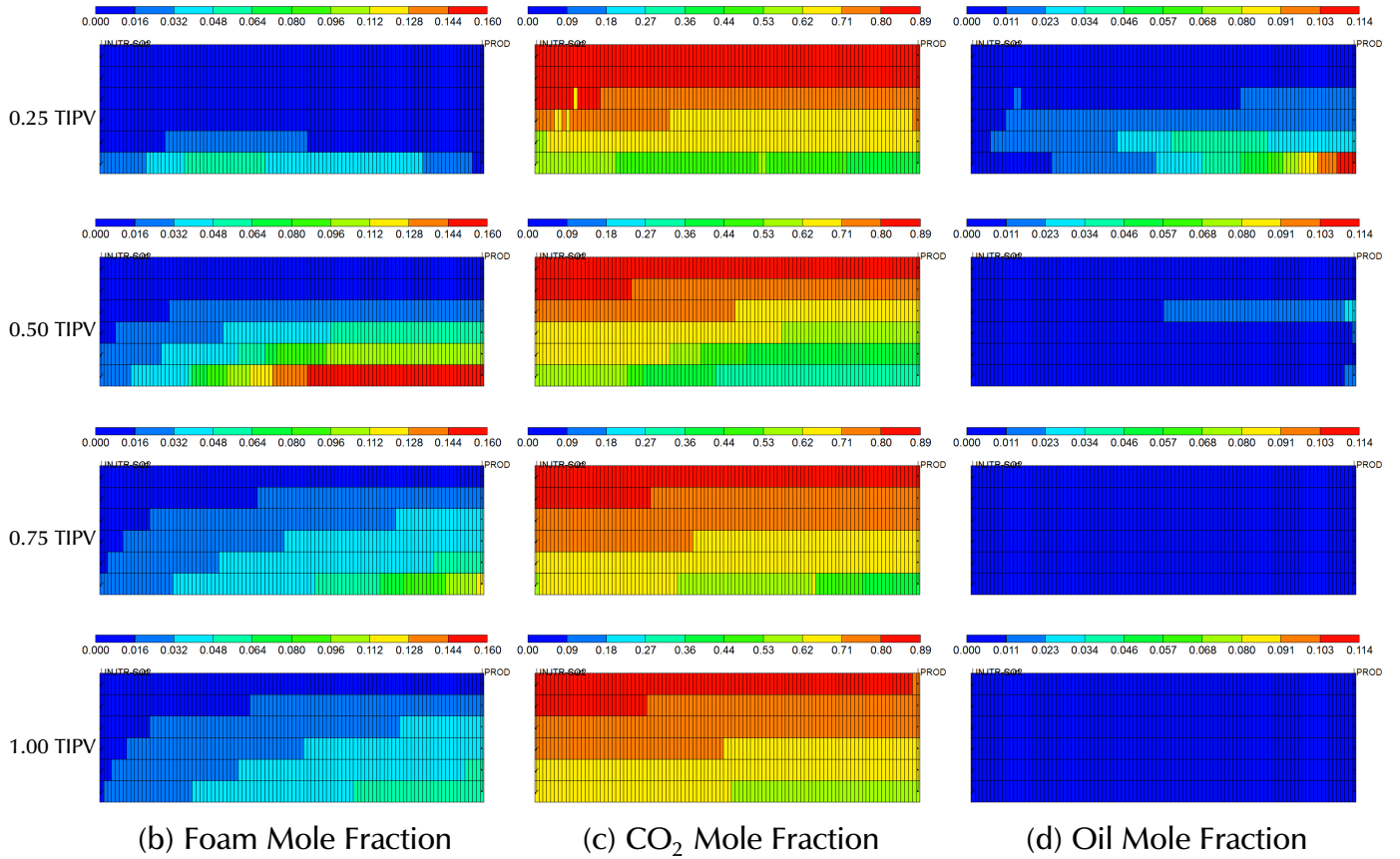
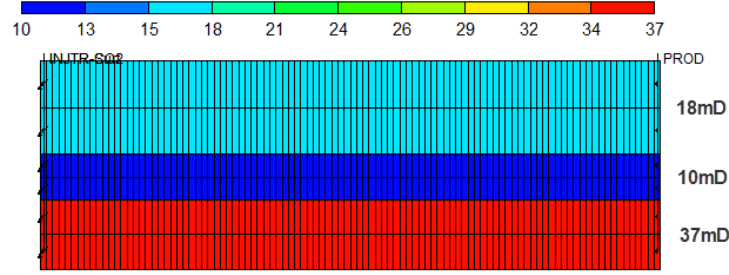


Figure 4.14: Property distribution for synthetic reservoir R1 during the co-injection of 0.5% wt surfactant solution and CO<sub>2</sub> showing (a) permeability distribution, and the global mole fraction of (b) foam, (c) CO<sub>2</sub>, and (d) oil, at 0.25, 0.50, 0.75 and 1.00 of total injected pore volume



(a) Permeability distribution for R2

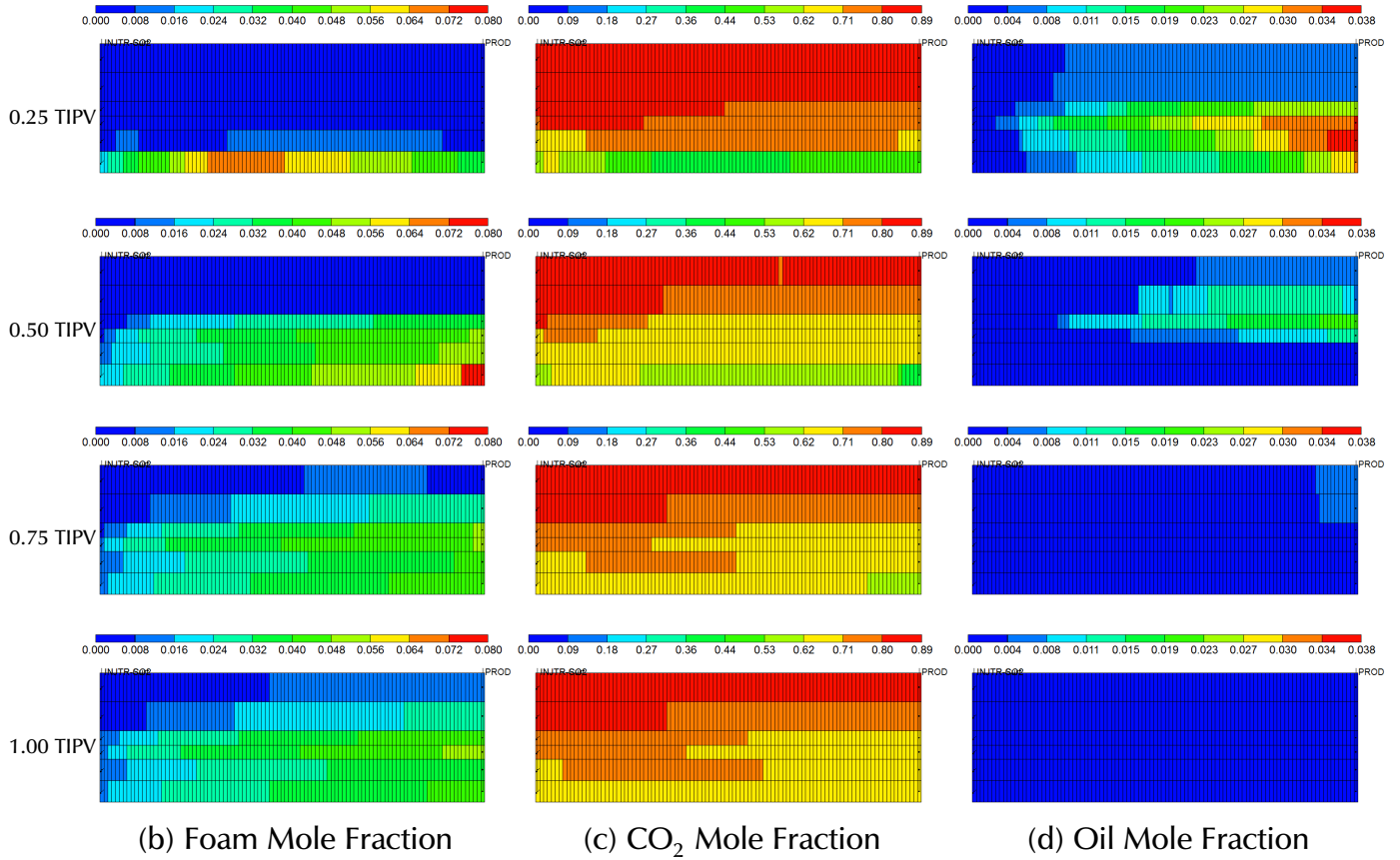
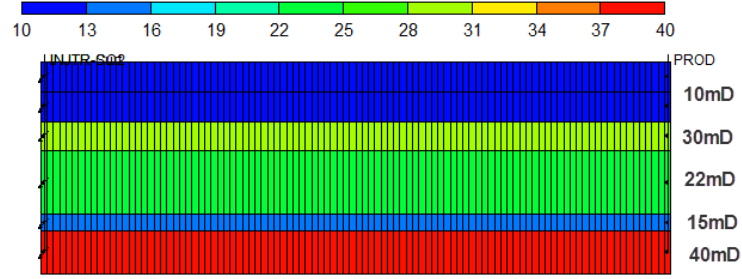


Figure 4.15: Property distribution for synthetic reservoir R2 during the co-injection of 0.5% wt surfactant solution and CO<sub>2</sub> showing (a) permeability distribution, and the global mole fraction of (b) foam, (c) CO<sub>2</sub>, and (d) oil, at 0.25, 0.50, 0.75 and 1.00 of total injected pore volume





(a) Permeability distribution for *R3*

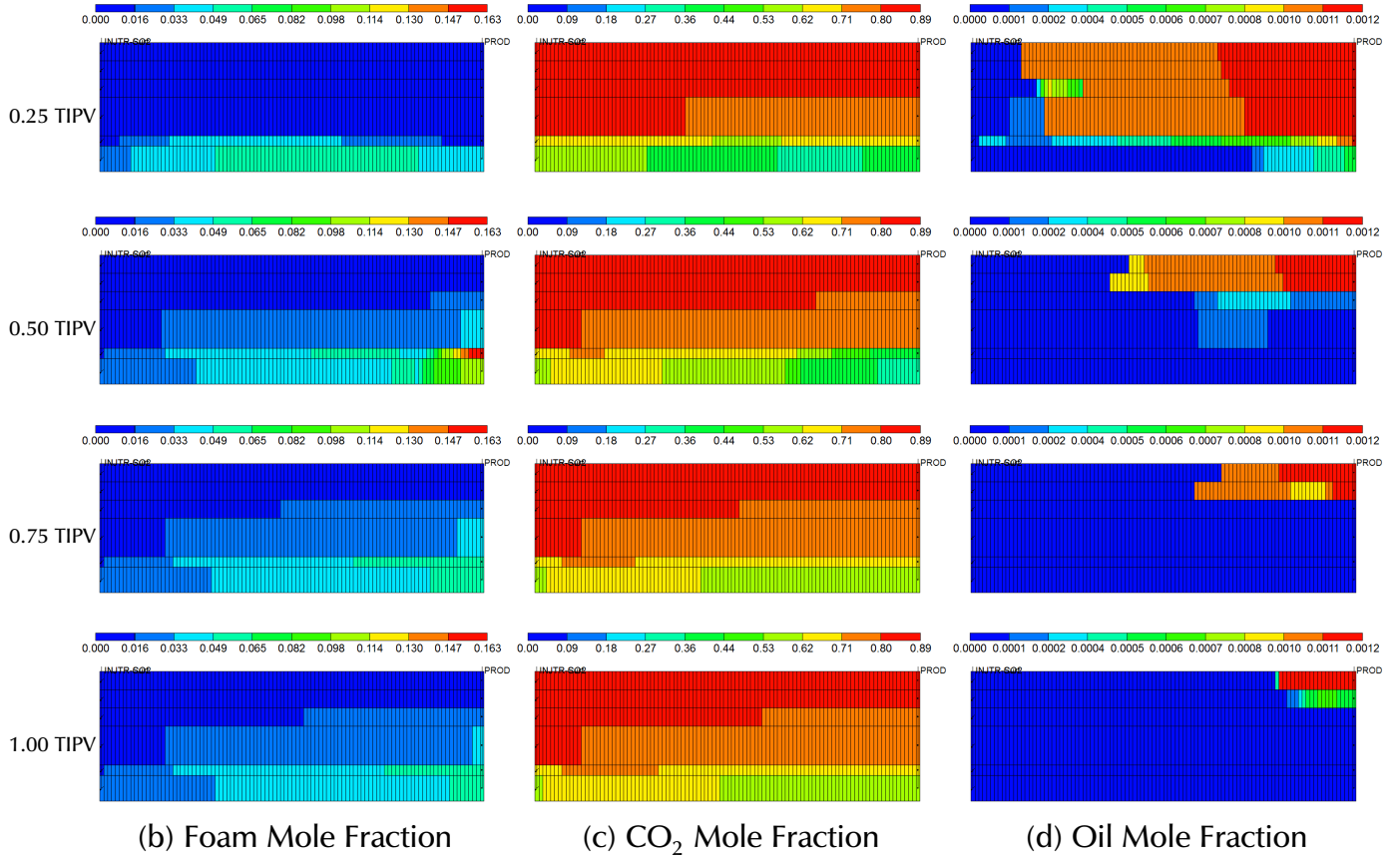


Figure 4.16: Property distribution for synthetic reservoir *R3* during the co-injection of 0.5% wt surfactant solution and  $\text{CO}_2$  showing (a) permeability distribution, and the global mole fraction of (b) foam, (c)  $\text{CO}_2$ , and (d) oil, at 0.25, 0.50, 0.75 and 1.00 of total injected pore volume

When pure CO<sub>2</sub> injection is carried out, the results tend to contradict the findings of this work. Greenkorn et al. (1965) investigated the challenges associated with scaling core-level miscible displacement to field scale. They found that recovery efficiency reduced as reservoir heterogeneity increased. Higher recovery efficiency was obtained from a homogeneous reservoir. Culpepper (1989) developed a one-dimensional, three-phase flow simulator with two of the phases (oleic and aqueous) being miscible and also found that an increase in permeability variation affected oil recovery. The generation of foam via the coinjection of CO<sub>2</sub> and surfactant, and its ability to act as a gas diverting agent is responsible for this contrast.

Yaghoobi et al. (1998) carried out research to investigate the effect of reservoir heterogeneity on CO<sub>2</sub> breakthrough during foam injection. They found that heterogeneity has a significant impact on foam flow, and they suggested that foam should be tested in heterogeneous systems to enable proper interpretation of its behavior in systems that appropriately describe reservoir conditions. It is therefore imperative to further analyze the impact of heterogeneity on pressure difference and oil recovery factor. This was carried out by incorporating the Dykstra-Parsons coefficient. The Dykstra-Parsons coefficient,  $V_{DP}$ , is a statistical measure of non-uniformity of a set of permeability distribution data (Dykstra and Parsons, 1950). More explanation on utilizing  $V_{DP}$  is provided in Chapter 5.

## 5 Design of Experiments

Design of Experiments (DoE) allow researchers to extract maximum information from a series of systematically conducted experiments or simulations to provide optimal information about the system. The use of DoE in this work will assist in developing a metamodel that is capable of predicting oil recovery performance and pressure difference for CO<sub>2</sub>-surfactant floods in field operations based on laboratory results. The metamodel will take into consideration, the effects of key parameters that enhance or hinder the successful implementation. Hoque (2010) defines a metamodel as a surrogate or substitute for a more complex and computationally intensive simulation model.

Zhang (2003) outlined the necessary steps that must be taken to develop a functioning predictive model. They are as follows:

1. selection of input variables and response variables
2. generating a sample of combinations for the input variables
3. running experiments for each combination in the sample to obtain corresponding responses
4. identifying influential variables
5. developing a response model that can be used as a metamodel with the ability to serve as a substitute for physical experiments

The dimensionless numbers derived previously served as input variables. Oil recovery and average pressure difference across the porous medium are considered as response variables. A Hammersley Sequence Sampling (HSS) design was used to generate and place sample points in the design space. These sample point where then used to model various reservoir scenarios.

### 5.1 Overview of Design of Experiments Methods

There are many designs available to generate a sample of combinations for input variables. These designs are mostly grouped under two categories: the classical design and the space

filling or modern design. In a classical design, it is believed that random errors exist in results measured during laboratory experiments. The classical design is mainly utilized in studies where randomness and non-repeatability are inherent. The errors present in classical designs do not exist in modern designs because the effect of randomness is minimized. Also, since modern designs are mainly utilized for computer simulations, the problems associated with non-repeatability is reduced (Giunta et al., 2003).

#### **5.1.1 Classical Design of Experiments**

Random variations that exist in physical experiments are accounted for by spreading the sample points around the design space and by taking replicates so as to allow an estimate of the random error independent of any lack of fit error (Simpson et al., 2001; NIST/SEMATECH, 2003). Examples of common classical designs include Box-Behnken designs, factorial designs (full and fractional), and central composite designs.

#### **5.1.2 Modern Design of Experiments**

The application of modern or space filling designs is based on the fact that there are no random errors during deterministic computer experiments. Hence, there is no need for replications and randomizations and sample points can be placed in the interior of the design space. Simpson et al. (2001) compared 4 types of space filling experimental designs to determine which strategy generates the most accurate and reliable approximations of complex engineering analysis. These designs include: Latin hypercubes, Hammersley Sequence Sampling, orthogonal arrays, and uniform designs. They concluded that Hammersley Sequence Sampling yielded more accurate approximations and proved to be a more effective method when using large sample sizes. Other researchers that have implemented Hammersley Sequence Sampling include: Diwekar and Kalagnanam (1996), Wong et al. (1997), Rafajlowicz and Schwabe (2006), Kalla (2008), and Hoque (2010).

### **5.2 Methodology**

Building a model to predict oil recovery factor and pressure difference required the establishment of minimum and maximum values for the previously utilized dimensionless parameters.

Minimum and maximum values for all dimensionless parameters except  $R_L$ , were selected by applying surfactant concentration as endpoints and using two values that corresponded with the values derived from laboratory experiments. This ensured that the selected endpoints fell within physically possible ranges. For  $R_L$ , the minimum and maximum values were determined by selecting two values whose mean equaled the values derived from laboratory experiments.

In order to analyze the impact of surfactant concentration on oil recovery factor and pressure difference, dimensionless surfactant concentration  $c_{surf}$  was added as a parameter. Surfactant concentration ranged from 0.1% wt to 0.5% wt.

An additional dimensionless factor, the Dykstra-Parsons Coefficient,  $V_{DP}$ , was included as an additional input variable to account for reservoir heterogeneity. It is defined as:

$$V_{DP} = \frac{k_{0.5} - k_{0.84}}{k_{0.5}} \quad (5.1)$$

where,

$k_{0.5}$  : median of the permeability

$k_{0.84}$  : one standard deviation in permeability below the median

The minimum and maximum values shown in Table 5.1 set the endpoints for the design space that will contain the sampling points. Values for  $V_{DP}$  range from 0 to 1, with 0 representing a completely homogeneous system, and 1 for a completely heterogeneous reservoir. In this study, minimum and maximum values for  $V_{DP}$  were chosen as 0.1 and 0.8 respectively.

A two-dimensional reservoir model with 100 gridblocks was used in the simulator. Parameters in the gas relative permeability reduction model and foam generation and sustenance model were obtained by interpolating between the results derived from the history-match of laboratory experiments for the 0.1% wt and 0.5% wt surfactant solution. Other parameters that were obtained from interpolation include: CO<sub>2</sub> viscosity, endpoint relative permeability for the second set of curves (foam present), and the wetting and nonwetting phase interpolation parameter for relative permeability data ( $DTRAPW$  and  $DTRAPN$ , respectively). The

dimensional parameters calculated from the dimensionless groups and used as input in the reservoir simulator are presented in Appendix C (Tables C.3, C.4, C.5, and C.6).

A simple MATLAB code based on Hammersley Sequence Sampling was used to generate the sampling points with values between 0 and 1 that consisted of 128 cases for the 9 dimensionless parameters. The MATLAB code is shown in Appendix D. The end points of the dimensionless numbers were interpolated with the raw design space to obtain intermediate values. Table C.1 shows the raw Hammersley Sequence Sampling space, while Table C.2 shows the actual values that were used for modeling.

Table 5.1: Minimum and maximum values for 9 dimensionless numbers

Groups	Min	Max
$R_L$	1.5	4.5
$M_{go}$	8.6	14.5
$N_{cap(ow)}$	$2.43 \times 10^{-6}$	$2.90 \times 10^{-6}$
$N_{G(og)}$	$4.19 \times 10^7$	$4.93 \times 10^7$
$N_{G(wo)}$	$2.66 \times 10^8$	$3.13 \times 10^8$
$V_{DP}$	0.1	0.8
$N_{pe(Lo1)}$	69	585
$N_{pe(To1)}$	245	2080
$c_{surf}$	0.1	0.5

### 5.2.1 Permeability Distribution

The permeability distribution used for each case was generated using a method outlined by Hirasaki (1984) and El-Khatib (2011). Permeability distribution of stratified, heterogeneous reservoirs are characterized by a log-normal distribution as:

$$p(k) = 1/2 \left( 1 + \left[ \frac{\ln(k/k_m)}{\sqrt{2}\sigma_k} \right] \right) \quad (5.2)$$

The term  $p(k)$ , which is the cumulative probability function, represents the fraction of the number of layers with permeability that is less than  $k$ . The term,  $k_m$ , is the mean permeability value of a particular system and  $\sigma_k$  is the standard deviation of the distribution. The relationship between  $\sigma_k$  and  $V_{DP}$  is:

$$\sigma_k = \ln \left[ \frac{1}{1 - V_{DP}} \right] \quad (5.3)$$

Permeability of a particular layer can be calculated from Equation 5.2:

$$k = k_m e^{\sqrt{2}\sigma_k \text{erf}^{-1}(1-2p(k))} \quad (5.4)$$

$$\ln(k) = \ln(k_m) + \sqrt{2}\sigma_k \text{erf}^{-1}(1-2p(k)) \quad (5.5)$$

Equation 5.5 can be represented by the equation of a straight line, which is of the form:

$$y = mx + b \quad (5.6)$$

with,

$$y = \ln(k)$$

$$x = \text{erf}^{-1}[1-2p(k)]$$

$$m = \sqrt{2}\sigma_k$$

$$b = \ln(k_m)$$

With a given value of  $V_{DP}$ , the standard deviation,  $\sigma_k$ , was calculated using Equation 5.3. The slope,  $\sqrt{2}\sigma_k$ , and the x-term,  $\text{erf}^{-1}[1-2p(k)]$  were then estimated. Values for  $k$  were generated for the cumulative probability function with values drawn randomly from a uniform distribution between 0 and 1.

### 5.2.2 Application of Regression Analysis

Regression Analysis is used to model and analyze the relationship between dependent and explanatory or independent variables. In this work, Regression Analysis was used to understand the nature of the relationship between the input variables, the dimensionless groups, and the system response via oil recovery factor and pressure difference. Regression was also used to generate a model that can predict oil recovery factor and pressure difference at locations not included within the sample space.

Two regression models, linear and pure quadratic, were analyzed in this work. They are respectively described by the following equations:

$$y = \beta_0 + \beta_1 x_1 + \beta_2 x_2 + \dots \beta_k x_k + \varepsilon, \quad \text{with } j = 1 \dots k \quad (5.7)$$

where,

$y$  : response variable

$x_j$  : regressors

$\beta_0$  : constant term or intersection

$\beta_j$  : regression coefficient of regressor

$\varepsilon$  : error term

$$y = \beta_0 + \beta_{l1}x_1 + \beta_{l2}x_2 + \dots\beta_{lk}x_k + \beta_{q1}x_1^2 + \beta_{q2}x_2^2 + \dots\beta_{qk}x_k^2 + \varepsilon, \quad \text{with } lj = qj = 1\dots k \quad (5.8)$$

where,

$y$  : response variable

$x_j$  : regressors

$\beta_0$  : constant term or intersection

$\beta_{lj}$  : linear term regression coefficient of regressor

$\beta_{qj}$  : quadratic term regression coefficient of regressor

$\varepsilon$  : error term

Regression Analysis was applied to the simulation results of the 128 cases that were developed using the Hammersley Sampling Sequence. The response variables studied were chosen to be oil recovery factor and pressure difference.

### 5.3 Results

The sampling points for the dimensionless groups utilized in the simulation models that were used to develop the models are shown in Tables C.1 and C.2. The dimensional properties required to obtain the dimensionless numbers were calculated and are shown in Tables C.3, C.4, C.5, and C.6. Initially, while carrying out some preliminary runs to gain some perspective on the nature of expected results, flow rates that corresponded with the velocity used in



the laboratory (approximately  $1.0\text{ft/day}$ ) were utilized. About 80% of the simulation runs failed, and flow rates were thereby reduced, along with other associated variables to keep the dimensionless numbers constant.

Table C.7 shows the values of oil recovery factor,  $RF$ , and differential pressure,  $\Delta p$ , obtained from the simulation runs for the 128 cases at the end of injection of  $8.0PV$  of surfactant solution and  $\text{CO}_2$ . The mean and standard deviation of the input and output parameters used to regression modeling are shown in Table 5.2.

Table 5.2: Basic descriptive statistics of input and output variables used in Experimental Design

Parameter	Mean	Std. Deviation
$RF$	0.6075	0.2119
Maximum $\Delta p$	130.5228	98.7821
$N_{pe(Lo1)}$	327.0000	150.7145
$N_{pe(To1)}$	1158.9301	537.9924
$R_L$	2.9890	0.8763
$M_{go}$	11.1087	1.7098
$N_{cap(ow)}$	$2.66 \times 10^{-6}$	$1.39 \times 10^{-7}$
$N_{G(og)}$	$4.55 \times 10^7$	$2.17 \times 10^6$
$N_{G(wo)}$	$2.90 \times 10^8$	$1.40 \times 10^7$
$V_{DP}$	0.4405	0.2079
$c_{surf}$	0.2963	0.1180

Linear and quadratic regression analysis were used to create models that were analyzed in order to determine the metamodel that provides the best fit for predicting oil recovery factor,  $RF$ , and pressure difference,  $\Delta p$ . For both  $RF$  and  $\Delta p$ , the quadratic regression model provided a slightly better fit than the linear model when actual values were compared with regressed values. The coefficients for calculating oil recovery factor and pressure difference obtained from linear and quadratic regression analysis are shown in Tables 5.3 and 5.4 respectively.

When carrying out an actual reservoir study, the coefficients obtained from the regression models, and thus the dimensionless numbers with the greatest or least impact might change based on the nature or environment of the model being analyzed. Also, response or dependent variables that appropriately describe the objectives of a particular field study can be selected.

R-squared values shown in Table 5.5 and the plots presented in Figures 5.1a, 5.1b, 5.2a, and 5.2b explain the relationship and fit between measured and regressed values of  $RF$  and  $\Delta p$ . The graphs presented show a very close fit for  $RF$  and a reasonable fit for  $\Delta p$ . This is an indication that the dimensionless groups utilized in this study provide better accuracy at predicting  $RF$  than they do for  $\Delta p$ . The fit obtained for maximum  $\Delta p$  is not as good as that calculated for  $RF$  because  $\Delta p$  is a dynamic variable that changes within each grid block with respect to time and has an additional difficulty in that it relies on the foam modeling parameters that are known to be very sensitive to small changes in parameter values. This continuous change is prone to fluctuations that ultimately affect the regression model. On the other hand,  $RF$  is a cumulative variable that is less prone to fluctuations.

Table 5.3: The coefficients for oil recovery factor and pressure difference obtained from linear regression analysis

Parameter	Symbol	$RF$ Coefficients	$\Delta p$ Coefficients
Intercept	$\beta_0$	1.917	-550.732
$N_{pe(Lo1)}$	$\beta_1$	$1.09 \times 10^{-4}$	$3.39 \times 10^{-2}$
$N_{pe(To1)}$	$\beta_2$	$-4.09 \times 10^{-5}$	$2.85 \times 10^{-3}$
$R_L$	$\beta_3$	$1.02 \times 10^{-2}$	-4.761
$M_{go}$	$\beta_4$	-0.11	33.345
$N_{cap(ow)}$	$\beta_5$	-3710.852	$4.54 \times 10^7$
$N_{G(og)}$	$\beta_6$	$1.22 \times 10^{-9}$	$4.64 \times 10^{-8}$
$N_{G(wo)}$	$\beta_7$	$2.92 \times 10^{-10}$	$-3.05 \times 10^{-7}$
$V_{DP}$	$\beta_8$	-0.457	-113.738
$c_{surf}$	$\beta_9$	-0.133	1123.729

### 5.3.1 Validation of the Regression Model

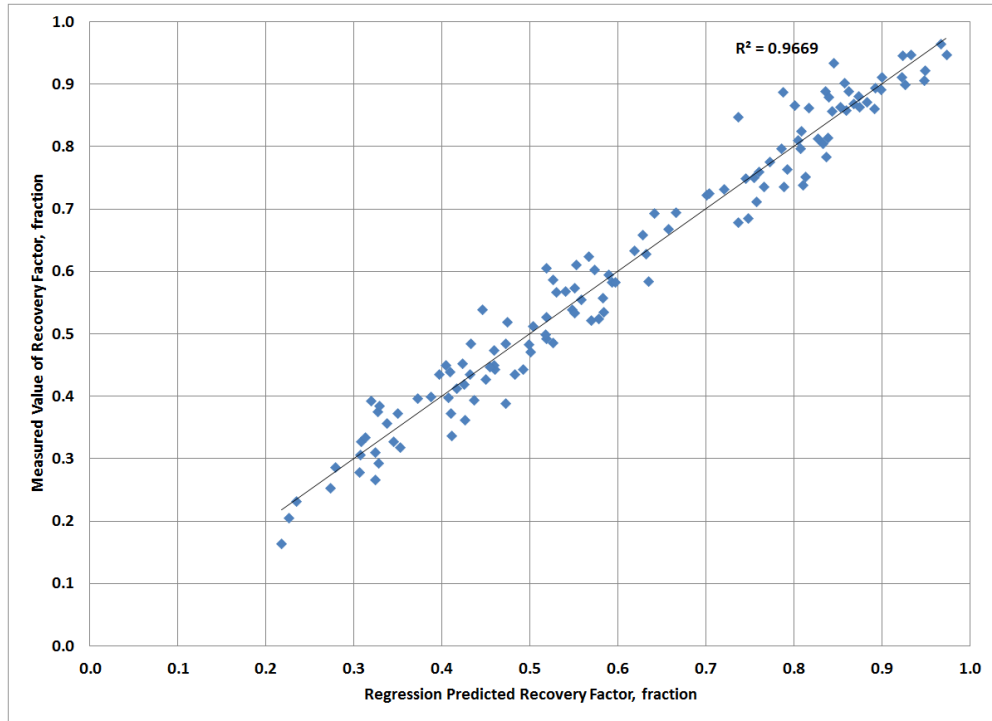
The linear and quadratic models were used to predict  $RF$  and  $\Delta p$  for 32 sample reservoirs for validation purposes. For parameters like  $R_L$ ,  $M_{go}$ ,  $N_{cap(ow)}$ ,  $N_{G(og)}$ ,  $N_{G(wo)}$ ,  $N_{pe(Lo1)}$ , and  $N_{pe(To1)}$ , the minimum and maximum values of the dimensionless numbers were extended beyond those used to develop the regression models. This was done to include some variance in the output. Minimum and maximum values of the dimensionless parameters are presented in Table 5.6. Table C.8 shows values of the dimensionless parameters utilized in the prediction cases. Tables C.9, C.10, C.11, and C.12 show the values of dimensional variables that were

Table 5.4: The coefficients for oil recovery factor and pressure difference obtained from quadratic regression analysis

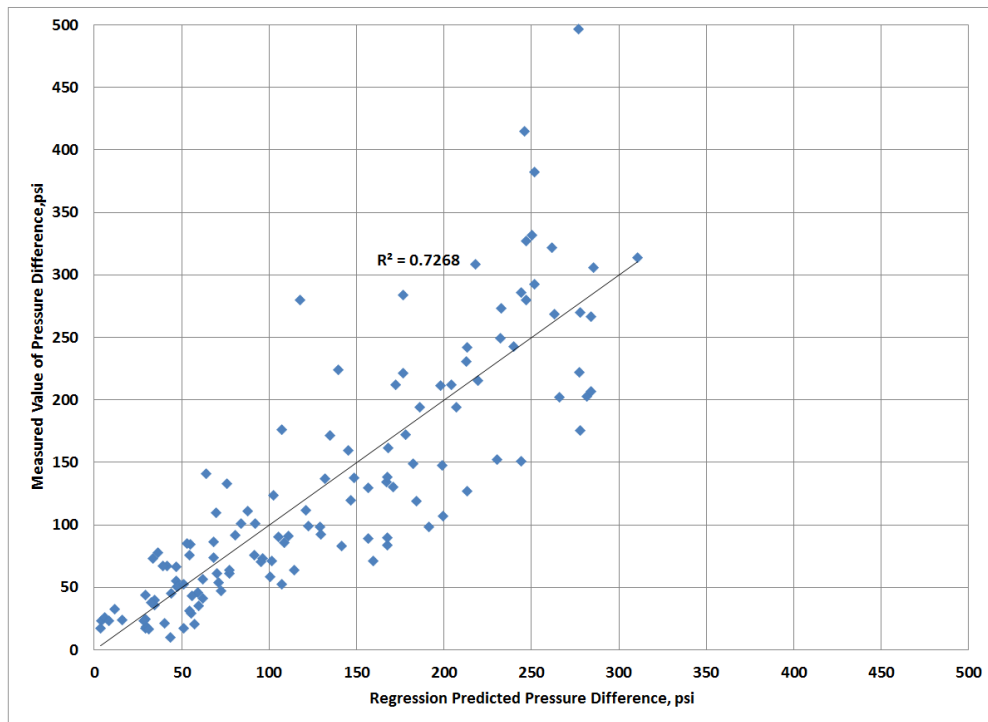
Parameter	Symbol	RF Coefficients	$\Delta p$ Coefficients
Intercept	$\beta_0$	57.379	$-6.68 \times 10^4$
$N_{pe(Lo1)}$	$\beta_1$	$3.55 \times 10^{-4}$	0.12
$N_{pe(To1)}$	$\beta_2$	$-1.51 \times 10^{-4}$	$40.5 \times 10^{-2}$
$R_L$	$\beta_3$	$4.62 \times 10^{-2}$	-1.174
$M_{go}$	$\beta_4$	-5.034	6393.852
$N_{cap(ow)}$	$\beta_5$	$4.71 \times 10^5$	$8.71 \times 10^8$
$N_{G(og)}$	$\beta_6$	$4.51 \times 10^{-8}$	$-8.64 \times 10^{-5}$
$N_{G(wo)}$	$\beta_7$	$-1.31 \times 10^{-8}$	$-1.04 \times 10^{-5}$
$V_{DP}$	$\beta_8$	-0.408	119.132
$c_{surf}$	$\beta_9$	-54.45	$6.41 \times 10^4$
$N_{pe(Lo1)}^2$	$\beta_{10}$	$-3.75 \times 10^{-7}$	$-1.31 \times 10^{-4}$
$N_{pe(To1)}^2$	$\beta_{11}$	$4.76 \times 10^{-8}$	$-1.91 \times 10^{-5}$
$R_L^2$	$\beta_{12}$	$-6.07 \times 10^{-3}$	-0.667
$M_{go}^2$	$\beta_{13}$	0.101	-141.523
$N_{cap(ow)}^2$	$\beta_{14}$	$-8.89 \times 10^{10}$	$-1.55 \times 10^{14}$
$N_{G(og)}^2$	$\beta_{15}$	$-4.86 \times 10^{-16}$	$9.52 \times 10^{-13}$
$N_{G(wo)}^2$	$\beta_{16}$	$2.30 \times 10^{-17}$	$1.75 \times 10^{-14}$
$V_{DP}^2$	$\beta_{17}$	$-7.19 \times 10^{-2}$	-259.537
$c_{surf}^2$	$\beta_{18}$	27.677	$-2.94 \times 10^4$

Table 5.5: R Squared values for linear and quadratic regression models

Model	R Square
Linear RF	0.9669
Linear $\Delta p$	0.7268
Quadratic RF	0.9752
Quadratic $\Delta p$	0.7467

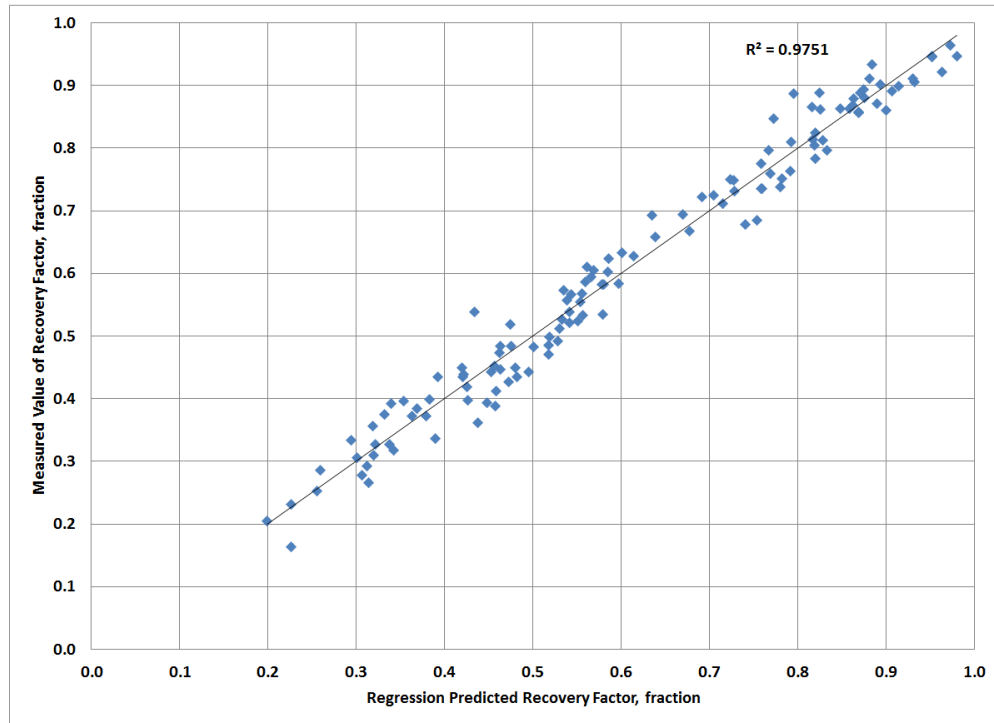


(a) Linear regression for  $RF$

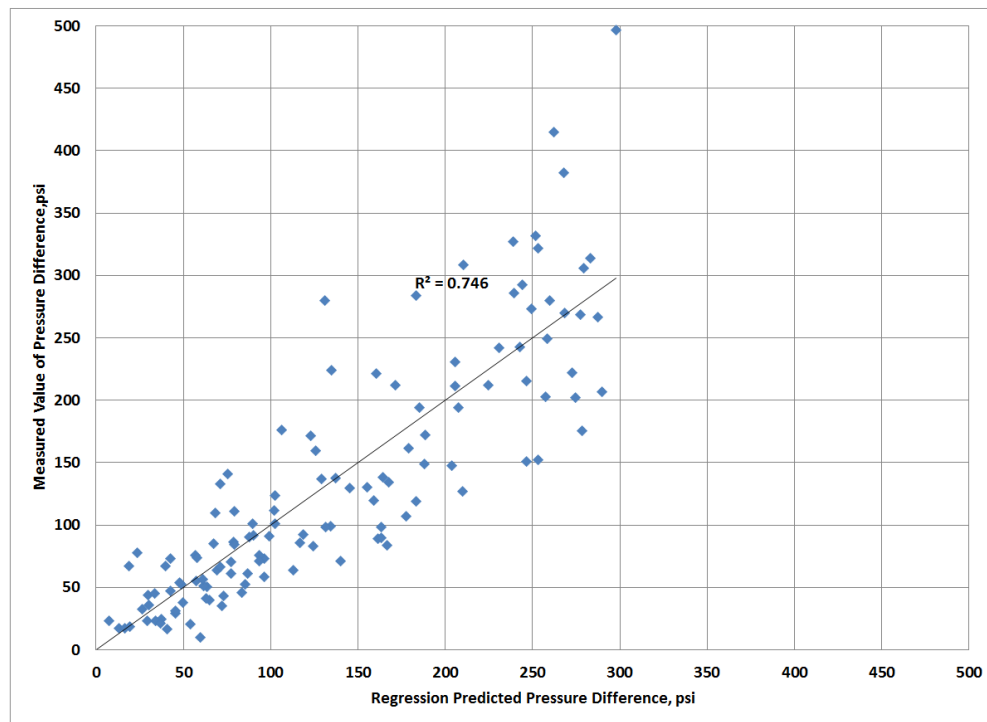


(b) Linear regression for  $\Delta p$

Figure 5.1: Scatter plot comparing measured and predicted  $RF$  and  $\Delta p$  for linear models



(a) Quadratic regression for  $RF$



(b) Quadratic regression for  $\Delta p$

Figure 5.2: Scatter plot comparing measured and predicted  $RF$  and  $\Delta p$  for quadratic models

used as input to the reservoir simulator. These values were calculated from the dimensionless parameters. The predicted results of  $RF$  and  $\Delta p$  are presented in Table C.13.

R-squared values obtained from the prediction data are shown in Table 5.7. Scatter plots showing the degree of fit between the actual and predicted values for  $R_L$  and  $\Delta p$  for the validation set are presented in Figures 5.3a, 5.3b, 5.4a, and 5.4b.

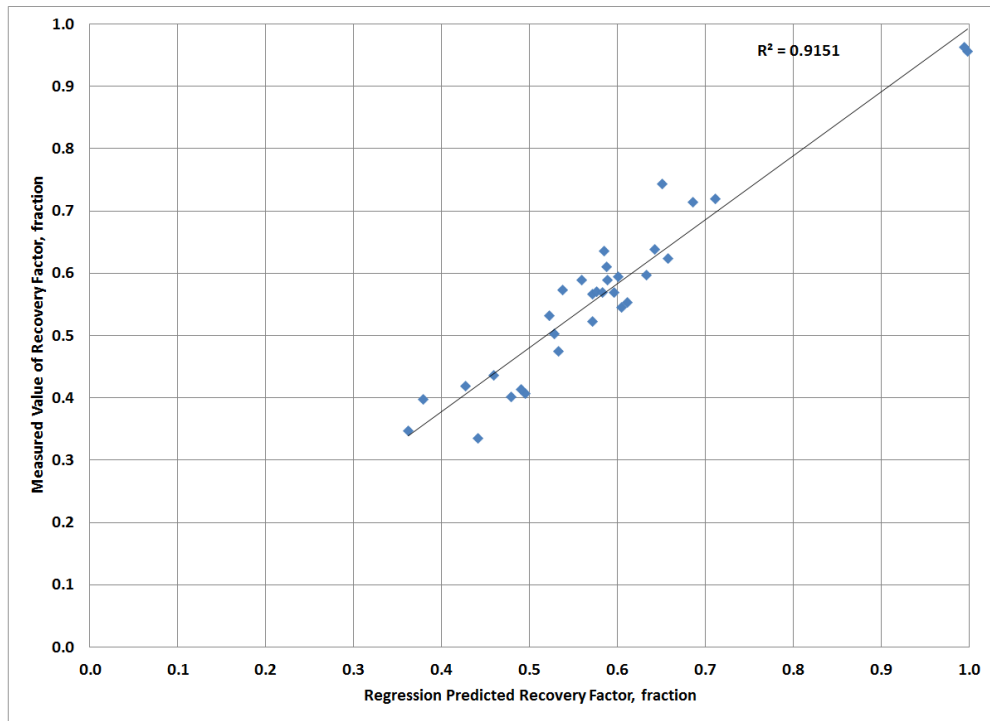
The linear regression model provided better results when compared to those obtained from the quadratic model. The lower values of R-squared obtained for the validation model, as compared to those obtained in the development model, are as a result of the extension of the minimum and maximum values of some of the dimensionless parameters. The linear model shows a very strong relationship for  $RF$  and an acceptable fit for  $\Delta p$ . In comparison to the linear model, the quadratic regression is unacceptable.

Table 5.6: Minimum and maximum values for dimensionless numbers for regression model validation

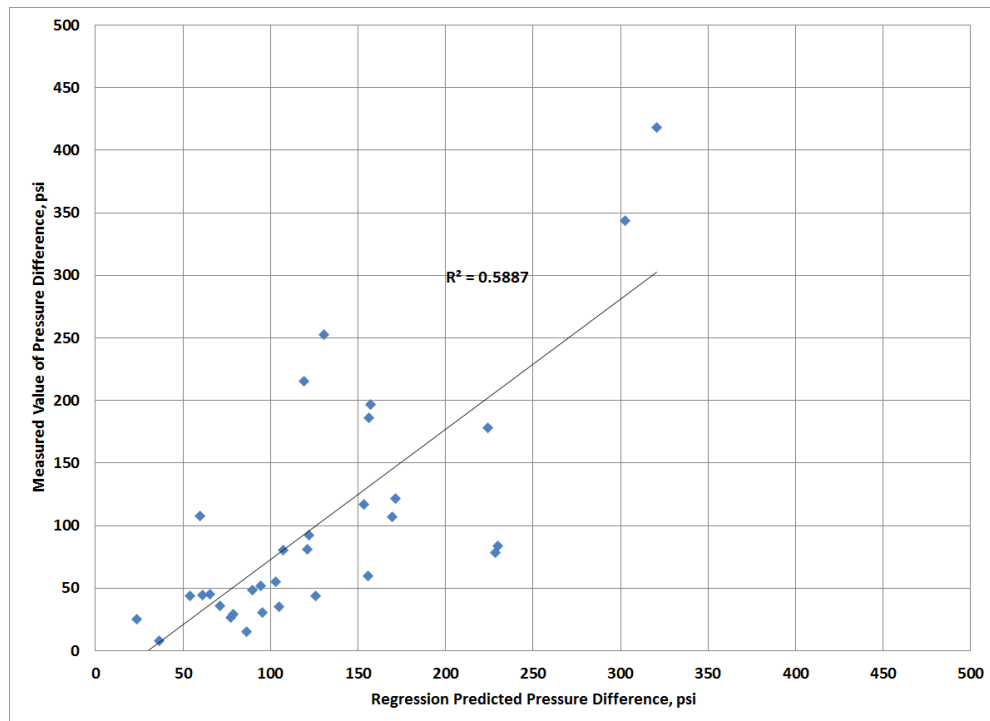
Groups	Min	Max
$R_L$	2	6
$M_{go}$	6	16
$N_{cap(ow)}$	$2.00 \times 10^{-6}$	$3.50 \times 10^{-6}$
$N_{G(og)}$	$3.50 \times 10^7$	$5.50 \times 10^7$
$N_{G(wo)}$	$2.00 \times 10^8$	$3.50 \times 10^8$
$V_{DP}$	0.1	0.8
$N_{pe(Lo1)}$	50	700
$N_{pe(To1)}$	200	2500
$c_{surf}$	0.1	0.5

Table 5.7: R Squared values for linear and quadratic regression models

Model	R Square
Linear $RF$	0.9151
Linear $\Delta p$	0.5887
Quadratic $RF$	0.4035
Quadratic $\Delta p$	0.3792

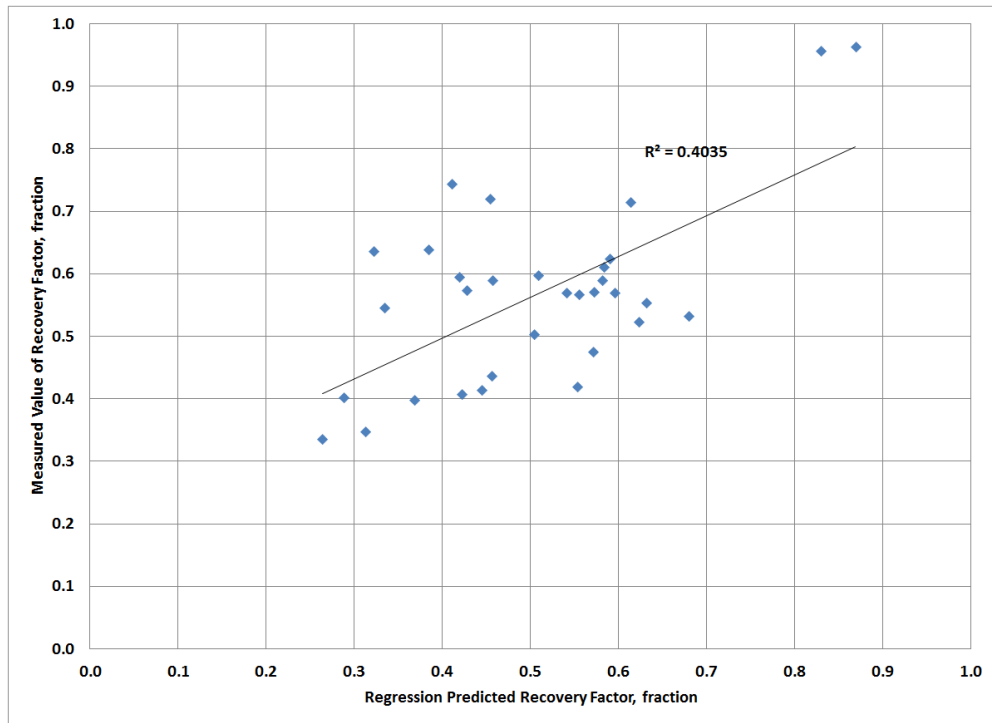


(a) Linear regression for  $RF$

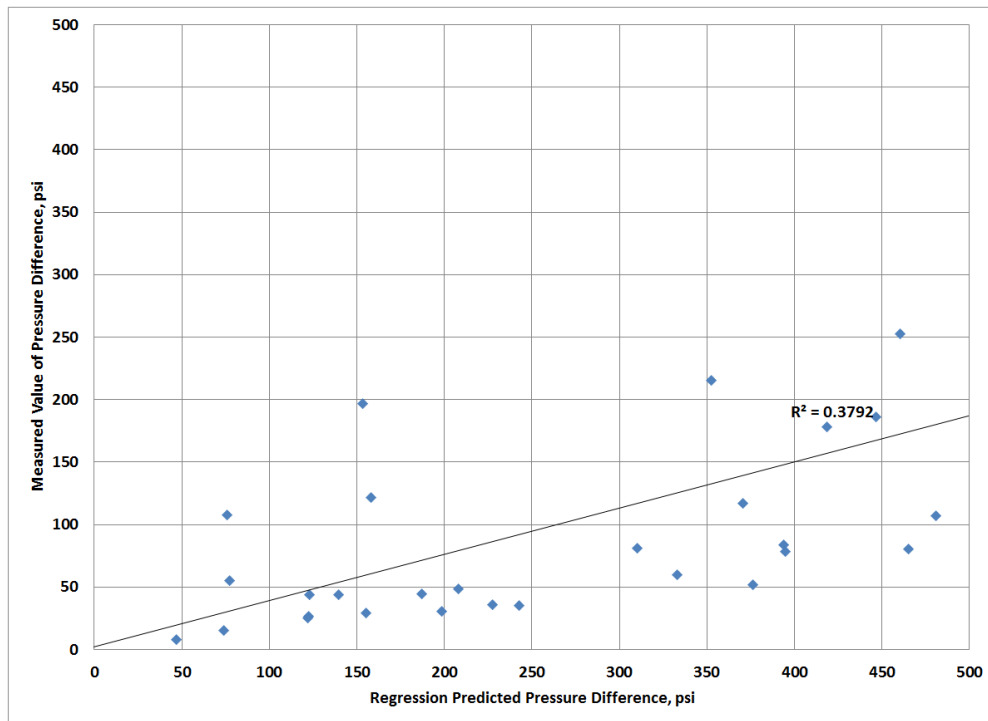


(b) Linear regression for  $\Delta p$

Figure 5.3: Scatter plot comparing measured and predicted  $RF$  and  $\Delta p$  for sample linear models



(a) Quadratic regression for  $RF$



(b) Quadratic regression for  $\Delta p$

Figure 5.4: Scatter plot comparing measured and predicted  $RF$  and  $\Delta p$  for sample quadratic models



### 5.3.2 Summary

Key dimensionless numbers that describe the behavior of surfactant-CO<sub>2</sub> injection are used to create a prediction model. Hammersley Sequence Sampling was used to generate a design space with 128 samples that was transformed to actual data by interpolating between the minimum and maximum values of the dimensionless parameters. The dimensionless numbers were used to calculate dimensional values that served as inputs to the simulator. Results from the simulation, recovery factor,  $RF$ , and pressure difference,  $\Delta p$ , along with the dimensionless numbers, were used to create a metamodel that can be used for prediction. To validate the model, 32 cases were tested and good results were obtained.

## 6 Conclusions and Recommendations

### 6.1 Conclusions

The noteworthy contributions of this study include the development of an appropriate methodology to carry out a history-match process for surfactant solution and CO<sub>2</sub> coinjection, validating the efficiency of traditional dimensionless numbers when applied to scaling from a laboratory model to field size, and the development of a model that can predict the behavior of a surfactant-CO<sub>2</sub> injection process based on dimensionless numbers. The major conclusions of this research are summarized below.

- Dimensionless numbers were developed using Inspectional Analysis (IA) and Dimensional Analysis (DA). In all, 45 dimensionless numbers were initially obtained. This number was reduced to 8 after eliminating groups that will have little or no impact (based on the nature of the relationship between some of the components and their predominant phase(s)) on the system being studied.
- Coreflood experiments were carried out and the results obtained provided information on the interaction of CO<sub>2</sub>, oil, brine and surfactant in porous media. The sequence of experiments are as follows: pore volume and porosity determination; absolute permeability measurement; oil flood to determine irreducible water and initial oil saturations, and endpoint relative permeability of oil in the presence of water; waterflood to calculate residual oil and initial water saturations, and endpoint permeability of water in the presence of oil; and, the simultaneous injection of CO<sub>2</sub> and, first, brine, and subsequently, 1.0 % wt surfactant solution to determine Mobility Reduction Factor (*MRF*). Finally, surfactant solution with 0.1 % wt and 0.5 % wt concentration was coinjected with CO<sub>2</sub> to generate foam, and displace oil.
- Experimental results show that a higher surfactant concentration yields a corresponding increase in pressure difference across the core, and hence more reduction in the residual oil saturation after waterflood. The simultaneous injection of CO<sub>2</sub> and surfactant solution

is effective in improving sweep efficiency in both homogeneous and heterogeneous systems.

- Borchardt et al. (1985), Yin et al. (2009), Bian et al. (2012) and Emadi et al. (2012) have conducted experimental studies to understand the mechanism of foam generation and propagation from CO<sub>2</sub> and surfactant solution in the presence of oil. The findings reported by these researchers were based solely on laboratory investigations as they did not utilize numerical simulation to further understand the behavior of their respective systems. One researcher, Ren (2012b), used history-matching to relate surfactant transport properties measured during core experiments to a simulator-derived *MRF*. While very good matches were obtained, Ren (2012b) reported that each of the fitted parameters that led to a good fit of pressure and saturation data may not represent actual foam physics. For the first time, a comprehensive study that interfaced laboratory experiments and numerical simulation, while maintaining realistic interactions between phases, was conducted.
- A numerical simulator was used to model the displacement of oil from a core using CO<sub>2</sub>-based foam. History-matching was used to fine-tune the laboratory model, obtain values for parameters used to calculate the relative permeability of CO<sub>2</sub> in the presence of foam, and to determine the generation rates for the modeling process that describes the formation and sustenance of foam. The use of the foam interpolation parameter and foam generation and sustenance modeling led to very good matches for recovery factor, *RF*, and pressure difference,  $\Delta p$ .
- Three synthetic reservoir models, with varying physical properties and equal dimensionless numbers with the laboratory model were designed. Results from the foam relative permeability interpolation parameters and the foam generation and sustenance modeling obtained from history-matching the coreflood experiments were applied to these synthetic cases. Similar results for recovery factor and pressure difference were obtained.

The variance observed in the results corresponded with the degree of heterogeneity of the synthetic models.  $RF$  reduced with heterogeneity, while  $\Delta p$  increased. Dykstra Parsons coefficient of permeability distribution was therefore included as an additional dimensionless number to account for heterogeneity.

- Hammersley Sequence Sampling was used to generate 128 sample points in a design space. The sample points were then transformed into the dimensionless numbers through which dimensional parameters were calculated for the 128 cases. A numerical simulator was used to obtain results for  $RF$  and  $\Delta p$ . Linear and quadratic regression methods were applied to model and analyze the relationship between dependent variables ( $RF$  and  $\Delta p$ ) and explanatory variables (dimensionless numbers). The quadratic model provided a better fit for the 128 cases. When applied to a prediction model of 32 cases, the linear model led to a more accurate fit. For both the linear and quadratic regression models, the fit obtained for  $RF$  was better than that obtained for maximum  $\Delta$ . This is because  $\Delta p$  is a dynamic variable that changes within each grid block with respect to time and has an additional difficulty in that it relies on the foam generation and sustenance modeling parameters that are known to be very sensitive to small changes in parameter values. On the other hand,  $RF$  is a cumulative variable that is less prone to fluctuations.

In general, a combination of laboratory experiments, numerical simulation models that encompass the use of a foam modeling technique based on stoichiometric relationships for the generation and sustenance of foam, a well defined use of the foam interpolation model, a statistical analytical methodology such as Design of Experiments is then required to extend the results from a core-scale model to field cases.

## **6.2 Recommendations**

The development of a methodology to predict the performance of a surfactant enhanced  $\text{CO}_2$  flood can be further enhanced by addressing some limitations that were observed while

carrying out this research work. Factors that can be considered so as to better understand the dynamics of foam, CO<sub>2</sub>, oil, brine, and surfactant propagation through porous media, the interaction and effect of dimensionless groups, and to improve the accuracy of prediction models include:

- The effect of foam generation propagation length can be included in further studies. Results obtained in this work show that strong foam is generated near the injector and moves across the system, with the weaker front approaching the producer. The ability to strengthen foam all through the reservoir will lead to a higher pressure difference and hence, an increase in oil recovery.
- A study to investigate the effect of contrasting permeability can be executed. A laboratory setup can be designed so as to provide the ability to inject from one pump, into multiple cores of varying permeability. Results from the multi-core system can be history-matched with a reservoir simulator, and applied to reservoir models.
- A better understanding of the physical meaning of the relative permeability interpolation parameters will give better insight into how each factor affects the relative permeability curves, the strength of the effect each variable has on system performance, and ultimately the application of these factors to build a more reliable prediction framework.
- Better understanding of the stoichiometric modeling of foam generation and sustenance from the simultaneous injection of CO<sub>2</sub> and surfactant solution, and the chemical effects of oil on the strength of foam. Results from this study will provide more accurate and physically meaningful values for stoichiometric coefficients and rates of reaction frequency that can be included in the modeling process.
- The adsorption of surfactant by the porous medium reduces the ability to generate strong foam. Including this factor in future studies will lead to a more realistic modeling approach. Liu et al. (2005), Liu et al. (2005), and Enick and Olsen (2011) published

results on the adsorption of surfactant by reservoir rocks. Similar studies tailored to the reservoir of interest can be carried out.

# References

- Afonja, G., R. G. Hughes, V. Nagineni, and L. Jin (2012). Simulation Study for Optimizing Injected Surfactant Volume in a Miscible Carbon Dioxide Flood. Paper presented at the SPETT 2012 Energy Conference and Exhibition, Port of Spain, Trinidad, 11-13 June. Paper Number: 158220-MS.
- Algharaib, M., R. Gharbi, and A. Malallah (2006). Scaling Immiscible Displacements in Porous Media with Horizontal Wells. *Transport in Porous Media* 65(1), 89–105.
- Bai, Y., J. Li, J. Zhou, and Q. Li (2008). Sensitivity Analysis of the Dimensionless Parameters in Scaling a Polymer Flooding Reservoir. *Transport in Porous Media* 73(37), 21.
- Behzadi, S. and B. Towler (2009). A New EOR Method. In *SPE Annual Technical Conference and Exhibition*, New Orleans, LA. Society of Petroleum Engineers. Paper Number: 123866-MS.
- Bernard, G. G., L. W. Holm, and C. P. Harvey (1980). Use of Surfactant to reduce CO<sub>2</sub> Mobility in Oil Displacement. *Society of Petroleum Engineers Journal* 20(4), 281–292.
- Bertin, H. J., O. G. Apaydin, L. M. Castanier, and A. R. Kavscek (1998). Foam Flow in Heterogenous Porous Media: Effect of Crossflow. In *SPE/DOE Symposium on IOR*, Tulsa, OK. Society of Petroleum Engineers. Paper Number: 39678-MS.
- Bian, Y., G. Penny, and N. Sheppard (2012). Surfactant Formulation Evaluation for Carbon Dioxide Foam Flooding in Heterogeneous Sandstone Reservoir. Paper presented at the SPE Improved Oil Recovery Symposium, Tulsa, OK, 14-18 April. Paper Number: 154018-MS.
- Birkhoff, G. (1950). *Hydrodynamics: A Study in Logic, Fact, and Similitude*. Princeton, NJ: Princeton University Press.
- Blackwell, R. J. (1959). Laboratory Studies of Microscopic Dispersion Phenomena. Paper presented at Joint SPE-AIChE Symposium, San Francisco, CA, 6-9 December. Paper Number: 1483-G.
- Borchardt, J., D. Bright, M. Dickson, and S. Wellington (1985). Surfactants for CO<sub>2</sub> Foam Flooding. Paper presented at the SPE Annual Technical Conference and Exhibition, Las Vegas, NV, 22-26 September. Paper Number: 14394-MS.
- Bridgman, P. W. (1922). *Dimensional Analysis*. New haven, CT: Yale University Press.
- Bruining, H., M. Darwish, and A. Rijnks (2012). Computation of the Longitudinal and Transverse Dispersion Coefficient in an Adsorbing Porous Medium Using Homogenization. *Transport in Porous Media* 91, 833–859.
- Buckingham, E. (1914). On Physically Similar Systems: Illustrating the use of Dimensional Analysis. *Phys. Rev.* 4, 345–376.
- Casteel, J. F. and N. F. Djabbarah (1988). Sweep Improvement in CO<sub>2</sub> Flooding by Use of Foaming Agents. *SPE Reservoir Engineering* 3(4), 1186–1192.
- Cense, A. and S. Berg (2009, September). The Viscous-Capillary Paradox in 2-Phase Flow in Porous Media. In *Proceedings of International Symposium of the Society of Core Analysts*, Noordwijk, The Netherlands. Society of Core Analysts (SCA). Paper Number: SCA2009-13.
- Chang, S. H., F. D. Martin, and R. B. Grigg (1994). Effect of Pressure on CO<sub>2</sub> Foam Displacements: A Micromodel Visualization Study. In *SPE/DOE 9th Symposium on IOR*, Tulsa, OK. Society of Petroleum Engineers. Paper Number: 27784-MS.

- Chen, S. (1991). *Investigation of Dispersivity as a Reservoir Rock Characteristics and its Determination from Well Logs*. Ph. D. thesis, University of Oklahoma.
- Chou, S. (1990). Percolation Theory of Foam in Porous Media. In *SPE/DOE Enhanced Oil Recovery Symposium*, Tulsa, OK. Society of Petroleum Engineers. Paper Number: 20239-MS.
- Claridge, E. L., B. M. Lescure, and M. W. Wang (1988). *Carbon Dioxide Foam Flooding - Laboratory Model and Computer Simulation of the Process*, Volume 373. American Chemical Society.
- CMG (2009). *User's Guide STARS*. Calgary, Canada: Computer Modelling Group.
- CMG (2012). *Chemical EOR Modelling with STARS*. Computer Modelling Group. Training manual given in class.
- Coombe, D. A., V. K. Shrivasta, A. K. Singhal, and J. Belgrave (1997). Numerical Simulation of Foam Flooding For Sweep Improvement. In *Annual Technical Meeting*, Calgary, Alberta. Petroleum Society of Canada. Paper Number: 97-58.
- Cosentino, L. (2001). *Integrated Reservoir Studies*. Fundamentals of Exploration and Production Series. Editions Technip.
- Culpepper, P. B. (1989). Simulation of a Miscible Carbon Dioxide Flood Using a Trapped Oil Function. Master's thesis, Texas Tech University.
- Diwekar, U. M. and J. R. Kalagnanam (1996). Robust Design Using an Efficient Sampling Technique. *Computers & Chemical Engineering* 20, Supplement 1(0), S389 – S394.
- Dykstra, H. and R. Parsons (1950). The Prediction of Oil Recovery by Waterflood. In *Secondary Recovery of Oil in the United States*, pp. 160–174. API.
- El-Khatib, N. A. F. (2011). The Modification of the Dykstra-Parsons Method for Inclined Stratified Reservoirs. Paper presented at SPE Middle East Oil and Gas Show, Manama, Bahrain, 6-9 March. Paper Number: 140960-MS.
- Emadi, A., M. Sohrabi, M. Jamiolahmady, and S. Ireland (2012). Visualization of Oil Recovery by CO<sub>2</sub>-Foam Injection: Effect of Oil Viscosity and Gas Type. Paper presented at the SPE Improved Oil Recovery Symposium, Tulsa, OK, 14-18 April. Paper Number: 152996-MS.
- Enick, R. M. (2009). Discussion on the Use of CO<sub>2</sub> Thickeners for Mobility Control and Oil Recovery. Private communication.
- Enick, R. M., E. J. Beckman, and A. Hamilton (2001). Novel CO<sub>2</sub>-Thickeners for Improved Mobility Control. Technical Report DOE-RA26-98BC15108, Department of Energy.
- Enick, R. M. and D. K. Olsen (2011). Mobility and Conformance Control for Carbon Dioxide Enhanced Oil Recovery (CO<sub>2</sub>-EOR) via Thickeners, Foams, and Gels – A Detailed Literature Review of 40 Years of Research. Technical Report DOE/NETL-2012/1540, National Energy Technology Laboratory.
- Fisher, A., R. Foulser, and S. Goodyear (1990). Mathematical Modeling of Foam Flooding. In *SPE/DOE Enhanced Oil Recovery Symposium*, Tulsa, OK. Society of Petroleum Engineers. Paper Number: 20195-MS.
- Focken, C. M. (1953). *Dimensional Methods and Their Applications*. London, England: Arnold.



- Foster, W. R. (1973, February). A Low-Tension Waterflooding Process. *Journal of Petroleum Technology* 25(2), 205–210.
- Garmeh, G. and R. T. Johns (2010). Upscaling of Miscible Floods in Heterogeneous Reservoirs Considering Reservoir Mixing. *SPE Reservoir Evaluation & Engineering* 13(5), 747–763.
- Gharbi, R., E. Peters, and A. Elkamel (1998). Scaling Miscible Fluid Displacements in Porous Media. *Energy & Fuels* 12(4), 801–811.
- Ghomian, Y. (2008). *Reservoir Simulation Studies for Coupled Carbon Dioxide Sequestration and Enhanced Oil Recovery*. Ph. D. thesis, The University of Texas at Austin.
- Giunta, A. A., S. F. J. Wojtkiewicz, and M. S. Eldred (2003). Overview of Modern Design of Experiments Methods for Computational Simulations. In Proceedings of the 41st AIAA Aerospace Sciences Meeting and Exhibit, Reno, NV, Jan. 6-9. Paper Number: AIAA 2003-0649.
- Green, D. W. and G. P. Willhite (1998). *Enhanced Oil Recovery*. Society of Petroleum Engineers.
- Greenkorn, R., C. Johnson, and R. Harding (1965). Miscible Displacement in a Controlled Natural System. *Journal of Petroleum Technology* 17(11), 1329–1335.
- Grigg, R. B., R. K. Svec, Z. W. Zeng, A. Mikhalin, Y. Liu, and G. Yin (2007). Improving Gas Flooding Efficiency. Technical Report DE-FG26-04NT15532, New Mexico Petroleum Recovery Research Center. 2nd Annual report.
- Grogan, A. T. and W. V. Pinczewski (1987). The Role of Molecular Diffusion Processes in Tertiary CO<sub>2</sub> Flooding. *Journal of Petroleum Technology* 39(5), 591–602.
- Grogan, A. T., W. V. Pinczewski, G. J. Ruskauff, and F. M. Orr (1988). Diffusion of CO<sub>2</sub> at Reservoir Conditions: Models and Measurements. *SPE Reservoir Engineering* 3(1), 93–102.
- Hackert, C. L., J. L. Ellzey, O. A. Ezekoye, and M. J. Hall (1996). Transverse Dispersion at High Peclet Numbers in Short Porous Media. *Experiments in Fluids* 21, 286–290.
- Hanssen, J. E., L. M. Surguchev, and I. Svorstol (1994). SAG Injection in a North Sea Stratified Reservoir: Flow Experiment and Simulation. In *European Petroleum Conference*, London, UK. Society of Petroleum Engineers. Paper Number: 28847-MS.
- Heller, J. P. (1994). *CO<sub>2</sub> Foams in Enhanced Oil Recovery*, Volume 242 of *Advances in Chemistry*. American Chemical Society.
- Heller, J. P., D. K. Dandge, R. J. Card, and L. G. Donaruma (1985). Direct Thickeners for Mobility Control of CO<sub>2</sub> Floods. *SPE Journal* 25(5), 679–686.
- Hirasaki, G. J. (1980). Scaling of Non-Equilibrium Phenomena in Surfactant Flooding. Paper presented at SPE/DOE Enhanced Oil Recovery Symposium, Tulsa, OK, 20-23 April. Paper Number: 8841-MS.
- Hirasaki, G. J. (1984). Properties of Log-Normal Permeability Distribution for Stratified Reservoirs. Unsolicited. Submitted to SPE for consideration for publication in one of its technical journals. Paper Number: 13416-MS.
- Hoque, S. (2010). *Development of Computational Fluid Dynamics based Multiple Linear and Neural Network Metamodels for Bioaerosol Fate and Transport in Indoor Environments*. Ph. D. thesis, Drexel University.

- Hrenya, C. (2007). Dimensional Analysis - Fluid Mechanics Lecture Notes. Available online at [ftp://ftp.colorado.edu/cuboulder/courses/chen3200/Lectures/DimAnal\\_1.pdf](ftp://ftp.colorado.edu/cuboulder/courses/chen3200/Lectures/DimAnal_1.pdf).
- Huang, E. and L. Holm (1988). Effect of WAG Injection and Rock Wettability on Oil recovery During CO<sub>2</sub> Flooding. *SPE Reservoir Engineering* 3(1), 119–129.
- Islam, M. R. and S. M. Farouq-Ali (1989). New Scaling Criteria for Polymer, Emulsion and Foam Flooding Experiments. *Journal of Canadian Petroleum Technology* 28(4), 79–87.
- Islam, M. R. and S. M. Farouq-Ali (1990). New Scaling Criteria For Chemical Flooding Experiments. *Journal of Canadian Petroleum Technology* 29(1), 29–36.
- Jackson, D. D., G. L. Andrews, and E. L. Claridge (1985). Optimum WAG Ratio vs. Rock Wettability in CO<sub>2</sub> Flooding. 60th Annual Technical Conference and Exhibition, Las Vegas, NV. Society of Petroleum Engineers. Paper Number: 14303-MS.
- Jensen, J. and F. Friedmann (1987). Physical and Chemical Effects of an Oil Phase on the Propagation of Foam in Porous Media. Paper presented at the SPE California Regional Meeting, 8-10 April, Ventura, CA.
- John, A. K., L. W. Lake, S. L. Bryant, and J. W. Jennings (2008). Investigation of Field Scale Dispersion. SPE/DOE Symposium on Improved Oil Recovery, Tulsa, OK. Society of Petroleum Engineers. Paper Number: 113429-MS.
- Jonoud, S. and M. D. Jackson (2008). New Criteria for the Validity of Steady-State Upscaling. *Transport in Porous Media* 71, 53–73.
- Kalla, S. (2008). *Reservoir Characterization Using Seismic Inversion Data*. Ph. D. thesis, Louisiana State University.
- Kam, S. and W. Rossen (2003). A Model for Foam Generation in Homogeneous Media. *SPE Journal* 8, 417–425.
- Khan, A. A., Y. Guo, D. Wessel-Berg, J. Kleppe, and D. Coombe (2006). Mobility control using foam - snorre/wfp fawag pilot revisited. PDF File, Stavanger, Norway.
- Kimber, K. and S. Farouq-Ali (1991). Scaled Physical Modeling of Steam-Injection Experiments. *SPE Reservoir Engineering* 6(4), 467–469.
- Koval, E. J. (1963). A Method for Predicting the Performance of Unstable Miscible Displacement in Heterogeneous Media. *SPE Journal* 3(2), 145–154.
- Kovscek, A. R., T. W. Patzek, and C. J. Radke (1995). FOAM3D: A Numerical Simulator for Mechanistic Prediction of Foam Displacement in Multidimensions. In *Report LBL-37200: Proceedings of the TOUGH Workshop*, Berkeley, CA, pp. 131–135.
- Kovscek, A. R. and C. J. Radke (1994). Fundamentals of Foam Transport in Porous Media. In L. L. Schramm (Ed.), *Foams - Fundamentals & Applications in the Petroleum Industry*, Chapter 3, pp. 115–163. Washington, DC: American Chemical Society.
- Kulkarni, M. M. (2003). Immiscible and Miscible Gas-Oil Displacement in Porous Media. Master's thesis, Louisiana State University, Baton Rouge, LA.
- Kulkarni, M. M. (2005). *Multiphase Mechanisms and Fluid Dynamics in Gas Injection Enhanced Oil Recovery Processes*. Ph. D. thesis, Louisiana State University.

- Lake, L. W. (1989). *Enhanced Oil Recovery*. Prentice Hall.
- Lake, L. W. and M. P. Walsh (2008). Enhanced Oil Recovery (EOR) Field Data Literature Search. Technical report, Department of Petroleum and Geosystems Engineering, University of Texas, Austin, TX.
- Langhaar, H. L. (1951). *Dimensional Analysis and Theory of Models*. New York, NY: Wiley.
- Leverett, M. C., W. B. Lewis, and M. E. True (1942). Dimensional-Model Studies of Oil-Field Behavior. *Trans. AIME* 146, 175–193.
- Lewis, E. (2008). *Sweep Efficiency in Miscible Enhanced Oil Recovery Processes*. Ph. D. thesis, University of Houston.
- Li, R., W. Yan, S. Liu, G. Hirasaki, and C. Miller (2010). Foam Mobility Control for Surfactant Enhanced Oil Recovery. *SPE Journal* 15(4), 928 – 942.
- Liu, Y., R. B. Grigg, and B. Bai (2005). Salinity, pH , and Surfactant Concentration Effects on CO<sub>2</sub>-Foam. Number 93095-MS. Society of Petroleum Engineers. Paper presented at the SPE International Symposium on Oilfield Chemistry, The Woodlands, TX, February 2 - 4, 2005.
- Liu, Y., R. B. Grigg, and R. K. Svec (2005). CO<sub>2</sub> Foam Behavior: Influence of Temperature, Pressure and Concentration of Surfactant. In *SPE Production and Operations Symposium*, Oklahoma City, OK. Society of Petroleum Engineers. paper Number: 94307-MS.
- Ma, K., S. L. Biswal, and G. J. Hirasaki (2012). Estimation of Parameters for Simulation of Steady State Foam Flow in Porous Media. Available online at [http://www.uwyo.edu/eori/\\_files/co2conference12/george\\_hirisaki\\_wyoming\\_july2012.pdf](http://www.uwyo.edu/eori/_files/co2conference12/george_hirisaki_wyoming_july2012.pdf).
- Moradi-Araghi, A., E. L. Johnston, D. R. Zomes, and K. J. Harpole (1997). Laboratory Evaluation of Surfactants for CO<sub>2</sub>-Foam Applications at the South Cowden Unit. In *International Symposium on Oilfield Chemistry*, Houston, TX. Society of Petroleum Engineers.
- Mwangi, P. (2010). An Experimental Study of Surfactant-Enhanced Waterflooding. Master's thesis, Louisiana State University.
- Nezhad, S. A. T., M. R. R. Mojarad, J. S. Paitakhti, J. S. Moghadas, and D. R. Farahmand (2006). Experimental Study on the Applicability of Water-Alternating-CO<sub>2</sub> Injection Secondary and Tertiary Recovery. Paper presented at the First International Oil Conference and Exhibition, Cancun, Mexico, 31 August-2 September. Paper Number: 103988-MS.
- NIST/SEMATECH (2003). A Glossary of DOE Terminology. Available online at <http://www.itl.nist.gov/div898/handbook/pri/section7/pri7.htm>.
- Novosad, J. J., K. Mannhardt, and A. Rendall (1989). The Interaction Between Foam And Crude Oils. Society of Petroleum Engineers. Paper presented at the 40th Annual Technical Meeting of the Petroleum Society of Canada, Banff, Canada, May 28 - 31, 1989.
- Panday, S. and M. Y. Corapcioglu (1989). Reservoir Transport Equations by Compositional Approach. *Transport in Porous Media* 4, 369–393.
- Patzek, T. W. (1998). *Description of Foam Flow in Porous Media by the Population Balance Method*, Volume 373 of ACS Symposium Series, Chapter 17, pp. 326–341. American Chemical Society.

- Perkins, T. K. and O. C. Johnston (1963). A Review of Diffusion and Dispersion in Porous Media. *SPE Journal* 3(1), 70–84.
- Pozzi, A. L. and J. Blackwell, R. (1963). Design of Laboratory Models for Study of Miscible Displacement. *SPE Journal* 3(1), 28 – 40.
- Pujol, L. and T. Boberg (1972). Scaling Accuracy of Laboratory Steam Flooding Models. Paper presented at the SPE California Regional Meeting, 8-10 November, Bakersfield, CA. Paper Number: 4191-MS.
- Rafajlowicz, E. and R. Schwabe (2006). Halton and Hammersley Sequences in Multivariate Nonparametric Regression. *Statistics and Probability Letters* 76(8), 803–812.
- Rai, K. (2008). Screening Model for Surfactant-Polymer Flooding Using Dimensionless Groups. Master's thesis, The University of Texas at Austin.
- Ren, G. (2012a). Discussion on the History-Matching Injection Pressure for Laboratory Data for CO<sub>2</sub>-Surfactant Injection. Personal communication.
- Ren, G. (2012b). *Dynamics of Supercritical CO<sub>2</sub>-Foam in Porous Media With Soluble CO<sub>2</sub> Surfactants*. Ph. D. thesis, The University of Texas at Austin.
- Renner, T. A. (1963). Measurement and Correlation of Diffusion Coefficients for CO<sub>2</sub> and Rich-Gas Applications. *SPE Journal* 3(1), 70–84.
- Rossen, W. R. (2000). Snap-off in Constricted Tubes and Porous Media. *Colloids and Surfaces A: Physicochemical and Engineering Aspects* 166(1-3), 101 – 107.
- Rossen, W. R. and P. A. Gauglitz (1990). Percolation Theory of Creation and Mobilization of Foams in Porous Media. *AIChE Journal* 36(8), 1176–1188.
- Rossen, W. R. and Z. H. Zhou (1995). Applying Fractional Flow Theory to Foam Processes at the Limiting Capillary Pressure. *SPE Advanced Technology Series* 3(1), 154–162.
- Rowe, H. G., S. D. York, and J. C. Ader (1981). Slaughter Estate Unit Tertiary Pilot Performance. *Journal of Petroleum Technology*, 613–620.
- Ruark, A. E. (1935). Inspectional Analysis: A Method Which Supplements Dimensional Analysis. *Journal of the Elisha Mitchell Scientific Society* 51(1), 127–133.
- Sahimi, M., M. R. Rasaei, and M. Haghighi (2006). Gas Injection and Fingering in Porous Media. In C. K. Ho and S. W. Webb (Eds.), *Gas Transport in Porous Media*, Volume 20 of *Theory and Applications of Transport in Porous Media*, pp. 133–168. Springer Netherlands.
- Salager, J. L. (1977). *Physico-chemical Properties of Surfactant - Water - Oil Mixtures: Phase Behavior, Microemulsion Formation and Interfacial Tension*. Ph. D. thesis, The University of Texas at Austin.
- Shen, C. (2006). *Experimental and Simulation Study of Foam in Porous Media*. Ph. D. thesis, The University of Texas at Austin.
- Sheng, J. (2011). *Modern Chemical Enhanced Oil Recovery - Theory and Practice*. Elsevier Inc.
- Shetty, S. (2011). Evaluation of Simultaneous Water and Gas Injection using CO<sub>2</sub>. Master's thesis, Louisiana State University.
- Shook, M. L., D. Li, and L. Lake (1992). Scaling Immiscible Flow Through Permeable Media by Inspectional Analysis. *In-Situ* 16(4), 311–350.

- Simpson, T. W., D. K. J. Lin, and W. Chen (2001). Sampling Strategies for Computer Experiments: Design and Analysis. *International Journal of Reliability and Applications* 2(3), 209–240.
- Sonin, A. (2001). *The Physical Basis of Dimensional Analysis*. Cambridge, MA: Department of Mechanical Engineering - MIT.
- Terry, R., A. Zaid, C. Angelos, and D. Whitman (1987). Polymerization in Supercritical CO<sub>2</sub> To Improve CO<sub>2</sub>/Oil Mobility Ratios. In *SPE International Symposium on Oilfield Chemistry*, San Antonio, TX, pp. 289–296. Society of Petroleum Engineers. Paper Number: 16270-MS.
- Tiab, D. and E. C. Donaldson (2011). *Petrophysics: Theory and Practice of Measuring Reservoir Rock and Fluid Transport Properties*. Gulf Professional Publishing.
- Tortopidis, S. and D. C. Shallcross (1994). Carbon Dioxide Foam Flood Studies Under Australian Reservoir Conditions. Paper presented at the SPE Asia Pacific Oil and Gas Conference, Melbourne, Australia, 7-10 November. Paper Number: 28811-MS.
- Tsau, J. S. and J. P. Heller (1992). Evaluation of Surfactants for CO<sub>2</sub>-Foam Mobility Control. Paper presented at SPE Permian Basin Oil and Gas Recovery Conference, Midland, TX, 18-20 March. Paper Number: 24013-MS.
- Tsau, J. S. and J. P. Heller (1996). How Can Selective Mobility Reduction of CO<sub>2</sub>-Foam Assist in Reservoir Floods? In *SPE Permian Oil and Gas Recovery Conference*, Midland, TX. Society of Petroleum Engineers. Paper Number: 35168-MS.
- Vikingstad, A. K. (2006). *Static and Dynamic Studies of Foam and Foam-Oil Interactions*. Ph.D Dissertation, University of Bergen, Bergen, Norway.
- Wassmuth, F., L. L. Schramm, K. Mannhardt, and L. Hodgins (2000). Scale-Up Evaluations and Simulations of Mobility Control Foams for Improved Oil Recovery. In L. L. Schramm (Ed.), *Surfactants: Fundamentals and Applications in the Petroleum Industry*, pp. 251–292.
- Whorton, L. P., E. R. Brownscombe, and A. B. Dyes (1952). A Method of Producing Oil by Means of Carbon Dioxide. United States Patent 2623596.
- Wong, T. T., W. S. Luk, and P. A. Heng (1997, November). Sampling with Hammersley and Halton points. *J. Graph. Tools* 2(2), 9–24.
- Wood, D. J., L. W. Lake, R. T. Johns, and V. Nunez (2008). A Screening Model for CO<sub>2</sub> Flooding and Storage in Gulf Coast Reservoirs Based on Dimensionless Groups. *SPE Reservoir Evaluation & Engineering* 11(3), 513–520.
- Xu, J. (2003). *Carbon dioxide Thickening Agents for Reduced CO<sub>2</sub> Mobility*. Ph. D. thesis, University of Pittsburgh.
- Yaghoobi, H. (1994). Laboratory Investigation of Parameters Affecting CO<sub>2</sub>-Foam Mobility in Sandstone at Reservoir Conditions. In *SPE Eastern Regional Meeting*, Charleston, WV. Society of Petroleum Engineers. Paper Number: 29168-MS.
- Yaghoobi, H., J. S. Tsau, and R. B. Grigg (1998). Effect of Foam on CO<sub>2</sub> Breakthrough: Is This Favorable to Oil Recovery? Paper presented at SPE Permian Basin Oil and Gas Recovery Conference, Midland, TX, 23-25 March. Paper Number: 39789-MS.

Yin, G., R. B. Grigg, and S. Yi (2009). Oil Recovery and Surfactant Adsorption during CO<sub>2</sub>-Foam Flooding. Paper presented at the Offshore Technology Conference, Houston, TX, 4-7 May. Paper Number: 19787-MS.

Zhang, J. (2003). *Performance-Based Seismic Design Using Designed Experiments and Neural Networks*. Ph. D. thesis, The University of British Columbia.

# Appendix A: Dimensionless Groups

The equations below show the mass balance transport equations for gas, oil and water phases respectively

$$\phi \frac{\partial}{\partial t} S_g c_{g1} = \frac{\partial}{\partial x} u_{gx} c_{g1} + \frac{\partial}{\partial z} u_{gz} c_{g1} \quad (\text{A.1})$$

$$\begin{aligned} \phi \frac{\partial}{\partial t} S_o c_{o1} + \phi \frac{\partial}{\partial t} S_o c_{o2} + \phi \frac{\partial}{\partial t} S_o c_{o4} = & \\ & \frac{\partial}{\partial x} u_{ox} c_{o1} + \frac{\partial}{\partial z} u_{oz} c_{o1} + \\ & \frac{\partial}{\partial x} u_{ox} c_{o2} + \frac{\partial}{\partial z} u_{oz} c_{o2} + \\ & \frac{\partial}{\partial x} u_{ox} c_{o4} + \frac{\partial}{\partial z} u_{oz} c_{o4} + \\ & \phi K_{L_{o1}} \frac{\partial^2}{\partial x^2} c_{o1} + \phi K_{T_{o1}} \frac{\partial^2}{\partial z^2} c_{o1} + \\ & \phi K_{L_{o2}} \frac{\partial^2}{\partial x^2} c_{o2} + \phi K_{T_{o2}} \frac{\partial^2}{\partial z^2} c_{o2} + \\ & \phi K_{L_{o4}} \frac{\partial^2}{\partial x^2} c_{o4} + \phi K_{T_{o4}} \frac{\partial^2}{\partial z^2} c_{o4} \end{aligned} \quad (\text{A.2})$$

$$\begin{aligned} \phi \frac{\partial}{\partial t} S_w c_{w1} + \phi \frac{\partial}{\partial t} S_w c_{w3} + \phi \frac{\partial}{\partial t} S_w c_{w4} = & \\ & \frac{\partial}{\partial x} u_{wx} c_{w1} + \frac{\partial}{\partial z} u_{wz} c_{w1} + \\ & \frac{\partial}{\partial x} u_{wx} c_{w3} + \frac{\partial}{\partial z} u_{wz} c_{w3} + \\ & \frac{\partial}{\partial x} u_{wx} c_{w4} + \frac{\partial}{\partial z} u_{wz} c_{w4} + \\ & \phi K_{L_{w1}} \frac{\partial^2}{\partial x^2} c_{w1} + \phi K_{T_{w1}} \frac{\partial^2}{\partial z^2} c_{w1} + \\ & \phi K_{L_{w3}} \frac{\partial^2}{\partial x^2} c_{w3} + \phi K_{T_{w3}} \frac{\partial^2}{\partial z^2} c_{w3} + \\ & \phi K_{L_{w4}} \frac{\partial^2}{\partial x^2} c_{w4} + \phi K_{T_{w4}} \frac{\partial^2}{\partial z^2} c_{w4} \end{aligned} \quad (\text{A.3})$$

## Constitutive Equations

$$u_{gx} = \frac{k_x k_{rg}}{\mu_g} \frac{\partial}{\partial x} p_g \quad (\text{A.4})$$

$$u_{gz} = \frac{k_z k_{rg}}{\mu_g} \frac{\partial}{\partial z} p_g \quad (\text{A.5})$$

$$u_{ox} = \frac{k_x k_{ro}}{\mu_o} \frac{\partial}{\partial x} p_o \quad (\text{A.6})$$

$$u_{oz} = \frac{k_z k_{ro}}{\mu_o} \frac{\partial}{\partial z} p_o \quad (\text{A.7})$$

$$u_{wx} = \frac{k_x k_{rw}}{\mu_w} \frac{\partial}{\partial x} p_w \quad (\text{A.8})$$

$$u_{wz} = \frac{k_z k_{rw}}{\mu_w} \frac{\partial}{\partial z} p_w \quad (\text{A.9})$$

$$p_{c_{ow}} = \sigma_{ow} \sqrt{\frac{\phi}{k}} j(S_w) \quad (\text{A.10})$$

$$p_{c_{go}} = \sigma_{go} \sqrt{\frac{\phi}{k}} j(S_o) \quad (\text{A.11})$$

### Saturation constraint

$$S_g + S_o + S_w = 1 \quad (\text{A.12})$$

### Initial and Boundary Conditions

$$S_w = S_{wi} \quad \text{at } t = 0, \forall x, z \quad (\text{A.13})$$

$$S_o = S_{oi} \quad \text{at } t = 0, \forall x, z \quad (\text{A.14})$$

$$c_{g1} = 0 \quad \text{at } t = 0, \forall x, z \quad (\text{A.15})$$

$$c_{o1} = 0 \quad \text{at } t = 0, \forall x, z \quad (\text{A.16})$$

$$c_{o2} = c_{2i} \quad \text{at } t = 0, \forall x, z \quad (\text{A.17})$$

$$c_{o4} = 0 \quad \text{at } t = 0, \forall x, z \quad (\text{A.18})$$

$$c_{w1} = 0 \quad \text{at } t = 0, \forall x, z \quad (\text{A.19})$$



$$c_{w3} = c_{3i} \quad \text{at } t = 0, \forall x, z \quad (\text{A.20})$$

$$c_{w4} = 0 \quad \text{at } t = 0, \forall x, z \quad (\text{A.21})$$

$$c_{g1} = c_{1j} \quad \text{at } x = 0, \forall t, z \quad (\text{A.22})$$

$$c_{o1} = 0 \quad \text{at } x = 0, \forall t, z \quad (\text{A.23})$$

$$c_{o2} = 0 \quad \text{at } x = 0, \forall t, z \quad (\text{A.24})$$

$$c_{o4} = 0 \quad \text{at } x = 0, \forall t, z \quad (\text{A.25})$$

$$c_{w1} = 0 \quad \text{at } x = 0, \forall t, z \quad (\text{A.26})$$

$$c_{w3} = 0 \quad \text{at } x = 0, \forall t, z \quad (\text{A.27})$$

$$c_{w4} = c_{4j} \quad \text{at } x = 0, \forall t, z \quad (\text{A.28})$$

$$p_g = \Delta p_g + \rho_g g (H - z) \quad \text{at } x = L, \forall t, z \quad (\text{A.29})$$

$$p_o = \Delta p_o + \rho_o g (H - z) \quad \text{at } x = L, \forall t, z \quad (\text{A.30})$$

$$p_w = \Delta p_w + \rho_w g (H - z) \quad \text{at } x = L, \forall t, z \quad (\text{A.31})$$

$$u_{gz} = u_{oz} = u_{wz} = 0 \quad \text{at } z = 0, \forall x, t \quad (\text{A.32})$$

$$u_{gz} = u_{oz} = u_{wz} = 0 \quad \text{at } z = H, \forall x, t \quad (\text{A.33})$$

$$\frac{1}{H} \int_0^H u_{gx} dz = u_T \quad \text{at } x = 0, \forall z, t \quad (\text{A.34})$$

## Multiplicative Factors

$$S_g = S_{gD} S_{gR} \quad (\text{A.35})$$

$$S_o = S_{oD} S_{oR} \quad (\text{A.36})$$

$$S_w = S_{wD} S_{wR} \quad (\text{A.37})$$

$$c_{g1} = c_{g1D} c_{g1R} \quad (\text{A.38})$$

$$c_{g2} = c_{g2D} c_{g2R} \quad (\text{A.39})$$

$$c_{o2} = c_{o2D} c_{o2R} \quad (\text{A.40})$$

$$c_{o4} = c_{o4D} c_{o4R} \quad (\text{A.41})$$

$$c_{w3} = c_{w3D} c_{w3R} \quad (\text{A.42})$$

$$c_{w4} = c_{w4D} c_{w4R} \quad (\text{A.43})$$

$$x = x_D x_R \quad (\text{A.44})$$

$$z = z_D z_R \quad (\text{A.45})$$

$$t = t_D t_R \quad (\text{A.46})$$

$$p_g = p_{gD} p_{gR} \quad (\text{A.47})$$

$$p_o = p_{oD} p_{oR} \quad (\text{A.48})$$

$$p_w = p_{wD} p_{wR} \quad (\text{A.49})$$

$$u_{gx} = u_{gxD} u_{gxR} \quad (\text{A.50})$$

$$u_{gz} = u_{gzD} u_{gzR} \quad (\text{A.51})$$

$$u_{ox} = u_{oxD} u_{oxR} \quad (\text{A.52})$$

$$u_{oz} = u_{ozD} u_{ozR} \quad (\text{A.53})$$

$$u_{wx} = u_{wxD} u_{wxR} \quad (\text{A.54})$$

$$u_{wz} = u_{wzD} u_{wzR} \quad (\text{A.55})$$

## Gas Dimensionless Groups

$$\phi \frac{\partial}{\partial t} S_g c_{g1} = \frac{\partial}{\partial x} u_{gx} c_{g1} + \frac{\partial}{\partial z} u_{gz} c_{g1} \quad (\text{A.56})$$

$$\phi \frac{S_{gR} c_{g1R}}{t_R} \frac{\partial}{\partial t_D} S_{gD} c_{g1D} = \frac{c_{g1R} u_{gxR}}{x_R} \frac{\partial}{\partial x_D} u_{gx_D} c_{g1D} + \frac{c_{g1R} u_{gzR}}{z_R} \frac{\partial}{\partial z_D} u_{gz_D} c_{g1D} \quad (\text{A.57})$$

$$\frac{\partial}{\partial t_D} S_{gD} c_{g1D} = \frac{u_{gxR} t_R}{\phi x_R S_{gR}} \frac{\partial}{\partial x_D} u_{gx_D} c_{g1D} + \frac{u_{gzR} t_R}{\phi z_R S_{gR}} \frac{\partial}{\partial z_D} u_{gz_D} c_{g1D} \quad (\text{A.58})$$

## Oil Dimensionless groups

$$\begin{aligned} \phi \frac{\partial}{\partial t} S_o c_{o1} + \phi \frac{\partial}{\partial t} S_o c_{o2} + \phi \frac{\partial}{\partial t} S_o c_{o4} = & \\ & \frac{\partial}{\partial x} u_{ox} c_{o1} + \frac{\partial}{\partial z} u_{oz} c_{o1} + \\ & \frac{\partial}{\partial x} u_{ox} c_{o2} + \frac{\partial}{\partial z} u_{oz} c_{o2} + \\ & \frac{\partial}{\partial x} u_{ox} c_{o4} + \frac{\partial}{\partial z} u_{oz} c_{o4} + \\ & \phi K_{L_{o1}} \frac{\partial^2}{\partial x^2} c_{o1} + \phi K_{T_{o1}} \frac{\partial^2}{\partial z^2} c_{o1} + \\ & \phi K_{L_{o2}} \frac{\partial^2}{\partial x^2} c_{o2} + \phi K_{T_{o2}} \frac{\partial^2}{\partial z^2} c_{o2} + \\ & \phi K_{L_{o4}} \frac{\partial^2}{\partial x^2} c_{o4} + \phi K_{T_{o4}} \frac{\partial^2}{\partial z^2} c_{o4} \end{aligned} \quad (\text{A.59})$$

$$\begin{aligned} \phi \frac{S_{oR} c_{o1R}}{t_R} \frac{\partial}{\partial t_D} S_{oD} c_{o1D} + \phi \frac{S_{oR} c_{o2R}}{t_R} \frac{\partial}{\partial t_D} S_{oD} c_{o2D} + \phi \frac{S_{oR} c_{o4R}}{t_R} \frac{\partial}{\partial t_D} S_{oD} c_{o4D} = & \\ & \frac{c_{o1R} u_{oxR}}{x_R} \frac{\partial}{\partial x_D} u_{ox_D} c_{o1D} + \frac{c_{o1R} u_{ozR}}{z_R} \frac{\partial}{\partial z_D} u_{oz_D} c_{o1D} + \\ & \frac{c_{o2R} u_{oxR}}{x_R} \frac{\partial}{\partial x_D} u_{ox_D} c_{o2D} + \frac{c_{o2R} u_{ozR}}{z_R} \frac{\partial}{\partial z_D} u_{oz_D} c_{o2D} + \\ & \frac{c_{o4R} u_{oxR}}{x_R} \frac{\partial}{\partial x_D} u_{ox_D} c_{o4D} + \frac{c_{o4R} u_{ozR}}{z_R} \frac{\partial}{\partial z_D} u_{oz_D} c_{o4D} + \\ & \phi \frac{K_{L_{o1}} c_{o1R}}{x_R^2} \frac{\partial^2}{\partial x_D^2} c_{o1D} + \phi \frac{K_{T_{o1}} c_{o1R}}{z_R^2} \frac{\partial^2}{\partial z_D^2} c_{o1D} + \\ & \phi \frac{K_{L_{o2}} c_{o2R}}{x_R^2} \frac{\partial^2}{\partial x_D^2} c_{o2D} + \phi \frac{K_{T_{o2}} c_{o2R}}{z_R^2} \frac{\partial^2}{\partial z_D^2} c_{o2D} + \\ & \phi \frac{K_{L_{o4}} c_{o4R}}{x_R^2} \frac{\partial^2}{\partial x_D^2} c_{o4D} + \phi \frac{K_{T_{o4}} c_{o4R}}{z_R^2} \frac{\partial^2}{\partial z_D^2} c_{o4D} \end{aligned} \quad (\text{A.60})$$

$$\begin{aligned}
& \frac{\partial}{\partial t_D} S_{0D} c_{01D} + \frac{\partial}{\partial t_D} S_{0D} c_{02D} + \frac{\partial}{\partial t_D} S_{0D} c_{04D} = \\
& \frac{u_{0x_R} t_R}{\phi x_R S_{0R}} \frac{\partial}{\partial x_D} u_{0x_D} c_{01D} + \frac{u_{0z_R} t_R}{\phi z_R S_{0R}} \frac{\partial}{\partial z_D} u_{0z_D} c_{01D} + \\
& \frac{u_{0x_R} t_R}{\phi x_R S_{0R}} \frac{\partial}{\partial x_D} u_{0x_D} c_{02D} + \frac{u_{0z_R} t_R}{\phi z_R S_{0R}} \frac{\partial}{\partial z_D} u_{0z_D} c_{02D} + \\
& \frac{u_{0x_R} t_R}{\phi x_R S_{0R}} \frac{\partial}{\partial x_D} u_{0x_D} c_{04D} + \frac{u_{0z_R} t_R}{\phi z_R S_{0R}} \frac{\partial}{\partial z_D} u_{0z_D} c_{04D} + \\
& \frac{K_{L_{01}} t_R}{x_R^2 S_{0R}} \frac{\partial^2}{\partial x_D^2} c_{01D} + \frac{K_{T_{01}} t_R}{z_R^2 S_{0R}} \frac{\partial^2}{\partial z_D^2} c_{01D} + \\
& \frac{K_{L_{02}} t_R}{x_R^2 S_{0R}} \frac{\partial^2}{\partial x_D^2} c_{02D} + \frac{K_{T_{02}} t_R}{z_R^2 S_{0R}} \frac{\partial^2}{\partial z_D^2} c_{02D} + \\
& \frac{K_{L_{04}} t_R}{x_R^2 S_{0R}} \frac{\partial^2}{\partial x_D^2} c_{04D} + \frac{K_{T_{04}} t_R}{z_R^2 S_{0R}} \frac{\partial^2}{\partial z_D^2} c_{04D}
\end{aligned} \tag{A.61}$$

### Water Dimensionless Group

$$\begin{aligned}
& \phi \frac{\partial}{\partial t} S_w c_{w1} + \phi \frac{\partial}{\partial t} S_w c_{w3} + \phi \frac{\partial}{\partial t} S_w c_{w4} = \\
& \frac{\partial}{\partial x} u_{wx} c_{w1} + \frac{\partial}{\partial z} u_{wz} c_{w1} + \\
& \frac{\partial}{\partial x} u_{wx} c_{w3} + \frac{\partial}{\partial z} u_{wz} c_{w3} + \\
& \frac{\partial}{\partial x} u_{wx} c_{w4} + \frac{\partial}{\partial z} u_{wz} c_{w4} + \\
& \phi K_{L_{w1}} \frac{\partial^2}{\partial x^2} c_{w1} + \phi K_{T_{w1}} \frac{\partial^2}{\partial z^2} c_{w1} + \\
& \phi K_{L_{w3}} \frac{\partial^2}{\partial x^2} c_{w3} + \phi K_{T_{w3}} \frac{\partial^2}{\partial z^2} c_{w3} + \\
& \phi K_{L_{w4}} \frac{\partial^2}{\partial x^2} c_{w4} + \phi K_{T_{w4}} \frac{\partial^2}{\partial z^2} c_{w4}
\end{aligned} \tag{A.62}$$

$$\begin{aligned}
& \phi \frac{S_{wR} c_{w1R}}{t_R} \frac{\partial}{\partial t_D} S_{wD} c_{w1D} + \phi \frac{S_{wR} c_{w3R}}{t_R} \frac{\partial}{\partial t_D} S_{wD} c_{w3D} + \phi \frac{S_{wR} c_{w4R}}{t_R} \frac{\partial}{\partial t_D} S_{wD} c_{w4D} = \\
& \frac{c_{w1R} u_{wR}}{x_R} \frac{\partial}{\partial x_D} u_{wD} c_{w1D} + \frac{c_{w1R} u_{wR}}{z_R} \frac{\partial}{\partial z_D} u_{wD} c_{w1D} + \\
& \frac{c_{w3R} u_{wR}}{x_R} \frac{\partial}{\partial x_D} u_{wD} c_{w3D} + \frac{c_{w3R} u_{wR}}{z_R} \frac{\partial}{\partial z_D} u_{wD} c_{w3D} + \\
& \frac{c_{w4R} u_{wR}}{x_R} \frac{\partial}{\partial x_D} u_{wD} c_{w4D} + \frac{c_{w4R} u_{wR}}{z_R} \frac{\partial}{\partial z_D} u_{wD} c_{w4D} + \\
& \phi \frac{K_{L_{w1}} c_{w1R}}{x_R^2} \frac{\partial^2}{\partial x_D^2} c_{w1D} + \phi \frac{K_{T_{w1}} c_{w1R}}{z_R^2} \frac{\partial^2}{\partial z_D^2} c_{w1D} + \\
& \phi \frac{K_{L_{w3}} c_{w3R}}{x_R^2} \frac{\partial^2}{\partial x_D^2} c_{w3D} + \phi \frac{K_{T_{w3}} c_{w3R}}{z_R^2} \frac{\partial^2}{\partial z_D^2} c_{w3D} + \\
& \phi \frac{K_{L_{w4}} c_{w4R}}{x_R^2} \frac{\partial^2}{\partial x_D^2} c_{w4D} + \phi \frac{K_{T_{w4}} c_{w4R}}{z_R^2} \frac{\partial^2}{\partial z_D^2} c_{w4D}
\end{aligned} \tag{A.63}$$

$$\begin{aligned}
& \frac{\partial}{\partial t_D} S_{wD} c_{w1D} + \frac{\partial}{\partial t_D} S_{wD} c_{w3D} + \frac{\partial}{\partial t_D} S_{wD} c_{w4D} = \\
& \frac{u_{wxR} t_R}{\phi x_R S_{wR}} \frac{\partial}{\partial x_D} u_{wxD} c_{w1D} + \frac{u_{wzR} t_R}{\phi z_R S_{wR}} \frac{\partial}{\partial z_D} u_{wzD} c_{w1D} + \\
& \frac{u_{wxR} t_R}{\phi x_R S_{wR}} \frac{\partial}{\partial x_D} u_{wxD} c_{w3D} + \frac{u_{wzR} t_R}{\phi z_R S_{wR}} \frac{\partial}{\partial z_D} u_{wzD} c_{w3D} + \\
& \frac{u_{wxR} t_R}{\phi x_R S_{wR}} \frac{\partial}{\partial x_D} u_{wxD} c_{w4D} + \frac{u_{wzR} t_R}{\phi z_R S_{wR}} \frac{\partial}{\partial z_D} u_{wzD} c_{w4D} + \\
& \frac{K_{Lw1} t_R}{x_R^2 S_{wR}} \frac{\partial^2}{\partial x_D^2} c_{w1D} + \frac{K_{Tw1} t_R}{z_R^2 S_{wR}} \frac{\partial^2}{\partial z_D^2} c_{w1D} + \\
& \frac{K_{Lw3} t_R}{x_R^2 S_{wR}} \frac{\partial^2}{\partial x_D^2} c_{w3D} + \frac{K_{Tw3} t_R}{z_R^2 S_{wR}} \frac{\partial^2}{\partial z_D^2} c_{w3D} + \\
& \frac{K_{Lw4} t_R}{x_R^2 S_{wR}} \frac{\partial^2}{\partial x_D^2} c_{w4D} + \frac{K_{Tw4} t_R}{z_R^2 S_{wR}} \frac{\partial^2}{\partial z_D^2} c_{w4D}
\end{aligned} \tag{A.64}$$

## Constitutive Equations Dimensionless Groups

### Gas Velocity

$$u_{gx_D} = \frac{k_x k_{rg} p_{gR}}{\mu_g u_{gxR} x_R} \frac{\partial}{\partial x_D} p_{gD} \tag{A.65}$$

$$u_{gz_D} = \frac{k_z k_{rg} p_{gR}}{\mu_g u_{gzR} z_R} \frac{\partial}{\partial z_D} p_{gD} \tag{A.66}$$

### Oil Velocity

$$u_{ox_D} = \frac{k_x k_{ro} p_{oR}}{\mu_o u_{oxR} x_R} \frac{\partial}{\partial x_D} p_{oD} \tag{A.67}$$

$$u_{oz_D} = \frac{k_z k_{ro} p_{oR}}{\mu_o u_{ozR} z_R} \frac{\partial}{\partial z_D} p_{oD} \tag{A.68}$$

### Water Velocity

$$u_{wx_D} = \frac{k_x k_{rw} p_{wR}}{\mu_w u_{wxR} x_R} \frac{\partial}{\partial x_D} p_{wD} \tag{A.69}$$

$$u_{wz_D} = \frac{k_z k_{rw} p_{wR}}{\mu_w u_{wzR} z_R} \frac{\partial}{\partial z_D} p_{wD} \tag{A.70}$$

### Capillary Pressure Dimensionless Groups

The variables:  $p_w$ ,  $p_o$ , and  $p_g$  are substituted with their respective multiplicative factors. The equations obtained are then divided through by the displacing fluid pressures. The equations obtained are:

$$p_{wD} - \frac{p_{oR}}{p_{wR}} p_{oD} = \sigma_{ow} \frac{\sqrt{\phi/k_x}}{p_{wR}} j(S_w) \quad (\text{A.71})$$

$$\frac{p_{oR}}{p_{gR}} p_{oD} - p_{gD} = \sigma_{go} \frac{\sqrt{\phi/k_x}}{p_{gR}} j(S_o) \quad (\text{A.72})$$

### Initial and Boundary Conditions Dimensionless Groups

$$S_{wD} = \frac{S_{wi}}{S_{wR}} \quad \text{at } t_D = 0, \forall x_D, z_D \quad (\text{A.73})$$

$$S_{oD} = \frac{S_{oi}}{S_{oR}} \quad \text{at } t_D = 0, \forall x_D, z_D \quad (\text{A.74})$$

$$c_{g1D} = 0 \quad \text{at } t_D = 0, \forall x_D, z_D \quad (\text{A.75})$$

$$c_{o1D} = 0 \quad \text{at } t_D = 0, \forall x_D, z_D \quad (\text{A.76})$$

$$c_{o2D} = \frac{c_{2i}}{c_{o2R}} \quad \text{at } t_D = 0, \forall x_D, z_D \quad (\text{A.77})$$

$$c_{o4D} = 0 \quad \text{at } t_D = 0, \forall x_D, z_D \quad (\text{A.78})$$

$$c_{w1D} = 0 \quad \text{at } t_D = 0, \forall x_D, z_D \quad (\text{A.79})$$

$$c_{w3D} = \frac{c_{3i}}{c_{w3R}} \quad \text{at } t_D = 0, \forall x_D, z_D \quad (\text{A.80})$$

$$c_{w4D} = 0 \quad \text{at } t_D = 0, \forall x_D, z_D \quad (\text{A.81})$$

$$c_{g1D} = \frac{c_{1j}}{c_{g1R}} \quad \text{at } x_D = 0, \forall t_D, z_D \quad (\text{A.82})$$

$$c_{o1D} = 0 \quad \text{at } x_D = 0, \forall t_D, z_D \quad (\text{A.83})$$

$$c_{o2D} = 0 \quad \text{at } x_D = 0, \forall t_D, z_D \quad (\text{A.84})$$

$$c_{o4D} = 0 \quad \text{at } x_D = 0, \forall t_D, z_D \quad (\text{A.85})$$

$$c_{w1D} = 0 \quad \text{at } x_D = 0, \forall t_D, z_D \quad (\text{A.86})$$

$$c_{w3D} = 0 \quad \text{at } x_D = 0, \forall t_D, z_D \quad (\text{A.87})$$

$$c_{w4D} = \frac{c_{4j}}{c_{w4R}} \quad \text{at } x_D = 0, \forall t_D, z_D \quad (\text{A.88})$$

$$p_{gD} = \frac{\Delta p_g}{p_{gR}} + \frac{\rho_g g z_R}{p_{gR}} \left( \frac{H}{z_R} - z_D \right) \quad \text{at } x_D = \frac{L}{x_R}, \forall t_D, z_D \quad (\text{A.89})$$

$$p_{oD} = \frac{\Delta p_o}{p_{oR}} + \frac{\rho_o g z_R}{p_{oR}} \left( \frac{H}{z_R} - z_D \right) \quad \text{at } x_D = \frac{L}{x_R}, \forall t_D, z_D \quad (\text{A.90})$$

$$p_{wD} = \frac{\Delta p_w}{p_{wR}} + \frac{\rho_w g z_R}{p_{wR}} \left( \frac{H}{z_R} - z_D \right) \quad \text{at } x_D = \frac{L}{x_R}, \forall t_D, z_D \quad (\text{A.91})$$

$$u_{gzD} = 0 \quad \text{at } z_D = 0, \forall x_D, t_D \quad (\text{A.92})$$

$$u_{ozD} = 0 \quad \text{at } z_D = 0, \forall x_D, t_D \quad (\text{A.93})$$

$$u_{wzD} = 0 \quad \text{at } z_D = 0, \forall x_D, t_D \quad (\text{A.94})$$

$$u_{gzD} = 0 \quad \text{at } z_D = \frac{H}{z_R}, \forall x_D, t_D \quad (\text{A.95})$$

$$u_{ozD} = 0 \quad \text{at } z_D = \frac{H}{z_R}, \forall x_D, t_D \quad (\text{A.96})$$

$$u_{wzD} = 0 \quad \text{at } z_D = \frac{H}{z_R}, \forall x_D, t_D \quad (\text{A.97})$$

$$\int_0^{\frac{H}{z_R}} u_{gxD} dz_D = \frac{Hu_T}{z_R u_{gxR}} \quad \text{at } x_D = 0, \forall z_D, t_D \quad (\text{A.98})$$

### Saturation Constraint Dimensionless Groups

$$\frac{S_{gR}}{S_{wR}} S_{gD} + \frac{S_{oR}}{S_{wR}} S_{oD} + S_{wD} = 1 \quad (\text{A.99})$$

The reference variables or scale factors can be considered to be arbitrary for convenience, as this enables the simplification of the dimensionless equations. Setting some of the dimensionless groups to 0, 1, or equal to another group, leads to the provision of simple relationships for some of the reference variables which can in turn be substituted into other dimensionless equations for elimination or simplification. **Table A.1** shows the first set dimensionless groups derived.

Table A.1: Initial Dimensionless Groups from Inspectional Analysis.

Group	Equation	Originating Equation
1	$\frac{u_{gx_R} t_R}{\phi x_R S_{gR}}$	Gas transport equation groups
2	$\frac{u_{gz_R} t_R}{\phi z_R S_{gR}}$	
3	$\frac{u_{ox_R} t_R}{\phi x_R S_{oR}}$	Oil transport equation groups
4	$\frac{u_{oz_R} t_R}{\phi z_R S_{oR}}$	
5	$\frac{K_{L_{o1}} t_R}{x_R^2 S_{oR}}$	
6	$\frac{K_{T_{o1}} t_R}{z_R^2 S_{oR}}$	
7	$\frac{K_{L_{o2}} t_R}{x_R^2 S_{oR}}$	
8	$\frac{K_{T_{o2}} t_R}{z_R^2 S_{oR}}$	
9	$\frac{K_{L_{o4}} t_R}{x_R^2 S_{oR}}$	
10	$\frac{K_{T_{o4}} t_R}{z_R^2 S_{oR}}$	
11	$\frac{u_{wx_R} t_R}{\phi x_R S_{wR}}$	Water transport equation groups
12	$\frac{u_{wz_R} t_R}{\phi z_R S_{wR}}$	
13	$\frac{K_{L_{w1}} t_R}{x_R^2 S_{wR}}$	
14	$\frac{K_{T_{w1}} t_R}{z_R^2 S_{wR}}$	
15	$\frac{K_{L_{w3}} t_R}{x_R^2 S_{wR}}$	
16	$\frac{K_{T_{w3}} t_R}{z_R^2 S_{wR}}$	
17	$\frac{K_{L_{w4}} t_R}{x_R^2 S_{wR}}$	
18	$\frac{K_{T_{w4}} t_R}{z_R^2 S_{wR}}$	

Table A.1 – Continued on Next Page . . .



Group	Equation	Originating Equation
19	$\frac{k_x k_{rg} p_{gR}}{\mu_g u_{gxR} x_R}$	Constitutive equations groups
20	$\frac{k_z k_{rg} p_{gR}}{\mu_g u_{gzR} z_R}$	
21	$\frac{k_x k_{ro} p_{oR}}{\mu_o u_{oxR} x_R}$	
22	$\frac{k_z k_{ro} p_{oR}}{\mu_o u_{ozR} z_R}$	
23	$\frac{k_x k_{rw} p_{wR}}{\mu_w u_{wxR} x_R}$	
24	$\frac{k_z k_{rw} p_{wR}}{\mu_w u_{wzR} z_R}$	
25	$\frac{p_{oR}}{p_{wR}}$	Capillary pressure, initial and boundary conditions, and saturation constraints groups
26	$\sigma_{ow} \frac{\sqrt{\phi/k}}{p_{wR}}$	
27	$\frac{p_{gR}}{p_{oR}}$	
28	$\sigma_{go} \frac{\sqrt{\phi/k}}{p_{oR}}$	
29	$\frac{S_{wi}}{S_{wR}}$	
30	$\frac{S_{oi}}{S_{oR}}$	
31	$\frac{c_{2i}}{c_{o2R}}$	
32	$\frac{c_{3i}}{c_{w3R}}$	
33	$\frac{c_{1j}}{c_{g1R}}$	
34	$\frac{c_{4j}}{c_{w4R}}$	
35	$\frac{\Delta p_g}{p_{gR}}$	
36	$\frac{\rho_g g z_R}{p_{gR}}$	
37	$\frac{\Delta p_o}{p_{oR}}$	
38	$\frac{\rho_o g z_R}{p_{oR}}$	

Table A.1 – Continued on Next Page . . .

Group	Equation	Originating Equation
39	$\frac{\Delta p_w}{p_{wR}}$	
40	$\frac{\rho_w g z_R}{p_{wR}}$	
41	$\frac{H}{z_R}$	
42	$\frac{L}{x_R}$	
43	$\frac{H u_T}{z_R u_{gxR}}$	
44	$\frac{S_{gR}}{S_{wR}}$	
45	$\frac{S_{oR}}{S_{wR}}$	

The reference velocity for all the phases were made equal with respect to direction of flow, and reference phase saturations were equalized and set to  $\Delta S$ .

$$u_{gxR} = u_{oxR} = u_{wxR} = u_{xR} \quad (\text{A.100})$$

$$u_{gzR} = u_{ozR} = u_{wzR} = u_{zR} \quad (\text{A.101})$$

$$S_{gR} = S_{oR} = S_{wR} = \Delta S \text{ and } \Delta S = 1 - S_{gr} - S_{or} - S_{wc} \quad (\text{A.102})$$

Thus, setting groups 41 and 42 to 1 yield:

$$x_R = L \quad (\text{A.103})$$

$$z_R = H \quad (\text{A.104})$$

As a result of setting groups 41 and 42 to equal 1, and also equating group 43 to 1, leads to:

$$u_{gxR} = u_T \quad (\text{A.105})$$

$$\text{and, } u_{gxR} = u_{xR} \quad (\text{A.106})$$

$$\text{therefore, } u_{oxR} = u_{wxR} = u_T \quad (\text{A.107})$$

This relationship also impacts groups 1, 3, and 11 by making them the same. Furthermore, a relationship for  $t_R$  can be obtained from these groups when the resulting equation is made equal to 1.

$$t_R = \frac{\phi L \Delta S}{u_T} \quad (\text{A.108})$$

Equating groups 2, 4 and 12 to 1, and substituting for  $t_R$  leads to:

$$u_{gzR} = u_{ozR} = u_{wzR} = u_{zR} = \frac{H}{L} u_T \quad (\text{A.109})$$

Setting groups 19, 21, and 23 to 1, and solving for pressure yields:

$$p_{gR} = \frac{Lu_T\mu_g}{k_x k_{rg}} \quad (\text{A.110})$$

$$p_{oR} = \frac{Lu_T\mu_o}{k_x k_{ro}} \quad (\text{A.111})$$

$$p_{wR} = \frac{Lu_T\mu_w}{k_x k_{rw}} \quad (\text{A.112})$$

Groups 35, 37, and 39 are set to zero, bearing the following relationships:

$$\Delta p_g = p_{gi} - p_w f \quad (\text{A.113})$$

$$\Delta p_o = p_{oi} - p_w f \quad (\text{A.114})$$

$$\Delta p_w = p_{wi} - p_w f \quad (\text{A.115})$$

$$\text{Therefore, } p_{gi} = p_{oi} = p_{wi} = p_w f \quad (\text{A.116})$$

For the concentration scale factors, injected surfactant concentration,  $c_{4j}$ , is selected as the major variable in scaling other fluid concentrations. Therefore, group 34 is set to 1 to obtain:

$$c_{4j} = c_{w4R} \quad (\text{A.117})$$

The other phase-component fluid concentrations are made equal, and set to injected surfactant concentration

$$c_{g1R} = c_{o2R} = c_{w3R} = c_{4j} \quad (\text{A.118})$$

In summary, the basic reference equation that are obtained which will be substituted into the dimensionless equations include:

$$u_{gxR} = u_{oxR} = u_{wxR} = u_{xR} = u_T \quad (\text{A.119})$$

$$u_{gzR} = u_{ozR} = u_{wzR} = u_{zR} = \frac{H}{L} u_T \quad (\text{A.120})$$

$$t_R = \frac{\phi L \Delta S}{u_T} \quad (\text{A.121})$$

$$S_{gR} = S_{oR} = S_{wR} = \Delta S \quad (\text{A.122})$$

$$p_{gR} = \frac{Lu_T\mu_g}{k_x k_{rg}} \quad (\text{A.123})$$

$$p_{oR} = \frac{Lu_T \mu_o}{k_x k_{ro}} \quad (\text{A.124})$$

$$p_{wR} = \frac{Lu_T \mu_w}{k_x k_{rw}} \quad (\text{A.125})$$

$$c_{g1R} = c_{o2R} = c_{w3R} = c_{4j} \quad (\text{A.126})$$

The longitudinal and transverse dispersion groups (5 through 10 and 13 through 18) are simplified as follows:

$$\frac{\phi K_{L_{o1}}}{Lu_T} \quad (\text{A.127})$$

$$\frac{\phi K_{T_{o1}} L}{H^2 u_T} \quad (\text{A.128})$$

$$\frac{\phi K_{L_{o2}}}{Lu_T} \quad (\text{A.129})$$

$$\frac{\phi K_{T_{o2}} L}{H^2 u_T} \quad (\text{A.130})$$

$$\frac{\phi K_{L_{o4}}}{Lu_T} \quad (\text{A.131})$$

$$\frac{\phi K_{T_{o4}} L}{H^2 u_T} \quad (\text{A.132})$$

$$\frac{\phi K_{L_{w1}}}{Lu_T} \quad (\text{A.133})$$

$$\frac{\phi K_{T_{w1}} L}{H^2 u_T} \quad (\text{A.134})$$

$$\frac{\phi K_{L_{w3}}}{Lu_T} \quad (\text{A.135})$$

$$\frac{\phi K_{T_{w3}} L}{H^2 u_T} \quad (\text{A.136})$$

$$\frac{\phi K_{L_{w4}}}{Lu_T} \quad (\text{A.137})$$

$$\frac{\phi K_{Tw^4} L}{H^2 u_T} \quad (\text{A.138})$$

The defined scale factors are substituted into the dimensionless equations to obtain:

$$u_{gz_D} = \frac{k_z L^2}{k_x H^2} \frac{\partial}{\partial z_D} p_{gD} \quad (\text{A.139})$$

$$u_{oz_D} = \frac{k_z L^2}{k_x H^2} \frac{\partial}{\partial z_D} p_{oD} \quad (\text{A.140})$$

$$u_{wz_D} = \frac{k_z L^2}{k_x H^2} \frac{\partial}{\partial z_D} p_{wD} \quad (\text{A.141})$$

$$p_{wD} - \frac{\mu_o k_{rw}}{\mu_w k_{ro}} = \sigma_{ow} k_{rw} \frac{\sqrt{\phi k_x}}{Lu_T \mu_w} j(S_w) \quad (\text{A.142})$$

$$\frac{\mu_o k_{rg}}{\mu_g k_{ro}} - p_{gD} = \sigma_{go} k_{rg} \frac{\sqrt{\phi k_x}}{Lu_T \mu_g} j(S_g) \quad (\text{A.143})$$

$$S_{wD} = 1 \quad (\text{A.144})$$

$$S_{oD} = 1 \quad (\text{A.145})$$

$$c_{o2D} = \frac{c_{2i}}{c_{4j}} \quad (\text{A.146})$$

$$c_{w3D} = \frac{c_{3i}}{c_{4j}} \quad (\text{A.147})$$

$$c_{g1D} = \frac{c_{1j}}{c_{4j}} \quad (\text{A.148})$$

$$c_{w4D} = 1 \quad (\text{A.149})$$

$$p_{gD} = \rho_g g H \frac{k_x k_{rg}}{Lu_T \mu_g} (1 - z_D) \quad (\text{A.150})$$

$$p_{oD} = \rho_o g H \frac{k_x k_{ro}}{Lu_T \mu_o} (1 - z_D) \quad (\text{A.151})$$

$$p_{wD} = \rho_w g H \frac{k_x k_{rw}}{Lu_T \mu_w} (1 - z_D) \quad (\text{A.152})$$

Below are the extracted dimensionless scaling groups:

$$G_1 = \frac{\phi K_{L_{o1}}}{Lu_T} \quad (\text{A.153})$$

$$G_2 = \frac{\phi K_{T_{o1}} L}{H^2 u_T} \quad (\text{A.154})$$

$$G_3 = \frac{\phi K_{L_{o2}}}{Lu_T} \quad (\text{A.155})$$

$$G_4 = \frac{\phi K_{T_{o2}} L}{H^2 u_T} \quad (\text{A.156})$$

$$G_5 = \frac{\phi K_{L_{o4}}}{Lu_T} \quad (\text{A.157})$$

$$G_6 = \frac{\phi K_{T_{o4}} L}{H^2 u_T} \quad (\text{A.158})$$

$$G_7 = \frac{\phi K_{L_{w1}}}{Lu_T} \quad (\text{A.159})$$

$$G_8 = \frac{\phi K_{T_{w1}} L}{H^2 u_T} \quad (\text{A.160})$$

$$G_9 = \frac{\phi K_{L_{w3}}}{Lu_T} \quad (\text{A.161})$$

$$G_{10} = \frac{\phi K_{T_{w3}} L}{H^2 u_T} \quad (\text{A.162})$$

$$G_{11} = \frac{\phi K_{L_{w4}}}{Lu_T} \quad (\text{A.163})$$

$$G_{12} = \frac{\phi K_{T_{w4}} L}{H^2 u_T} \quad (\text{A.164})$$

$$G_{13} = \frac{k_z L^2}{k_x H^2} \quad (\text{A.165})$$

$$G_{14} = \frac{\mu_o k_{rw}}{\mu_w k_{ro}} \quad (\text{A.166})$$

$$G_{15} = \frac{\mu_o k_{rg}}{\mu_g k_{ro}} \quad (\text{A.167})$$

$$G_{16} = \sigma_{ow} k_{rw} \frac{\sqrt{\phi k_x}}{Lu_T \mu_w} \quad (\text{A.168})$$

$$G_{17} = \sigma_{go} k_{ro} \frac{\sqrt{\phi k_x}}{Lu_T \mu_o} \quad (\text{A.169})$$

$$G_{18} = \rho_g g H \frac{k_x k_{rg}}{Lu_T \mu_g} \quad (\text{A.170})$$

$$G_{19} = \rho_o g H \frac{k_x k_{ro}}{Lu_T \mu_o} \quad (\text{A.171})$$

$$G_{20} = \rho_w g H \frac{k_x k_{rw}}{Lu_T \mu_w} \quad (\text{A.172})$$

$$G_{21} = \frac{c_{2i}}{c_{4j}} \quad (\text{A.173})$$

$$G_{22} = \frac{c_{3i}}{c_{4j}} \quad (\text{A.174})$$

$$G_{23} = \frac{c_{1j}}{c_{4j}} \quad (\text{A.175})$$

## Appendix B: Auxiliary Laboratory Experiments

The results obtained from auxiliary experiments are summarized in this section. The auxiliary experiments include:

1. porosity and permeability determination
2. oil flood to connate water saturation
3. waterflood to residual oil saturation

Table B.1 below shows the properties of the core used in the experiments.

Table B.1: Summary of results from auxiliary experiments

Length, <i>cm</i>	7.65
Diameter, <i>cm</i>	2.56
Porosity	0.332
Permeability ( <i>mD</i> )	19.96

Properties of the fluids used are presented below in Table B.2

Table B.2: Properties of fluids

Fluid	$\mu$ , <i>cp</i> (24°C, 2500 <i>psi</i> )	$\rho$ , <i>g/cm<sup>3</sup></i> (24°C, 2500 <i>psi</i> )	$\rho$ , <i>g/cm<sup>3</sup></i> (24°C, 14.7 <i>psi</i> )
Decane	1.03	0.7388	0.7273
2% wt CaCl <sub>2</sub>	1.10	1.01	1.009
CO <sub>2</sub>	0.0901	0.8948	0.0018
CD-1045 Surfactant	200		1.07

Table B.3 shows the results for fluid volumes used to calculate core pore volume and porosity.

Brine was injected at rates of 1.0 cc/min, 1.5 cc/min, 2.0 cc/min, 2.5 cc/min and 3.0 cc/min, for 1 pore volume each. Pressure difference across the core was obtained and used to determine permeability. Table B.4 below presents the average pressure difference for each flow rate that was used to calculate absolute permeability.

Decane was injected into the core to displace brine. This process enabled the calculation of irreducible water and initial oil saturations. The results are presented in Table B.5.



Table B.3: Fluid volumes used to calculate core pore volume and porosity

Initial volume of brine in pump, $cm^3$	122.26
Final volume of brine in pump, $cm^3$	46.32
Total volume of brine injected, $cm^3$	75.94
Initial volume of brine in production unit, $cm^3$	249.47
Final volume of brine in production unit, $cm^3$	200
Total volume of brine produced, $cm^3$	49.47
Total volume of brine left in system, $cm^3$	26.47
System dead volume, $cm^3$	13.4
Volume of brine left in core (Pore Volume), $cm^3$	13.07
Bulk volume of core, $cm^3$	39.37
Porosity	0.332

Table B.4: Flow rates and corresponding average  $\Delta p$  used to determine absolute permeability

Flow rate $cm^3/min$	Average $\Delta p$ $psi$	Permeability $mD$
1.00	23.98	16.70
1.50	31.64	18.99
2.00	40.74	19.66
2.50	45.81	21.85
3.00	53.19	22.59

Table B.5: Fluid volumes used to calculate irreducible water and initial oil saturations from oil injection

Initial volume of decane in pump, $cm^3$	183.78
Final volume of decane in pump, $cm^3$	132.4
Total volume of decane injected, $cm^3$	51.38
Initial volume of decane in production unit, $cm^3$	206.45
Final volume of decane in production unit, $cm^3$	180
Total volume of decane produced, $cm^3$	26.45
Total volume of decane left in system, $cm^3$	24.93
System dead volume, $cm^3$	13.4
Volume of decane left in core, $cm^3$	11.53
Volume of brine left in core, $cm^3$	1.54
Irreducible water saturation	0.12
Initial oil saturation	0.88

After oil injection and the determination of  $S_{wirr}$  and  $S_{oi}$ , brine was injected into the core to displace oil and initial water and residual oil saturations were determined. The results are presented in Table B.6.

Table B.6: Fluid volumes used to calculate initial water and residual oil saturations from waterflood

Initial volume of brine in pump, $cm^3$	226.51
Final volume of brine in pump, $cm^3$	172.28
Total volume of brine injected, $cm^3$	54.23
Initial volume of decane in production unit, $cm^3$	186.26
Final volume of decane in production unit, $cm^3$	181
Total volume of decane produced, $cm^3$	5.26
Volume of decane left in core, $cm^3$	6.27
Volume of brine left in core, $cm^3$	6.80
Initial water saturation	0.52
Residual oil saturation to waterflood	0.48

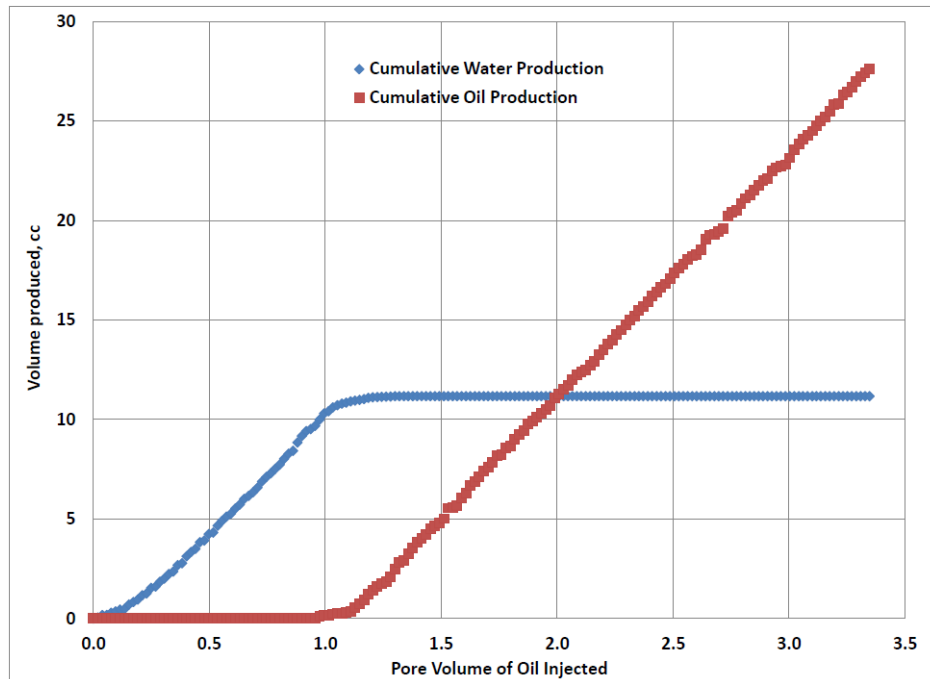
Results for fluid saturations remaining in the core after surfactant and  $CO_2$  coinjection are shown below in Table B.7.

Table B.7: Fluid saturations after surfactant and  $CO_2$  coinjection

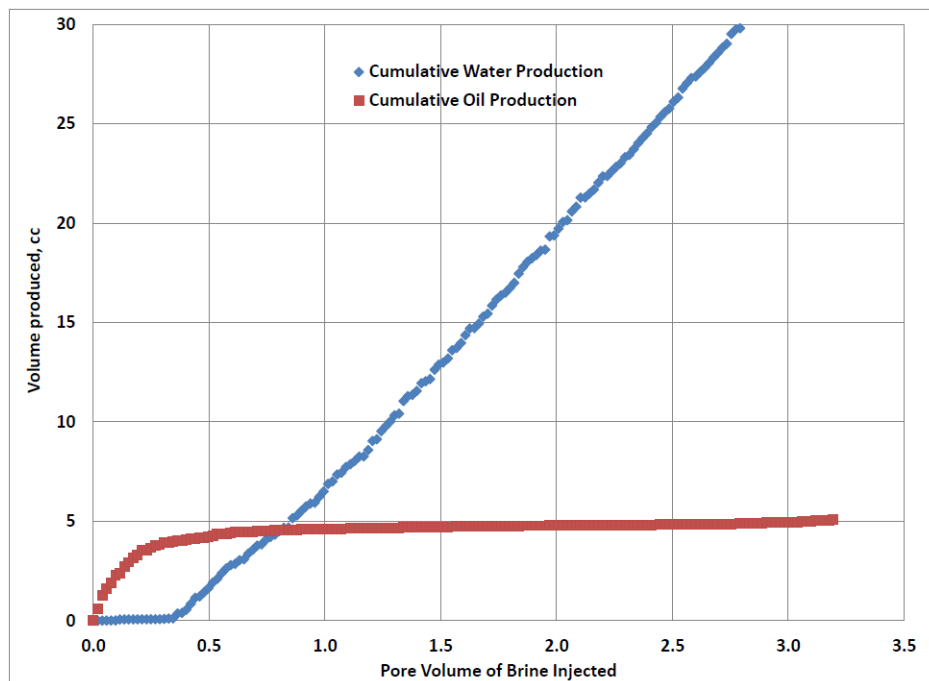
	0.1% wt	0.5% wt
Surfactant solution + brine saturation after coinjection	0.26	0.20
Oil saturation after coinjection	0.11	0.085
$CO_2$ saturation after coinjection	0.63	0.71

Graphs of cumulative oil and water produced during oil flood and waterflood procedures that were carried out before the coinjection of 0.1% wt and 0.5% wt surfactant solution are shown below in Figures B.1 and B.2.

Figures B.3 and Figures B.4 respectively illustrate the effect of surfactant concentration on pressure drop and foam mobility. These plots show the raw data (without the application of moving average) for pressure difference and foam mobility.

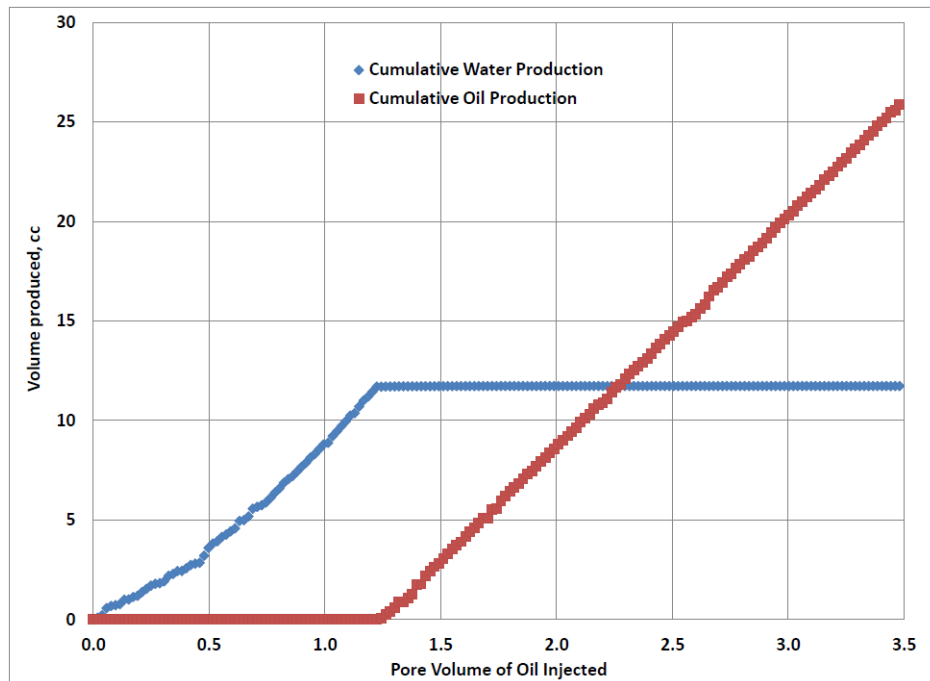


(a) Oil flood

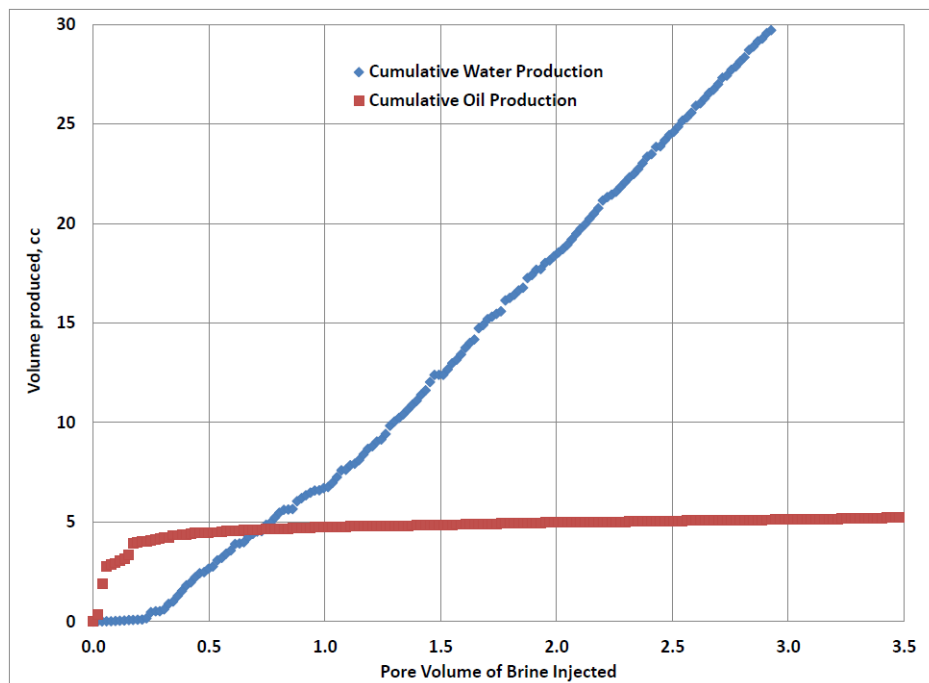


(b) Waterflood

Figure B.1: Cumulative oil and water produced for oil flood carried out before the coinjection of CO<sub>2</sub> and 0.1% wt surfactant solution



(a) Oil flood



(b) Waterflood

Figure B.2: Cumulative oil and water produced for oil flood carried out before the coinjection of CO<sub>2</sub> and 0.5% wt surfactant solution

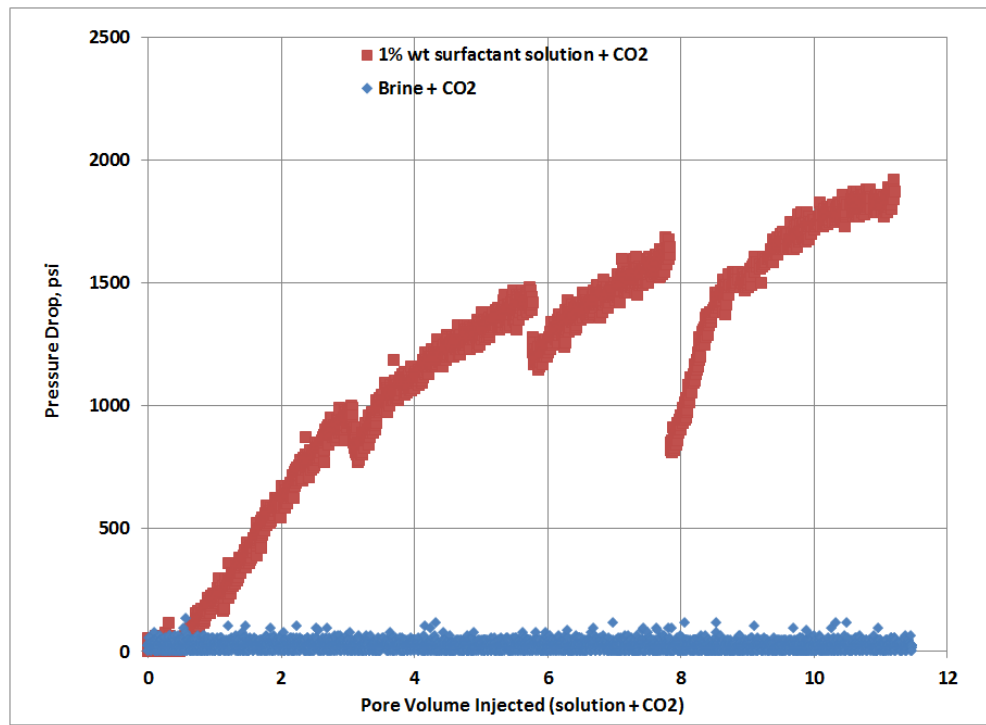


Figure B.3: Raw data of pressure difference for coinjection of CO<sub>2</sub> with brine (no surfactant) and coinjection of CO<sub>2</sub> with a solution of brine and 1.0% wt surfactant in a 1" (dia.) × 3" (long) Berea core

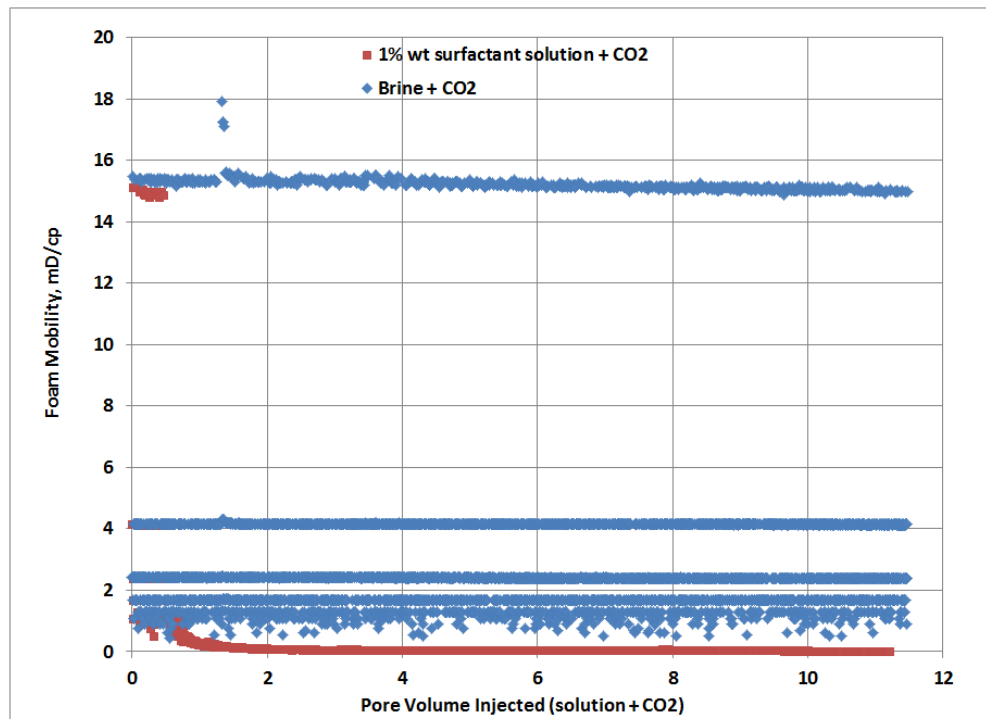


Figure B.4: Raw data of foam mobility for coinjection of CO<sub>2</sub> with brine (no surfactant) and maximum surfactant concentration (1.0% wt) in a 1" (dia.) × 3" (long) Berea core

## Appendix C: Inputs and Outputs for Design of Experiments

Hammersley Sequence Sampling technique was used to obtain 128 raw sampling points shown below in Table C.1. The actual values of dimensionless numbers that were obtained by interpolating and transforming the raw sampling points are shown in Table C.2. The dimensional parameters calculated from the dimensionless groups and used as input in the reservoir simulator are presented in Tables C.3, C.4, C.5, and C.6. Simulator-obtained results and linear- and quadratic-regression predicted values of  $RF$  and  $\Delta p$  for 128 cases are shown in Table C.7.

The linear and quadratic regression models obtained from the 128 cases were used to predict the output of 32 new models. Table C.8 shows values of the dimensionless parameters utilized in the prediction cases. Tables C.9, C.10, C.11, and C.12 show the values of dimensional variables that were used as input to the reservoir simulator. These values were calculated from the dimensionless parameters. The predicted results of  $RF$  and  $\Delta p$  are presented in Table C.13.

The following parameters were constant in all the cases:

$$g, cm/s^2 = 980.7$$

$$\mu_o, cp = 1.295$$

$$\mu_w, cp = 1.10$$

$$\sigma_{ow}, dyn/cm = 49$$

Table C.1: Raw sampling points defining the design space for dimensionless groups for 128 runs

Cases	$N_{pe(Lo1)}$	$N_{pe(To1)}$	$R_L$	$M_{go}$	$N_{cap(ow)}$	$N_{G(og)}$	$N_{G(wo)}$	$V_{DP}$	$c_{surf}$
1	0.0078	0.5	0.3333	0.2	0.1429	0.0909	0.0769	0.0588	0.0526
2	0.0156	0.25	0.6667	0.4	0.2857	0.1818	0.1538	0.1176	0.1053
3	0.0234	0.75	0.1111	0.6	0.4286	0.2727	0.2308	0.1765	0.1579
4	0.0313	0.125	0.4444	0.8	0.5714	0.3636	0.3077	0.2353	0.2105
5	0.0391	0.625	0.7778	0.04	0.7143	0.4545	0.3846	0.2941	0.2632
6	0.0469	0.375	0.2222	0.24	0.8571	0.5455	0.4615	0.3529	0.3158
7	0.0547	0.875	0.5556	0.44	0.0204	0.6364	0.5385	0.4118	0.3684
8	0.0625	0.0625	0.8889	0.64	0.1633	0.7273	0.6154	0.4706	0.4211

Table C.1: (continued)

Cases	$N_{pe(Lo1)}$	$N_{pe(To1)}$	$R_L$	$M_{go}$	$N_{cap(ow)}$	$N_{G(og)}$	$N_{G(wo)}$	$V_{DP}$	$c_{surf}$
9	0.0703	0.5625	0.037	0.84	0.3061	0.8182	0.6923	0.5294	0.4737
10	0.0781	0.3125	0.3704	0.08	0.449	0.9091	0.7692	0.5882	0.5263
11	0.0859	0.8125	0.7037	0.28	0.5918	0.0083	0.8462	0.6471	0.5789
12	0.0938	0.1875	0.1481	0.48	0.7347	0.0992	0.9231	0.7059	0.6316
13	0.1016	0.6875	0.4815	0.68	0.8776	0.1901	0.0059	0.7647	0.6842
14	0.1094	0.4375	0.8148	0.88	0.0408	0.281	0.0828	0.8235	0.7368
15	0.1172	0.9375	0.2593	0.12	0.1837	0.3719	0.1598	0.8824	0.7895
16	0.125	0.0313	0.5926	0.32	0.3265	0.4628	0.2367	0.9412	0.8421
17	0.1328	0.5313	0.9259	0.52	0.4694	0.5537	0.3136	0.0035	0.8947
18	0.1406	0.2813	0.0741	0.72	0.6122	0.6446	0.3905	0.0623	0.9474
19	0.1484	0.7813	0.4074	0.92	0.7551	0.7355	0.4675	0.1211	0.0028
20	0.1563	0.1563	0.7407	0.16	0.898	0.8264	0.5444	0.1799	0.0554
21	0.1641	0.6563	0.1852	0.36	0.0612	0.9174	0.6213	0.2388	0.108
22	0.1719	0.4063	0.5185	0.56	0.2041	0.0165	0.6982	0.2976	0.1607
23	0.1797	0.9063	0.8519	0.76	0.3469	0.1074	0.7751	0.3564	0.2133
24	0.1875	0.0938	0.2963	0.96	0.4898	0.1983	0.8521	0.4152	0.2659
25	0.1953	0.5938	0.6296	0.008	0.6327	0.2893	0.929	0.474	0.3186
26	0.2031	0.3438	0.963	0.208	0.7755	0.3802	0.0118	0.5329	0.3712
27	0.2109	0.8438	0.0123	0.408	0.9184	0.4711	0.0888	0.5917	0.4238
28	0.2188	0.2188	0.3457	0.608	0.0816	0.562	0.1657	0.6505	0.4765
29	0.2266	0.7188	0.679	0.808	0.2245	0.6529	0.2426	0.7093	0.5291
30	0.2344	0.4688	0.1235	0.048	0.3673	0.7438	0.3195	0.7682	0.5817
31	0.2422	0.9688	0.4568	0.248	0.5102	0.8347	0.3964	0.827	0.6343
32	0.25	0.0156	0.7901	0.448	0.6531	0.9256	0.4734	0.8858	0.687
33	0.2578	0.5156	0.2346	0.648	0.7959	0.0248	0.5503	0.9446	0.7396
34	0.2656	0.2656	0.5679	0.848	0.9388	0.1157	0.6272	0.0069	0.7922
35	0.2734	0.7656	0.9012	0.088	0.102	0.2066	0.7041	0.0657	0.8449
36	0.2813	0.1406	0.0494	0.288	0.2449	0.2975	0.7811	0.1246	0.8975
37	0.2891	0.6406	0.3827	0.488	0.3878	0.3884	0.858	0.1834	0.9501
38	0.2969	0.3906	0.716	0.688	0.5306	0.4793	0.9349	0.2422	0.0055
39	0.3047	0.8906	0.1605	0.888	0.6735	0.5702	0.0178	0.301	0.0582
40	0.3125	0.0781	0.4938	0.128	0.8163	0.6612	0.0947	0.3599	0.1108
41	0.3203	0.5781	0.8272	0.328	0.9592	0.7521	0.1716	0.4187	0.1634
42	0.3281	0.3281	0.2716	0.528	0.1224	0.843	0.2485	0.4775	0.2161
43	0.3359	0.8281	0.6049	0.728	0.2653	0.9339	0.3254	0.5363	0.2687
44	0.3438	0.2031	0.9383	0.928	0.4082	0.0331	0.4024	0.5952	0.3213
45	0.3516	0.7031	0.0864	0.168	0.551	0.124	0.4793	0.654	0.374
46	0.3594	0.4531	0.4198	0.368	0.6939	0.2149	0.5562	0.7128	0.4266
47	0.3672	0.9531	0.7531	0.568	0.8367	0.3058	0.6331	0.7716	0.4792
48	0.375	0.0469	0.1975	0.768	0.9796	0.3967	0.7101	0.8304	0.5319
49	0.3828	0.5469	0.5309	0.968	0.0029	0.4876	0.787	0.8893	0.5845
50	0.3906	0.2969	0.8642	0.016	0.1458	0.5785	0.8639	0.9481	0.6371
51	0.3984	0.7969	0.3086	0.216	0.2886	0.6694	0.9408	0.0104	0.6898
52	0.4063	0.1719	0.642	0.416	0.4315	0.7603	0.0237	0.0692	0.7424
53	0.4141	0.6719	0.9753	0.616	0.5743	0.8512	0.1006	0.128	0.795
54	0.4219	0.4219	0.0247	0.816	0.7172	0.9421	0.1775	0.1869	0.8476
55	0.4297	0.9219	0.358	0.056	0.8601	0.0413	0.2544	0.2457	0.9003
56	0.4375	0.1094	0.6914	0.256	0.0233	0.1322	0.3314	0.3045	0.9529
57	0.4453	0.6094	0.1358	0.456	0.1662	0.2231	0.4083	0.3633	0.0083
58	0.4531	0.3594	0.4691	0.656	0.309	0.314	0.4852	0.4221	0.0609
59	0.4609	0.8594	0.8025	0.856	0.4519	0.405	0.5621	0.481	0.1136
60	0.4688	0.2344	0.2469	0.096	0.5948	0.4959	0.6391	0.5398	0.1662
61	0.4766	0.7344	0.5802	0.296	0.7376	0.5868	0.716	0.5986	0.2188
62	0.4844	0.4844	0.9136	0.496	0.8805	0.6777	0.7929	0.6574	0.2715
63	0.4922	0.9844	0.0617	0.696	0.0437	0.7686	0.8698	0.7163	0.3241
64	0.5	0.0078	0.3951	0.896	0.1866	0.8595	0.9467	0.7751	0.3767
65	0.5078	0.5078	0.7284	0.136	0.3294	0.9504	0.0296	0.8339	0.4294
66	0.5156	0.2578	0.1728	0.336	0.4723	0.0496	0.1065	0.8927	0.482
67	0.5234	0.7578	0.5062	0.536	0.6152	0.1405	0.1834	0.9516	0.5346
68	0.5313	0.1328	0.8395	0.736	0.758	0.2314	0.2604	0.0138	0.5873

Table C.1: (continued)

Cases	$N_{pe(Lo1)}$	$N_{pe(To1)}$	$R_L$	$M_{go}$	$N_{cap(ow)}$	$N_{G(og)}$	$N_{G(wo)}$	$V_{DP}$	$c_{surf}$
69	0.5391	0.6328	0.284	0.936	0.9009	0.3223	0.3373	0.0727	0.6399
70	0.5469	0.3828	0.6173	0.176	0.0641	0.4132	0.4142	0.1315	0.6925
71	0.5547	0.8828	0.9506	0.376	0.207	0.5041	0.4911	0.1903	0.7452
72	0.5625	0.0703	0.0988	0.576	0.3499	0.595	0.568	0.2491	0.7978
73	0.5703	0.5703	0.4321	0.776	0.4927	0.686	0.645	0.308	0.8504
74	0.5781	0.3203	0.7654	0.976	0.6356	0.7769	0.7219	0.3668	0.903
75	0.5859	0.8203	0.2099	0.024	0.7784	0.8678	0.7988	0.4256	0.9557
76	0.5938	0.1953	0.5432	0.224	0.9213	0.9587	0.8757	0.4844	0.0111
77	0.6016	0.6953	0.8765	0.424	0.0845	0.0579	0.9527	0.5433	0.0637
78	0.6094	0.4453	0.321	0.624	0.2274	0.1488	0.0355	0.6021	0.1163
79	0.6172	0.9453	0.6543	0.824	0.3703	0.2397	0.1124	0.6609	0.169
80	0.625	0.0391	0.9877	0.064	0.5131	0.3306	0.1893	0.7197	0.2216
81	0.6328	0.5391	0.0041	0.264	0.656	0.4215	0.2663	0.7785	0.2742
82	0.6406	0.2891	0.3374	0.464	0.7988	0.5124	0.3432	0.8374	0.3269
83	0.6484	0.7891	0.6708	0.664	0.9417	0.6033	0.4201	0.8962	0.3795
84	0.6563	0.1641	0.1152	0.864	0.105	0.6942	0.497	0.955	0.4321
85	0.6641	0.6641	0.4486	0.104	0.2478	0.7851	0.574	0.0173	0.4848
86	0.6719	0.4141	0.7819	0.304	0.3907	0.876	0.6509	0.0761	0.5374
87	0.6797	0.9141	0.2263	0.504	0.5335	0.9669	0.7278	0.1349	0.59
88	0.6875	0.1016	0.5597	0.704	0.6764	0.0661	0.8047	0.1938	0.6427
89	0.6953	0.6016	0.893	0.904	0.8192	0.157	0.8817	0.2526	0.6953
90	0.7031	0.3516	0.0412	0.144	0.9621	0.2479	0.9586	0.3114	0.7479
91	0.7109	0.8516	0.3745	0.344	0.1254	0.3388	0.0414	0.3702	0.8006
92	0.7188	0.2266	0.7078	0.544	0.2682	0.4298	0.1183	0.4291	0.8532
93	0.7266	0.7266	0.1523	0.744	0.4111	0.5207	0.1953	0.4879	0.9058
94	0.7344	0.4766	0.4856	0.944	0.5539	0.6116	0.2722	0.5467	0.9584
95	0.7422	0.9766	0.8189	0.184	0.6968	0.7025	0.3491	0.6055	0.0139
96	0.75	0.0234	0.2634	0.384	0.8397	0.7934	0.426	0.6644	0.0665
97	0.7578	0.5234	0.5967	0.584	0.9825	0.8843	0.503	0.7232	0.1191
98	0.7656	0.2734	0.93	0.784	0.0058	0.9752	0.5799	0.782	0.1717
99	0.7734	0.7734	0.0782	0.984	0.1487	0.0744	0.6568	0.8408	0.2244
100	0.7813	0.1484	0.4115	0.032	0.2915	0.1653	0.7337	0.8997	0.277
101	0.7891	0.6484	0.7449	0.232	0.4344	0.2562	0.8107	0.9585	0.3296
102	0.7969	0.3984	0.1893	0.432	0.5773	0.3471	0.8876	0.0208	0.3823
103	0.8047	0.8984	0.5226	0.632	0.7201	0.438	0.9645	0.0796	0.4349
104	0.8125	0.0859	0.856	0.832	0.863	0.5289	0.0473	0.1384	0.4875
105	0.8203	0.5859	0.3004	0.072	0.0262	0.6198	0.1243	0.1972	0.5402
106	0.8281	0.3359	0.6337	0.272	0.1691	0.7107	0.2012	0.2561	0.5928
107	0.8359	0.8359	0.9671	0.472	0.312	0.8017	0.2781	0.3149	0.6454
108	0.8438	0.2109	0.0165	0.672	0.4548	0.8926	0.355	0.3737	0.6981
109	0.8516	0.7109	0.3498	0.872	0.5977	0.9835	0.432	0.4325	0.7507
110	0.8594	0.4609	0.6831	0.112	0.7405	0.0826	0.5089	0.4913	0.8033
111	0.8672	0.9609	0.1276	0.312	0.8834	0.1736	0.5858	0.5502	0.856
112	0.875	0.0547	0.4609	0.512	0.0466	0.2645	0.6627	0.609	0.9086
113	0.8828	0.5547	0.7942	0.712	0.1895	0.3554	0.7396	0.6678	0.9612
114	0.8906	0.3047	0.2387	0.912	0.3324	0.4463	0.8166	0.7266	0.0166
115	0.8984	0.8047	0.572	0.152	0.4752	0.5372	0.8935	0.7855	0.0693
116	0.9063	0.1797	0.9053	0.352	0.6181	0.6281	0.9704	0.8443	0.1219
117	0.9141	0.6797	0.0535	0.552	0.7609	0.719	0.0533	0.9031	0.1745
118	0.9219	0.4297	0.3868	0.752	0.9038	0.8099	0.1302	0.9619	0.2271
119	0.9297	0.9297	0.7202	0.952	0.0671	0.9008	0.2071	0.0242	0.2798
120	0.9375	0.1172	0.1646	0.192	0.2099	0.9917	0.284	0.083	0.3324
121	0.9453	0.6172	0.4979	0.392	0.3528	0.0008	0.3609	0.1419	0.385
122	0.9531	0.3672	0.8313	0.592	0.4956	0.0917	0.4379	0.2007	0.4377
123	0.9609	0.8672	0.2757	0.792	0.6385	0.1826	0.5148	0.2595	0.4903
124	0.9688	0.2422	0.6091	0.992	0.7813	0.2735	0.5917	0.3183	0.5429
125	0.9766	0.7422	0.9424	0.0016	0.9242	0.3644	0.6686	0.3772	0.5956
126	0.9844	0.4922	0.0905	0.2016	0.0875	0.4553	0.7456	0.436	0.6482
127	0.9922	0.9922	0.4239	0.4016	0.2303	0.5462	0.8225	0.4948	0.7008
128	1	0.0039	0.7572	0.6016	0.3732	0.6371	0.8994	0.5536	0.7535



Table C.2: Actual sampling points defining the design space for dimensionless groups for 128 runs

Cases	$N_{pe(Lo1)}$	$N_{pe(To1)}$	$R_L$	$M_{go}$	$N_{cap(ow)} \times 10^{-6}$	$N_{G(og)} \times 10^7$	$N_{G(wo)} \times 10^8$	$V_{DP}$	$c_{surf}$
1	69	1166.13	2.5	13.98	2.49	4.25	2.69	0.1404	0.1208
2	73.06	701.94	3.52	13.5	2.56	4.32	2.73	0.1834	0.1428
3	77.13	1630.32	1.83	13.04	2.63	4.39	2.77	0.2264	0.1647
4	81.19	469.84	2.84	12.62	2.7	4.46	2.81	0.2693	0.1867
5	85.25	1398.22	3.86	12.22	2.77	4.53	2.84	0.3123	0.2087
6	89.31	934.03	2.17	11.85	2.84	4.6	2.88	0.3552	0.2306
7	93.38	1862.41	3.18	11.5	2.43	4.67	2.92	0.3982	0.2526
8	97.44	353.79	4.2	11.17	2.5	4.73	2.96	0.4412	0.2746
9	101.5	1282.17	1.6	10.85	2.57	4.8	3	0.4841	0.2965
10	105.57	817.98	2.62	10.56	2.64	4.87	3.03	0.5271	0.3185
11	109.63	1746.36	3.63	10.28	2.71	4.19	3.07	0.57	0.3405
12	113.69	585.89	1.94	10.01	2.78	4.26	3.11	0.613	0.3624
13	117.76	1514.27	2.96	9.76	2.85	4.33	2.66	0.656	0.3844
14	121.82	1050.08	3.97	9.52	2.44	4.4	2.7	0.6989	0.4064
15	125.88	1978.46	2.28	9.29	2.51	4.47	2.73	0.7419	0.4283
16	129.94	295.77	3.29	9.07	2.58	4.53	2.77	0.7848	0.4503
17	134.01	1224.15	4.31	8.87	2.65	4.6	2.81	0.1	0.4723
18	138.07	759.96	1.71	8.67	2.72	4.67	2.85	0.143	0.4942
19	142.13	1688.34	2.73	14.48	2.79	4.74	2.89	0.1859	0.1
20	146.2	527.87	3.75	13.96	2.86	4.81	2.92	0.2289	0.122
21	150.26	1456.25	2.05	13.47	2.45	4.88	2.96	0.2718	0.1439
22	154.32	992.05	3.07	13.02	2.52	4.2	3	0.3148	0.1659
23	158.39	1920.43	4.09	12.6	2.59	4.27	3.04	0.3578	0.1879
24	162.45	411.82	2.39	12.2	2.66	4.33	3.07	0.4007	0.2098
25	166.51	1340.2	3.41	11.83	2.73	4.4	3.11	0.4437	0.2318
26	170.57	876.01	4.42	11.48	2.8	4.47	2.66	0.4866	0.2538
27	174.64	1804.39	1.53	11.15	2.87	4.54	2.7	0.5296	0.2757
28	178.7	643.91	2.54	10.84	2.46	4.61	2.74	0.5726	0.2977
29	182.76	1572.29	3.56	10.54	2.53	4.68	2.77	0.6155	0.3197
30	186.83	1108.1	1.86	10.26	2.6	4.75	2.81	0.6585	0.3416
31	190.89	2036.48	2.88	10	2.67	4.82	2.85	0.7014	0.3636
32	194.95	266.76	3.9	9.75	2.74	4.88	2.89	0.7444	0.3855
33	199.02	1195.14	2.2	9.51	2.81	4.2	2.93	0.7874	0.4075
34	203.08	730.95	3.22	9.28	2.88	4.27	2.96	0.1025	0.4295
35	207.14	1659.33	4.24	9.06	2.47	4.34	3	0.1455	0.4514
36	211.2	498.85	1.64	8.86	2.54	4.41	3.04	0.1884	0.4734
37	215.27	1427.23	2.65	8.66	2.61	4.48	3.08	0.2314	0.4954
38	219.33	963.04	3.67	14.45	2.68	4.55	3.12	0.2744	0.1012
39	223.39	1891.42	1.98	13.93	2.75	4.62	2.66	0.3173	0.1231
40	227.46	382.81	2.99	13.45	2.82	4.68	2.7	0.3603	0.1451
41	231.52	1311.19	4.01	13	2.89	4.75	2.74	0.4032	0.1671
42	235.58	847	2.32	12.58	2.48	4.82	2.78	0.4462	0.189
43	239.65	1775.38	3.33	12.18	2.55	4.89	2.82	0.4892	0.211
44	243.71	614.9	4.35	11.81	2.62	4.21	2.85	0.5321	0.2329
45	247.77	1543.28	1.75	11.46	2.69	4.28	2.89	0.5751	0.2549
46	251.83	1079.09	2.77	11.13	2.76	4.35	2.93	0.6181	0.2769
47	255.9	2007.47	3.78	10.82	2.83	4.42	2.97	0.661	0.2988
48	259.96	324.78	2.09	10.53	2.9	4.48	3	0.704	0.3208
49	264.02	1253.16	3.11	10.25	2.43	4.55	3.04	0.7469	0.3428
50	268.09	788.97	4.12	9.99	2.5	4.62	3.08	0.7899	0.3647
51	272.15	1717.35	2.43	9.73	2.57	4.69	3.12	0.1051	0.3867
52	276.21	556.88	3.45	9.5	2.63	4.76	2.67	0.148	0.4087
53	280.28	1485.26	4.46	9.27	2.7	4.83	2.7	0.191	0.4306
54	284.34	1021.07	1.56	9.05	2.77	4.9	2.74	0.2339	0.4526
55	288.4	1949.45	2.58	8.85	2.84	4.22	2.78	0.2769	0.4746
56	292.46	440.83	3.6	8.65	2.44	4.28	2.82	0.3199	0.4965
57	296.53	1369.21	1.9	14.42	2.51	4.35	2.86	0.3628	0.1023

Table C.2: (continued)

Cases	$N_{pe(L01)}$	$N_{pe(T01)}$	$R_L$	$M_{gv}$	$N_{cap(ow)} \times 10^{-6}$	$N_{G(og)} \times 10^7$	$N_{G(wo)} \times 10^8$	$V_{DP}$	$c_{surf}$
58	300.59	905.02	2.92	13.91	2.58	4.42	2.89	0.4058	0.1243
59	304.65	1833.4	3.94	13.42	2.64	4.49	2.93	0.4487	0.1462
60	308.72	672.92	2.24	12.97	2.71	4.56	2.97	0.4917	0.1682
61	312.78	1601.3	3.26	12.55	2.78	4.63	3.01	0.5347	0.1902
62	316.84	1137.11	4.27	12.16	2.85	4.7	3.05	0.5776	0.2121
63	320.9	2065.49	1.68	11.79	2.45	4.77	3.08	0.6206	0.2341
64	324.97	252.25	2.69	11.44	2.52	4.83	3.12	0.6635	0.2561
65	329.03	1180.63	3.71	11.12	2.59	4.9	2.67	0.7065	0.278
66	333.09	716.44	2.01	10.81	2.65	4.22	2.71	0.7495	0.3
67	337.16	1644.82	3.03	10.51	2.72	4.29	2.75	0.7924	0.322
68	341.22	484.35	4.05	10.23	2.79	4.36	2.78	0.1076	0.3439
69	345.28	1412.73	2.35	9.97	2.86	4.43	2.82	0.1505	0.3659
70	349.35	948.54	3.37	9.72	2.46	4.5	2.86	0.1935	0.3879
71	353.41	1876.92	4.39	9.48	2.53	4.57	2.9	0.2365	0.4098
72	357.47	368.3	1.79	9.26	2.59	4.63	2.93	0.2794	0.4318
73	361.54	1296.68	2.81	9.04	2.66	4.7	2.97	0.3224	0.4538
74	365.6	832.49	3.82	8.84	2.73	4.77	3.01	0.3653	0.4757
75	369.66	1760.87	2.13	8.64	2.8	4.84	3.05	0.4083	0.4977
76	373.72	600.39	3.14	14.39	2.87	4.91	3.09	0.4513	0.1035
77	377.79	1528.77	4.16	13.88	2.47	4.23	3.12	0.4942	0.1254
78	381.85	1064.58	2.47	13.4	2.54	4.3	2.67	0.5372	0.1474
79	385.91	1992.96	3.48	12.95	2.6	4.37	2.71	0.5801	0.1694
80	389.98	310.28	4.5	12.53	2.67	4.43	2.75	0.6231	0.1913
81	394.04	1238.66	1.5	12.14	2.74	4.5	2.79	0.6661	0.2133
82	398.1	774.47	2.52	11.77	2.81	4.57	2.82	0.709	0.2353
83	402.17	1702.85	3.53	11.43	2.88	4.64	2.86	0.752	0.2572
84	406.23	542.37	1.84	11.1	2.48	4.71	2.9	0.7949	0.2792
85	410.29	1470.75	2.86	10.79	2.55	4.78	2.94	0.1101	0.3012
86	414.35	1006.56	3.87	10.5	2.61	4.85	2.98	0.1531	0.3231
87	418.42	1934.94	2.18	10.22	2.68	4.92	3.01	0.196	0.3451
88	422.48	426.32	3.19	9.96	2.75	4.23	3.05	0.239	0.3671
89	426.54	1354.7	4.21	9.71	2.82	4.3	3.09	0.2819	0.389
90	430.61	890.51	1.61	9.47	2.89	4.37	3.13	0.3249	0.411
91	434.67	1818.89	2.63	9.25	2.49	4.44	2.68	0.3679	0.4329
92	438.73	658.42	3.65	9.03	2.56	4.51	2.71	0.4108	0.4549
93	442.8	1586.8	1.95	8.82	2.62	4.58	2.75	0.4538	0.4769
94	446.86	1122.61	2.97	8.63	2.69	4.65	2.79	0.4968	0.4988
95	450.92	2050.99	3.99	14.37	2.76	4.72	2.83	0.5397	0.1046
96	454.98	281.26	2.29	13.85	2.83	4.78	2.86	0.5827	0.1266
97	459.05	1209.64	3.31	13.38	2.9	4.85	2.9	0.6256	0.1486
98	463.11	745.45	4.32	12.93	2.43	4.92	2.94	0.6686	0.1705
99	467.17	1673.83	1.73	12.51	2.5	4.24	2.98	0.7116	0.1925
100	471.24	513.36	2.74	12.12	2.57	4.31	3.02	0.7545	0.2145
101	475.3	1441.74	3.76	11.75	2.64	4.38	3.05	0.7975	0.2364
102	479.36	977.55	2.06	11.41	2.71	4.45	3.09	0.1126	0.2584
103	483.43	1905.93	3.08	11.08	2.78	4.52	3.13	0.1556	0.2803
104	487.49	397.31	4.1	10.77	2.84	4.58	2.68	0.1986	0.3023
105	491.55	1325.69	2.4	10.48	2.44	4.65	2.72	0.2415	0.3243
106	495.61	861.5	3.42	10.21	2.51	4.72	2.75	0.2845	0.3462
107	499.68	1789.88	4.44	9.94	2.58	4.79	2.79	0.3274	0.3682
108	503.74	629.41	1.54	9.7	2.65	4.86	2.83	0.3704	0.3902
109	507.8	1557.79	2.55	9.46	2.72	4.93	2.87	0.4134	0.4121
110	511.87	1093.6	3.57	9.23	2.79	4.25	2.91	0.4563	0.4341
111	515.93	2021.98	1.88	9.02	2.85	4.32	2.94	0.4993	0.4561
112	519.99	339.29	2.89	8.81	2.45	4.38	2.98	0.5422	0.478
113	524.05	1267.67	3.91	8.62	2.52	4.45	3.02	0.5852	0.5
114	528.12	803.48	2.22	14.34	2.59	4.52	3.06	0.6282	0.1058
115	532.18	1731.86	3.23	13.83	2.66	4.59	3.1	0.6711	0.1277
116	536.24	571.38	4.25	13.35	2.73	4.66	3.13	0.7141	0.1497
117	540.31	1499.76	1.65	12.91	2.8	4.73	2.68	0.757	0.1717

Table C.2: (continued)

Cases	$N_{pe(Lo1)}$	$N_{pe(To1)}$	$R_L$	$M_{gv}$	$N_{cap(ow)} \times 10^{-6}$	$N_{G(og)} \times 10^7$	$N_{G(wo)} \times 10^8$	$V_{DP}$	$c_{surf}$
118	544.37	1035.57	2.67	12.49	2.86	4.8	2.72	0.8	0.1936
119	548.43	1963.95	3.68	12.1	2.46	4.87	2.76	0.1152	0.2156
120	552.5	455.34	1.99	11.73	2.53	4.93	2.79	0.1581	0.2376
121	556.56	1383.72	3.01	11.39	2.6	4.18	2.83	0.2011	0.2595
122	560.62	919.53	4.02	11.06	2.67	4.25	2.87	0.244	0.2815
123	564.68	1847.9	2.33	10.76	2.74	4.32	2.91	0.287	0.3035
124	568.75	687.43	3.35	10.47	2.81	4.39	2.95	0.33	0.3254
125	572.81	1615.81	4.36	10.19	2.87	4.46	2.98	0.3729	0.3474
126	576.87	1151.62	1.76	9.93	2.47	4.53	3.02	0.4159	0.3694
127	580.94	2080	2.78	9.68	2.54	4.6	3.06	0.4588	0.3913
128	585	245	3.8	9.45	2.61	4.67	3.1	0.5018	0.4133

Table C.3: Part 1: Dimensional properties calculated from dimensionless numbers

Case	L cm	H cm	$\phi$	$k_1$ mD	$k_2$ mD	$k_3$ mD	$k_4$ mD	$k_5$ mD
1	8636.43	3448.8	0.37	51.29	61.55	67.05	72.41	79.48
2	6341.2	1801.01	0.34	125.04	159.6	179.01	198.4	224.77
3	5643.91	3090.25	0.387	26	35.42	40.96	46.66	54.66
4	7212.81	2536.95	0.384	25.95	37.87	45.23	53.05	64.36
5	5883.42	1524.27	0.3	37.45	58.79	72.67	87.88	110.67
6	6314.58	2916.3	0.395	79.12	134.23	172.11	215.07	281.82
7	7969.66	2504.6	0.337	54.33	100.16	133.54	172.82	236.28
8	5327.49	1268.83	0.331	33.57	67.65	94.06	126.39	180.87
9	8782.19	5487.43	0.344	42.09	93.41	135.88	190.16	285.87
10	8344.92	3188.55	0.397	5.53	13.63	20.83	30.47	48.32
11	2341.56	644.37	0.386	34.99	96.73	156	239.47	402.76
12	2900.66	1495.7	0.352	20.07	62.97	107.8	174.57	313.26
13	7757.99	2624.43	0.375	11.61	41.98	76.82	132.06	254.8
14	3032.99	763.44	0.316	17.98	76.32	150.62	277.06	580.33
15	7319.99	3213	0.302	1.69	8.63	18.58	36.95	85.1
16	9165.5	2781.66	0.356	8.17	52.01	124.14	270.84	697.75
17	8382.76	1944.18	0.389	122.83	139.45	148.02	156.16	166.63
18	5856.07	3417.83	0.361	81.3	97.9	106.84	115.54	127.06
19	3900.2	1428.58	0.319	126.29	161.8	181.79	201.8	229.06
20	2854.52	761.84	0.313	96.74	132.3	153.28	174.9	205.27
21	9289.04	4526.16	0.301	104.18	152.66	182.7	214.64	260.95
22	4419.75	1440.11	0.353	32.41	51.11	63.31	76.71	96.82
23	2752.46	673.67	0.324	39.47	67.28	86.45	108.24	142.18
24	3495.65	1461.87	0.362	43.62	80.83	108.02	140.09	192.03
25	9288.06	2725.41	0.345	50.38	102.1	142.31	191.67	275.05
26	2106.2	476.01	0.391	33.56	74.93	109.31	153.35	231.24
27	6281.38	4118.66	0.373	44.7	110.87	169.95	249.24	396.61
28	2220.95	873.76	0.326	11.15	31.05	50.24	77.35	130.57
29	3941.71	1107.66	0.338	5.07	16.03	27.54	44.75	80.63
30	5359.23	2875.1	0.311	14.98	54.63	100.38	173.21	335.72
31	3770.07	1308.71	0.324	3.37	14.45	28.64	52.92	111.41
32	9341.29	2396.74	0.364	5.93	30.69	66.44	132.82	307.75
33	7837.09	3557.58	0.34	8.66	55.89	134.31	294.79	764.99
34	5859.74	1819.98	0.394	47.73	54.37	57.81	61.07	65.28
35	5849.48	1380.77	0.342	32.33	39.07	42.71	46.26	50.96
36	7937.19	4845.44	0.34	67.08	86.26	97.09	107.95	122.76
37	6812.65	2566.15	0.346	57.31	78.69	91.34	104.4	122.77
38	4846.03	1319.89	0.315	89.6	131.85	158.11	186.08	226.72
39	8545.12	4322.29	0.339	9.94	15.74	19.54	23.72	30
40	6716.94	2243.67	0.34	73.32	125.59	161.74	202.92	267.2
41	4389.72	1094.57	0.365	63.62	118.49	158.72	206.29	283.52

Table C.3: (continued)

Case	L cm	H cm	$\phi$	$k_1$ mD	$k_2$ mD	$k_3$ mD	$k_4$ mD	$k_5$ mD
42	2818.63	1217.08	0.301	14.76	30.08	42.03	56.74	81.65
43	5154.15	1546.57	0.324	48.52	108.97	159.41	224.2	339.09
44	5386.33	1238.42	0.31	7.22	18.03	27.72	40.76	65.08
45	2657.25	1517.52	0.315	11.02	30.91	50.18	77.5	131.29
46	9891.6	3573.84	0.3	19.41	61.87	106.7	173.94	314.68
47	8199.41	2166.57	0.32	21.6	79.5	146.7	254.08	494.72
48	9788.08	4683.39	0.34	9.38	40.67	81.03	150.33	318.19
49	9857.42	3172.96	0.368	10.42	54.54	118.76	238.6	556.22
50	8029.97	1947.4	0.394	5.08	33.23	80.41	177.55	464.15
51	7710.62	3174.57	0.32	45.05	51.5	54.84	58.02	62.12
52	6054.08	1757.04	0.389	59.91	72.65	79.55	86.29	95.24
53	2925.32	655.56	0.314	34.33	44.31	49.96	55.63	63.39
54	8430.37	5394.54	0.386	16.02	22.08	25.67	29.39	34.64
55	4086	1584.03	0.342	50.32	74.36	89.35	105.34	128.62
56	7025.06	1953.45	0.351	77.05	122.57	152.47	185.43	235.12
57	9234.35	4855.91	0.347	38.03	65.45	84.48	106.21	140.19
58	7291.42	2498.42	0.3	71.03	132.96	178.53	232.54	320.43
59	9781	2485.55	0.355	47.31	96.93	135.81	183.76	265.2
60	8185	3653.06	0.371	31.86	71.98	105.59	148.88	225.86
61	3789.12	1163.26	0.347	32.38	81.36	125.47	185.02	296.39
62	7225.26	1690.49	0.394	17.36	49.02	79.86	123.71	210.35
63	6072.15	3623.58	0.333	17.21	55.3	95.74	156.61	284.48
64	6360.48	2362.32	0.32	22.23	82.57	153	266.01	520.33
65	2128.91	573.95	0.373	5.79	25.35	50.76	94.58	201.25
66	3558.4	1766.27	0.351	11.94	63.27	138.54	279.78	656.26
67	5155.37	1700.67	0.309	2.8	18.6	45.31	100.67	265.14
68	6438.37	1590.46	0.304	140.81	161.5	172.25	182.5	195.75
69	5176.61	2199.48	0.327	25.42	30.94	33.94	36.87	40.77
70	6775.29	2010.3	0.338	47.24	61.2	69.13	77.11	88.03
71	3817.19	870.11	0.302	99.6	137.84	160.59	184.17	217.47
72	9345.44	5224.7	0.354	102.59	152.24	183.28	216.46	264.88
73	8296.09	2957.14	0.314	13.06	20.87	26.01	31.7	40.28
74	8350.05	2184.63	0.399	44.71	77.31	100.02	125.99	166.71
75	2934.6	1379.29	0.357	71.15	133.87	180.2	235.22	324.97
76	2545.67	809.6	0.357	53.98	111.21	156.22	211.88	306.64
77	2800.81	673.09	0.355	52.58	119.51	175.81	248.52	378.19
78	9220.92	3738.42	0.374	19.88	50.29	77.8	115.04	184.9
79	7056.79	2025.91	0.397	8.94	25.44	41.58	64.61	110.27
80	2304.21	512.05	0.365	15.36	49.76	86.47	141.93	258.88
81	6166.14	4110.76	0.373	21.44	80.35	149.53	260.97	512.86
82	2154.06	855.89	0.303	5.6	24.79	49.88	93.36	199.72
83	2309.58	653.63	0.324	7.35	39.41	86.81	176.21	415.9
84	8965.06	4875.2	0.359	6.81	45.92	112.64	251.83	668.29
85	9193.33	3219.35	0.318	153.55	176.72	188.79	200.31	215.23
86	3249.79	839.22	0.315	142.25	173.76	190.91	207.71	230.09
87	2882.84	1323.72	0.359	46.29	60.21	68.13	76.11	87.06
88	4493.48	1406.6	0.392	51.52	71.6	83.57	96	113.59
89	4378.25	1039.64	0.343	43.37	64.63	77.96	92.24	113.11
90	7835.63	4857.89	0.366	46.76	75.06	93.77	114.47	145.81
91	4342.84	1651.46	0.357	22.79	39.6	51.35	64.81	85.97
92	5538.44	1518.86	0.396	10.28	19.45	26.24	34.32	47.55
93	7733.33	3961.98	0.398	58.99	122.22	172.14	234.02	339.64
94	6004.52	2022.66	0.304	52.06	119.06	175.64	248.92	379.96
95	6024.78	1511.73	0.301	29.72	75.68	117.44	174.14	280.85
96	5255.23	2294.06	0.377	25.07	71.83	117.83	183.63	314.57
97	6310.68	1907.97	0.366	15.74	51.41	89.69	147.7	270.53
98	5040.86	1165.72	0.348	17.68	66.86	124.97	218.95	432.3
99	4751.3	2752.88	0.399	5.33	23.85	48.22	90.65	194.96
100	9148.41	3335.58	0.371	3.06	16.61	36.8	75.09	178.37

Table C.3: (continued)

Case	L cm	H cm	$\phi$	$k_1$ mD	$k_2$ mD	$k_3$ mD	$k_4$ mD	$k_5$ mD
101	7680.84	2043.09	0.389	2.93	20.05	49.54	111.44	298.01
102	9987.79	4837.05	0.352	114.72	132.48	141.76	150.63	162.13
103	2131.11	691.56	0.389	58.86	72.17	79.42	86.54	96.04
104	6175.66	1506.87	0.305	71.93	93.91	106.45	119.11	136.51
105	3612.11	1502.69	0.318	51.77	72.23	84.47	97.19	115.24
106	5604.85	1638.6	0.332	13.49	20.19	24.41	28.93	35.55
107	7685.48	1732.04	0.384	54.23	87.45	109.47	133.9	170.95
108	8373.24	5445.45	0.322	24.63	43.01	55.89	70.69	94
109	8206.24	3212.6	0.336	26.02	49.46	66.9	87.71	121.82
110	2968.05	831.12	0.341	58.46	121.8	171.99	234.36	341.12
111	8050.72	4290.13	0.348	11.86	27.28	40.36	57.34	87.8
112	8239.94	2847.93	0.31	11.03	28.26	43.99	65.42	105.86
113	6733.05	1721.99	0.391	20.32	58.64	96.52	150.9	259.46
114	9957.76	4494.63	0.357	6.33	20.84	36.49	60.31	110.92
115	4512.04	1395.96	0.346	22.28	85.04	159.64	280.77	556.98
116	3143.83	739.91	0.312	15.82	71.46	145.21	274.21	592.93
117	7422.53	4496.79	0.375	8.75	48.08	107.13	219.75	525.29
118	4888.27	1832.62	0.384	3.07	21.35	53.11	120.24	324.03
119	9113.25	2473.67	0.365	114.08	132.2	141.68	150.76	162.57
120	7988.95	4015.48	0.34	74.22	91.32	100.67	109.86	122.15
121	8456.74	2813.03	0.399	54.74	71.74	81.47	91.3	104.84
122	4530.11	1126.05	0.312	14.45	20.24	23.71	27.33	32.47
123	5595.08	2402.92	0.33	55.65	83.65	101.31	120.29	148.16
124	5400.74	1614.48	0.375	61.59	99.76	125.15	153.37	196.27
125	8416.7	1929.58	0.395	29.65	52.01	67.75	85.86	114.46
126	9769.52	5539.54	0.351	26.84	51.3	69.56	91.39	127.27
127	5411.73	1946.43	0.32	47.72	99.99	141.57	193.36	282.25
128	2675.56	704.64	0.384	43.39	100.43	149.01	212.26	326.03

Table C.4: Part 2: Dimensional properties calculated from dimensionless numbers

Case	$Q_{CO_2}$ $cm^3 min^{-1}$	$Q_{surf}$ $cm^3 min^{-1}$	$D_{Lo1} \times 10^{-2}$ $cm^2 min^{-1}$	$D_{To1} \times 10^{-4}$ $cm^2 min^{-1}$	$\mu_{CO_2}$ cp	$C_{surf} \times 10^{-5}$ mole frac	$N_c^{ref}$ $10^{-6}$
1	2542.03	847.34	9.64	9.1	0.129	7.27	4.7
2	1593.37	531.12	16.74	14.06	0.134	8.6	4.92
3	2602.98	867.66	6.87	9.75	0.139	9.92	5.13
4	1488.65	496.22	7.13	15.24	0.143	11.24	5.35
5	861.45	287.15	11.36	4.65	0.148	12.56	5.56
6	4663.28	1554.43	13.1	26.72	0.153	13.89	5.77
7	2069.87	689.96	11.13	5.52	0.157	15.21	5.99
8	690.81	230.27	9.46	14.78	0.162	16.53	6.2
9	9756.13	3252.04	10.86	33.56	0.167	17.85	6.42
10	1405.51	468.5	3.67	6.93	0.171	19.17	6.63
11	579.74	193.25	10.29	4.9	0.176	20.5	6.84
12	2171.35	723.78	9.37	48.37	0.181	21.82	7.06
13	2187.01	729	7.44	6.62	0.185	23.14	7.27
14	575.34	191.78	10.37	7.63	0.19	24.46	7.49
15	1547.45	515.82	3.85	4.72	0.195	25.79	7.7
16	2503.57	834.52	8.55	34.59	0.199	27.11	7.92
17	1309.69	436.56	7.43	4.38	0.204	28.43	8.13
18	5074.87	1691.62	6.81	42.12	0.209	29.75	8.34
19	1789.55	596.52	10.06	11.36	0.125	6.02	4.5
20	657.79	219.26	9.42	18.6	0.13	7.34	4.71
21	6716.87	2238.96	8.98	22	0.134	8.67	4.93
22	870.09	290.03	4.54	7.51	0.139	9.99	5.14
23	369.37	123.12	5.82	2.88	0.144	11.31	5.36

Table C.4: (continued)

Case	$Q_{CO_2}$ $cm^3 min^{-1}$	$Q_{surf}$ $cm^3 min^{-1}$	$D_{Lo1} \times 10^{-2}$ $cm^2 min^{-1}$	$D_{To1} \times 10^{-4}$ $cm^2 min^{-1}$	$\mu_{CO_2}$ $cp$	$C_{surf} \times 10^{-5}$ <b>mole frac</b>	$N_c^{ref}$ $10^{-6}$
24	1582.28	527.43	5.86	40.44	0.148	12.63	5.57
25	2455.01	818.34	7.13	7.63	0.153	13.95	5.78
26	299.07	99.69	5.56	5.54	0.158	15.28	6
27	9673.12	3224.37	7.34	30.55	0.162	16.6	6.21
28	579.7	193.23	3.85	16.56	0.167	17.92	6.43
29	403.66	134.55	2.8	2.57	0.172	19.24	6.64
30	3967.7	1322.57	5.9	28.61	0.176	20.57	6.86
31	649.12	216.37	3.08	3.48	0.181	21.89	7.07
32	1393.41	464.47	4.26	20.5	0.186	23.21	7.28
33	5428.26	1809.42	6.63	22.76	0.19	24.53	7.5
34	1114.72	371.57	3.28	8.81	0.195	25.86	7.71
35	476.57	158.86	2.75	1.92	0.2	27.18	7.93
36	6737.23	2245.74	4.24	66.83	0.204	28.5	8.14
37	2205.07	735.02	4.08	8.74	0.209	29.82	8.35
38	1113.75	371.25	5.99	10.12	0.125	6.09	4.51
39	2456.88	818.96	1.98	5.98	0.13	7.41	4.73
40	2499.81	833.27	5.75	38.15	0.135	8.74	4.94
41	930.13	310.04	5.37	5.9	0.139	10.06	5.15
42	797.39	265.8	2.85	14.78	0.144	11.38	5.37
43	1420.48	473.49	5.26	6.4	0.149	12.7	5.58
44	376.44	125.48	2.34	4.9	0.153	14.02	5.8
45	1597.04	532.35	3.15	16.5	0.158	15.35	6.01
46	3595.31	1198.44	4.91	14.96	0.163	16.67	6.22
47	1937.88	645.96	5.51	4.91	0.167	17.99	6.44
48	5850.46	1950.15	3.93	72.1	0.172	19.31	6.65
49	2739.37	913.12	3.69	8.05	0.177	20.64	6.87
50	1091.21	363.74	2.92	5.83	0.181	21.96	7.08
51	2235.2	745.07	2.62	7.05	0.186	23.28	7.3
52	1083.89	361.3	2.64	11.03	0.191	24.6	7.51
53	255.23	85.08	2.64	2.5	0.195	25.93	7.72
54	4432.55	1477.52	1.56	17.77	0.2	27.25	7.94
55	1516.2	505.4	3.33	7.42	0.205	28.57	8.15
56	1509.65	503.22	3.61	18.55	0.209	29.89	8.37
57	5467.09	1822.36	2.78	16.64	0.125	6.16	4.52
58	2756.6	918.87	4.76	18.56	0.13	7.48	4.74
59	1834.77	611.59	3.58	3.85	0.135	8.8	4.95
60	4318.76	1439.59	3.08	28.15	0.139	10.13	5.17
61	1066.51	355.5	3.67	6.76	0.144	11.45	5.38
62	974.81	324.94	2.63	4.02	0.149	12.77	5.59
63	5053	1684.33	2.92	16.16	0.153	14.09	5.81
64	2695.97	898.66	3.94	70	0.158	15.42	6.02
65	285.09	95.03	2	4.06	0.163	16.74	6.24
66	2781.76	927.25	3.62	41.46	0.168	18.06	6.45
67	1063.42	354.47	2.43	5.42	0.172	19.38	6.66
68	1297.29	432.43	4.25	18.26	0.177	20.71	6.88
69	1410.34	470.11	1.78	7.87	0.182	22.03	7.09
70	1107.36	369.12	2.1	6.8	0.186	23.35	7.31
71	580.1	193.37	3.65	3.58	0.191	24.67	7.52
72	9429.76	3143.25	3.4	103.29	0.196	25.99	7.73
73	1324.04	441.35	1.48	5.23	0.2	27.32	7.95
74	1453.53	484.51	2.32	6.99	0.205	28.64	8.16
75	2284.24	761.41	3.56	16.53	0.21	29.96	8.38
76	871.88	290.63	3.39	21.33	0.126	6.23	4.53
77	502.54	167.51	3.09	4.41	0.13	7.55	4.75
78	3247.8	1082.6	2	11.79	0.135	8.87	4.96
79	944.83	314.94	1.41	2.26	0.14	10.2	5.18
80	276.49	92.16	2.28	14.14	0.144	11.52	5.39
81	9087.77	3029.26	3.01	42.5	0.149	12.84	5.6
82	676.62	225.54	2.2	17.87	0.154	14.16	5.82

Table C.4: (continued)

Case	$Q_{CO_2}$ $cm^3 min^{-1}$	$Q_{surf}$ $cm^3 min^{-1}$	$D_{Lo1} \times 10^{-2}$ $cm^2 min^{-1}$	$D_{To1} \times 10^{-4}$ $cm^2 min^{-1}$	$\mu_{CO_2}$ $cp$	$C_{surf} \times 10^{-5}$ <b>mole frac</b>	$N_c^{ref}$ $10^{-6}$
83	505.09	168.36	2.79	5.28	0.158	15.49	6.03
84	7209.12	2403.04	2.49	55.09	0.163	16.81	6.25
85	3551.45	1183.82	3.22	11.01	0.168	18.13	6.46
86	708.61	236.2	3.34	9.17	0.172	19.45	6.68
87	1224.84	408.28	1.79	8.16	0.177	20.78	6.89
88	1013.42	337.81	1.85	18	0.182	22.1	7.1
89	565.76	188.59	2.09	3.72	0.186	23.42	7.32
90	7801.4	2600.47	2.19	40.78	0.191	24.74	7.53
91	1040.69	346.9	1.42	4.92	0.196	26.06	7.75
92	510.63	170.21	0.94	4.72	0.2	27.39	7.96
93	6594.15	2198.05	2.46	18.01	0.205	28.71	8.17
94	2312.95	770.98	3.33	15.06	0.21	30.03	8.39
95	1089.25	363.08	2.82	3.91	0.126	6.3	4.55
96	2980.39	993.46	2.32	71.38	0.131	7.62	4.76
97	1550.46	516.82	2.13	7.4	0.135	8.94	4.97
98	723.47	241.16	2.22	7.39	0.14	10.27	5.19
99	2771.24	923.75	1.24	11.66	0.145	11.59	5.4
100	1926.63	642.21	1.21	14.76	0.149	12.91	5.62
101	1044.73	348.24	1.39	3.24	0.154	14.23	5.83
102	6799.6	2266.53	2.29	26.37	0.159	15.56	6.04
103	502.45	167.48	1.59	4.24	0.163	16.88	6.26
104	981.79	327.26	2.4	17.51	0.168	18.2	6.47
105	1280.63	426.88	1.75	11.23	0.173	19.52	6.69
106	545.56	181.85	0.92	4.54	0.177	20.84	6.9
107	973.3	324.43	1.73	2.46	0.182	22.17	7.12
108	6520.34	2173.45	1.52	51.3	0.187	23.49	7.33
109	2617.49	872.5	1.63	8.12	0.191	24.81	7.54
110	802.27	267.42	2.63	9.67	0.196	26.13	7.76
111	3943.51	1314.5	1.28	9.29	0.201	27.46	7.97
112	1532.64	510.88	1.29	23.6	0.205	28.78	8.19
113	1054.37	351.46	1.56	4.22	0.21	30.1	8.4
114	3100.88	1033.63	1.08	14.46	0.126	6.37	4.56
115	1434.38	478.13	2.4	7.08	0.131	7.69	4.77
116	573.58	191.19	2.63	13.65	0.136	9.01	4.98
117	8026.93	2675.64	1.94	25.61	0.14	10.34	5.2
118	1487.87	495.96	1.38	10.21	0.145	11.66	5.41
119	1770	590	1.76	3.62	0.15	12.98	5.63
120	4633.45	1544.48	1.63	50.01	0.154	14.3	5.84
121	1995.5	665.17	1.28	5.7	0.159	15.63	6.06
122	332.4	110.8	0.91	3.42	0.164	16.95	6.27
123	2613.67	871.22	1.81	10.23	0.168	18.27	6.48
124	1401.37	467.12	1.82	13.43	0.173	19.59	6.7
125	974.57	324.86	1.3	2.42	0.178	20.91	6.91
126	6058.31	2019.44	1.27	20.44	0.182	22.24	7.13
127	1995.02	665.01	2.04	7.39	0.187	23.56	7.34
128	561.82	187.27	1.8	29.77	0.192	24.88	7.55

Table C.5: Part 3: Dimensional properties calculated from dimensionless numbers

Case	DTRAPW1	DTRAPN1	DTRAPW2	DTRAPN2	$k_{rgcw}$	$k_{rwiro}$	$k_{rocv}$
1	3.05	4.92	0.17	0.14	0.06	0.38	0.41
2	3.11	4.84	0.34	0.31	0.06	0.38	0.42
3	3.16	4.76	0.5	0.47	0.05	0.39	0.43
4	3.22	4.67	0.66	0.64	0.05	0.4	0.44
5	3.27	4.59	0.83	0.8	0.05	0.4	0.45

Table C.5: (continued)

Case	DTRAPW1	DTRAPN1	DTRAPW2	DTRAPN2	$k_{rgcw}$	$k_{rwiro}$	$k_{rocv}$
6	3.33	4.51	0.99	0.97	0.04	0.41	0.46
7	3.38	4.43	1.15	1.13	0.04	0.42	0.47
8	3.44	4.35	1.32	1.3	0.04	0.43	0.49
9	3.49	4.26	1.48	1.47	0.03	0.43	0.5
10	3.55	4.18	1.65	1.63	0.03	0.44	0.51
11	3.6	4.1	1.81	1.8	0.03	0.45	0.52
12	3.66	4.02	1.97	1.96	0.02	0.45	0.53
13	3.71	3.93	2.14	2.13	0.02	0.46	0.54
14	3.77	3.85	2.3	2.29	0.02	0.47	0.55
15	3.82	3.77	2.47	2.46	0.01	0.48	0.56
16	3.88	3.69	2.63	2.62	0.01	0.48	0.57
17	3.93	3.6	2.79	2.79	0.01	0.49	0.59
18	3.99	3.52	2.96	2.96	0	0.5	0.6
19	3	5	0.02	-0.02	0.06	0.37	0.4
20	3.05	4.92	0.18	0.15	0.06	0.38	0.41
21	3.11	4.84	0.34	0.31	0.06	0.38	0.42
22	3.16	4.75	0.51	0.48	0.05	0.39	0.43
23	3.22	4.67	0.67	0.65	0.05	0.4	0.44
24	3.27	4.59	0.84	0.81	0.05	0.4	0.45
25	3.33	4.51	1	0.98	0.04	0.41	0.46
26	3.38	4.42	1.16	1.14	0.04	0.42	0.48
27	3.44	4.34	1.33	1.31	0.04	0.43	0.49
28	3.49	4.26	1.49	1.47	0.03	0.43	0.5
29	3.55	4.18	1.65	1.64	0.03	0.44	0.51
30	3.6	4.09	1.82	1.81	0.03	0.45	0.52
31	3.66	4.01	1.98	1.97	0.02	0.46	0.53
32	3.71	3.93	2.15	2.14	0.02	0.46	0.54
33	3.77	3.85	2.31	2.3	0.02	0.47	0.55
34	3.82	3.76	2.47	2.47	0.01	0.48	0.56
35	3.88	3.68	2.64	2.63	0.01	0.48	0.58
36	3.93	3.6	2.8	2.8	0.01	0.49	0.59
37	3.99	3.52	2.97	2.97	0	0.5	0.6
38	3	5	0.03	-0.01	0.06	0.37	0.4
39	3.06	4.91	0.19	0.16	0.06	0.38	0.41
40	3.11	4.83	0.35	0.32	0.06	0.38	0.42
41	3.17	4.75	0.52	0.49	0.05	0.39	0.43
42	3.22	4.67	0.68	0.65	0.05	0.4	0.44
43	3.28	4.58	0.84	0.82	0.05	0.41	0.45
44	3.33	4.5	1.01	0.99	0.04	0.41	0.46
45	3.39	4.42	1.17	1.15	0.04	0.42	0.48
46	3.44	4.34	1.34	1.32	0.04	0.43	0.49
47	3.5	4.25	1.5	1.48	0.03	0.43	0.5
48	3.55	4.17	1.66	1.65	0.03	0.44	0.51
49	3.61	4.09	1.83	1.81	0.03	0.45	0.52
50	3.66	4.01	1.99	1.98	0.02	0.46	0.53
51	3.72	3.92	2.16	2.15	0.02	0.46	0.54
52	3.77	3.84	2.32	2.31	0.02	0.47	0.55
53	3.83	3.76	2.48	2.48	0.01	0.48	0.56
54	3.88	3.68	2.65	2.64	0.01	0.48	0.58
55	3.94	3.6	2.81	2.81	0.01	0.49	0.59
56	3.99	3.51	2.97	2.97	0	0.5	0.6
57	3.01	4.99	0.03	0	0.06	0.37	0.4
58	3.06	4.91	0.2	0.17	0.06	0.38	0.41
59	3.12	4.83	0.36	0.33	0.06	0.38	0.42
60	3.17	4.74	0.53	0.5	0.05	0.39	0.43
61	3.23	4.66	0.69	0.66	0.05	0.4	0.44
62	3.28	4.58	0.85	0.83	0.05	0.41	0.45
63	3.34	4.5	1.02	0.99	0.04	0.41	0.47
64	3.39	4.41	1.18	1.16	0.04	0.42	0.48



Table C.5: (continued)

Case	DTRAPW1	DTRAPN1	DTRAPW2	DTRAPN2	$k_{rgcw}$	$k_{rwiro}$	$k_{rocv}$
65	3.45	4.33	1.34	1.33	0.04	0.43	0.49
66	3.5	4.25	1.51	1.49	0.03	0.43	0.5
67	3.55	4.17	1.67	1.66	0.03	0.44	0.51
68	3.61	4.09	1.84	1.82	0.03	0.45	0.52
69	3.66	4	2	1.99	0.02	0.46	0.53
70	3.72	3.92	2.16	2.15	0.02	0.46	0.54
71	3.77	3.84	2.33	2.32	0.02	0.47	0.55
72	3.83	3.76	2.49	2.49	0.01	0.48	0.57
73	3.88	3.67	2.66	2.65	0.01	0.48	0.58
74	3.94	3.59	2.82	2.82	0.01	0.49	0.59
75	3.99	3.51	2.98	2.98	0	0.5	0.6
76	3.01	4.99	0.04	0.01	0.06	0.37	0.4
77	3.06	4.9	0.21	0.17	0.06	0.38	0.41
78	3.12	4.82	0.37	0.34	0.06	0.38	0.42
79	3.17	4.74	0.53	0.51	0.05	0.39	0.43
80	3.23	4.66	0.7	0.67	0.05	0.4	0.44
81	3.28	4.58	0.86	0.84	0.05	0.41	0.45
82	3.34	4.49	1.03	1	0.04	0.41	0.47
83	3.39	4.41	1.19	1.17	0.04	0.42	0.48
84	3.45	4.33	1.35	1.33	0.04	0.43	0.49
85	3.5	4.25	1.52	1.5	0.03	0.43	0.5
86	3.56	4.16	1.68	1.67	0.03	0.44	0.51
87	3.61	4.08	1.84	1.83	0.03	0.45	0.52
88	3.67	4	2.01	2	0.02	0.46	0.53
89	3.72	3.92	2.17	2.16	0.02	0.46	0.54
90	3.78	3.83	2.34	2.33	0.02	0.47	0.55
91	3.83	3.75	2.5	2.49	0.01	0.48	0.57
92	3.89	3.67	2.66	2.66	0.01	0.49	0.58
93	3.94	3.59	2.83	2.83	0.01	0.49	0.59
94	4	3.5	2.99	2.99	0	0.5	0.6
95	3.01	4.98	0.05	0.02	0.06	0.37	0.4
96	3.07	4.9	0.21	0.18	0.06	0.38	0.41
97	3.12	4.82	0.38	0.35	0.06	0.38	0.42
98	3.18	4.74	0.54	0.51	0.05	0.39	0.43
99	3.23	4.65	0.71	0.68	0.05	0.4	0.44
100	3.29	4.57	0.87	0.85	0.05	0.41	0.46
101	3.34	4.49	1.03	1.01	0.04	0.41	0.47
102	3.4	4.41	1.2	1.18	0.04	0.42	0.48
103	3.45	4.32	1.36	1.34	0.04	0.43	0.49
104	3.51	4.24	1.53	1.51	0.03	0.44	0.5
105	3.56	4.16	1.69	1.67	0.03	0.44	0.51
106	3.62	4.08	1.85	1.84	0.03	0.45	0.52
107	3.67	3.99	2.02	2.01	0.02	0.46	0.53
108	3.73	3.91	2.18	2.17	0.02	0.46	0.54
109	3.78	3.83	2.34	2.34	0.02	0.47	0.56
110	3.84	3.75	2.51	2.5	0.01	0.48	0.57
111	3.89	3.66	2.67	2.67	0.01	0.49	0.58
112	3.95	3.58	2.84	2.83	0.01	0.49	0.59
113	4	3.5	3	3	0	0.5	0.6
114	3.01	4.98	0.06	0.03	0.06	0.37	0.4
115	3.07	4.9	0.22	0.19	0.06	0.38	0.41
116	3.12	4.81	0.39	0.36	0.06	0.39	0.42
117	3.18	4.73	0.55	0.52	0.05	0.39	0.43
118	3.23	4.65	0.72	0.69	0.05	0.4	0.44
119	3.29	4.57	0.88	0.85	0.05	0.41	0.46
120	3.34	4.48	1.04	1.02	0.04	0.41	0.47
121	3.4	4.4	1.21	1.19	0.04	0.42	0.48
122	3.45	4.32	1.37	1.35	0.04	0.43	0.49
123	3.51	4.24	1.53	1.52	0.03	0.44	0.5

Table C.5: (continued)

Case	DTRAPW1	DTRAPN1	DTRAPW2	DTRAPN2	$k_{rgcw}$	$k_{rwiro}$	$k_{rocv}$
124	3.56	4.15	1.7	1.68	0.03	0.44	0.51
125	3.62	4.07	1.86	1.85	0.03	0.45	0.52
126	3.67	3.99	2.03	2.01	0.02	0.46	0.53
127	3.73	3.91	2.19	2.18	0.02	0.46	0.54
128	3.78	3.83	2.35	2.35	0.02	0.47	0.56

Table C.6: Part 4: Dimensional properties calculated from dimensionless numbers

Case	$es$	$ev$	$S_o^{max}$	$eo$	$\Gamma_m$	$\Gamma_{pn}$	$mole_{surf}^{-1} min^{-1}$	$mole_{surf}^{-1} min^{-1}$
1	0.13	0.47	0.8	1.06	2.0003	2.0047	1.61	13.85
2	0.15	0.47	0.81	1.04	2.0005	2.0063	5.8	46.4
3	0.16	0.46	0.81	1.02	2.0008	2.0079	3.34	24.91
4	0.17	0.45	0.82	1	2.0011	2.0095	2.35	16.34
5	0.19	0.45	0.82	0.98	2.0014	2.0111	6.19	40.32
6	0.2	0.44	0.83	0.96	2.0017	2.0126	6.79	41.46
7	0.21	0.43	0.83	0.94	2.0019	2.0142	3.96	22.67
8	0.22	0.43	0.83	0.92	2.0022	2.0158	8.18	44.05
9	0.24	0.42	0.84	0.9	2.0025	2.0174	3.75	18.97
10	0.25	0.41	0.84	0.88	2.0028	2.019	1.52	7.24
11	0.26	0.41	0.85	0.86	2.0031	2.0205	58.23	261.56
12	0.28	0.4	0.85	0.84	2.0033	2.0221	37.15	157.33
13	0.29	0.39	0.86	0.82	2.0036	2.0237	4.42	17.66
14	0.3	0.39	0.86	0.8	2.0039	2.0253	43.15	162.67
15	0.32	0.38	0.87	0.78	2.0042	2.0268	2.93	10.44
16	0.33	0.37	0.87	0.76	2.0045	2.0284	4.43	14.89
17	0.34	0.37	0.87	0.74	2.0047	2.03	4.9	15.55
18	0.36	0.36	0.88	0.73	2.005	2.0316	9.76	29.26
19	0.12	0.48	0.8	1.08	2	2.0033	16.08	148.4
20	0.13	0.47	0.8	1.06	2.0003	2.0048	30.63	262.36
21	0.15	0.47	0.81	1.04	2.0006	2.0064	2.99	23.82
22	0.16	0.46	0.81	1.02	2.0008	2.008	7.23	53.68
23	0.17	0.45	0.82	1	2.0011	2.0096	25.74	178.57
24	0.19	0.45	0.82	0.98	2.0014	2.0111	17.28	112.17
25	0.2	0.44	0.83	0.96	2.0017	2.0127	3.19	19.43
26	0.21	0.43	0.83	0.94	2.002	2.0143	51.82	295.94
27	0.23	0.43	0.84	0.92	2.0022	2.0159	8.2	44.03
28	0.24	0.42	0.84	0.9	2.0025	2.0175	36.69	185.22
29	0.25	0.41	0.84	0.88	2.0028	2.019	8.98	42.68
30	0.26	0.41	0.85	0.86	2.0031	2.0206	10.87	48.67
31	0.28	0.4	0.85	0.84	2.0034	2.0222	12.14	51.26
32	0.29	0.39	0.86	0.82	2.0036	2.0238	2.9	11.53
33	0.3	0.39	0.86	0.8	2.0039	2.0254	6.76	25.42
34	0.32	0.38	0.87	0.78	2.0042	2.0269	6.32	22.41
35	0.33	0.37	0.87	0.76	2.0045	2.0285	5.59	18.74
36	0.34	0.37	0.87	0.74	2.0048	2.0301	4.92	15.56
37	0.36	0.36	0.88	0.72	2.005	2.0317	6.76	20.19
38	0.12	0.48	0.8	1.08	2	2.0033	9.6	88.25
39	0.13	0.47	0.8	1.06	2.0003	2.0049	1.1	9.37
40	0.15	0.47	0.81	1.04	2.0006	2.0065	5.56	44.16
41	0.16	0.46	0.81	1.02	2.0009	2.0081	13.03	96.43
42	0.17	0.45	0.82	1	2.0011	2.0096	17.91	123.86
43	0.19	0.45	0.82	0.98	2.0014	2.0112	10.55	68.27
44	0.2	0.44	0.83	0.96	2.0017	2.0128	4.56	27.68
45	0.21	0.43	0.83	0.94	2.002	2.0144	26.83	152.75
46	0.23	0.43	0.84	0.92	2.0023	2.016	3.2	17.1

Table C.6: (continued)

Case	$es$	$ev$	$S_o^{max}$	$eo$	$\Gamma_{rn}$	$\Gamma_{pn}$	$r_1$ $mole_{surf}^{-1} min^{-1}$	$r_2$ $mole_{surf}^{-1} min^{-1}$
47	0.24	0.42	0.84	0.9	2.0025	2.0175	5.53	27.8
48	0.25	0.41	0.84	0.88	2.0028	2.0191	2.92	13.84
49	0.27	0.41	0.85	0.86	2.0031	2.0207	2.84	12.69
50	0.28	0.4	0.85	0.84	2.0034	2.0223	3.57	15.02
51	0.29	0.39	0.86	0.82	2.0037	2.0239	3.66	14.53
52	0.31	0.39	0.86	0.8	2.0039	2.0254	6.27	23.5
53	0.32	0.38	0.87	0.78	2.0042	2.027	28.13	99.5
54	0.33	0.37	0.87	0.76	2.0045	2.0286	2.1	7
55	0.34	0.37	0.87	0.74	2.0048	2.0302	19.97	63
56	0.36	0.36	0.88	0.72	2.0051	2.0318	7.65	22.81
57	0.12	0.48	0.8	1.08	2	2.0034	1.66	15.23
58	0.13	0.47	0.8	1.06	2.0003	2.005	4.9	41.66
59	0.15	0.47	0.81	1.04	2.0006	2.0066	2.19	17.35
60	0.16	0.46	0.81	1.02	2.0009	2.0082	2.87	21.19
61	0.17	0.45	0.82	1	2.0011	2.0097	16.99	117.07
62	0.19	0.45	0.82	0.98	2.0014	2.0113	3.56	22.94
63	0.2	0.44	0.83	0.96	2.0017	2.0129	5.92	35.79
64	0.21	0.43	0.83	0.94	2.002	2.0145	7.7	43.67
65	0.23	0.43	0.84	0.92	2.0023	2.016	36.85	196.46
66	0.24	0.42	0.84	0.9	2.0026	2.0176	25.12	126.01
67	0.25	0.41	0.84	0.88	2.0028	2.0192	8.44	39.85
68	0.27	0.41	0.85	0.86	2.0031	2.0208	9.94	44.25
69	0.28	0.4	0.85	0.84	2.0034	2.0224	6.77	28.41
70	0.29	0.39	0.86	0.82	2.0037	2.0239	4.87	19.28
71	0.31	0.39	0.86	0.8	2.004	2.0255	27.99	104.55
72	0.32	0.38	0.87	0.78	2.0042	2.0271	4.55	16.04
73	0.33	0.37	0.87	0.76	2.0045	2.0287	2.61	8.69
74	0.35	0.37	0.88	0.74	2.0048	2.0303	4.23	13.3
75	0.36	0.36	0.88	0.72	2.0051	2.0318	54.73	162.59
76	0.12	0.48	0.8	1.08	2	2.0035	33.74	307.73
77	0.14	0.47	0.81	1.06	2.0003	2.0051	27.18	230.13
78	0.15	0.47	0.81	1.04	2.0006	2.0067	1.73	13.64
79	0.16	0.46	0.81	1.02	2.0009	2.0082	2.22	16.35
80	0.17	0.45	0.82	1	2.0012	2.0098	35.65	244.73
81	0.19	0.45	0.82	0.98	2.0014	2.0114	6.96	44.71
82	0.2	0.44	0.83	0.96	2.0017	2.013	44.12	265.82
83	0.21	0.43	0.83	0.94	2.002	2.0146	51.29	290.05
84	0.23	0.43	0.84	0.92	2.0023	2.0161	3.19	16.97
85	0.24	0.42	0.84	0.9	2.0026	2.0177	4.13	20.64
86	0.25	0.41	0.84	0.88	2.0028	2.0193	35.97	169.36
87	0.27	0.41	0.85	0.86	2.0031	2.0209	25.66	113.85
88	0.28	0.4	0.85	0.84	2.0034	2.0224	11.46	47.92
89	0.29	0.39	0.86	0.82	2.0037	2.024	14.24	56.18
90	0.31	0.39	0.86	0.8	2.004	2.0256	4.87	18.13
91	0.32	0.38	0.87	0.78	2.0042	2.0272	10.72	37.7
92	0.33	0.37	0.87	0.76	2.0045	2.0288	4.54	15.06
93	0.35	0.37	0.88	0.74	2.0048	2.0303	6.33	19.86
94	0.36	0.36	0.88	0.72	2.0051	2.0319	14.81	43.86
95	0.12	0.48	0.8	1.08	2.0001	2.0036	6.08	55.2
96	0.14	0.47	0.81	1.06	2.0003	2.0052	6.99	58.97
97	0.15	0.47	0.81	1.04	2.0006	2.0067	4.76	37.32
98	0.16	0.46	0.81	1.02	2.0009	2.0083	8.24	60.34
99	0.18	0.45	0.82	1	2.0012	2.0099	5.5	37.63
100	0.19	0.45	0.82	0.98	2.0015	2.0115	1.52	9.76
101	0.2	0.44	0.83	0.96	2.0017	2.0131	2.61	15.68
102	0.22	0.43	0.83	0.94	2.002	2.0146	2.69	15.17
103	0.23	0.43	0.84	0.92	2.0023	2.0162	42.99	227.76
104	0.24	0.42	0.84	0.9	2.0026	2.0178	8.12	40.46
105	0.25	0.41	0.84	0.88	2.0029	2.0194	18.14	85.12

Table C.6: (continued)

Case	$es$	$ev$	$S_o^{max}$	$eo$	$\Gamma_{rn}$	$\Gamma_{pn}$	$r_{r1}$ $mole_{surf}^{-1} min^{-1}$	$r_{r2}$ $mole_{surf}^{-1} min^{-1}$
106	0.27	0.41	0.85	0.86	2.0031	2.0209	4.16	18.38
107	0.28	0.4	0.85	0.84	2.0034	2.0225	4.33	18.07
108	0.29	0.39	0.86	0.82	2.0037	2.0241	3.34	13.13
109	0.31	0.39	0.86	0.8	2.004	2.0257	3.88	14.42
110	0.32	0.38	0.87	0.78	2.0043	2.0273	50.07	175.54
111	0.33	0.37	0.87	0.76	2.0045	2.0288	3.45	11.41
112	0.35	0.37	0.88	0.74	2.0048	2.0304	3.44	10.75
113	0.36	0.36	0.88	0.72	2.0051	2.032	6.47	19.1
114	0.12	0.48	0.8	1.07	2.0001	2.0037	1	9.04
115	0.14	0.47	0.81	1.06	2.0004	2.0052	11.55	97.05
116	0.15	0.47	0.81	1.04	2.0006	2.0068	27.63	216.03
117	0.16	0.46	0.81	1.02	2.0009	2.0084	3.88	28.27
118	0.18	0.45	0.82	1	2.0012	2.01	6.74	45.96
119	0.19	0.45	0.82	0.98	2.0015	2.0116	2.6	16.61
120	0.2	0.44	0.83	0.96	2.0018	2.0131	3.31	19.83
121	0.22	0.43	0.83	0.94	2.002	2.0147	2.44	13.71
122	0.23	0.43	0.84	0.92	2.0023	2.0163	6.32	33.37
123	0.24	0.42	0.84	0.9	2.0026	2.0179	8.69	43.17
124	0.26	0.41	0.85	0.88	2.0029	2.0195	9.77	45.69
125	0.27	0.41	0.85	0.86	2.0032	2.021	3	13.23
126	0.28	0.4	0.85	0.84	2.0034	2.0226	2.27	9.45
127	0.29	0.39	0.86	0.82	2.0037	2.0242	12.44	48.79
128	0.31	0.39	0.86	0.8	2.004	2.0258	46.63	172.62

Table C.7: Measured and linear- and quadratic-regression predicted values of  $RF$  and  $\Delta p$ 

Case	$RF$			$\Delta p$		
	Measured	Linear Model	Quadratic Model	Measured	Linear Model	Quadratic Model
1	0.3718	0.4097	0.3786	29.47	55.33	45.43
2	0.3889	0.4722	0.4575	20.58	57.50	54.00
3	0.5388	0.4464	0.4332	109.98	69.71	68.36
4	0.5669	0.5304	0.5430	133.23	75.95	70.84
5	0.4851	0.5259	0.5173	61.05	77.43	77.17
6	0.5387	0.5481	0.5412	73.26	96.29	96.30
7	0.5675	0.5406	0.5557	63.85	77.22	69.22
8	0.6589	0.6285	0.6388	110.99	87.55	79.02
9	0.5243	0.5779	0.5505	85.58	108.78	116.69
10	0.6324	0.6191	0.6003	280.17	117.64	130.73
11	0.5828	0.5928	0.5799	98.83	122.40	134.22
12	0.6274	0.6316	0.6139	119.55	146.85	159.04
13	0.5821	0.5971	0.5779	161.88	167.85	179.14
14	0.5840	0.6343	0.5970	89.12	156.47	161.57
15	0.5349	0.5834	0.5794	221.41	176.51	160.43
16	0.6938	0.6659	0.6701	98.47	191.13	163.43
17	0.9468	0.9732	0.9520	202.98	281.43	257.36
18	0.9638	0.9669	0.9729	313.76	310.43	283.19
19	0.3563	0.3372	0.3189	17.20	50.92	12.92
20	0.4353	0.4316	0.4204	31.20	54.24	45.28
21	0.3363	0.4109	0.3896	10.05	43.62	59.68
22	0.4427	0.4605	0.4525	66.82	46.59	71.12
23	0.4498	0.4590	0.4801	55.44	46.92	57.34
24	0.5860	0.5260	0.5593	86.44	68.30	78.59
25	0.5269	0.5190	0.5331	60.88	70.32	86.88
26	0.6102	0.5522	0.5611	100.90	92.02	102.62
27	0.4711	0.5004	0.5174	64.16	114.10	112.76
28	0.6018	0.5739	0.5847	123.98	102.30	102.37

Table C.7: (continued)

Case	$RF$			$\Delta p$		
	Measured	Linear Model	Quadratic Model	Measured	Linear Model	Quadratic Model
29	0.5545	0.5580	0.5531	175.92	107.22	106.30
30	0.5219	0.5699	0.5411	98.16	129.23	131.61
31	0.5334	0.5511	0.5560	171.67	134.84	122.92
32	0.6923	0.6409	0.6344	137.82	148.58	137.15
33	0.5572	0.5824	0.5382	84.03	167.61	166.41
34	0.9055	0.9484	0.9323	322.04	261.51	253.26
35	0.8990	0.9262	0.9144	327.31	246.91	238.96
36	0.9212	0.9493	0.9629	270.22	277.61	268.39
37	0.9461	0.9232	0.9522	306.14	285.46	279.40
38	0.3183	0.3523	0.3423	17.61	29.31	16.45
39	0.3922	0.3191	0.3394	75.88	54.61	56.77
40	0.4521	0.4237	0.4561	35.32	59.88	71.92
41	0.4190	0.4253	0.4256	45.63	59.28	83.32
42	0.4470	0.4546	0.4630	84.30	54.75	79.25
43	0.4271	0.4501	0.4722	43.45	56.01	73.08
44	0.4919	0.5188	0.5280	141.23	63.99	75.45
45	0.4842	0.4722	0.4753	101.04	84.00	89.41
46	0.4992	0.5174	0.5188	76.13	91.43	93.17
47	0.5118	0.5036	0.5300	70.20	95.51	77.27
48	0.6243	0.5665	0.5853	112.01	120.80	101.72
49	0.5731	0.5512	0.5346	70.97	101.44	93.31
50	0.5948	0.5892	0.5657	91.31	111.04	98.94
51	0.8808	0.8733	0.8750	230.91	212.81	205.70
52	0.9115	0.9227	0.9301	242.68	239.76	242.72
53	0.9111	0.8995	0.8814	279.82	246.93	259.88
54	0.8939	0.8921	0.8743	496.84	276.77	297.79
55	0.9018	0.8578	0.8932	266.77	283.97	287.35
56	0.9470	0.9328	0.9800	221.88	277.43	272.67
57	0.2864	0.2793	0.2588	18.64	29.62	19.41
58	0.3276	0.3448	0.3377	16.55	31.08	40.64
59	0.3724	0.3498	0.3628	24.82	29.01	37.46
60	0.4387	0.4087	0.4215	50.34	47.33	63.23
61	0.3977	0.4070	0.4258	51.01	47.76	61.78
62	0.4736	0.4592	0.4624	85.13	53.04	67.40
63	0.4125	0.4164	0.4583	52.33	51.32	48.78
64	0.6048	0.5186	0.5690	56.68	61.96	60.88
65	0.4426	0.4924	0.4955	91.46	80.43	90.11
66	0.4827	0.4985	0.5004	58.58	100.61	96.26
67	0.4355	0.4828	0.4815	90.50	105.28	87.81
68	0.8710	0.8828	0.8897	107.28	199.50	177.44
69	0.8878	0.8360	0.8240	308.86	218.07	210.48
70	0.8629	0.8742	0.8587	194.08	206.80	207.52
71	0.8634	0.8525	0.8476	127.33	213.31	209.63
72	0.8600	0.8916	0.8995	151.20	244.20	246.33
73	0.8684	0.8675	0.8619	382.46	251.44	267.62
74	0.8917	0.8991	0.9066	268.44	262.97	277.41
75	0.9336	0.8451	0.8842	206.67	283.76	289.82
76	0.2775	0.3067	0.3060	23.51	28.39	33.96
77	0.3061	0.3076	0.3002	23.19	4.26	29.11
78	0.3754	0.3272	0.3320	39.66	34.55	64.74
79	0.3848	0.3285	0.3685	73.20	33.61	42.38
80	0.4835	0.4331	0.4632	66.91	41.52	39.67
81	0.3989	0.3872	0.3831	41.08	62.00	62.89
82	0.3933	0.4364	0.4476	74.08	68.42	57.81
83	0.3616	0.4266	0.4377	53.67	71.29	47.96
84	0.5191	0.4739	0.4748	47.31	72.34	42.64
85	0.7628	0.7922	0.7916	70.86	159.26	140.17
86	0.8042	0.8334	0.8185	90.06	167.47	163.03
87	0.8876	0.7878	0.7954	194.44	185.90	185.26

Table C.7: (continued)

Case	RF			$\Delta p$		
	Measured	Linear Model	Quadratic Model	Measured	Linear Model	Quadratic Model
88	0.8572	0.8590	0.8692	211.73	198.17	205.59
89	0.8141	0.8386	0.8173	212.03	204.29	224.65
90	0.7830	0.8366	0.8201	249.22	232.00	258.19
91	0.8663	0.8010	0.8160	273.21	232.54	249.46
92	0.8880	0.8618	0.8707	415.21	246.05	262.16
93	0.8251	0.8087	0.8198	201.92	266.09	274.55
94	0.8790	0.8393	0.8632	175.87	277.95	278.24
95	0.1639	0.2175	0.2259	24.00	16.03	-9.22
96	0.3276	0.3080	0.3209	35.77	34.25	30.18
97	0.3338	0.3126	0.2936	37.88	32.75	49.47
98	0.3968	0.3726	0.3531	32.73	11.76	26.41
99	0.3104	0.3243	0.3192	44.05	29.15	29.92
100	0.4498	0.4047	0.4196	78.00	36.50	23.54
101	0.4348	0.3969	0.3922	67.33	38.99	18.69
102	0.6848	0.7484	0.7537	83.46	141.56	124.41
103	0.8465	0.7363	0.7721	159.64	145.12	125.81
104	0.7969	0.8074	0.8331	130.05	170.75	154.96
105	0.7349	0.7655	0.7595	134.42	167.04	167.71
106	0.8101	0.8045	0.7927	284.26	176.55	183.23
107	0.7963	0.7854	0.7671	148.65	182.26	188.10
108	0.7378	0.8100	0.7799	242.13	213.00	230.81
109	0.7361	0.7881	0.7586	215.72	219.55	246.49
110	0.7520	0.8127	0.7818	152.42	230.10	253.03
111	0.7590	0.7604	0.7683	331.90	250.13	251.53
112	0.8570	0.8434	0.8684	285.81	243.83	239.38
113	0.8615	0.8170	0.8254	292.43	251.73	244.04
114	0.2052	0.2263	0.1991	25.86	6.09	-10.71
115	0.2315	0.2345	0.2259	17.40	3.48	-1.69
116	0.2661	0.3240	0.3139	23.33	8.30	7.47
117	0.2528	0.2735	0.2558	21.18	40.10	36.70
118	0.2925	0.3282	0.3120	45.51	44.19	33.59
119	0.6676	0.6572	0.6767	52.43	107.06	85.42
120	0.7318	0.7209	0.7279	92.64	129.44	118.63
121	0.7220	0.7008	0.6915	136.90	132.00	128.98
122	0.7487	0.7455	0.7268	224.18	139.57	134.71
123	0.7245	0.7036	0.7046	129.51	156.68	145.26
124	0.7749	0.7729	0.7586	138.51	167.39	164.39
125	0.7505	0.7550	0.7237	211.87	172.50	171.48
126	0.7115	0.7574	0.7147	172.34	178.07	188.34
127	0.6785	0.7368	0.7409	119.16	184.24	183.43
128	0.8121	0.8277	0.8285	147.41	198.68	203.65

Table C.8: Sampling points defining the design space for dimensionless groups for 32 prediction runs

Cases	$N_{pe(Lo1)}$	$N_{pe(To1)}$	$R_L$	$M_{go}$	$N_{cap(ow)} \times 10^{-6}$	$N_{G(og)} \times 10^7$	$N_{G(wo)} \times 10^8$	$V_{DP}$	$c_{surf}$
1	50	1368.85	3.35	13.98	3.30	3.68	2.12	0.1413	0.1211
2	70.97	765.57	4.75	13.50	3.06	3.88	2.24	0.1852	0.1434
3	91.94	1972.13	2.42	13.04	2.82	4.08	2.37	0.2292	0.1657
4	112.9	463.93	3.82	12.62	2.58	4.27	2.49	0.2731	0.188
5	133.87	1670.49	5.22	12.22	2.34	4.47	2.62	0.317	0.2103
6	154.84	1067.21	2.88	11.85	2.10	4.67	2.74	0.3609	0.2326
7	175.81	2273.77	4.29	11.50	3.50	4.87	2.87	0.4048	0.2548
8	196.77	313.11	5.69	11.17	3.26	5.07	2.99	0.4487	0.2771
9	217.74	1519.67	2.10	10.85	3.02	5.27	3.12	0.4926	0.2994
10	238.71	916.39	3.51	10.56	2.78	5.46	3.24	0.5365	0.3217

Table C.8: (continued)

Cases	$N_{pe(L01)}$	$N_{pe(T01)}$	$R_L$	$M_{gv}$	$N_{cap(ow)} \times 10^{-6}$	$N_{G(og)} \times 10^7$	$N_{G(wo)} \times 10^8$	$V_{DP}$	$c_{surf}$
11	259.68	2122.95	4.91	10.28	2.55	3.5	3.37	0.5804	0.344
12	280.65	614.75	2.57	10.01	2.31	3.7	3.49	0.6244	0.3663
13	301.61	1821.31	3.97	9.76	2.07	3.9	2	0.6683	0.3886
14	322.58	1218.03	5.38	9.52	3.47	4.09	2.13	0.7122	0.4109
15	343.55	2424.59	3.04	9.29	3.23	4.29	2.25	0.7561	0.4331
16	364.52	237.71	4.44	9.07	2.99	4.49	2.37	0.8	0.4554
17	385.48	1444.26	5.84	8.87	2.75	4.69	2.5	0.1	0.4777
18	406.45	840.98	2.26	8.67	2.51	4.89	2.62	0.1439	0.5
19	427.42	2047.54	3.66	14.48	2.27	5.09	2.75	0.1878	0.1
20	448.39	539.34	5.06	13.96	2.03	5.28	2.87	0.2317	0.1223
21	469.35	1745.9	2.73	13.47	3.43	5.48	3	0.2756	0.1446
22	490.32	1142.62	4.13	13.02	3.19	3.52	3.13	0.3196	0.1669
23	511.29	2349.18	5.53	12.60	2.95	3.72	3.25	0.3635	0.1891
24	532.26	388.52	3.19	12.20	2.72	3.91	3.38	0.4074	0.2114
25	553.23	1595.08	4.60	11.83	2.48	4.11	3.5	0.4513	0.2337
26	574.19	991.8	6.00	11.48	2.24	4.31	2.01	0.4952	0.256
27	595.16	2198.36	2.00	11.15	2.00	4.51	2.13	0.5391	0.2783
28	616.13	690.16	3.40	10.84	3.40	4.71	2.26	0.583	0.3006
29	637.1	1896.72	4.81	10.54	3.16	4.91	2.38	0.6269	0.3229
30	658.06	1293.44	2.47	10.26	2.92	5.1	2.51	0.6708	0.3452
31	679.03	2500	3.87	10.00	2.68	5.3	2.63	0.7148	0.3674
32	700	200	5.27	9.75	2.44	5.5	2.76	0.7587	0.3897

Table C.9: Part 1: Dimensional properties for cases to be predicted

Case	L cm	H cm	$\phi$	$k_1$ mD	$k_2$ mD	$k_3$ mD	$k_4$ mD	$k_5$ mD
1	5490.97	1638.78	0.342	83.08	99.82	108.82	116.41	131.16
2	7853.79	1652.3	0.398	66.93	85.66	96.2	105.33	123.66
3	11538.21	4776.57	0.37	177.13	242.35	280.83	315.11	386.34
4	8094.58	2120.01	0.313	155.22	227.91	273.03	314.4	403.6
5	7063.43	1352.95	0.311	10.9	17.24	21.4	25.33	34.14
6	6093.63	2113.56	0.369	93.57	160.44	206.73	252.02	357.84
7	11887.95	2773.86	0.302	102.72	191.91	257.46	323.9	486.25
8	10016.79	1760.94	0.341	79.99	163.9	229.63	298.85	476.4
9	5346.54	2541.26	0.376	8.2	18.57	27.27	36.81	62.63
10	5203.71	1484.02	0.369	47.18	119.15	184.17	258.82	472.64
11	6853.77	1396.14	0.392	41.37	117.78	192.61	282.87	558.44
12	5705.66	2218.87	0.394	4.11	13.36	23.27	35.88	77.25
13	9092.07	2287.87	0.384	3.8	14.34	26.78	43.64	103.56
14	6310.62	1173.71	0.341	7.31	32.79	66.37	115.16	305.39
15	12161.7	4001.93	0.389	14.79	80.94	179.96	335.98	1014.29
16	6919.46	1557.89	0.327	12.59	87.46	217.59	443.51	1564.08
17	12472.53	2134.19	0.311	40.67	46.17	49.01	51.35	55.77
18	9806.21	4339.53	0.385	50.15	60.47	66.03	70.73	79.88
19	6658.99	1818.23	0.393	192.89	247.83	278.81	305.69	359.78
20	5794.7	1144.08	0.306	45.93	63.1	73.26	82.32	101.19
21	9286.86	3405.18	0.323	58.47	86.22	103.49	119.36	153.65
22	7416.15	1795.73	0.351	131.18	208.59	259.41	307.59	415.82
23	9547.79	1725.77	0.321	58.17	100.24	129.45	158.1	225.19
24	10340.43	3236.64	0.307	103.29	193.97	260.87	328.82	495.33
25	7417.07	1613.32	0.338	68.16	140.44	197.29	257.29	411.67
26	11021.61	1836.93	0.308	38.5	87.71	129.17	174.8	298.55
27	9855.65	4927.82	0.382	41.41	105.28	163.25	229.98	421.82
28	5707.5	1677.39	0.33	22.51	64.56	105.94	156.01	309.49
29	10953.4	2279.49	0.345	5.5	18.04	31.54	48.78	105.59
30	5968.2	2418.69	0.363	16.99	64.79	121.57	198.77	474.55

Table C.9: (continued)

Case	L cm	H cm	$\phi$	$k_1$ mD	$k_2$ mD	$k_3$ mD	$k_4$ mD	$k_5$ mD
31	9947.2	2570.25	0.363	22.76	103.12	209.82	365.51	976.16
32	8347.04	1583.06	0.332	4.69	25.97	58.08	108.95	331.66

Table C.10: Part 2: Dimensional properties for cases to be predicted

Case	$Q_{CO_2}$ $cm^3 min^{-1}$	$Q_{surf}$ $cm^3 min^{-1}$	$D_{Lo1} \times 10^{-2}$ $cm^2 min^{-1}$	$D_{To1} \times 10^{-4}$ $cm^2 min^{-1}$	$\mu_{CO_2}$ cp	$C_{surf} \times 10^{-5}$ mole frac	$N_c^{ref}$ $10^{-6}$
1	1519.67	506.56	24.23	7.88	0.129	7.29	4.71
2	946.68	315.56	12.86	5.27	0.134	8.63	4.92
3	8527.22	2842.41	16.9	13.5	0.139	9.97	5.14
4	2172.98	724.33	14.77	24.65	0.144	11.32	5.36
5	259.2	86.4	3.2	0.94	0.148	12.66	5.58
6	2059.52	686.51	6.56	11.44	0.153	14	5.79
7	3401.11	1133.7	13.2	5.56	0.158	15.34	6.01
8	1441.99	480.66	9.26	17.98	0.163	16.68	6.23
9	1811.08	603.69	2.44	7.9	0.167	18.02	6.44
10	1532.05	510.68	5.48	11.61	0.172	19.37	6.66
11	971.72	323.91	4.48	2.27	0.177	20.71	6.88
12	938.39	312.8	1.31	9.05	0.182	22.05	7.1
13	609.37	203.12	1.22	1.28	0.186	23.39	7.31
14	617.79	205.93	3.43	3.14	0.191	24.73	7.53
15	5804.26	1934.75	4.4	6.75	0.196	26.07	7.75
16	1604.05	534.68	5.12	39.76	0.201	27.42	7.97
17	632.65	210.88	1.93	1.51	0.205	28.76	8.18
18	3543.08	1181.03	1.57	14.88	0.21	30.1	8.4
19	1711.87	570.62	2.74	4.26	0.125	6.02	4.5
20	359.2	119.73	1.55	5.01	0.13	7.36	4.72
21	4003.74	1334.58	2.82	10.19	0.134	8.7	4.93
22	2066.16	688.72	3.68	9.26	0.139	10.05	5.15
23	974.99	325	2.54	1.81	0.144	11.39	5.37
24	4160.01	1386.67	3.35	44.97	0.149	12.73	5.59
25	1151.36	383.79	2.34	3.84	0.153	14.07	5.8
26	740.32	246.77	1.82	2.93	0.158	15.41	6.02
27	6035.59	2011.86	1.44	9.72	0.163	16.75	6.24
28	1668.4	556.13	2.22	17.11	0.168	18.1	6.46
29	823.03	274.34	1.05	1.53	0.172	19.44	6.67
30	3123.54	1041.18	1.78	14.86	0.177	20.78	6.89
31	2587.94	862.65	2.11	3.82	0.182	22.12	7.11
32	569.72	189.91	1.09	13.71	0.187	23.46	7.32

Table C.11: Part 3: Dimensional properties for cases to be predicted

Case	DTRAPW1	DTRAPN1	DTRAPW2	DTRAPN2	$k_{rgcw}$	$k_{rwiro}$	$k_{rocw}$
1	3.05	4.92	0.17	0.14	0.06	0.38	0.41
2	3.11	4.84	0.34	0.31	0.06	0.38	0.42
3	3.16	4.75	0.51	0.48	0.05	0.39	0.43
4	3.22	4.67	0.67	0.65	0.05	0.4	0.44
5	3.28	4.59	0.84	0.81	0.05	0.4	0.45
6	3.33	4.5	1.01	0.98	0.04	0.41	0.46
7	3.39	4.42	1.17	1.15	0.04	0.42	0.48
8	3.44	4.34	1.34	1.32	0.04	0.43	0.49



Table C.11: (continued)

Case	DTRAPW1	DTRAPN1	DTRAPW2	DTRAPN2	$k_{rgcw}$	$k_{rwiro}$	$k_{rocv}$
9	3.5	4.25	1.5	1.49	0.03	0.43	0.5
10	3.55	4.17	1.67	1.65	0.03	0.44	0.51
11	3.61	4.09	1.84	1.82	0.03	0.45	0.52
12	3.67	4	2	1.99	0.02	0.46	0.53
13	3.72	3.92	2.17	2.16	0.02	0.46	0.54
14	3.78	3.83	2.34	2.33	0.02	0.47	0.55
15	3.83	3.75	2.5	2.5	0.01	0.48	0.57
16	3.89	3.67	2.67	2.66	0.01	0.49	0.58
17	3.94	3.58	2.83	2.83	0.01	0.49	0.59
18	4	3.5	3	3	0	0.5	0.6
19	3	5	0.02	-0.02	0.06	0.37	0.4
20	3.06	4.92	0.18	0.15	0.06	0.38	0.41
21	3.11	4.83	0.35	0.32	0.06	0.38	0.42
22	3.17	4.75	0.52	0.49	0.05	0.39	0.43
23	3.22	4.67	0.68	0.66	0.05	0.4	0.44
24	3.28	4.58	0.85	0.82	0.05	0.41	0.45
25	3.33	4.5	1.01	0.99	0.04	0.41	0.47
26	3.39	4.41	1.18	1.16	0.04	0.42	0.48
27	3.45	4.33	1.35	1.33	0.04	0.43	0.49
28	3.5	4.25	1.51	1.5	0.03	0.43	0.5
29	3.56	4.16	1.68	1.66	0.03	0.44	0.51
30	3.61	4.08	1.85	1.83	0.03	0.45	0.52
31	3.67	4	2.01	2	0.02	0.46	0.53
32	3.72	3.91	2.18	2.17	0.02	0.46	0.54

Table C.12: Part 4: Dimensional properties for cases to be predicted

Case	$es$	$ev$	$S_o^{max}$	$eo$	$\Gamma_m$	$\Gamma_{pn}$	$r_{r1}$ $mole_{surf}^{-1}min^{-1}$	$r_{r2}$ $mole_{surf}^{-1}min^{-1}$
1	0.13	0.47	0.8	1.06	2.0003	2.0048	7.26	62.38
2	0.15	0.47	0.81	1.04	2.0006	2.0064	2.83	22.55
3	0.16	0.46	0.81	1.02	2.0008	2.008	2.35	17.46
4	0.17	0.45	0.82	1	2.0011	2.0096	5.38	37.35
5	0.19	0.45	0.82	0.98	2.0014	2.0112	1.91	12.37
6	0.2	0.44	0.83	0.96	2.0017	2.0128	6.35	38.56
7	0.21	0.43	0.83	0.94	2.002	2.0144	3.98	22.69
8	0.23	0.43	0.84	0.92	2.0023	2.016	4.59	24.56
9	0.24	0.42	0.84	0.9	2.0025	2.0176	4.9	24.63
10	0.25	0.41	0.84	0.88	2.0028	2.0192	13.24	62.57
11	0.27	0.41	0.85	0.86	2.0031	2.0208	7.04	31.33
12	0.28	0.4	0.85	0.84	2.0034	2.0224	3.34	13.98
13	0.29	0.39	0.86	0.82	2.0037	2.024	1.36	5.37
14	0.31	0.39	0.86	0.8	2.004	2.0256	8.79	32.74
15	0.32	0.38	0.87	0.78	2.0042	2.0272	3.34	11.74
16	0.33	0.37	0.87	0.76	2.0045	2.0288	13.15	43.6
17	0.35	0.37	0.88	0.74	2.0048	2.0304	1.66	5.2
18	0.36	0.36	0.88	0.72	2.0051	2.032	2.39	7.04
19	0.12	0.48	0.8	1.08	2	2.0033	4.51	41.67
20	0.13	0.47	0.8	1.06	2.0003	2.0049	3.74	32.01
21	0.15	0.47	0.81	1.04	2.0006	2.0065	2.94	23.38
22	0.16	0.46	0.81	1.02	2.0009	2.0081	6.62	49.06
23	0.17	0.45	0.82	1	2.0011	2.0097	3.02	20.88
24	0.19	0.45	0.82	0.98	2.0014	2.0113	3.71	23.98
25	0.2	0.44	0.83	0.96	2.0017	2.0129	5.48	33.15
26	0.21	0.43	0.83	0.94	2.002	2.0145	2.1	11.9
27	0.23	0.43	0.84	0.92	2.0023	2.0161	2.23	11.9

Table C.12: (continued)

Case	$es$	$ev$	$S_o^{max}$	$eo$	$\Gamma_{rn}$	$\Gamma_{pn}$	$r_{r1}$ $mole_{surf}^{-1} min^{-1}$	$r_{r2}$ $mole_{surf}^{-1} min^{-1}$
28	0.24	0.42	0.84	0.9	2.0026	2.0177	11.09	55.52
29	0.25	0.41	0.84	0.88	2.0028	2.0193	1.53	7.23
30	0.27	0.41	0.85	0.86	2.0031	2.0209	9.37	41.56
31	0.28	0.4	0.85	0.84	2.0034	2.0225	4.28	17.87
32	0.29	0.39	0.86	0.82	2.0037	2.0241	3.35	13.19

Table C.13: Measured and linear- and quadratic-regression predicted values of  $RF$  and  $\Delta p$  for prediction cases

Case	$RF$			$\Delta p$		
	Measured	Linear Model	Quadratic Model	Measured	Linear Model	Quadratic Model
1	0.3972	0.3793	0.3686	35.51	104.76	242.70
2	0.4367	0.4592	0.4559	48.83	89.45	208.16
3	0.4191	0.4273	0.5536	15.28	86.42	73.93
4	0.4750	0.5331	0.5718	26.53	77.01	122.36
5	0.5029	0.5285	0.5040	107.75	59.57	75.85
6	0.5887	0.5591	0.5817	45.48	65.40	-17.03
7	0.5733	0.5376	0.4285	44.02	125.60	123.09
8	0.7429	0.6510	0.4106	80.96	120.83	310.34
9	0.6354	0.5843	0.3228	252.79	130.48	460.15
10	0.6381	0.6423	0.3848	92.75	121.78	514.18
11	0.5950	0.6003	0.4197	80.53	107.12	464.93
12	0.6240	0.6569	0.5908	215.75	118.85	352.50
13	0.6108	0.5874	0.5836	186.04	156.23	446.33
14	0.5969	0.6328	0.5094	178.48	224.00	418.51
15	0.5668	0.5711	0.5550	84.03	229.93	393.89
16	0.7136	0.6854	0.6139	78.76	228.16	394.79
17	0.9559	0.9981	0.8297	343.82	302.30	505.26
18	0.9623	0.9942	0.8693	418.25	320.70	518.68
19	0.3469	0.3624	0.3127	7.86	36.45	46.88
20	0.4015	0.4795	0.2886	25.43	23.40	121.90
21	0.3346	0.4412	0.2638	30.59	95.16	198.36
22	0.4073	0.4948	0.4224	29.23	78.83	155.25
23	0.4134	0.4901	0.4453	44.89	61.28	187.12
24	0.5699	0.5764	0.5725	36.24	71.12	227.37
25	0.5227	0.5715	0.6237	43.85	53.93	139.52
26	0.5688	0.5826	0.5415	51.82	94.47	376.04
27	0.5314	0.5223	0.6798	55.04	103.04	77.30
28	0.5536	0.6115	0.6318	121.76	171.14	157.86
29	0.5695	0.5957	0.5956	197.08	157.29	153.46
30	0.5447	0.6046	0.3348	106.99	169.48	480.97
31	0.5892	0.5886	0.4573	59.61	155.55	332.75
32	0.7201	0.7108	0.4541	116.82	153.10	370.28

## Appendix D: Code for Hammersley Sequence Sampling

The following is a sample MATLAB code used to generate based on Hammersley Sequence Sampling method to obtain sampling points for the dimensionless groups.

```
function [z]= Hammersley(N, k)

z=zeros(N,k);

p=primes(1.0474e5);

for n=1:N
    z(n,1)=n/N;
    for i=2:k
        R=p((i-1));
        %Convert n into base R notation
        m=fix(log(n)/log(R));
        base=zeros(1,m+1);
        phi=zeros(1,m+1);
        coefs=zeros(m+1,1);
        for j=0:m
            base(j+1)=R^j;
            phi(j+1)=R^(-j-1);
        end
        remain=n;
        for j=m+1:-1:1
            coefs(j)=fix((remain)/base(j));
            remain=remain-coefs(j)*base(j);
        end
        z(n,i)=phi*coefs;
    end
end
```

end

end

# Appendix E: Nomenclature

## English Abbreviations

EOR	Enhanced Oil Recovery
WAG	Water Alternating Gas
MRF	Mobility Reduction Factor
TIPV	Total Injected Pore Volume

## Subscripts

$1$	CO <sub>2</sub> component
$2$	Decane component
$3$	Brine component
$4$	Surfactant component
$D$	Dimensionless quantity
$g$	Gaseous phase
$i$	Initial state
$j$	Injection state
$m$	Phase (g, o, and w)
$n$	Component (1, 2, 3 and 4)
$o$	Oleic phase
$R$	Reference quantity
$T$	Total quantity
$w$	Aqueous phase
$x$	x-direction
$z$	z-direction

## English Symbols

Symbol	Quantity	Unit
$A$	Area	$L^2$
$D_{nm}$	Diffusion coefficient of component $n$ in phase $m$	$L^2/t$
$D_{L(nm)}$	Longitudinal diffusion coefficient of component $n$ in phase $m$	$L^2/t$
$D_{T(nm)}$	Transverse diffusion coefficient of component $n$ in phase $m$	$L^2/t$
$DTRAPW1$	Wetting phase interpolation parameter for first set of $k_r$ curves	
$DTRAPW2$	Wetting phase interpolation parameter for second set of $k_r$ curves	
$DTRAPN1$	Non-wetting phase interpolation parameter for first set of $k_r$ curves	
$DTRAPN2$	Non-wetting phase interpolation parameter for second set of $k_r$ curves	
$d_p$	Mean particle diameter	$L$
$F$	Formation electric resistivity factor	
$eo$	Oil exponent term	
$es$	Surfactant exponent term	
$ev$	Capillary number exponent term	
$H$	Reservoir thickness	$L$
$k_x$	Horizontal permeability	$L^2$
$k_z$	Vertical permeability	$L^2$
$k_{rg}^f$	Adjusted relative permeability of gas in the presence of foam	
$k_{rm}$	Relative permeability of phase $m$	
$k_{row}$	Relative permeability of oil-water system	
$k_{rog}$	Relative permeability of oil-gas system	

$k_{rgcw}$	Relative permeability of gas at connate water	
$k_{rocw}$	Relative permeability of oil at connate water	
$k_{rwiro}$	Relative permeability of water at irreducible oil	
$K_L$	Longitudinal dispersion coefficient of component $n$ in phase $m$	$L^2/t$
$K_T$	Transverse dispersion coefficient of component $n$ in phase $m$	$L^2/t$
$M_{go}$	Mobility ratio of gas-oil system	
$M_{ow}$	Mobility ratio of oil-water system	
$M$	Molecular weight	$M/mole$
$M_n$	Molecular weight of component $n$	$M/mole$
$N_{cap(go)}$	Capillary number of gas-oil system	
$N_{cap(ow)}$	Gravity number of oil-water system	
$N_c^{ref}$	Reference capillary number	
$N_{G(go)}$	Gravity number of gas-oil system	
$N_{G(ow)}$	Capillary number of oil-water system	
$N_{peL(nm)}$	Longitudinal Peclet number of component $n$ in phase $m$	
$N_{peT(nm)}$	Transverse Peclet number of component $n$ in phase $m$	
$p$	Pressure	$M/(Lt^2)$
$Q$	Flow rate	$L^3/t$
$R_L$	Reservoir aspect ratio	
$r_r$	Reaction rate of new component generation	$mole^{-1}t^{-1}$
$S_o$	Local oil saturation for $k_{rg}$ modification	
$S_o^{max}$	Maximum oil saturation for $k_{rg}$ modification	
$S_m$	Saturation of phase $m$	

$S_{or}$	Residual oil saturation	
$S_{wc}$	Connate water saturation	
$u$	Velocity	$L/t$
$u_m$	Velocity of phase $m$	$L/t$
$u_T$	Total fluid velocity	$L/t$
$V$	Volume	$L^3$
$V_n$	Volume of component $n$	$L^3$
$V_{DP}$	Dykstra Parsons coefficient	
$w_s$	Local surfactant concentration in grid block	
$w_s^{max}$	Maximum surfactant concentration	
$x$	Spatial variable in horizontal direction	
$z$	Spatial variable in vertical direction	



## Greek Symbols

Symbol	Quantity	Unit
$\Delta p$	Pressure difference	$M/(Lt^2)$
$\phi$	Porosity	
$\mu$	Viscosity	$M/Lt$
$\mu_m$	Viscosity of phase $m$	$M/Lt$
$\rho$	Density	$M/L^3$
$\rho_m$	Density of phase $m$	$M/L^3$
$\sigma$	Interfacial tension	$M/t^2$
$\sigma_k$	Standard deviation of permeability distribution	
$\sigma_{go}$	Gas-oil interfacial tension	$M/t^2$
$\sigma_{ow}$	Water-oil interfacial tension	$M/t^2$
$\lambda$	Fluid mobility	$L^3t/M$
$\lambda_m$	Mobility of phase $m$	$L^3t/M$
$\tau$	Time scale factor	
$\Gamma_{rn}$	Reacting component $n$ stoichiometric coefficient	
$\Gamma_{pn}$	Producing component $n$ stoichiometric coefficient	

## Vita

Gbolahan Afonja was born in Port Harcourt, Rivers, Nigeria. He attended the Nigerian Navy Secondary School, Abeokuta, and pursued a Bachelor's degree in Electrical Engineering from Morgan State University, Baltimore, MD, which he received in 2004. Gbolahan continued his education at West Virginia University, Morgantown, WV, where he obtained his Master's degree in Petroleum and Natural Gas Engineering. In August, 2013, he will receive the degree of Doctor of Philosophy from Louisiana State University's Craft and Hawkins Department of Petroleum Engineering.